



UNIVERSITY OF
BIRMINGHAM

TRIBOLOGY OF BALL-AND-SOCKET
TOTAL DISC ARTHROPLASTY

by

PARSHIA MOGHADAS MOBARAKEH

A thesis submitted to
University of Birmingham
for the degree of
DOCTOR OF PHILOSOPHY

School of Mechanical Engineering
University of Birmingham
April 2012

UNIVERSITY OF
BIRMINGHAM

University of Birmingham Research Archive

e-theses repository

This unpublished thesis/dissertation is copyright of the author and/or third parties. The intellectual property rights of the author or third parties in respect of this work are as defined by The Copyright Designs and Patents Act 1988 or as modified by any successor legislation.

Any use made of information contained in this thesis/dissertation must be in accordance with that legislation and must be properly acknowledged. Further distribution or reproduction in any format is prohibited without the permission of the copyright holder.

ABSTRACT

Total disc arthroplasty (TDA) can be used to replace a degenerated intervertebral disc in the spine. There are different designs of TDAs, but one of the most common is a ball-and-socket combination. Contact between the bearing surfaces of such designs can result in high frictional torque, which can then result in wear and implant loosening. This study was designed to determine the effects of change in design factors, such as dimensions and material combinations, on friction and wear of ball-and-socket TDAs. Friction tests were carried out on generic models with ball radii 10, 12, 14 and 16 mm. Three material combinations were investigated; metal-on-metal, metal-on-polymer and for the first time polymer-on-metal. Wear tests were performed on metal-on-polymer Charité® TDAs and generic metal-on-metal models to compare the wear rate under the same conditions. Friction test results showed that polymer-on-metal TDAs create less friction than metal-on-polymer and metal-on-metal TDAs. Wear test results showed that under the same conditions, metal-on-metal TDAs create 23 times less wear debris than metal-on-polymer. The results were in agreement with studies on total hip arthroplasty (THA). The results of this work suggest possible alternatives for future TDA designs.

My darling mum and dad,

...I am still a little child, only with greater curiosity and more questions...

To my beloved mum, dad and sister

ACKNOWLEDGMENTS

A great supervisor believes in you, unselfishly helps you and leads you, and sometimes pokes you with a sharp stick called "truth". It is hard to overstate my gratitude to my great supervisors Professor David Hukins and Dr. Duncan Shepherd for their unconditional help and inspirational guidance throughout this work; without them this work would not have been possible.

I would like to thank Mr. Carl Hingley, Mr. Lee Gauntlett, Mr. Peter Thornton, Mr. Alan Saywell, Dr. James Bowen, Dr. Hossein Ostadi, Mr. Gerry Dunne (Westley Engineering Ltd.), Dr. Michelle Holder and Mr. David Cunningham (University of Strathclyde) for their technical support which made the experimental aspects of this thesis possible.

My special thanks go also to my true friends who were always there for me and supported me with their love.

I wish I could put in words and thank my mother for her endless love and unconditional help, inspiration, encouragement and support throughout this work. Without her, I could not finish this work. I would also like to thank my beloved sister, Armita, for her love and support throughout this work.

TABLE OF CONTENTS

Chapter 1. Introduction	1
Chapter 2. Background	6
2.1 Chapter overview	6
2.2 Introduction	7
2.3 The anatomy of the spine	8
2.3.1. Regions of the spine	8
2.3.2. Motions of the spine.....	10
2.3.3. The vertebra	12
2.3.4. The intervertebral disc	15
2.3.5. The ligaments.....	19
2.3.6. Load and load bearing properties of the intervertebral disc	19
2.4 Neck and back pain	21
2.5 Aging and degeneration	21
2.6 Treatment of neck and back pain	23
2.7 Total disc arthroplasty	25
2.8 Failure of TDA	30
2.9 Possible steps towards improving TDAs	33
2.9.1. Introduction	33
2.9.2. How dimension-related problems can be improved	33
2.9.3. How material-related problems can be improved	35
2.10 General testing conditions for the experimental studies of TDAs	36
2.10.1. Introduction	36
2.10.2. Selection of load, range of motion and frequency according to the standards	36
2.10.3. Lubrication	38
2.10.4. Lubrication regime and friction	40
2.11 Summary	43

Chapter 3. General Materials and Methods	45
3.1 Chapter overview	45
3.2 Materials	46
3.2.1. Disc design	46
3.2.1.1. <i>Introduction</i>	46
3.2.1.2. <i>Metal-on-metal friction tests</i>	46
3.2.1.3. <i>Metal and polymer friction tests</i>	47
3.2.1.4. <i>Metal-on-metal wear test</i>	48
3.2.1.5. <i>Charité® wear test</i>	48
3.2.2. Disc manufacture	49
3.2.3. Testing equipment	52
3.2.3.1. <i>Bose Spine Simulator</i>	52
3.2.3.2. <i>Bose ElectroForce® Test Instrument</i>	56
3.3 Methods	58
3.3.1. Preparation of the samples	58
3.3.2. Surface roughness measurements	59
3.3.2.1. <i>Introduction</i>	59
3.3.2.2. <i>Non-contact method</i>	60
3.3.2.3. <i>Contact method</i>	62
3.3.3. General testing conditions for the current study according to the ISO and ASTM standards	65
3.3.3.1. <i>Friction tests</i>	65
3.3.3.2. <i>Wear tests</i>	66
3.4 Summary	67

Chapter 4. Effect of Lubricants on the Friction in Total Disc Arthroplasty	68
4.1 Chapter overview	68
4.2 Introduction	69
4.3 Materials and methods	70
4.3.1. Introduction	70
4.3.2. Fixtures	71
4.3.3. Lubricant preparation	74
4.3.4. Viscosity measurement of the lubricants	75
4.3.5. Preparation of the metal samples	77
4.3.6. Frictional torque	77
4.3.7. Statistical analysis	79

4.3.8. Stribeck analysis	80
4.4 Results	81
4.4.1. Frictional torque analysis	81
4.4.2. Lubrication regime analysis	86
4.5 Discussion	90
4.6 Summary	94
Chapter 5. Effect of Ball Radius on the Friction in Metal-on-Metal Total Disc Arthroplasty	96
5.1 Chapter overview	96
5.2 Introduction	97
5.3 Materials and methods	97
5.3.1. Introduction	97
5.3.2. Frictional torque	99
5.3.3. Stribeck analysis	100
5.4 Results	100
5.4.1. Frictional torque analysis	100
5.4.2. Lubrication regime analysis	104
5.5 Discussion	107
5.6 Summary	109
Chapter 6. Polymer-on-Metal or Metal-on-Polymer Total Disc Arthroplasty? Effect of Material Combination on the Friction	110
6.1 Chapter overview	110
6.2 Introduction	111
6.3 Materials and methods	111
6.3.1. Introduction	111
6.3.2. Frictional torque	114
6.3.3. Statistical analysis	114
6.3.4. Stribeck analysis	115
6.4 Results	115
6.4.1. Frictional torque analysis	115

6.4.2. Lubrication regime analysis	121
6.5 Discussion	121
6.6 Summary	126
Chapter 7. Wear of Total Disc Arthroplasty	127
7.1 Chapter overview	127
7.2 Introduction	128
7.3 Materials and methods	129
7.3.1. Materials	129
7.3.1.1. <i>Implant and fixtures for the Charité® wear test</i>	129
7.3.1.2. <i>Implant and fixtures for the metal-on-metal wear test</i>	132
7.3.1.3. <i>Testing equipment</i>	132
7.3.2. Methods	132
7.3.2.1. <i>Preparing samples for measurement</i>	132
7.3.2.2. <i>Gravimetric measurement</i>	133
7.3.2.3. <i>Volumetric measurement</i>	134
7.3.2.4. <i>Surface roughness measurements of the metal samples</i>	136
7.3.2.5. <i>Lubricant preparation</i>	137
7.3.2.6. <i>Viscosity measurement of the lubricant</i>	137
7.3.2.7. <i>Performing the tests</i>	138
7.3.2.8. <i>Statistical analysis</i>	141
7.4 Results	144
7.4.1. Wear study of the Charité® cores	144
7.4.2. Wear study of the metal-on-metal samples	147
7.4.3. Surface study of the metal-on-metal samples	150
7.4.4. Comparison between wear of the Charité® TDAs and the metal-on-metal samples	154
7.5 Discussion	155
7.5.1. The Charité® TDA	155
7.5.2. Wear of metal-on-metal samples	157
7.5.3. Comparison between wear of the Charité® TDAs and the metal-on-metal samples	159
7.6 Summary	159

Chapter 8. General Conclusions	160
Appendix A	166
Appendix B	183
Appendix C	187
Appendix D	191
Appendix E	196
References	200

LIST OF FIGURES

Figure 2.1. Regions of the spine (author’s own photographs, adapted from Kurtz and Edidin, 2006)	9
Figure 2.2. The anatomic reference directions (author’s own photographs, adapted from Kurtz and Edidin, 2006)	11
Figure 2.3. The kinematic motions of the spine (author’s own diagrams, adapted from Kurtz and Edidin, 2006).....	12
Figure 2.4. Examples of a) cervical, b) thoracic and c) lumbar vertebrae: IAP- inferior articular process, L- lamina, P- pedicle, SAP- superior articular process, SP- spinous process, TP- traverse process, VB- vertebral body. The numbers 1, 2 and 3 indicate the vertebral body, pedicle and posterior process sections of the vertebra, respectively (author’s own drawings of typical vertebrae, adapted from Bogduck, (2005), Joseph (1986) and Middleditch and Oliver(2005)).	14
Figure 2.5. Typical structure of an intervertebral disc (author’s own drawing, adapted from Bogduk (2005), Guerin and Elliott (2006) and Hukins (1988))	16
Figure 2.6. Typical shape for a) cervical, b) thoracic and c) lumbar intervertebral discs (author’s own drawing, adapted from Hukins (1988))	17
Figure 2.7. Indication of height, depth and width of the disc	34
Figure 2.8. The a) boundary, b) mixed and c) fluid film lubrication between two articulating surfaces	40
Figure 2.9. The Stribeck curve (adapted from Scholes and Unsworth (2006b))	42
Figure 3.1. The Maverick™ TDA	47
Figure 3.2. The cobalt chrome block has been (A) cut and (B) shaped to form the desired sample. It was then (C) highly polished with a Black and Decker Bench Grinder	50
Figure 3.3. The Black and Decker Bench Grinder.....	50

Figure 3.4. The side view of four TDAs with radii of 10, 12, 14 and 16 mm and identical spherical base diameter of 18 mm	51
Figure 3.5. The generic metal-on-metal ball (left) and socket (right) sample with 10 mm ball radius	51
Figure 3.6. The generic metal ball (left) and polymer socket (right) sample with 10 mm ball radius	52
Figure 3.7. The Bose SDWS-1 Spine Simulator with uni-axial Bose 1010CCH-1K-B load cell. The arrows show direction of motions and the green point at the centre indicates the Centre of Rotation.....	53
Figure 3.8. The Bose SDWS-1 Spine Simulator, with multi-axial AMTI MC3-6-1000 load cell: A) desktop computer, B) heating controller and C) actuators	54
Figure 3.9. The bath assembly (A) is mounted with the split clamps and screws (B) to the heating block of the spine simulator (C). The clearance between the top and bottom plate after assembly is 100 mm	55
Figure 3.10. The Bose ElectroForce® 3330 Series II Test Instrument	57
Figure 3.11. The average surface roughness Ra in 2D (left) and the average surface roughness Sa in 3D (right)	60
Figure 3.12. The MicroXAM2 interferometer	61
Figure 3.13. The Taylor Hobson Form Talysurf-120L.....	62
Figure 3.14. Surface roughness measurements of a) metal and b) polymer samples with ball radius 10 mm. The sampling length is 1.25×1.25 mm	64
Figure 4.1. The generic metal-on-metal samples with a) 10 mm and b) 16 mm ball radii. The endplates are designed to enable easy fixation to the spine simulator	70
Figure 4.2. The distance from the top plate to COR of the Bose spine simulator (42.5 mm) and to the bottom plate (100 mm).....	71
Figure 4.3. A 2D example of the sample with 16 mm ball radius, fitted to the fixtures. The red point indicates the COR of the sample, which is 42.5 mm to the top plate of the simulator.	72

Figure 4.4. A 2D example of the sample with 10 mm ball radius, fitted to the same fixtures as those for the 16 mm sample. The red point indicates the COR of the sample, which has been adjusted to correct position by 9 mm extra plate, bringing the COR back to 42.5 mm. The cross indicates the COR of 10 mm sample, if the fixture were fitted to the simulator's top plate without the 9 mm extra plate.....	73
Figure 4.5. The top fixture (left) and the extra plate (right)	74
Figure 4.6. The AR-G2 cone-on-plate rheometer	76
Figure 4.7. The Bose Spine Simulator with the 10 mm sample inside a) before and b) after adding lubricant	78
Figure 4.8. Mean frictional torque plotted against frequency, for the samples with 16 mm ball radius in diluted calf serum (✕) and Ringer's solution (•) for axial rotation. Error bars represent 95% confidence intervals	82
Figure 4.9 Mean frictional torque plotted against frequency, for the samples with 16 mm ball radius in diluted calf serum (✕) and Ringer's solution (•) for lateral bending. Error bars represent 95% confidence intervals	83
Figure 4.10. Mean frictional torque plotted against frequency, for the samples with 16 mm ball radius in diluted calf serum (✕) and Ringer's solution (•) for flexion. Error bars represent 95% confidence intervals	84
Figure 4.11. Mean frictional torque plotted against frequency, for the samples with 16 mm ball radius in diluted calf serum (✕) and Ringer's solution (•) for extension. Error bars represent 95% confidence intervals	85
Figure 4.12. Stribeck curves for sample with a ball radius of 16 mm for diluted calf serum (✕) and Ringer's solution (•), operated in axial rotation. A third order polynomial has been fitted to the points	86
Figure 4.13. Stribeck curves for sample with a ball radius of 16 mm for diluted calf serum (✕) and Ringer's solution (•), operated in lateral bend. A third order polynomial has been fitted to the points	87
Figure 4.14. Stribeck curves for sample with a ball radius of 16 mm for diluted calf serum (✕) and Ringer's solution (•), operated in flexion. A third order polynomial has been fitted to the points.....	88

Figure 4.15. Stribeck curves for sample with a ball radius of 16 mm for diluted calf serum (×) and Ringer’s solution (•), operated in extension. A third order polynomial has been fitted to the points..... 89

Figure 4.16. Maximum mean frictional torque plotted against maximum angular motion for sample with a ball radius of 16 mm for diluted calf serum (×) ($R^2 = 0.67$) and Ringer’s solution (•) ($R^2 = 0.91$). Regression lines are fitted through the data points 93

Figure 5.1. Mean frictional torque plotted against frequency for the sample with a ball radius of 10 mm, in flexion, under the loads of 50 (■), 600 (▲), 1200 (×) and 2000 N (◆). Error bars represent standard deviations; when error bars are not shown they are smaller than the symbols used to represent the data points..... 101

Figure 5.2. Mean frictional torque plotted against load for flexion at a frequency of 1 Hz, for implants with ball radii of 10 (■) ($R^2 = 0.99$, $p = 0.004$), 12 (▲) ($R^2 = 0.98$, $p = 0.012$), 14 (×) ($R^2 = 0.98$, $p = 0.009$) and 16 mm (◆) ($R^2 = 0.99$, $p = 0.006$). Error bars represent standard deviations; when error bars are not shown they are smaller than the symbols used to represent the data points. Regression lines are fitted through the data points 102

Figure 5.3. Mean frictional torque against radius for a frequency of 1 Hz in flexion motion, under the loads of 50 (■) ($R^2 = 0.95$, $p = 0.028$), 600 (▲) ($R^2 = 0.98$, $p = 0.011$), 1200 (×) ($R^2 = 0.95$, $p = 0.025$) and 2000 N (◆) ($R^2 = 0.99$, $p = 0.006$). Error bars represent standard deviations; when error bars are not shown they are smaller than the symbols used to represent the data points. Regression lines are fitted through the data points..... 103

Figure 5.4. Stribeck curves for sample with a ball radius of 10 mm, under loads of 600 (▲), 1200 (×) and 2000 N (◆), operated in flexion. A third order polynomial has been fitted to the points..... 104

Figure 5.5. Stribeck curves for sample with a ball radius of 12 mm, under loads of 600 (▲), 1200 (×) and 2000 N (◆), operated in flexion. A third order polynomial has been fitted to the points..... 105

Figure 5.6. Stribeck curves for sample with a ball radius of 14 mm, under loads of 600 (▲), 1200 (×) and 2000 N (◆), operated in flexion. A third order polynomial has been fitted to the points..... 106

Figure 5.7. Stribeck curves for sample with a ball radius of 16 mm, under loads of 600 (▲), 1200 (×) and 2000 N (◆), operated in flexion. A third order polynomial has been fitted to the points..... 107

Figure 6.1. The generic model with polymer socket (top right) on metal ball (top left), and metal socket (bottom left) on polymer ball (bottom right) with 10 mm ball radius 112

Figure 6.2. Mean frictional torque plotted against frequency, in axial rotation, for the samples with 10 mm ball radius in polymer socket/metal ball (×) and metal socket/polymer ball (▲) combination, and samples with 14 mm ball radius in polymer socket/metal ball (×) and metal socket/polymer ball (▲) combination. Error bars represent 95% confidence intervals; where error bars are not shown, they are smaller than the data points 116

Figure 6.3. Mean frictional torque plotted against frequency, in extension between 0° to -3°, for the samples with 10 mm ball radius in polymer socket/metal ball (×) and metal socket/polymer ball (▲) combination, and samples with 14 mm ball radius in polymer socket/metal ball (×) and metal socket/polymer ball (▲) combination. Error bars represent 95% confidence intervals; where error bars are not shown, they are smaller than the data points..... 117

Figure 6.4. Mean frictional torque plotted against frequency, in flexion between 0° to 6°, for the samples with 10 mm ball radius in polymer socket/metal ball (×) and metal socket/polymer ball (▲) combination, and samples with 14 mm ball radius in polymer socket/metal ball (×) and metal socket/polymer ball (▲) combination. Error bars represent 95% confidence intervals; where error bars are not shown, they are smaller than the data points..... 119

Figure 6.5. Mean frictional torque plotted against frequency, in flexion between 0° to 2°, for the samples with 10 mm ball radius in polymer socket/metal ball (×) and metal socket/polymer ball (▲) combination, and samples with 14 mm ball radius in polymer socket/metal ball (×) and metal socket/polymer ball (▲) combination. Error bars represent 95% confidence intervals; where error bars are not shown, they are smaller than the data points..... 120

Figure 6.6. Stribeck curves for the samples with 10 mm ball radius in polymer socket/metal ball (×) and metal socket/polymer ball (▲) combination, and samples with 14 mm ball radius in polymer socket/metal ball (×) and metal socket/polymer ball (▲) combination, in axial rotation. A third order polynomial has been fitted to the points 122

Figure 6.7. Stribeck curves for the samples with 10 mm ball radius in polymer socket/metal ball (×) and metal socket/polymer ball (▲) combination, and samples with 14 mm ball radius in polymer socket/metal ball (×) and metal socket/polymer ball (▲) combination, in flexion between 0° to 6°. A third order polynomial has been fitted to the points 123

Figure 7.1. The Charité® TDA	129
Figure 7.2. The endplate (A), fixture (B) and lid (C).....	131
Figure 7.3. The assembly method of the Charité® endplate to the fixture. a) The metal endplate is placed into the fixture, and b) the lid is placed on top to secure the endplate in place	131
Figure 7.4. a) The SkyScan-1172 High-resolution desk-top MicroCT system and b) the Charite® core inside a grooved packaging foam	135
Figure 7.5. An example of a) two measurements with correlation at line of equality and b) Bland-Altman graph with results in agreement (author’s own graphs, adapted from Bland and Altman, 1986)	143
Figure 7.6. The mean mass loss of the Charité® cores. A regression line is fitted through the data points ($R^2 = 0.99$, $p = 0.00$). Error bars represent standard deviations	144
Figure 7.7. The mean volume loss of the Charité® cores. A regression line is fitted through the data points ($R^2 = 0.99$, $p = 0.00$). Error bars represent standard deviations	145
Figure 7.8. The Bland-Altman graph, with the difference between the means of the values from the two measurement methods against the means.....	146
Figure 7.9. The 3D microCT images of the UHMWPE Charité® core a) brand new and b) after 5 million cycles of wear test	147
Figure 7.10. The mean mass loss of the metal-on-metal samples. A regression line is fitted through the data points (for 0 to 1 million cycles, $R^2 = 0.99$, $p = 0.046$; for 1 to 5 million cycles, $R^2 = 0.99$, $p = 0.00$). Error bars represent standard deviations	149
Figure 7.11. The mean volume loss of the metal-on-metal samples. A regression line is fitted through the data points (for 0 to 1 million cycles, $R^2 = 0.99$, $p = 0.046$; for 1 to 5 million cycles, $R^2 = 0.99$, $p = 0.00$). Error bars represent standard deviations	150
Figure 7.12. The average surface roughness of metal-on-metal samples (for 0 to 1 million cycles, $R^2 = 0.98$, $p = 0.039$; for 1 to 5 million cycles, $R^2 = 0.94$, $p = 0.012$). Error bars represent standard deviations	152

Figure 7.13. The 3D Taylor Hobson Form Talysurf-120L surface roughness measurement images of a ball sample a) when brand new, b) after 1 million cycles and c) after 5 million cycles 153

Figure 7.14. The mean volume loss of the Charité® cores (◆) and metal-on-metal samples (■). A regression line is fitted through the data points. Error bars represent standard deviations; when error bars are not shown they are smaller than the symbols used to represent the data points 154

LIST OF TABLES

Table 2.1. The average range of motion for human intervertebral disc (Adams and Hutton, 1988; Bogduk, 2005; White and Panjabi, 1990).....	18
Table 2.2. Examples of TDAs, based on information in Anderson et al. (2006), Gwynne (2010), Kurtz (2006) and Wang et al. (2011) (author’s own drawings and photographs)	26
Table 2.3. The recommended load values for wear testing of TDAs, by ISO and ASTM standards (ASTM F2423-05; BS ISO 18192-1:2008)	37
Table 2.4. The range of motion for cervical region (ASTM F2423-05; BS ISO 18192-1:2008)	37
Table 2.5. The range of motion for lumbar region (ASTM F2423-05; BS ISO 18192-1:2008)	38
Table 3.1. The suggested values for different motions, compressive load and diluted calf serum protein concentration, for testing lumbar TDAs (ASTM F2423-05; BS ISO 18192-1:2008).....	66
Table 4.1. The average surface roughness (Sa) of metal ball and socket samples with ball radii 10 and 16 mm, based on six measurements.....	77
Table 4.2. Some of the major compositions of lubricants (Fogh-Andersen, 1995; Sherwood, 2011; Harsha and Joyce, 2011; Streicher et al.1996).....	90
Table 5.1. The average surface roughness (Sa) of metal ball and socket samples with ball radii 10, 12, 14 and 16 mm, after six measurements	98
Table 6.1. The average surface roughness (Sa) of polymer and metal samples, after six measurements.....	113
Table 7.1. Required angular displacements for lumbar TDA wear test, by the BS ISO 18192-1:2008	139
Table 7.2. Load parameters for lumbar TDA wear test, by the BS ISO 18192-1:2008.....	139

Table 7.3. The average surface roughness (Sa) of brand new metal ball and socket samples, after six measurements 151

Table 7.4. The average surface roughness (Sa) of metal ball and socket samples after 5 million cycles, after six measurements 151

Chapter 1

Introduction

The aims of the work presented in this thesis were to investigate the tribology of ball-and-socket total disc arthroplasty (TDA) under laboratory conditions. This work is aimed towards developing a better understanding of ball-and-socket TDAs and how their life and performance can be improved for future designs.

To achieve the aims, the following objectives were set:

- to compare between calf serum and Ringer's solution, in order to identify the most appropriate lubricant for laboratory tests on TDAs
- to design generic TDA models with different ball radii, in order to investigate the effect of change in ball radius on performance of ball-and-socket TDAs
- to design generic TDA models with different material combinations, in order to investigate the effect of change in material combination on performance of ball-and-socket TDAs
- to compare the wear rate of a metal-on-metal and metal-on-polymer TDAs, by performing wear tests under identical conditions

Laboratory experiments on TDAs are carried out to simulate performance in the body, in order to develop a better understanding of the tribological behaviour and performance of these designs. It is important that the *in vitro* tests are reliable; therefore, the testing conditions need to mimic what TDAs experience in the body, as closely as possible. When a TDA is implanted, it is lubricated by the surrounding body fluid. This means that the *in vitro* tests need to include a lubricant similar to that in the body. The intervertebral joint is assumed to be lubricated by interstitial fluid (Shaheen and Shepherd, 2007; Yao and Gu, 2006), which

may have composition between Ringer's solution and diluted calf serum (Fogh-Andersen, 1995; Sherwood, 2011; Streicher et al.1996). Both lubricants have been used in previous studies; yet, it is not clear which one can be used as the alternative lubricant for *in vitro* studies of TDAs; this was investigated as the first objective of this work.

Ball-and-socket TDAs have been commercially available since 1987 (Kurtz, 2006) and like any other implant, they have experienced failure. The main reasons for failure are associated with the design factors, such as dimensions and material combination, and creation of wear debris as a result of ball-and-socket surface contact. Unlike total hip arthroplasty (THA), no systematic studies have been performed to investigate the effect of changes in dimensions and materials on the performance of TDAs. As part of the objectives of this work, the effect of change in ball radius, as a major design factor for ball-and-socket TDAs, has been investigated.

The majority of TDAs have metal-on-metal (metal socket on metal ball) or metal-on-polymer (metal socket on polymer ball) material combination. Polymer-on-metal (polymer socket on metal ball) THA was initiated by Charnley as a means of reducing friction between the articulating surfaces (Hall et al., 1994; Joyce, 2009). The combination of metal and polymer for TDAs is the other way round. Therefore, with regards to changing the material combination as the third objective of this work, the effect of reverse material combination (i.e. polymer socket on metal ball) was investigated to understand whether such a material combination offers a better performance for TDAs.

As creation of wear debris is considered to be a reason for failure and further problems, it is important to develop an understanding of the wear rate of TDAs with different material combinations. Previous studies have investigated the wear rate for metal-on-metal and metal-on-polymer TDAs. However, as they have been performed with different equipments and under different testing conditions, the results may not be comparable. Therefore, as the final objective of this work, the wear rate of TDAs with both material combinations is investigated, and a true comparison is developed.

To meet the objectives of this work, the studies that were performed are described in the chapters summarised below.

Chapter 2 provides the reader with necessary background information for understanding the importance of the work. It describes the anatomy of the spine, including the intervertebral disc. The major reason behind the need for TDAs is described, followed by a description of different types of TDAs and the reasons for failure. Finally, the reasons for selecting ball radius and material combination as important factors for improving the performance of TDAs are described.

In *Chapter 3*, the common material and methods used in this work are described. The chapter includes the design and manufacturing process of the generic TDA models, followed by an introduction to the equipments used for performing experiments. Methods of preparing samples for testing and general testing conditions are also described.

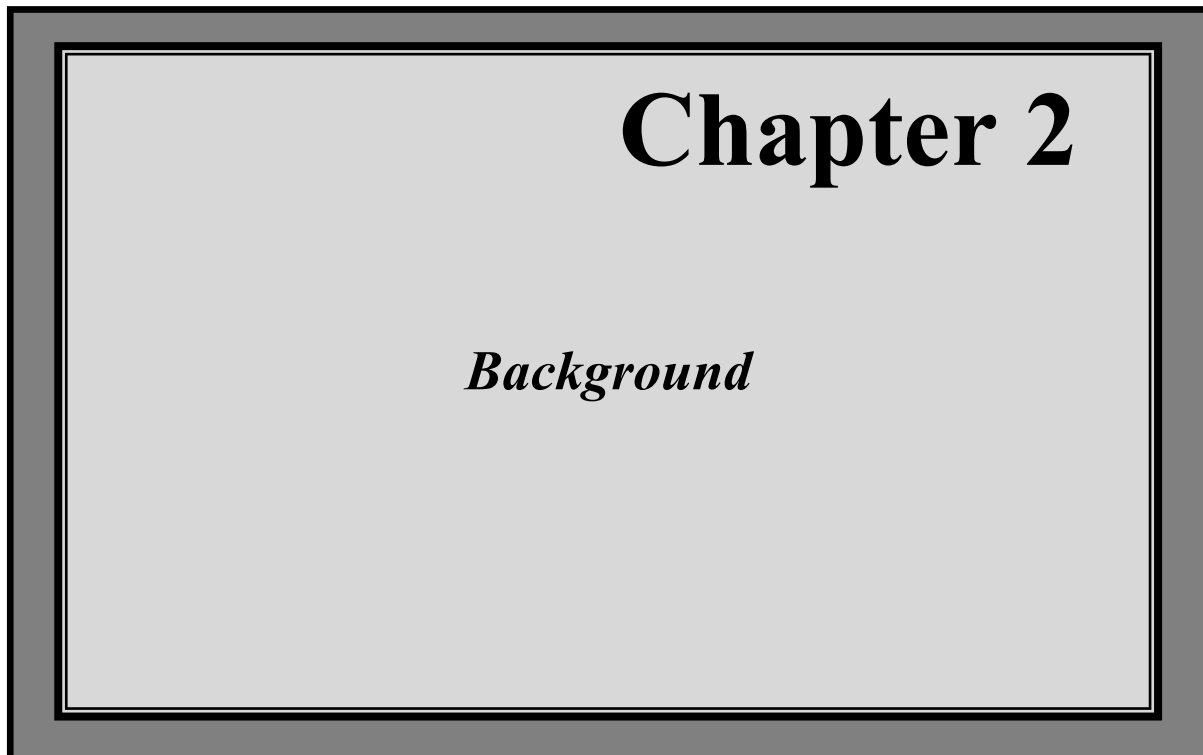
As one of the factors that affects the results, *Chapter 4* presents the study on the effect of lubricant on friction in TDAs. In this part of the work, two most commonly used lubricants, diluted calf serum and Ringer's solution, are compared and the lubricant for the remaining studies in this work is introduced.

Chapter 5 presents the study on the effect of change in ball radius on the friction of ball-and-socket TDAs. In this chapter, four generic metal-on-metal TDA models with different ball radii are examined under similar conditions and the dimensions that give the best performance identified.

The comparison between metal-on-polymer and polymer-on-metal TDAs is presented in *Chapter 6*. In this chapter, two samples with different ball radii were tested from each group of material combination. The results are compared and the material combination with better performance is introduced.

Chapter 7 includes the study of the wear of metal-on-metal and metal-on-polymer TDAs. In this part of the study, generic models of metal-on-metal TDA are compared with commercially available metal-on-polymer TDA, the Charité® (Depuy Spine, Raynham, MA, USA). The tests were performed under similar conditions and the wear rates of both types of TDAs are compared.

Finally, in *Chapter 8*, overall conclusions towards the alternative TDA design is provided.



2.1. Chapter overview

This chapter provides the background information and the thinking process towards the aims and objectives of the work presented in this thesis. It starts with an introduction to why total disc arthroplasty (TDA) is required (§ 2.2), followed by an introduction to the anatomy of the spine (§ 2.3). An insight on neck and back pain is provided in § 2.4, followed by a brief description of aging and disc degeneration as potential reasons for pain in § 2.5, as well as possible methods of treatment in § 2.6. Commercially available TDAs and the possible reasons for their failure are reviewed in § 2.7 and § 2.8. In § 2.9, possible approaches towards improving the design and minimising the failure of ball-and-socket TDAs are described. Section 2.10 includes some of the *in vitro* testing conditions. The chapter closes with a summary of the background information in § 2.11.

2.2. Introduction

TDA is an artificial implant which is used to replace a natural intervertebral disc. One of the main reasons for implantation of TDAs is to overcome problems associated with disc degeneration. Most people experience some degree of disc degeneration in their lives. The onset and progression of degeneration may be associated with aging, genetics, life style or environment (Bogduk, 2005; Guerin and Elliott, 2006; Modic and Ross, 2007; White et al., 2010). The degenerated disc undergoes dramatic change in structure, composition and mechanical properties. With degeneration, not only the nature and functionality of the disc is affected, but it may also lead to further problems. For example, studies show that it may be associated with pain and discomfort in the neck and back (Evans, et al., 2005; Hughes et al., 2012; Modic and Ross, 2007; Orozco et al., 2011). Neck and back pain, in particular low back pain (LBP), are major concerns as one third of the population suffers from some degree of neck and back pain during their lifetime. LBP itself is among the top ten reasons for patients visiting doctors and despite this fact, its causes and consequently methods of management are poorly understood (Guerin and Elliott, 2006; McGregor and Hukins, 2009; National Institute for Health and Clinical Excellence, 2009). TDAs are designed as a means of eliminating the pain associated with aging and degeneration of the intervertebral disc. As they replace the natural disc, their function and performance is expected to be as close to that of natural disc as possible. However, studies show that to date, this has not been the case. Clinical studies report various types of failure and malfunction of the implants. This highlights the vital importance and desperate need for improving the design of TDAs.

To understand how TDAs can be improved, it is first important to understand the anatomy of the spine and how and under what conditions TDAs are expected to perform (§ 2.3). Then possible reasons for TDA malfunction and failure need to be studied, to develop a better understanding of the functionality of the current TDAs and to avoid repeating similar mistakes for future designs (more details in §2.8). Finally, based on the knowledge towards the expected performance and reasons for failure, alternative changes in TDA design can be proposed. The following section is an introduction to the anatomy of the spine and understanding the natural intervertebral disc.

2.3. The Anatomy of the Spine

2.3.1 Regions of the spine

The spine is divided into five regions and each includes a specific number of vertebrae, some of which are fused whilst others are separated by intervertebral discs. The regions are called *cervical*, *thoracic*, *lumbar*, *sacral* and the *coccyx* (Figure 2.1). The *cervical* region comprise seven vertebrae, namely C1 through C7, with C1 being the first from the skull. The cervical vertebrae provide flexibility and range of motion for support of the head. The intervertebral discs are named based on their adjacent vertebrae. For example, the disc between C2 and C3 is identified by C2-C3. Following the cervical vertebrae, the next region is *thoracic* which consists of twelve vertebrae (T1 through T12). The thoracic vertebrae support ribs and organs within the rib area (Bogduk, 2005; Joseph, 1986; Kurtz and Edidin, 2006; Middleditch and Oliver, 2005). After the thoracic region, there are five *lumbar* vertebrae (L1 through L5) that

are subjected to the highest forces and moments of the spine (Kurtz and Edidin, 2006). The next region, the *sacrum*, consists of five vertebrae (S1 through S5) and attaches the spine to the iliac bones of the pelvis at L5-S1. The sacrum is said to be fused (Bogduk, 2005; Joseph, 1986; Middleditch and Oliver, 2005). However, Wicke (1998) reported some form of cartilage between S1 and S2. The final region, the *coccyx*, is connected to the S5 and is also referred to as the tail bone. It has four fused vertebrae (Bogduk, 2005; Joseph, 1986; Kurtz and Edidin, 2006; Middleditch and Oliver, 2005).

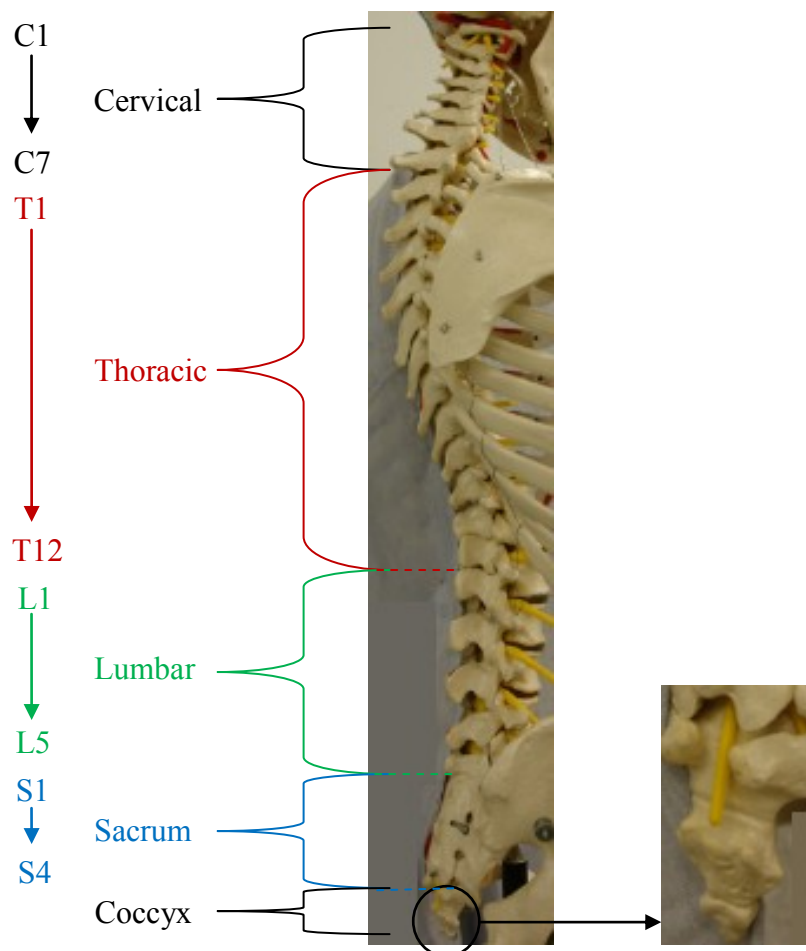


Figure 2.1. Regions of the spine (author's own photographs, adapted from Kurtz and Edidin, 2006)

2.3.2. Motions of the spine

When communicating with surgeons, designing implants and performing experiments, it is important to use an identical vocabulary for anatomic directions and motions. The upward and downward vertical directions are known as *superior* and *inferior*, respectively. The front position of the human body is called *anterior*, whilst the back is referred to as *posterior*. The *lateral* direction is the left and right side of the body and the *medial* is towards the middle of the body. Figure 2.2 shows the anatomic directions graphically.

There are four kinematic motions in the spine. *Flexion* and *extension* are when the body is bending anteriorly and posteriorly, respectively. Bending sideways is known as *lateral bending* and rotating is *axial torsion* or *axial rotation*. The kinematic motions are shown in Figure 2.3.

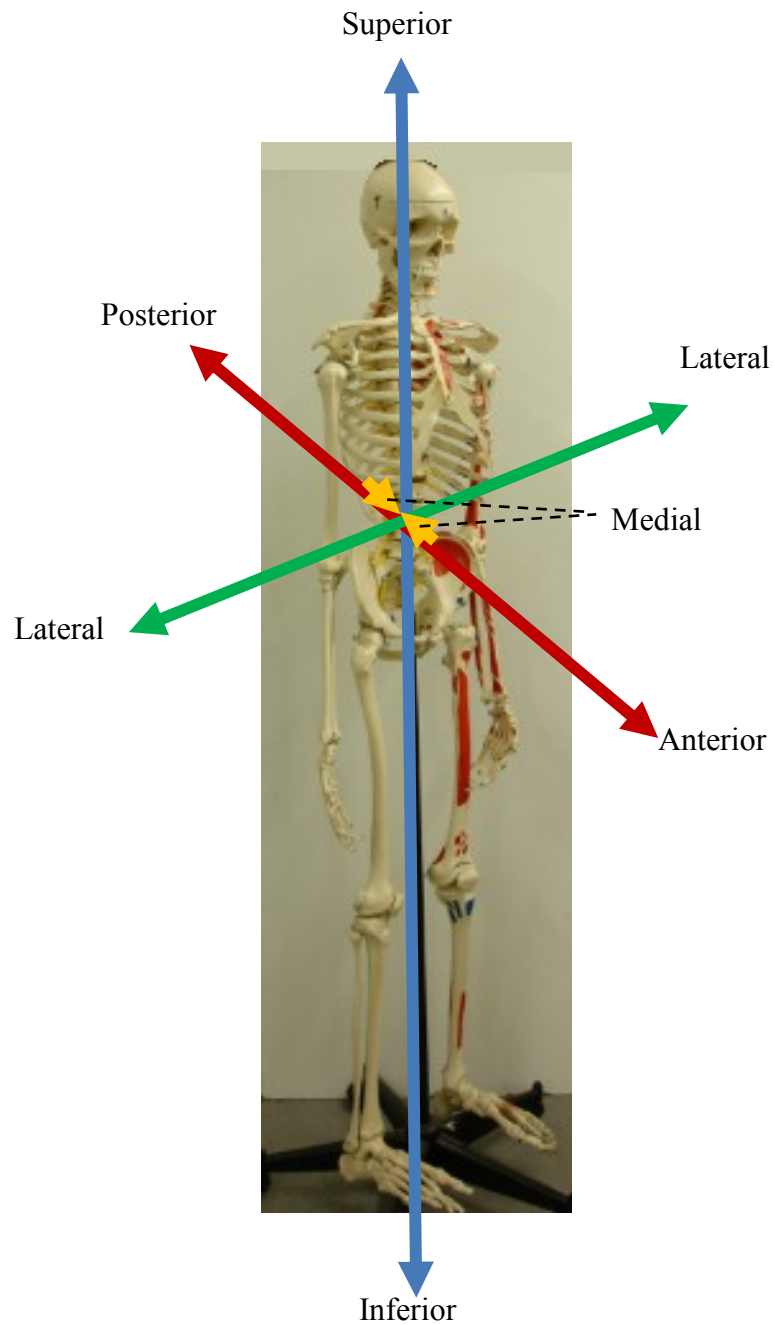


Figure 2.2. *The anatomic reference directions (author's own photographs, adapted from Kurtz and Edidin, 2006)*

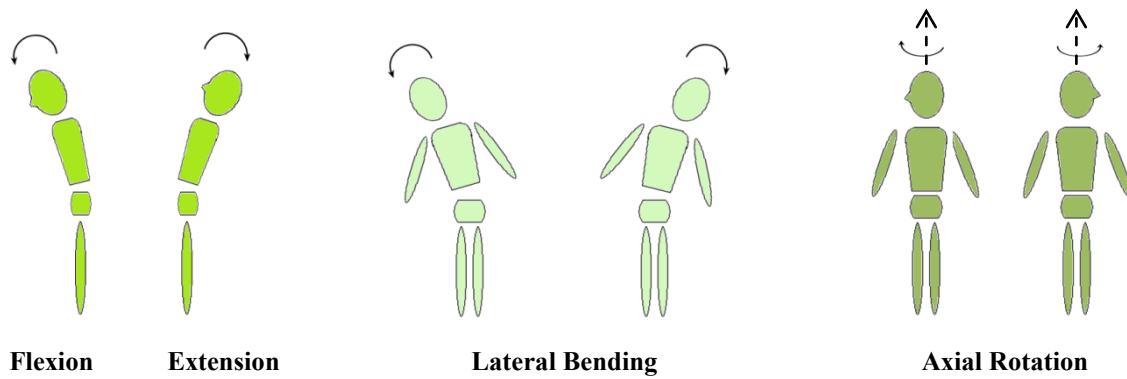


Figure 2.3. *The kinematic motions of the spine (author's own diagrams, adapted from Kurtz and Edidin, 2006)*

2.3.3. The vertebra

The vertebrae protect the spinal cord and the cauda equina, and transfer load to one another, intervertebral discs and other parts such as the pelvis. The vertebrae in each region have different shapes, but they all consist of three main components: the *vertebral body*, *pedicles* and *posterior elements* (Bogduk, 2005; Joseph, 1986).

The *vertebral body* (Figure 2.4) has roughly flat inferior and superior surfaces that are dedicated to sustain compressive loads applied to the spine and transmit it to the adjacent vertebra below. It is considered to be the main load-bearing component of a vertebra (Bogduk, 2005; Kurtz and Edidin, 2006). It has a rough anterior surface that is slightly concave and a slightly flat posterior surface (Joseph, 1986). The *pedicles* (Figure 2.4) are the stout pillars of bone, projecting from the back of the vertebral body. The projected bones form a shallow superior vertebral notch and a much deeper inferior vertebral notch (Bogduk,

2005; Joseph, 1986). The pedicles are the only connections between the vertebral body and the posterior elements. The loads sustained by any of the posterior elements are channelled towards the pedicles and from there transmitted to vertebral bodies (Bogduk, 2005). The *posterior elements* of a vertebra are the *laminae*, the *articular processes*, the *spinous processes* and the *transverse processes* (Figure 2.4). A lamina projects from each pedicle. The two laminae meet posteriorly and fuse together in the midline. Each lamina is extended and enlarged inferiorly and superiorly into a mass of bone to form the *inferior articular process* and *superior articular process*. The inferior articular processes of the superior vertebra forms two *facet joints*, one on each side, with the superior articular process of the inferior vertebra. The spinous processes project posteriorly from the junction of laminae. The transverse processes anteriorly arise from the vertebral body, inferiorly from the junction of the pedicle and the laminae, and posteriorly from the articular processes. It can be observed in Figure 2.4 that the posterior elements have irregular shapes and various bars of bone are projected in all direction. This enables muscles that act in different directions to move the vertebrae in different directions through the tendons which attach muscle to bone (Bogduk, 2005; Joseph, 1986; Middleditch and Oliver, 2005).

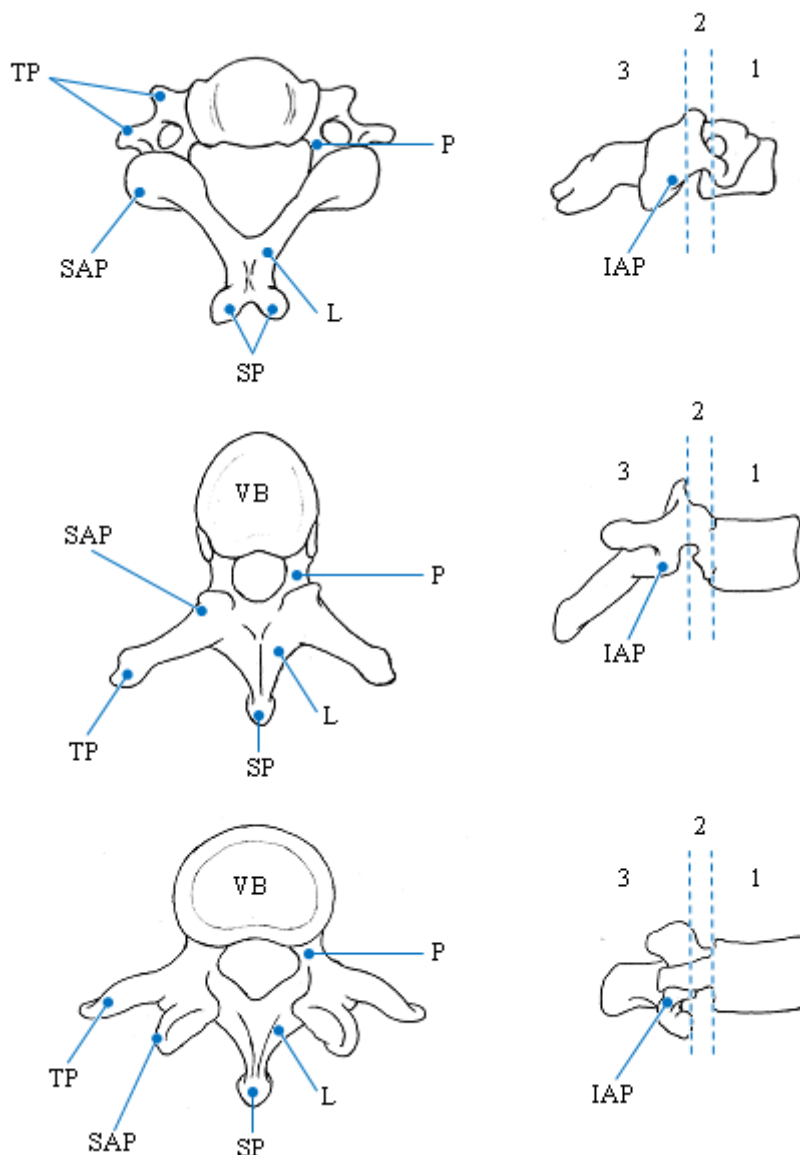


Figure 2.4. Examples of a) cervical, b) thoracic and c) lumbar vertebrae: IAP- inferior articular process, L- lamina, P- pedicle, SAP- superior articular process, SP- spinous process, TP- traverse process, VB- vertebral body. The numbers 1, 2 and 3 indicate the vertebral body, pedicle and posterior process sections of the vertebra, respectively (author's own drawings of typical vertebrae, adapted from Bogduck, (2005), Joseph (1986) and Middleditch and Oliver (2005)).

2.3.4. The intervertebral disc

The intervertebral discs impart flexibility and mobility to the spine and allow motions of the body (Hardy, 1982; White and Panjabi, 1990). One of the major functions of the intervertebral discs is providing support against spinal loads; they act as the prime components to transmit load from one vertebral body to the next (Hukins, 1987; Middleditch and Oliver, 2005). Therefore, the discs need to be stiff enough to maintain such stability. On the other hand, they need to be soft enough to allow flexibility and motion in different directions (Guerin and Elliott, 2006). The structure of the intervertebral disc has three main components that provide a load bearing mechanism as well as flexibility; these components are the *nucleus pulposus*, the *annulus fibrosus* and the *endplates* (Figure 2.5) (Guerin and Elliott, 2006; Marcolongo et al., 2006). The matrix of the disc consists of *proteoglycans*, *collagen fibres*, *elastic fibres* and *water*. The water content varies with age and degeneration. It also changes with the amount of load on the disc. In total, about 85% of the disc consists of water, which falls to about 70-75% in a mature disc (Bogduck, 2005; Guerin and Elliott, 2006; Middleditch and Oliver, 2005). Collagen fibres provide tensile reinforcement in tissues (Hukins and Aspden, 1985). The intervertebral disc is stiff in compression because the nucleus acts like the fluid in a pressure vessel, the collagen fibres are angled so that they are placed in tension by this internal pressure and so provide reinforcement (Broberg and von Essen, 1980; Hickey and Hukins, 1980; Klein et al., 1983; McNally and Arridge, 1995). This structure is flexible in bending and torsion but the collagen fibres provide reinforcement because some of them are strained by these movements (Hickey and Hukins, 1980; Klein and Hukins, 1982). Bending of the intervertebral joint is also restricted by the spinal ligaments whose collagen fibres reorient when they are strained so stiffening them and, consequently, the intervertebral joint (Hukins et al., 1990).

The *nucleus pulposus* (Figure 2.5) is a semi-solid gel comprising 40-60% of the disc. The position of the nucleus varies in different regions of the spine; for example, it is positioned posteriorly in the cervical and lumbar regions, whilst it is more central in thoracic region (Bogduk, 2005; Middleditch and Oliver, 2005). The *annulus fibrosus* (Figure 2.5) is a ring of coaxial layers, also known as lamellae, of collagen fibres that surround the nucleus pulposus. The collagen fibre layers are oriented in alternating angles and embedded in a proteoglycan matrix. Such properties assist in withstanding loads in multiple directions (Guerin and Elliott, 2006; Hickey and Hukins, 1980; Middleditch and Oliver, 2005). The cartilaginous *endplates* (Figure 2.5) form a border and separate the disc from an adjacent vertebral body; therefore, every disc consists of two endplates. One of the functions of the endplate is forming a barrier through which water and nutrients can pass between the nucleus pulposus and vertebra (Guerin and Elliott, 2006; Middleditch and Oliver, 2005).

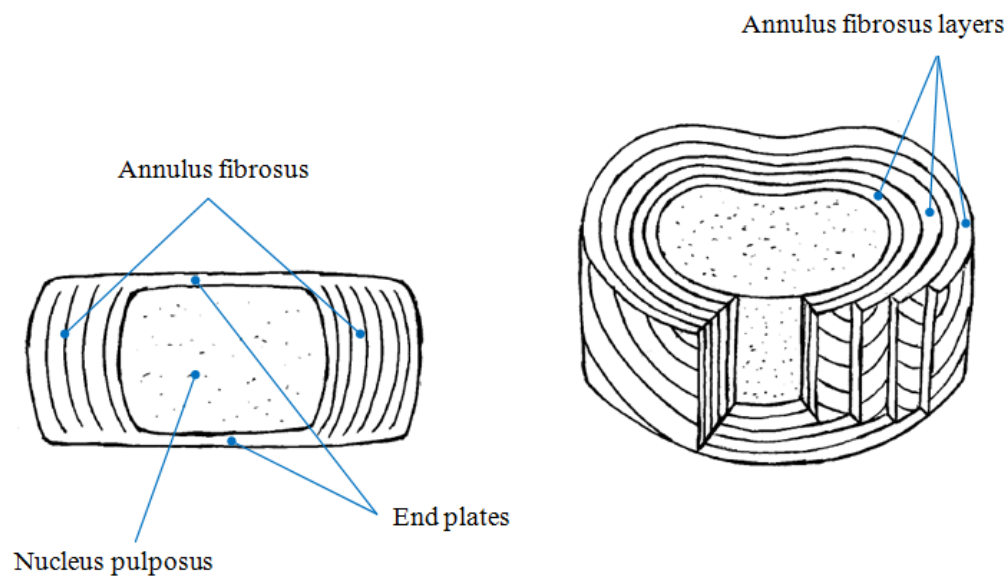


Figure 2.5. Typical structure of an intervertebral disc (author's own drawing, adapted from Bogduk (2005), Guerin and Elliott (2006) and Hukins (1988))

The shape of each disc corresponds to the adjacent vertebral body and hence varies in different spinal regions. The intervertebral discs have an elliptical shape in the cervical region, a rounded triangle (or heart) shape in the thoracic region and a kidney shape in the lumbar region (Hukins, 1988). The difference in shapes can be observed in Figure 2.6.



Figure 2.6. Typical shape for a) cervical, b) thoracic and c) lumbar intervertebral discs

(author's own drawing, adapted from Hukins (1988))

Depending on the spinal region, the intervertebral disc experiences different ranges of motion. Table 2.1 presents the average range of motions for each disc segment and all three angular motions.

Table 2.1. The average range of motion for human intervertebral disc (Adams and Hutton, 1988; Bogduk, 2005; White and Panjabi, 1990)

Disc Segment	Average range of motion (°)		
	Flexion/Extension	Lateral bend	Axial rotation
C2-C3	9	10	9
C3-C4	14	11	12
C4-C5	13	11	13
C5-C6	18	8	10
C6-C7	16	7	9
C7-T1	10	4	8
T1-T2	4	5	14
T2-T3	4	6	8
T3-T4	4	6	8
T4-T5	4	6	8
T5-T6	4	6	8
T6-T7	5	6	8
T7-T8	6	6	8
T8-T9	6	6	7
T9-T10	6	6	4
T10-T11	9	7	2
T11-T12	12	9	2
T12-L1	12	8	2
L1-L2	12	6	2
L2-L3	14	6	2
L3-L4	15	8	2
L4-L5	17	6	2
L5-S1	25	3	5

2.3.5. The ligaments

The ligaments hold vertebrae and discs together and extend along the spinal column. Together with discs, they provide a mechanically stable joint (Hukins, 1987). There are different types of ligaments. The anterior longitudinal ligament (ALL) is firmly attached to the edge of the vertebral body and the disc. It runs over the entire anterior surface of the spinal column. From the posterior aspect, the vertebral body and disc are attached by the posterior longitudinal ligament (PLL). The PLL posteriorly covers the vertebral bodies down to the coccyx. The supraspinous ligament (SSL) originates in the ligamentum nuchae (LN) and connects the tips of the spinous processes from C7 to sacrum. The interspinous ligament (ISL) connects adjacent spinous processes. It runs from the anterior inferior aspect of the spinous process above to the posterior superior aspect of the spinous process below. The capsular ligament (CL) is attached beyond the margins of the adjacent articular process. The ligament flavum (LF) connects the anterior inferior edge of the lamina above to the posterior superior border of the lamina below (Panjabi et al., 1978). Some of the ligaments limit the mobility of the joint, but all act to protect against separation of vertebral bodies during bending movements (Adams et al., 1980).

2.3.6. Load and load bearing properties of the intervertebral disc

The main constituent of the disc is water. The nucleus is the mostly hydrated part of the disc and therefore is isotropic and not very compressible. This helps to transfer load equally to any direction (Hukins, 1992). Since the nucleus is surrounded by the annulus, it cannot swell freely, meaning that the nucleus experiences a high internal pressure, known as the swelling pressure (Urban and Maroudas, 1981). This allows the disc to act like an inflated tyre. The

swelling pressure has a radial component, which is balanced by tangential tensile stress in the annulus, and an axial component which is balanced by compression (Hukins, 1987). The discs are subjected to compressive loads which arise from tension in the ligaments and muscles (Maroudas and Urban, 1980). Under axial compression, the height of the nucleus decreases and radial and even pressure is exerted onto the surrounding annulus. This pressure is balanced by tension in the collagen fibres. The axial pressure is exerted towards the endplates, which is then transmitted to the adjacent vertebrae.

The pressure on the disc increases when it is subjected to external load. It varies with the position of the body and the method by which the external load is exerted, for example by exercise or lifting. It is not exactly clear at which position the spine experiences the maximum load. In a study by Nachemson (1976), it has been stated that the spine experiences maximum loading in the upright unsupported sitting position, whilst holding an external weight. In another study the worst-case activity has been described as when a 200 N weight is lifted with back bent and knees straight (Kurtz, 2006). The load bearing of the discs varies in different levels. Moving towards the sacral region, the load becomes greater. As an example, nearly 60% of external loads are applied on L5-S1 intervertebral disc (Middleditch and Oliver, 2005; Nachemson, 1976). The lumbar region experiences an average of 1000 to 5300 N load in compression and 1800 N in tension (Panjabi et al., 1978).

2.4. Neck and back pain

Neck and back pain are considered as leading causes of long term pain, disability and morbidity (Basho et al., 2011; McGregor and Hukins, 2009). The treatment for neck and back pain costs the National Health Service (NHS) more than £1000 million per year (National Institute for Health and Clinical Excellence, 2009). In the USA, the cost of treatment is estimated as \$25 billion per year (Frymoyer and Cats-Baril, 1991). Over 70% of the population suffer from some degree of neck and back pain, but in most cases the patients tend to recover from the pain after two weeks of non-surgical treatment; for example, after conservative care, activity modification and physiotherapy (Cairns et al., 1984; Marcolongo et al., 2006; Punt et al., 2009). However, some patients experience pain which lasts longer than 3 months and is unlikely to recover spontaneously. Such sufferers rarely return to work after two years of absence (Hammonds et al., 1978; Deyo et al., 2006). This has an impact on the treatment cost and industry cost. Therefore, understanding the causes is crucial. Disc degeneration is a common cause of back and neck pain (Dang, 2007; Wang et al., 2011; Williams and Sambrook, 2011).

2.5. Aging and degeneration

Like other organs, the structure, composition and mechanical properties of discs change throughout life (Kurtz, 2006; Lyons et al., 1981; Virgin, 1951). With aging, total content of proteoglycans within the nucleus pulposus decreases and the ratio of collagen-proteoglycan

binding increases, which may affect the ability to attract and retain water. This may lead the nucleus pulposus to lose water (Gower and Pedrini, 1969; Lyons et al., 1981). As a result, it becomes less like a liquid and more like a solid (Iatridis et al., 1996) and the mechanical and biochemical properties are affected (Guerin and Elliott, 2006). The dehydrated disc becomes stiffer, which leads to the transfer of the compressive load directly to the annulus fibrosus, leaving the disc vulnerable to mechanical injury and degeneration. It also results in annular bulging and loss of disc height (Dang, 2007; Harris and MacNab, 1954; Vernon-Roberts and Pirie, 1977). The degeneration affects the organisation of the annulus fibrosus layers and makes some of them thicker (Farfan et al., 1972; Marchand and Ahmed, 1990). The degenerated annulus may experience radial tears, cracks and fissures under increased and unevenly transmitted pressure (Adams et al., 2000). When the pressure in the nucleus decreases, the annulus no longer bulges uniformly outwards and does not act like an inflated tyre; instead, it bulges inwards and outwards, which results in more damage to the annulus and loss of disc height (Meakin and Hukins, 2000). This results in an abnormal response to the loading of the spinal segments, which in time may result in loss of ability to move beyond normal limits (Dang, 2007).

The degeneration of the disc may result in pain. For example, the nucleus may migrate within the annulus fibres and irritate the nerves, which then results in pain. Nucleus herniation may also lead to inflammation or nerve compression. The loss of disc height may partially dislocate the facet joints, which can lead to osteoarthritis and pain (Fujiwara et al., 1999; Koes et al., 2001). Depending on the severity of degeneration, type of pain and condition of the patient, surgical (such as artificial disc replacement) or non-surgical (such as medication)

methods are implemented to treat the pain. The methods of treatment of neck and back pain are described in the following section.

2.6. Treatment of neck and back pain

There are two categories of treatment for neck and back pain: conservative and surgical. In the conservative method, the patient is treated by rest, medication, activity modification and exercise, physiotherapy and rehabilitation. Most patients are expected to recover from the pain, following the conservative treatment. However, some sufferers do not fully recover and require surgical treatment (Ahn 2002; Bush et al., 1992).

There are different surgical treatments. Surgical decompression and/or fusion are considered as conventional options for surgical treatment of the discs (Dang, 2007; Porchet and Metcalf, 2004). In *surgical decompression*, the herniated nucleus or any anatomical structure, such as bones or ligaments, which compresses the spinal nerve is excised. It may have a short-term satisfactory effect in relieving pain, but in the long term (5 years post-operation) it may lead to further degeneration and pain (Abramovitz and Neff, 1991).

In *Spinal fusion*, the degenerated disc is removed and the spinal segment is held in place by bone graft and sometimes internal fixation, such as metal rods, screws, plates and fusion cages. In spinal fusion, the motion at the damaged spinal segment is eliminated. The main advantage of this treatment is that the disc height is preserved. One of the main disadvantages is that fusion can lead to accelerated adjacent-level disc degeneration, which may be a result

of immobilisation of the functional spinal unit by fusion (Kurtz, 2006; Erkan et al., 2009; Grupp et al., 2010). In a study by Gillet (2003) a 20% rate of lumbar adjacent-level disc disease was reported in a series of 106 lumbar fusion patients with 2 to 15 years of follow-up.

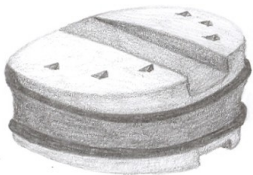

Nucleus replacement is implemented when only the nucleus is causing the disc to bulge outwards and impinge on nerve roots. In this method of treatment, the degenerated nucleus is removed and replaced by a prosthetic device. It is possible that degeneration is interrupted if the nucleus is excised before the annulus and the endplates are severely damaged (Dang, 2007). However, in nucleus replacement, there is always the risk that the nucleus is treated after the remaining disc segments have been affected. This may result in further treatment, including complete removal of the synthetic nucleus and degenerated annulus.

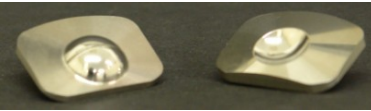
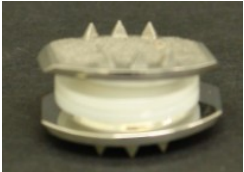
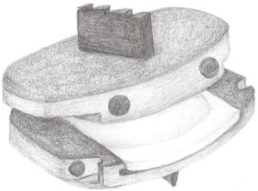
Artificial disc replacement is another method of treatment which includes complete removal of the degenerated disc which is then replaced by a TDA. Unlike fusion, the discs undergoing artificial disc replacement treatment are able to preserve motion (Bertagnoli et al., 2005; Cunningham et al., 2009; Hallab et al., 2003; McAfee et al. 2005; Kurtz, 2006). The following section presents a background study on TDAs to familiarise the reader with the design and function of the implants.

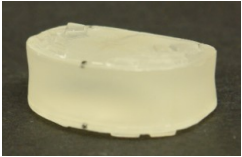
2.7. Total disc arthroplasty

Since 1970, TDAs underwent various modifications and they only became commercially available since 1987 (Kurtz, 2006). The main feature of TDAs is their ability to preserve motion, which is achieved by having either a ball-and-socket structure or a flexible elastomer as their main body. The idea of a ball-and-socket design for TDA is analogous to the bearing concept of total hip arthroplasty (THA). However, the natural disc does not have a ball-and-socket configuration and therefore implementing the concept for TDA may not seem very sensible. Despite this, ball-and-socket TDAs are still more common than TDAs with a flexible elastomer body. Table 2.2 presents examples of TDAs that have been commercially available.

Table 2.2. Examples of TDAs, based on information in Anderson et al. (2006), Gwynne (2010), Kurtz (2006) and Wang et al. (2011) (author's own drawings and photographs)

	Commercial name (availability)	Main feature	Material combination	Reasons for failure
	Acroflex (available in 1988- discontinued)	- one component - non articulating surfaces - ability to perform flexion/extension, lateral bend, axial rotation and compression	Hexsyn -based polyolefin rubber core fused to two porous coated titanium endplates	- fracture of the polymer core - creation of wear debris -bone loss -implant loosening
	Bryan® (available since 2000)	- one component - non articulating surfaces - ability to perform flexion/extension, lateral bend, axial rotation and compression	polyurethane (PU) nucleus (core), surrounded by a PU sheath, with two titanium endplates covered by titanium porous coating	-no reports on failure

	<p>Maverick™ (available since 2002)</p>	<ul style="list-style-type: none"> - two components - ball and socket articulation - ability to perform flexion/extension, lateral bend and axial rotation 	<p>cobalt-chrome-molybdenum alloy, hydroxyapatite-coated at the bone-contacting side</p>	<ul style="list-style-type: none"> -metal wear debris result in toxicity, inflammatory response, bone loss and implant loosening
	<p>Charité® (available since 1987)</p>	<ul style="list-style-type: none"> - three components; two endplates and a core with two convex surfaces - ball and socket articulation - ability to perform flexion/extension, lateral bend and axial rotation 	<p>cobalt chromium endplates coated with titanium calcium phosphate, and an ultra-high molecular weight polyethylene (UHMWPE) sliding core</p>	<ul style="list-style-type: none"> - wear of the polymer core - fracture of the core edge - anterior migration - bone loss - implant loosening
	<p>ProDisc® II (available since 1999)</p>	<ul style="list-style-type: none"> - three components; two endplates and a core with a convex surface that slides and locks into the bottom endplate - ball and socket articulation - ability to perform flexion/extension, lateral bend and axial rotation 	<p>cobalt chromium endplates coated with titanium spray on bone-contacting side and an UHMWPE core</p>	<ul style="list-style-type: none"> - wear of the polymer core - polymer core migration - bone loss - implant loosening

	Cadisc™-L (available since 2009)	-one component -non articulating surfaces -ability to perform flexion/extension, lateral bend, axial rotation and compression	polycarbonate polyurethane with hard endplate regions, a lower modulus for nucleus region and a higher modulus for annulus region	-no reports on failure
---	-------------------------------------	---	---	------------------------

Typical examples of a ball-and-socket TDA are the Maverick™ (Medtronic, Minneapolis, USA), Charité®, and ProDisc® (Synthes, West Chester, PA, USA). The ball-and-socket TDAs consist of at least one convex surface (ball), articulating against a concave surface (socket). The dimensions of the ball and socket components are design-dependent, but are within the range of a natural disc (more details on dimensions of natural disc in § 2.9.2). Different material combinations have been reported for ball-and-socket TDAs. Typical examples are: metal-on-metal, metal-on-polymer and polymer-on-polymer. For the first two combinations, the metal is medical grade titanium alloy, medical grade cobalt chrome alloy or medical grade stainless steel. The polymer in metal-on-polymer combination is mostly ultra high molecular weight polyethylene (UHMWPE) (Kurtz, 2006). For polymer-on-polymer combination, different medical grades of polyether ether ketone (PEEK) are used (Grupp et al., 2010; Scholes and Unsworth, 2010). Among all types of TDAs, metal-on-metal and metal-on-polymer are the most popular material combinations. Depending on the design of the ball-and-socket TDA, the number of components may vary, but they consist of at least two components.

Bryan® (Medtronic Sofamor Danek, Memphis, TN, USA) and Cadisc™-L (Ranier Technology Ltd., Cambridge, UK) are examples of TDAs that do not include an articulation of a convex on concave surface; instead, they comprise an elastomeric polymer body, which in some cases (for example in Bryan®) is held in place by two metal endplates. Similar to ball-and-socket TDAs, the overall dimensions are design-dependent, but lie within the range of the natural disc.

2.8 Failure of TDA

Looking at Table 2.2 and other studies on TDA, the major reasons for the implant failure are design-related. Design-related factors include geometry and shape, dimensions and material combination. Some of the design-related problems are detected after *in vitro* experiments, whilst in some cases they only appear after implantation. As an example, the AcroFlex went through three phases of design development since its first implantation in 1988. When the implant was first tested *in vitro* for strength in axial compression and fatigue over 10 million cycles under 448 N axial load, evidence of local material failure was observed; yet tests were judged to be successful at the time (Steffee, 1992). After implantation, some of them failed due to fracture of the polymer core and creation of wear debris (Kurtz, 2006). The third generation of the same implant used similar material combination as the first generation, but the geometry of the endplates was changed. It was tested for strength in compression and compressive shear. However, as it did not have articulating surfaces, no wear tests were performed. Then in the animal testing of the same implant, evidence of wear debris and localised foreign body reaction was observed (Kurtz, 2006). After implanted into the human, further problems such as tears of the polymer core, bone loss (osteolysis) and consequently implant loosening was observed; the AcroFlex is no longer available.

Charité® is a ball-and-socket implant with combination of a metal and polymer. It is expected that when two solid surfaces articulate at all times, they create friction. Also, as a result of this articulation, wear of the material, in particular the softer material occurs (Hutchings, 1992); this results in creation of wear particles. Studies on Charité® and similar implants, such as ProDisc® and Maverick™, show evidence of wear debris both *in vitro* and

in vivo. Studies on THA report complications and problems associated with wear particles. Hip joints are synovial joints and are lubricated by synovial fluid, which is secreted from synovial capsules. When THA is implanted, the wear particles may accumulate in the synovial capsules and in long term result in inflammatory response of the adjacent tissues, bone loss and implant loosening (Affatato et al., 2008; Anderson et al., 2006; Jin et al., 1997). TDAs are not enclosed by synovial capsules. However, wear debris is still a major concern, as it may still affect the adjacent tissues, result in inflammatory response and could lead to bone loss and implant loosening. In a study on metal-on-metal Prestige Cervical Disc by Anderson et al. (2006), chronic inflammatory response was observed as a result of metallic wear debris. Therefore, wear particles are considered as a major problem, in particular for ball-and-socket TDAs (David, 2005; Kurtz et al., 2007).

In the Maverick™, the identical material for ball and socket was selected because of the low wear rate of the similar material combination observed in THAs (Clarke et al., 2000). However, *in vitro* wear studies show that the metal-on-metal TDAs can create 0.43 ± 0.05 mm³ of wear particles per million testing cycles (Paré et al., 2007). This may be enough to cause toxicity, infection of adjacent tissues, bone loss and implant loosening, as has been seen in metal-on-metal THAs (Affatato et al., 2008; Jin et al., 1997).

Studies on the Charité® show that the polymer core, in particular the rim, may experience fracture, radial cracking and plastic deformation under axial load. The rim is thin (about 1 mm), which makes it vulnerable to load. The core has a 2-sided convex feature. Therefore, when implanted, it is important that the centre of rotation (COR) of the ball is aligned as closely as possible with that of the spine in the region of interest. Failure to do so may result

in fracture of the rim, ejection of the polymer core or partial dislocation. Such problems occur as a result of poor design (David, 2005; Kurtz et al., 2007). Subsidence of the implant is another design-related issue which was particularly observed in the first generation of Charité® (Charité SB I) as a result of small endplates, and hence small contact area between the endplate surface and the adjacent vertebrae (Kurtz, 2006). The ProDisc® also involves design-related complications. For example, the endplates are designed in such way that the surgeon needs to make a groove onto the adjacent vertebrae, in order to slide the TDA in the disc space for implantation. This may result in vertebral split fracture as has been reported in the literature (Shim et al., 2005). Also, similar to the Charité®, if the COR of the ball is not aligned with that of the spine in the region of interest, partial subsidence of the endplates, anterior migration or partial ejection of the UHMWPE core may occur.

Despite the catastrophic failure of the Acroflex design, no other major reports are available on the failure of TDAs with flexible elastomeric body. This is either because they have shown a good performance so far, such as Bryan®, or they are newly introduced to the market and no long history of clinical performance is available, such as Cadisc™-L. The ball-and-socket TDAs have been implanted since 1987 and more studies on their performance and failure are available. Despite knowing that they fail, not many studies have been performed on how failure can be minimised or how performance can be improved. Therefore, the objectives of this work were set for a small contribution towards improving the ball-and-socket TDAs.

2.9. Possible steps towards improving TDAs

2.9.1. Introduction

It was mentioned in the previous section that the design-related problems in ball-and-socket TDAs often lead to creation of wear debris, and consequently toxicity, bone loss and implant loosening. This, in addition to studies on THAs, could mean that by improving the design factors such as geometry, dimension and material combination, creation of wear debris can be reduced and hence, implant malfunction, bone loss and implant loosening may be controlled. In this work, effect of change of dimension and material combination are studied.

2.9.2. How dimension-related problems can be improved

In ball-and-socket TDAs, the main dimensions are a) overall dimensions for height, depth and width, b) radii of ball and socket and c) radial clearance between the ball and socket. Depending on the individual, the height (Figure 2.7) of the natural intervertebral discs may range between 4.2 to 7.5 mm for the cervical region and 6.2 to 15 mm for the lumbar region (Berry et al., 1987; Bogduk, 2005; Gilad and Nissan, 1986; Yoganandan et al., 2001). The average depth and width (Figure 2.7) of a cervical vertebral body is 14.5-19.2 mm \times 16.5-22.5 mm (depth \times width), and for lumbar it is 31-37 mm \times 48-56 mm (Berry et al., 1987; Gilad and Nissan, 1986; Panjabi et al., 1991). Therefore, the overall dimensions of the TDAs need to be within these ranges. From the experience of the first generation of Charité® TDA (Charité SB I), it was learned that the overall dimensions need to be as close to that of natural disc as possible (Kurtz, 2006). Since the ability to alter the overall dimensions is limited, it was not considered as the main focus for this study; instead, the primary focus was set on the radii of the ball and socket.

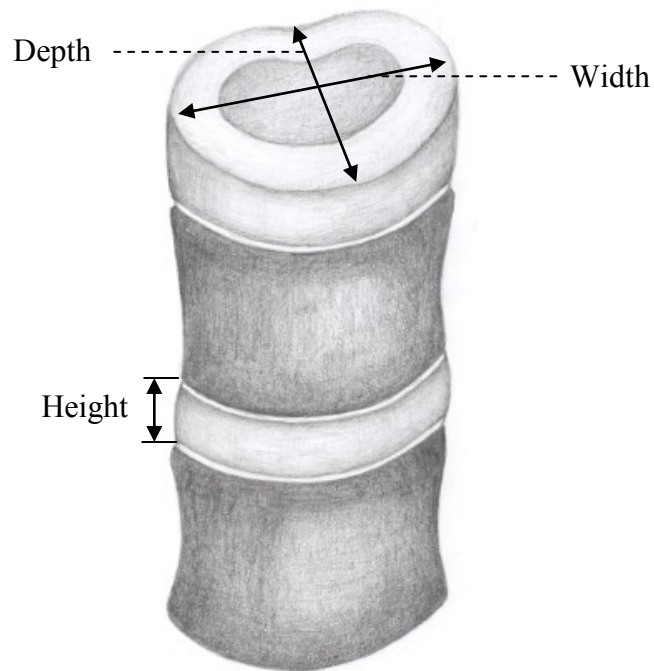


Figure 2.7. Indication of height, depth and width of the disc

Studies on THAs show numerous variations in wear rate as ball radius changes (Bishop et al., 2008; Streicher et al., 1996). Therefore, it was thought to be worth investigating for TDAs; however, no studies under identical conditions have been performed to understand the effect of change in ball radius on performance of such implants. Therefore, part of the current work was focused on investigating the effect of ball radius on performance of TDA, which is presented in Chapter 5.

It should be noted that the size of radial clearance will also affect the tribological performance of TDAs, as seen in THAs (Jacobs et al., 1998; Scholes et al., 2000a; Scott and Schroeder, 1997). However, this was not the primary subject of this study.

2.9.3. How material-related problems can be improved

It was mentioned in § 2.7 that the majority of ball-and-socket TDAs have a metal-on-metal or metal-on-polymer combination. Since the ball and socket are articulating against each other at all times, it is almost impossible to avoid wear. On the other hand, there is a limited choice of material for TDAs. Therefore, it is important to select the most appropriate material combination to reduce wear as much as possible.

The wear rate of metal-on-metal TDAs is reported to be less than that for metal-on-polymer (Paré et al., 2007; Scholes et al., 2001). Therefore, metal-on-metal TDAs might be preferred. However, the number of commercially available TDAs with metal-on-polymer combination is more than metal-on-metal. Hence, the question is how such a material combination can be improved. In THAs, the articulation of a metal femoral head (ball) against polymer acetabular cup (socket) was initiated by Charnley (his THA was named after him) (Hall et al., 1994; Joyce, 2009). TDAs have been designed with the material combination the other way round, with a polymer ball articulating against a metal socket. Typical examples include the Charité® and the ProDisc-L®. The effect of reverse material combination for ball and socket has never been studied before; therefore, it is not clear whether such material combination really benefits TDAs. This question is answered in the study that is presented in Chapter 6.

With regards to effect of material combination on creation of wear debris, there is a further area of interest. As was mentioned above, studies show that the wear rate of metal-on-metal TDAs is less than that for the metal-on-polymer combination. However, unlike THAs, the wear rate of both types of TDAs has never been studied under equivalent conditions before and hence, the wear rates in the literature may not be comparable. Chapter 7 of this work

presents the study on investigation of the wear rate of metal-on-metal and metal-on-polymer TDAs under the same conditions.

2.10. General testing conditions for the experimental studies of TDAs

2.10.1. Introduction

When performing experimental studies *in vitro*, the testing condition and environment need to be close to what TDAs may experience when implanted into the spine. It is important to apply appropriate load, range of motion and frequency. Also, as the TDA is naturally lubricated, the choice of lubricant to be used in the tests and understanding of the lubrication regime between the articulating surfaces are important. The following sections describe the general testing conditions for experimental studies of TDAs.

2.10.2. Selection of load, range of motion and frequency according to the standards

It was previously mentioned (§ 2.3.2 and § 2.3.6) that the intervertebral discs undergoes different motions and loads. Therefore, to assure comparability as much as possible, the experiments need to be performed under similar loads and motions to what the intervertebral disc experiences.

The experimental tests on TDAs are guided by the International Organization for Standardization (ISO), in particular BS ISO 18192-1:2008, and the American Society for Testing and Materials (ASTM), in particular ASTM F2423-05 (new version of the standard BS ISO 18192-1 became available since 2011). Depending on the spine region, various loads

and ranges of motion are suggested for testing. It should be noted that both standards only suggest values for cervical and lumbar regions. The recommended load values are presented in Table 2.3. The recommendations by BS ISO 18192-1:2008 and ASTM F2423-05 for range of motion for cervical and lumbar TDAs are shown in Tables 2.4 and 2.5, respectively.

Table 2.3. The recommended load values for wear testing of TDAs, by ISO and ASTM standards (ASTM F2423-05; BS ISO 18192-1:2008)

	Load (N)	
	Cervical region	Lumbar region
BS ISO 18192-1:2008	Sinusoidal with 50 (Min) 150 (Max)	Sinusoidal with 600 (Min) 2000 (Max)
ASTM F2423-05	Constant 100	Constant 1200

Table 2.4. The range of motion for cervical region (ASTM F2423-05; BS ISO 18192-1:2008)

	Range of motion (°)			
	Flexion	Extension	Lateral bend	Axial rotation
BS ISO 18192-1:2008	7.5	7.5	± 6	± 4
ASTM F2423-05	7.5	7.5	± 6	± 6

Table 2.5. The range of motion for lumbar region (ASTM F2423-05; BS ISO 18192-1:2008)

	Range of motion (°)			
	Flexion	Extension	Lateral bend	Axial rotation
BS ISO 18192-1:2008	6	3	± 2	± 2
ASTM F2423-05	7.5	7.5	± 6	± 3

The frequency of the movements in the intervertebral discs depends on the type of activity. As it may be difficult to perform the experiments under many different frequencies, the BS ISO 18192-1:2008 and ASTM F2423-05 standards suggest a frequency of 1 Hz for angular motions and 2 Hz for loads. They also suggest that other frequencies for angular motions can be chosen, but must not exceed 2 Hz.

2.10.3. Lubrication

When a TDA is implanted, it is lubricated by the surrounding body fluid. Therefore, in an experiment, the TDA needs to be lubricated with fluid similar to that in the body. Natural hip and knee joints are lubricated by synovial fluid (Gale et al, 2007; Wang et al., 2008b). The intervertebral joint is not a synovial joint and is assumed to be lubricated by interstitial fluid (Shaheen and Shepherd, 2007; Yao and Gu, 2006). This means that the desired lubricant needs to have similar properties to that in interstitial fluid, and therefore, selecting a proper lubricant is important.

Various tribological tests have been performed on THA and total knee arthroplasty (TKA), in which different lubricants have been used. Harsha and Joyce (2011) divide these lubricants into two groups. The first group is non-physiological fluids, which contain no proteins, for example, de-ionised water and Ringer's solution. The second group are physiological fluids, which contain protein, such as calf serum. The composition of the fluid is important as it could have an appreciable effect on the results of any tribological tests. For example, the protein concentration may affect the friction between the articulating surfaces (Brockett et al., 2008; Harsha and Joyce, 2011; Scholes and Unsworth, 2000; Wang et al., 2004).

Calf serum is the most common lubricant used for *in vitro* experiments on artificial joints such as THA and TKA (Joyce, 2009), as it is believed to have properties that are close to those of synovial fluid. Calf serum is also the lubricant recommended by the standard BS ISO 18192-1:2008 for the wear testing of TDAs (the standard ASTM F2423-05 recommends bovine serum as the lubricant), despite intervertebral joints not being synovial and so not lubricated by synovial fluid. Diluted calf serum has been used in several studies on wear of TDAs (Paré et al., 2007; Prokopovich et al., 2011; Serhan et al., 2006). The composition of the fluid that lubricates the bearing surfaces in TDAs is not fully understood, but is likely to be somewhere between Ringer's solution and diluted calf serum (Fogh-Andersen, 1995; Sherwood, 2011; Streicher et al. 1996). Therefore, as part of the studies in this work, both lubricants were tested and the desired lubricant for TDA experiments was selected. This study is presented in Chapter 4.

2.10.4. Lubrication regime and friction

The lubrication regime will affect the wear of a ball-and-socket TDA. As was mentioned in the previous section, when a TDA is implanted, it may be lubricated by the natural interstitial fluid; however, the nature of the lubrication regime could vary for different designs of TDAs. Depending on the lubrication regime, the articulating surfaces may still be in direct contact (boundary lubrication), partly separated by the fluid (mixed lubrication) or fully separated by the fluid (fluid film lubrication) (Dowson and Jin, 2006; Hall et al., 1994). Figure 2.8 presents an exaggeration of each lubrication regime, graphically.

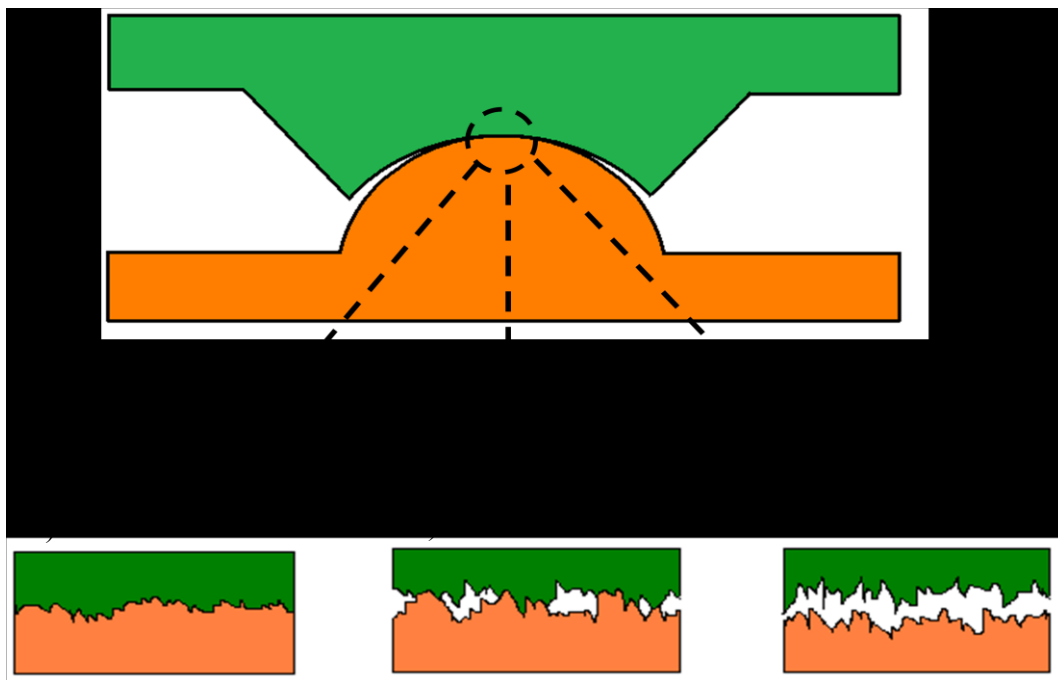


Figure 2.8. The a) boundary, b) mixed and c) fluid film lubrication between two articulating surfaces

In an experiment, it would be very difficult to see the contact between the articulating surfaces. In studies on THAs, *Stribeck analysis* is performed to indicate the lubrication regime under which the implant acts (Scholes and Unsworth, 2006b; Smith et al., 2001a). This may be also applicable to TDAs for better understanding the lubrication regime between the articulating surfaces. In Stribeck analysis, the relationship between the friction factor, f , and Sommerfeld number, Z , are determined. The friction factor is related to frictional torque, T , applied load, L , and radius, r , of the bearing surfaces by

$$f = \frac{T}{rL} \quad 1$$

(Scholes and Unsworth, 2000). The Sommerfeld number is related to the viscosity of the lubricant, η , entraining velocity of the bearing surfaces, u , r and L by

$$Z = \frac{\eta r}{L} \quad 2$$

(Scholes and Unsworth, 2000). The entraining velocity of the bearing surfaces, is conventionally defined by

$$u = \frac{v}{2} = \tau\phi \quad 3$$

where v is the angular velocity and τ is the frequency at which the test was performed (Mattei et al., 2011; Shaheen and Shepherd, 2007; Wang et al., 2008a).

Stribeck analysis is performed by plotting a *Stribeck curve*, which is a graph of f against Z . The shape of the graph enables the lubrication regime to be predicted. When f decreases, with increasing Z , a mixed lubrication regime is indicated, whereas an increasing f with increasing Z , indicates a fluid film regime. A constant f indicates a boundary lubrication regime (Jones et al., 2009; Scholes and Unsworth, 2000). An example of a Stribeck curve and each lubrication regime is presented in Figure 2.9.

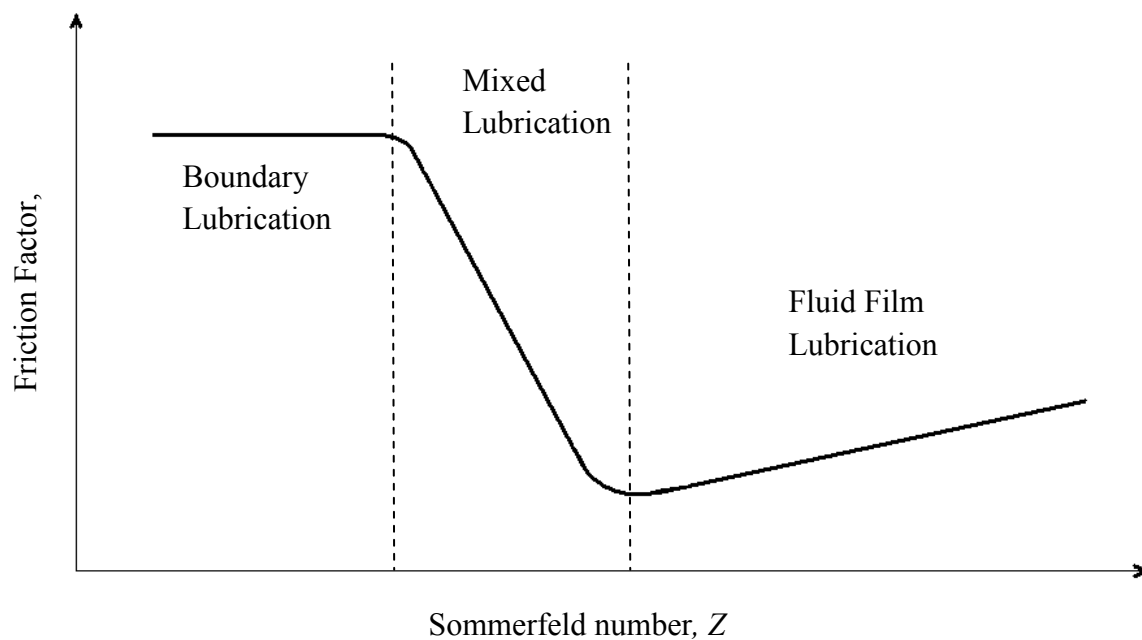


Figure 2.9. *The Stribeck curve (adapted from Scholes and Unsworth (2006b))*

Friction in the boundary lubrication regime is the highest (Hutchings, 1992); hence, it is possible that more wear debris is created. Although there is no simple relationship between wear and friction, it is expected that implants which offer less friction perform better (Crockett et al., 2009). Therefore, creation of wear particles can be minimised if the articulating surfaces are in less contact and less friction is created between the surfaces. For this reason, an understanding of the friction created by the implant will help to understand the possible lubrication regime and hence, identify the alternative ball radius and material combination. This method was implemented in Chapters 4 to 6, to find the ball radius and material combination that offers less friction and better lubrication.

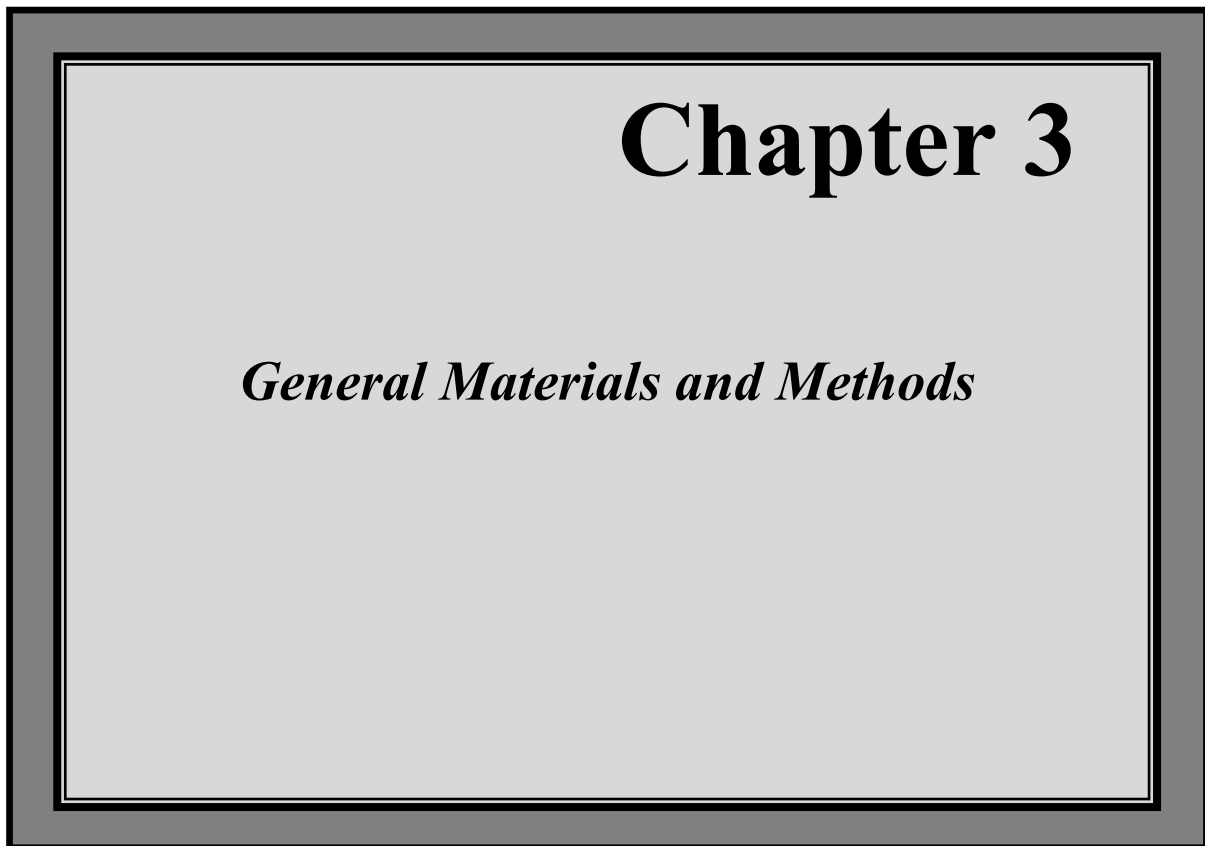
2.11. Summary

The spinal column consists of five regions and 33 vertebrae, some of which are fused. The non-fused vertebrae are usually separated by intervertebral discs. The intervertebral disc may experience functional deterioration as a result of aging and degeneration. Depending on the degree of degeneration, there are non-surgical and surgical methods of treatment. One surgical method is disc replacement, in which the degenerated disc is removed and a TDA is implanted.

TDA's consist of either ball-and-socket or flexible elastomeric body. During the life of the TDA's, they may experience design-related problems, which in the long term can result in implant malfunction and failure. Such problems include fracture of the components, migration, plastic deformation and wear debris creation. Wear debris itself can lead to further

problems such as toxicity, inflammatory response of the adjacent tissues, bone loss and implant loosening. To reduce these problems, particularly in ball-and-socket models, TDAs need to be improved. As the majority of the problems mentioned are associated with the design of the implant, the improvement can be achieved by changing one or some of the design factors, such as geometry, dimensions and material combination.

As part of the main objectives of this work, the effects of changes in ball radius and material combination on the performance of the TDAs were investigated and the results are presented in the following chapters. Also, to gain an insight on how much wear particles are created under similar *in vitro* conditions, a series of wear tests were performed on metal-on-metal and a metal-on-polymer TDAs; the results are presented in Chapter 7.



3.1. Chapter overview

In this chapter the common materials and methods used in this study are presented. In § 3.2.1 the design of the generic models for the total disc arthroplasty (TDA) is described, before the manufacturing method is explained in § 3.2.2. A review of the testing equipments is provided in § 3.2.3. The methods for preparing the samples for testing and surface roughness measurements are presented in § 3.3.1 and § 3.3.2, respectively. General testing conditions for friction and wear tests are explained in § 3.3.3. Finally, a brief summary of the whole chapter is provided in § 3.4

3.2. Materials

3.2.1. Disc design

3.2.1.1. Introduction

The majority of the experiments in this study were performed on generic ball-and-socket models of TDA, which were designed based on the dimensions and geometry of existing TDAs, such as the Maverick™, Charité®, and ProDisc-L®. The tests performed in this study were friction and wear tests. Friction tests were divided into two groups: 1) metal-on-metal, and 2) metal and polymer combinations. The wear tests were also divided into two groups: 1) metal-on-metal wear on the generic models and 2) metal-on-polymer wear of the Charité® TDA.

3.2.1.2. Metal-on-metal friction tests

In this series of tests, generic ball-and-socket models were designed based on the metal-on-metal Maverick™ device. The Maverick™ consists of bearing surfaces manufactured from cobalt chrome molybdenum alloy (Co-27Cr-5.5Mo-0.06C) (ASTM F 1537 – 08) with a ball radius of 10 mm and radial clearance of 0.015 mm between the ball and socket (Figure 3.1). The roughness of the Maverick™ bearing surfaces was measured in-house (more details in § 3.3.2) and the value of average roughness, (see § 3.3.2.1), was found to be 0.05 ± 0.001 μm (mean \pm standard deviation).

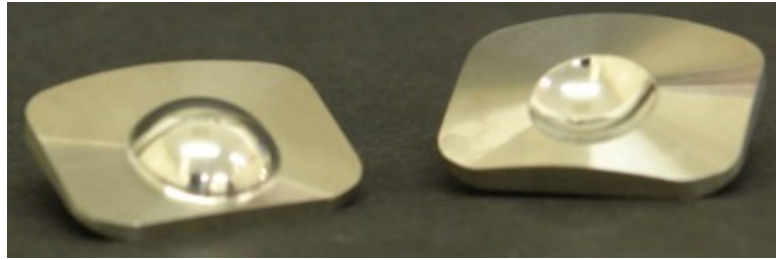


Figure 3.1. *The Maverick™ TDA*

As one of the objectives of this study was to compare the results from different radii in order to find the most appropriate (Chapter 5), the ball radii were selected to be 10, 12, 14 and 16 mm. The first three ball radii were selected based on existing designs of TDA: Maverick™ with ball radius 10 mm (in-house measurements) Charité® with ball radius 12.5 (Charité® Artificial Disc, 2006) and ProDisc-L® with ball radius 14.25 mm (Rawlinson et al., 2007). There is no commercially available TDA with 16 mm ball radius; this dimension was selected to increase the range of radii investigated. The radial clearance between the articulating surfaces was 0.015 mm, similar to that in the Maverick™ device. Also, the spherical base diameter of the balls, which is the diameter of the edge between the ball and the surface, for all samples, was 18 mm. The endplates were designed to fit to fixtures by screws (details on fixtures can be found in Chapter 4, § 4.3.2).

3.2.1.3. Metal and polymer friction tests

This series included two ball-and-socket models of TDAs; one design had a metal socket/polymer ball and the other a polymer socket/metal ball. The metal in each design was Co-27Cr-5.5Mo-0.06C (as described in § 3.2.1.2) and the polymer was ultra high molecular weight polyethylene (UHMWPE) (ASTM F 2848 – 10), similar to that in the Charité® and

ProDisc-L® TDAs. In both groups, two ball radii of 10 and 14 mm were used, with each radius having a radial clearance of 0.35 mm between the ball and socket, similar to the metal-on-polymer ProDisc-L® TDA (Rawlinson et al., 2007). Like the metal-on-metal samples, the spherical base diameter was 18 mm, to enable comparison between geometrically similar samples in this study. The R_a values of the metal and polymer samples were selected based on the in-house measurements of the Maverick™ and the Charite® TDAs, where R_a (\pm standard deviation) for metal and polymer bearing surfaces were 0.05 ± 0.001 and 0.80 ± 0.052 μm , respectively (it should be noted that the surface roughness of metal endplates of the Charité® device was measured in-house, using the method described in § 3.3.2.3, giving the value of 0.01 ± 0.001 μm . The manufacturer (§ 3.2.2) could not achieve such low roughness value; hence, the metal samples were designed with surface roughness similar to that in the Maverick™ device).

3.2.1.4. Metal-on-metal wear test

In this test the generic metal-on-metal samples with 10 mm ball radius (detailed in § 3.2.1.2) underwent wear testing for 5 million cycles. This is explained in more detail in Chapter 7.

3.2.1.5. Charité® wear test

In this experiment the existing Charité® TDAs were tested for 5 million cycles. The test was similar to the metal-on-metal wear test, as described in Chapter 7.

3.2.2. Disc manufacture

To be able to manufacture the samples, the engineering drawings of each sample were produced using SolidWorks2009 software (Dassault Systèmes SolidWorks Corp., Massachusetts, USA) (the engineering drawings can be found in Appendix A). Using the engineering drawings, the metal and polymer samples were manufactured and highly polished by Westley Engineering Ltd. (Birmingham, UK). The samples were machined from bar, using MIKRON VCP600 and WS71D Machining Centres (Rottweil, Germany), and cut to appropriate dimension, by Charmilles Robofil 4031 SI Wire Cutting machine (MAC-TEC e.K., Emmelshausen, Germany (Figure 3.2.A and B). A Black & Decker Bench Grinder (Berkshire, UK) with two grades of Carbrax medium and fine greasy, manufactured by Canning-Lippert Ltd. (Birmingham, UK), was then used to highly polish the surfaces (Figure 3.2.C). As polishing the polymer samples were difficult due to physical properties, they were initially polished by a small Harrison lathe (West Yorkshire, UK), then polished with a very fine grade of Wet & Dry and with Brasso® metal polish (Reckitt Benckiser North America, Inc., Parsippany, NJ, USA); then they were polished by Black & Decker Bench Grinder. For the final surface finish the grinding wheel was replaced by a polishing mop (Figure 3.3).

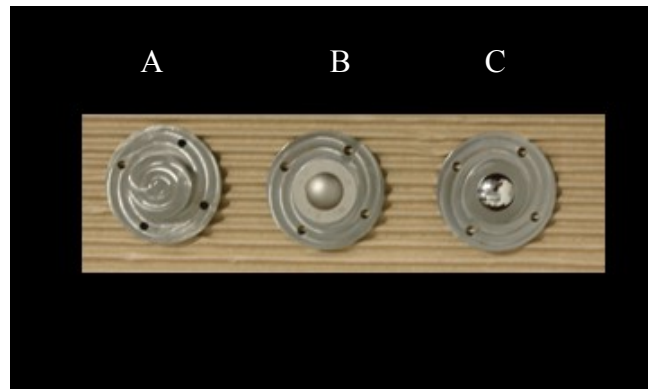


Figure 3.2. The cobalt chrome block has been (A) cut and (B) shaped to form the desired sample. It was then (C) highly polished with a Black and Decker Bench Grinder

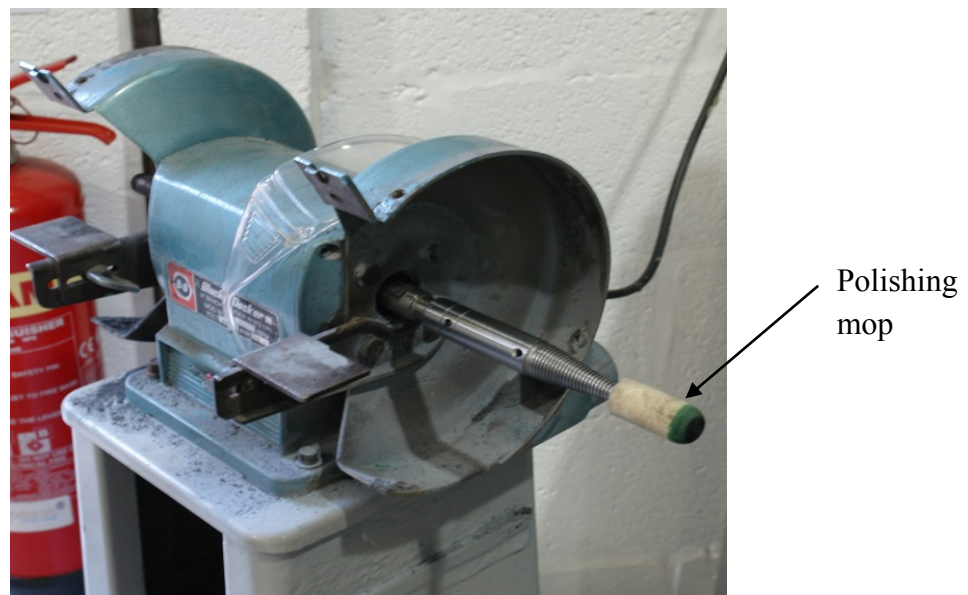


Figure 3.3. The Black and Decker Bench Grinder

Figure 3.4 presents the side view of samples with ball radii 10, 12, 14 and 16 mm; in this picture, the difference between the shape of the ball implants can be clearly seen. Figure 3.5 shows the generic metal-on-metal model with 10 mm ball radius. An example of a polymer and metal sample with ball radius 10 mm can be seen in Figure 3.6.

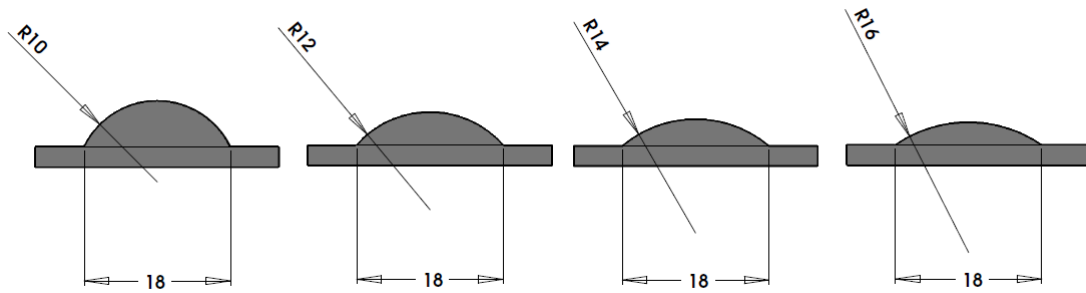


Figure 3.4. The side view of four TDAs with radii of 10, 12, 14 and 16 mm and identical spherical base diameter of 18 mm



Figure 3.5. The generic metal-on-metal ball (left) and socket (right) sample with 10 mm ball radius

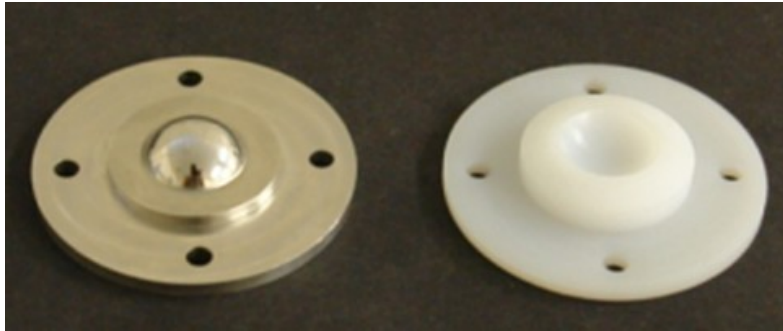


Figure 3.6. *The generic metal ball (left) and polymer socket (right) sample with 10 mm ball radius*

3.2.3. Testing equipment

3.2.3.1. Bose Spine Simulator

The majority of the experiments were performed using three single station Bose SDWS-1 Spine Simulators (Bose Corporation, ElectroForce Systems Group, Eden Prairie, MN, USA). All three simulators have 6 degrees of freedom and enable $\pm 15^\circ$ flexion/extension, $\pm 12^\circ$ lateral bend, $\pm 9^\circ$ axial rotation and 3 kN axial load.

Two of the simulators are fitted with a uni-axial Bose 1010CCH-1K-B load cell (Bose Corporation, ElectroForce Systems Group, Eden Prairie, MN, USA), that were calibrated every 12 months by the manufacturer (Figure 3.7). The uni-axial load cell does not offer frictional torque measurement. Therefore, it is more suitable for wear tests.

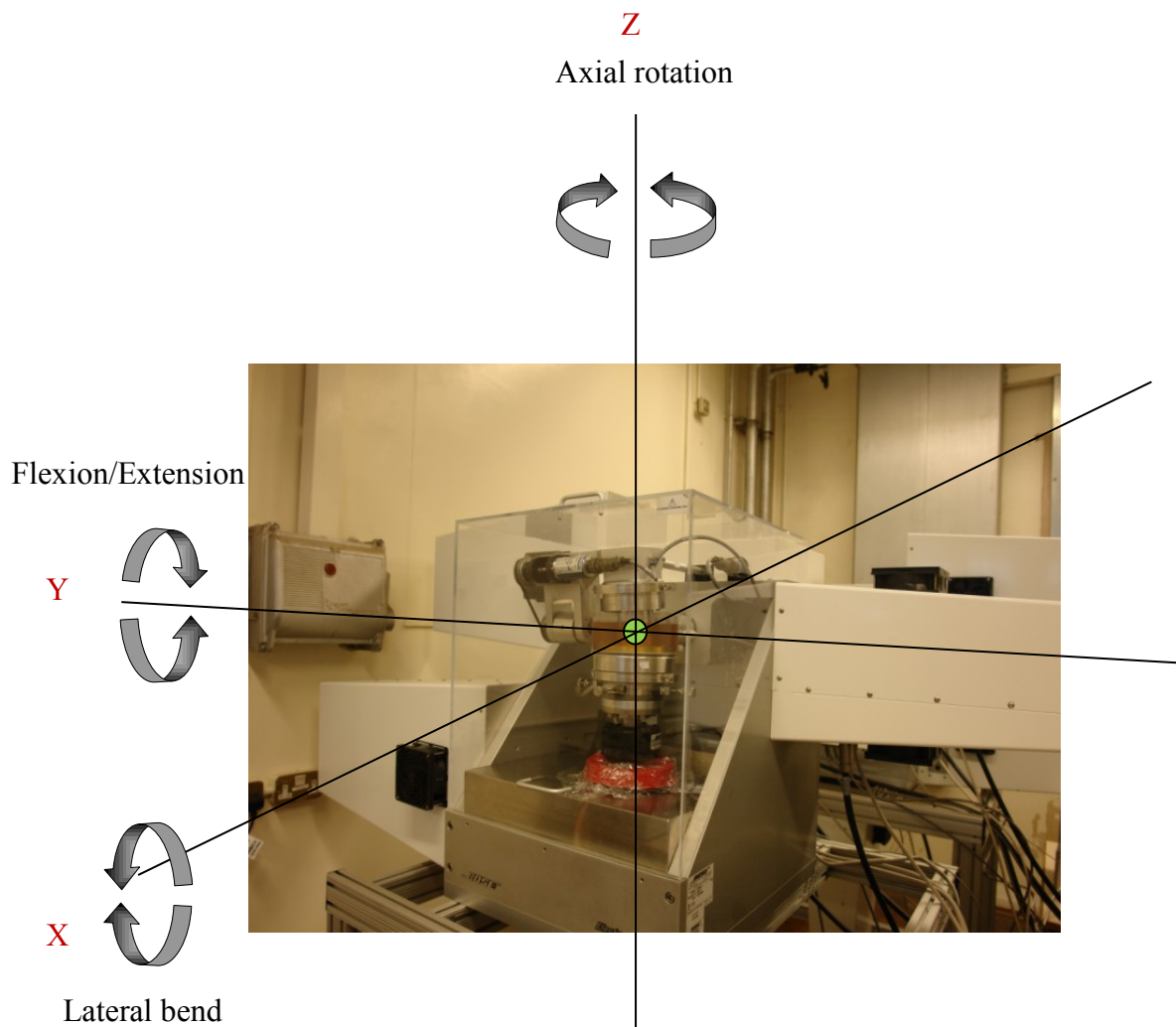


Figure 3.7. The Bose SDWS-1 Spine Simulator with uni-axial Bose 1010CCH-1K-B load cell. The arrows show direction of motions and the green point at the centre indicates the Centre of Rotation

The third simulator is fitted with a multi-axial AMTI MC3-6-1000 load cell (Berkshire, England), that was calibrated every 12 months by the manufacturer. This load cell enables frictional torque measurement, with precision of 0.01 N.m; therefore, it was used for friction

tests (Figure 3.8). To avoid damage to the load cell, limits are defined by the manufacturer for each motion. If the frictional torque exceed ± 15 N.m, the machine automatically triggers and the test stops.

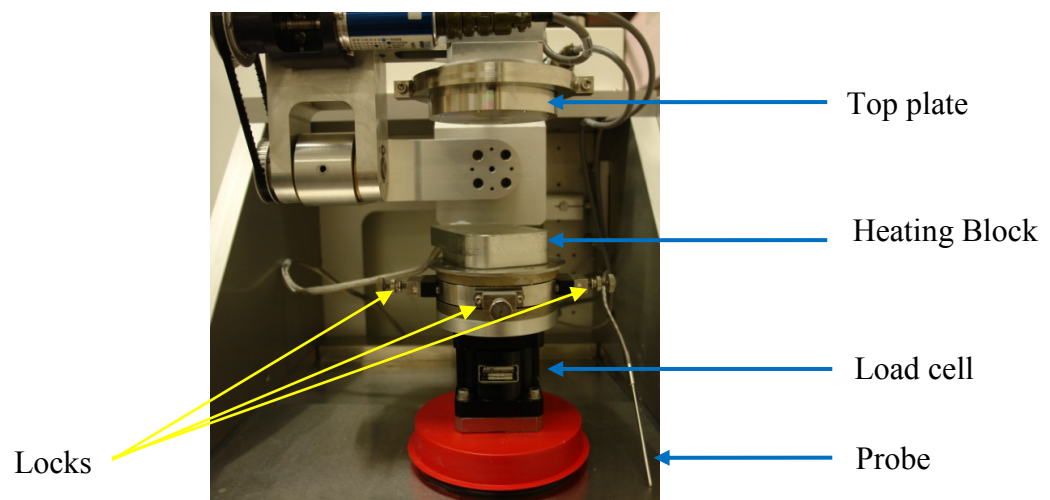
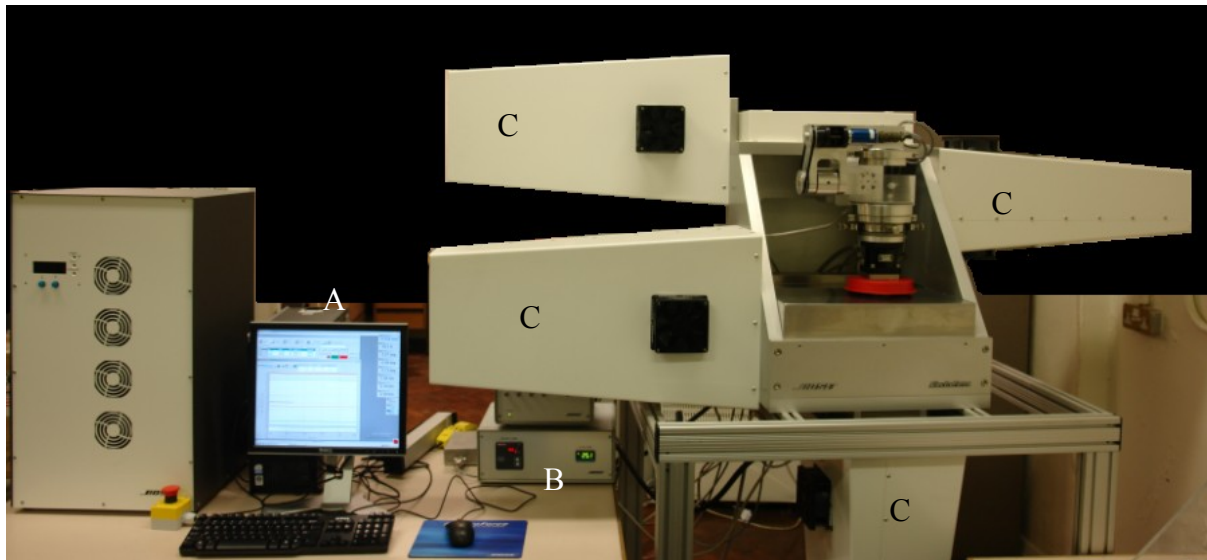


Figure 3.8. The Bose SDWS-1 Spine Simulator, with multi-axial AMTI MC3-6-1000 load cell: A) desktop computer, B) heating controller and C) actuators

All three spine simulators are connected to desktop computers and controlled by WinTest® 4.1 software (Bose Corporation, ElectroForce Systems Group, Eden Prairie, MN, USA). The software provides data acquisition, waveform generation and instrument control. It controls the linear actuators that run the simulators' movements. There are four actuators in each simulator; two move the bottom plate to perform axial rotation and axial compression, whilst the other two move the top plate to perform flexion/extension and lateral bend (Figure 3.8).

The simulators are fitted with a temperature controlled Perspex chamber, which is fixed to the bottom plate, forming a bath (Figure 3.9). The temperature is controlled by the software, through a probe that is connected to the chamber's wall. The heating is supplied by a heating block, on which the bath is fitted. The heating is controlled by a heating controller, which is also connected to the computer and controlled by the software.

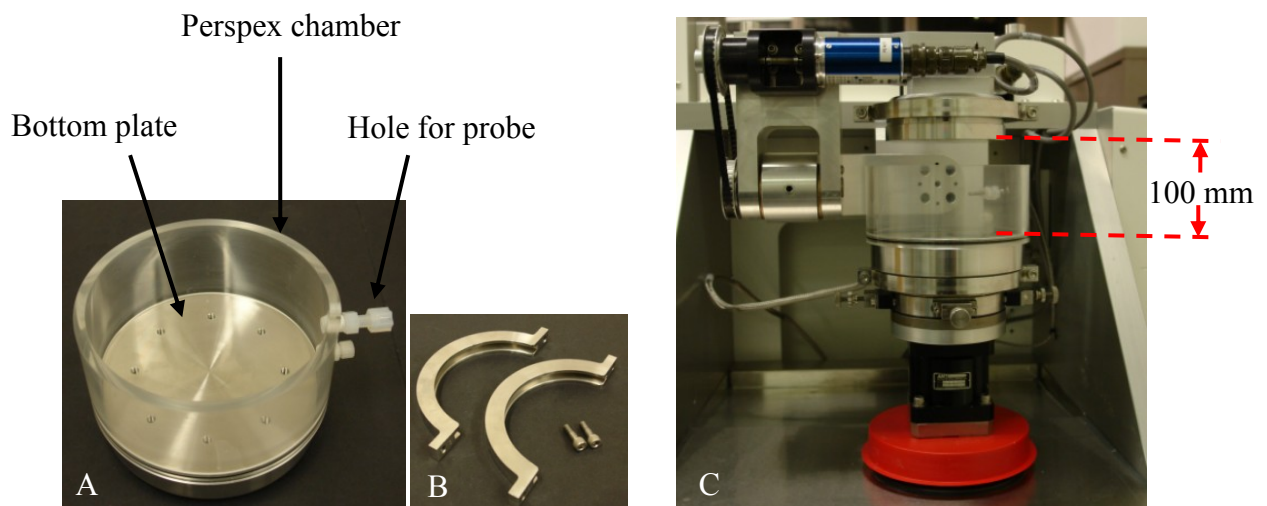


Figure 3.9. The bath assembly (A) is mounted with the split clamps and screws (B) to the heating block of the spine simulator (C). The clearance between the top and bottom plate after assembly is 100 mm

The top and bottom plates are fixed to the spine simulator, using split clamps. The clearance between the two plates, at zero position of the bottom plate, is 100 mm. The bottom plate can travel ± 12 mm in the vertical direction, from the zero position. The top plate cannot vertically move. The bottom plate can also move ± 5 mm in the horizontal (X and Y) direction if required (see Figure 3.7 for directions). It includes four screw-type locks that can lock the plate completely, so it will not move during testing.

3.2.3.2. The Bose ElectroForce® Test Instrument

The Bose ElectroForce® 3330 Series II Test Instrument (Bose Corporation, ElectroForce Systems Group, Eden Prairie, MN, USA) was used as the load soak control station for the wear testing of the Charité® TDAs. This was necessary as recommended by standards BS ISO 18192-1:2008 and ASTM F2423-05 to investigate fluid uptake of the polymer during testing. This machine has a single actuator that offers axial displacement and compression, only. It is fitted with a 3 kN load cell (Bose 1010CCH-1K-B) that was calibrated every 12 months by the manufacturer. Like the spine simulators, it is connected to a desktop computer and controlled by WinTest® 4.1. The Test Instrument is fitted with a temperature controlled Perspex fluid bath, the same as the simulators, which is also fixed to the heating block (Figure 3.10). The temperature control and heating mechanism are the same as the simulators.

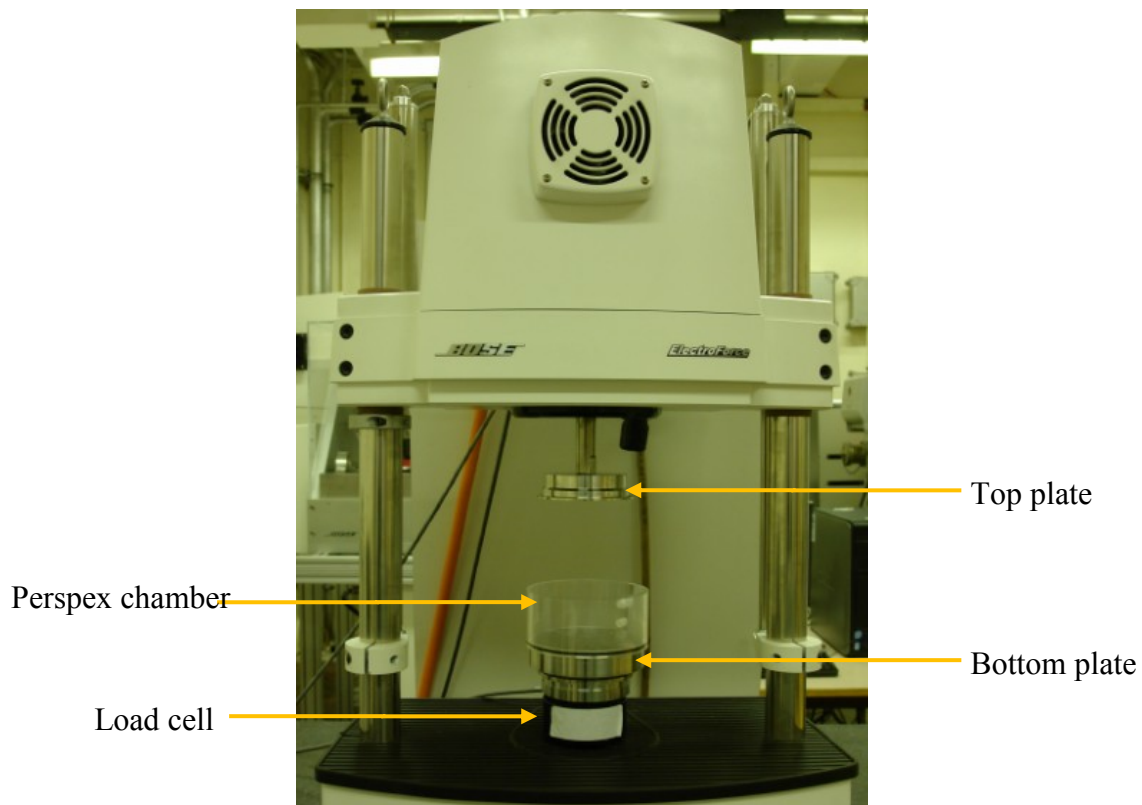


Figure 3.10. *The Bose ElectroForce® 3330 Series II Test Instrument*

The top and bottom plates are fixed to the machine, using split clamps and screws, similar to that in the spine simulators. The clearance between the two plates, when the top plate is at its highest position and the bottom plate is at zero position, is 400 mm. The top plate can be manually moved up and down and get fixed at any desired position within this distance. The top plate can be also controlled by the software to travel ± 12 mm in vertical direction. The bottom plate is stationary.

3.3. Methods

3.3.1. Preparation of the samples

The following procedures are based on the standard BS ISO 14242-2 and the Standard Operating Protocol for Spine Wear Simulator Studies (SOP01.6) of the Institute of Medical and Biological Engineering, University of Leeds. The latter was used to enable comparison of the Charité® wear results between those obtained in this study (Chapter 7) and those obtained at the Institute of Medical and Biological Engineering.

Regardless of the type of the test, before testing, the specimens were checked with the naked eye to ensure they are visually clean, contaminant free and free from scratches or other damage; if the components were not visually clean, they were cleaned with 70% alcohol/water solution (Sigma-Aldrich, St. Louis, MO, USA) before the start of the test. They were then soaked in solution of Virkon disinfectant powder (Antec International, Sudbury, UK) diluted with tap water, for at least 2 hours and no longer than 24 hours, to destroy bacterial contamination (for 10 mg of powder, 1 litre water was used). UHMWPE components were soaked in the Virkon disinfectant solution for a maximum of 20 minutes. After that, the specimens were washed once with tap water and twice with distilled water and allowed to dry in the open air, whilst kept on low lint clean-room wipes (Cleanroom shop, Cumbria, UK). The samples were then ultrasonically cleaned in a propan-2-ol bath (Scientific Laboratory Supplies, Town, East Yorkshire, UK), then washed again with acetone (Sigma-Aldrich, St. Louis, MO, USA) to remove any traces of grease or dirt. Finally, they were dried and wiped over with low lint clean-room wipes and kept in plastic boxes at room temperature

for 48 hours. After 48 hours, the surface roughness of each sample was measured (more details in § 3.3.2).

The polymer samples were soaked in distilled water and kept at 37° C in a Petri dish for two weeks before the start of each test to allow for any fluid uptake to stabilise (recommended by SOP01.6).

3.3.2. Surface roughness measurements

3.3.2.1. Introduction

Surface roughness defines the texture of a surface and is characterised by peaks and valleys. The mean value between the peaks and valleys is called average roughness. If the measurement is performed in two dimensions (2D), the average roughness is conventionally denoted by R_a ; if it is in three dimensions (3D), it is R_q (Taylor Hobson, 1990). Figure 3.11 explains the difference between the two measurements. It can be seen that in the case of 2D measurement, the results only give the average roughness along one line on the surface at the time, whereas in the case of 3D measurement, a 3D model of the surface profile of the area of interest is produced.

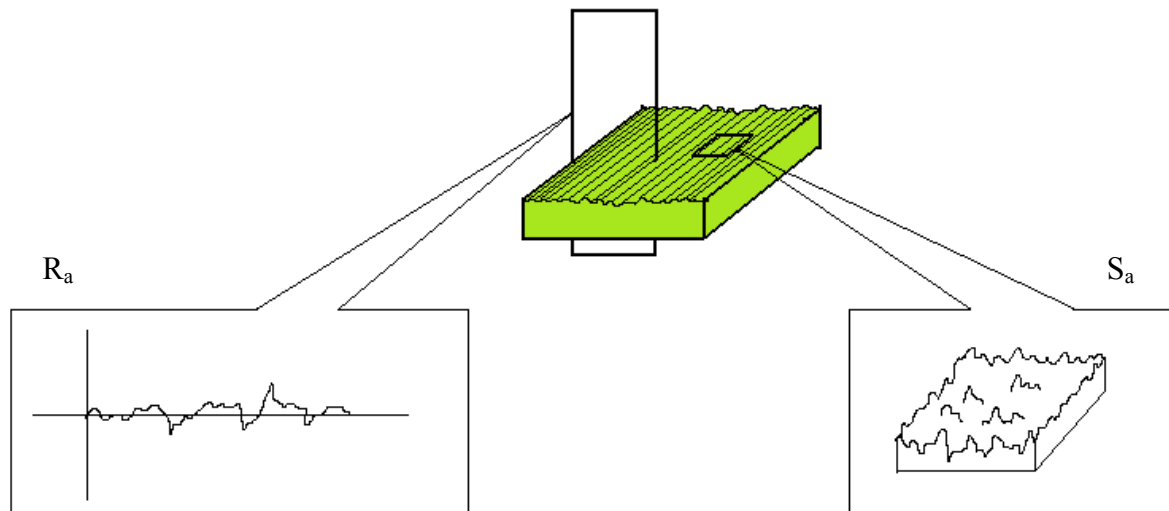


Figure 3.11. The average surface roughness R_a in 2D (left) and the average surface roughness S_a in 3D (right)

There are different methods for measuring the surface roughness. They can be divided into contact or non-contact methods. Both methods were available for surface roughness measurements required in this work. Each method was suited to different sizes of specimen. Therefore, the method was selected according to the specimen size.

3.3.2.2 Non-contact method

The non-contact method was used to measure the surface roughness of the UHMWPE components of the Charité® TDAs (the UHMWPE core). There were two reasons for this selection. First, the UHMWPE core has two convex faces, which made it difficult to adjust it to a certain position and assure no movements or damage to the surface as a result of direct surface contact. Therefore, it was easier to use a method that does not include direct contact to the surface. Second, the size of the component was suitable for the non-contact equipment.

The measurements were obtained using a MicroXAM2 interferometer (Omniscan, Wrexham, UK) (Figure 3.12). The interferometer enabled 3D surface mapping of the implants with accuracy of ± 0.01 mm. In this method, the surface of the specimen is not in direct contact with the machine; instead, the image of the surface is obtained from the interference of the light beams which are scattered by the surface. The image is then processed using Scanning Probe Image Processor software (Image Metrology, Horsholm, Denmark).

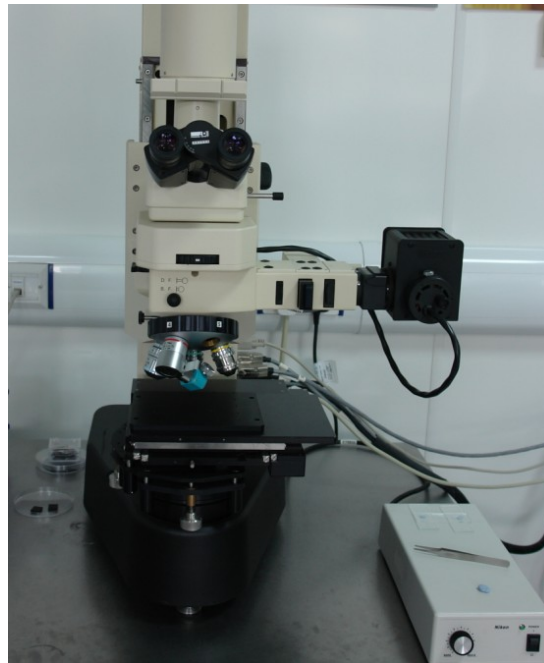


Figure 3.12. The MicroXAM2 interferometer

3.3.2.3 Contact method

The generic samples and the Charité® metal endplates were too big for the MicroXAM2 interferometer and, therefore, a Taylor Hobson Form Talysurf-120L (Leicester, UK) stylus profiler was used. Unlike the interferometer, the latter uses direct contact of a diamond-tip stylus to the surface for measurement (Figure 3.13). The diameter of the tip was 4 μm and the cone angle was 60°.

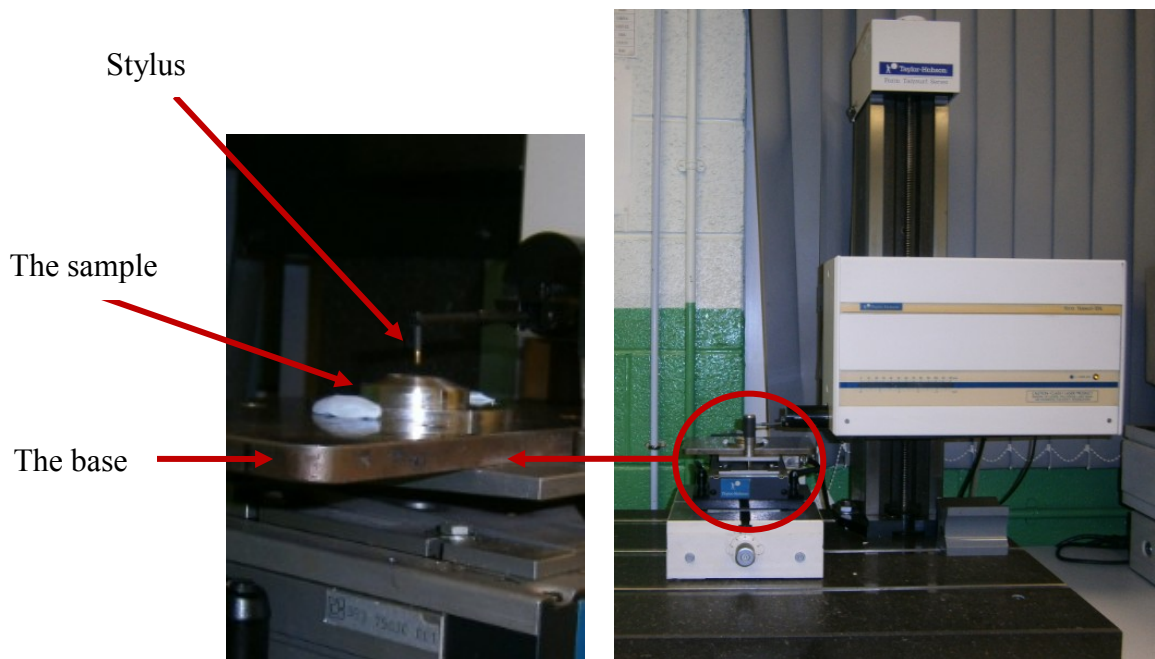


Figure 3.13. The Taylor Hobson Form Talysurf-120L

To perform measurements, the samples were placed on the base of the profiler and held in place by Bostik Blu-Tack® (Paris, France). The stylus tip was carefully placed very close to the surface of the sample (about 2 mm above the surface), using a manual control module. Then, using a computer-controlled function, the stylus was moved down until it fully touched

the surface. The stylus then had to be set to a desired axial travelling distance. Also, the measurements had to be selected to be performed in either 2D or 3D. For all the specimens in this study, the standard 1.25×1.25 mm travel distance for 3D measurement was selected (Taylor Hobson, 1990). Once the travelling distance was specified, the measurement started by the stylus moving along the surface from and up to the given travelling distance. After finishing the first row, the stylus moved to the starting point to start the second row. This was repeated until the measurement was complete. The data was collected by a Microsoft Disk Operating System (MS-DOS) operated computer. Once it finished, data was transferred to a Windows operated computer for analysis.

The data was analysed using the TalyMap Universal 3.1.8 software (Taylor Hobson Limited, Leicester, UK) (Figure 3.14). The first step was to filter the data to remove any high frequency data that resulted from noise and vibration. This was achieved by using what is known as profile filter cut-off wavelength (λ_c) (or roughness cut-off wavelength), which defines the intersection between roughness and waviness components (BS ISO 4287:1997). The standard cut-off wavelengths of a profile filter are 0.08, 0.25, 0.8, 2.5 and 8 mm (BS ISO 3274:1996). The filters were selected according to the recommendations of the standards BS ISO 3274:1996 and BS ISO 4288:1996, the stylus tip radius and expected surface roughness values. In case the expected surface roughness values are not known, there is a booklet provided by the Taylor Hobson Limited, in which there are metal samples with different surface roughness. Therefore, the desired sample can be visually compared with those in the booklet and the range of roughness can be estimated. The stylus tip radius in this experiment was $2 \mu\text{m}$ and the expected surface roughness for metal samples was between 0.02 and $0.1 \mu\text{m}$. Therefore, according to the standards, the appropriate cut-off wavelength was 0.25 mm.

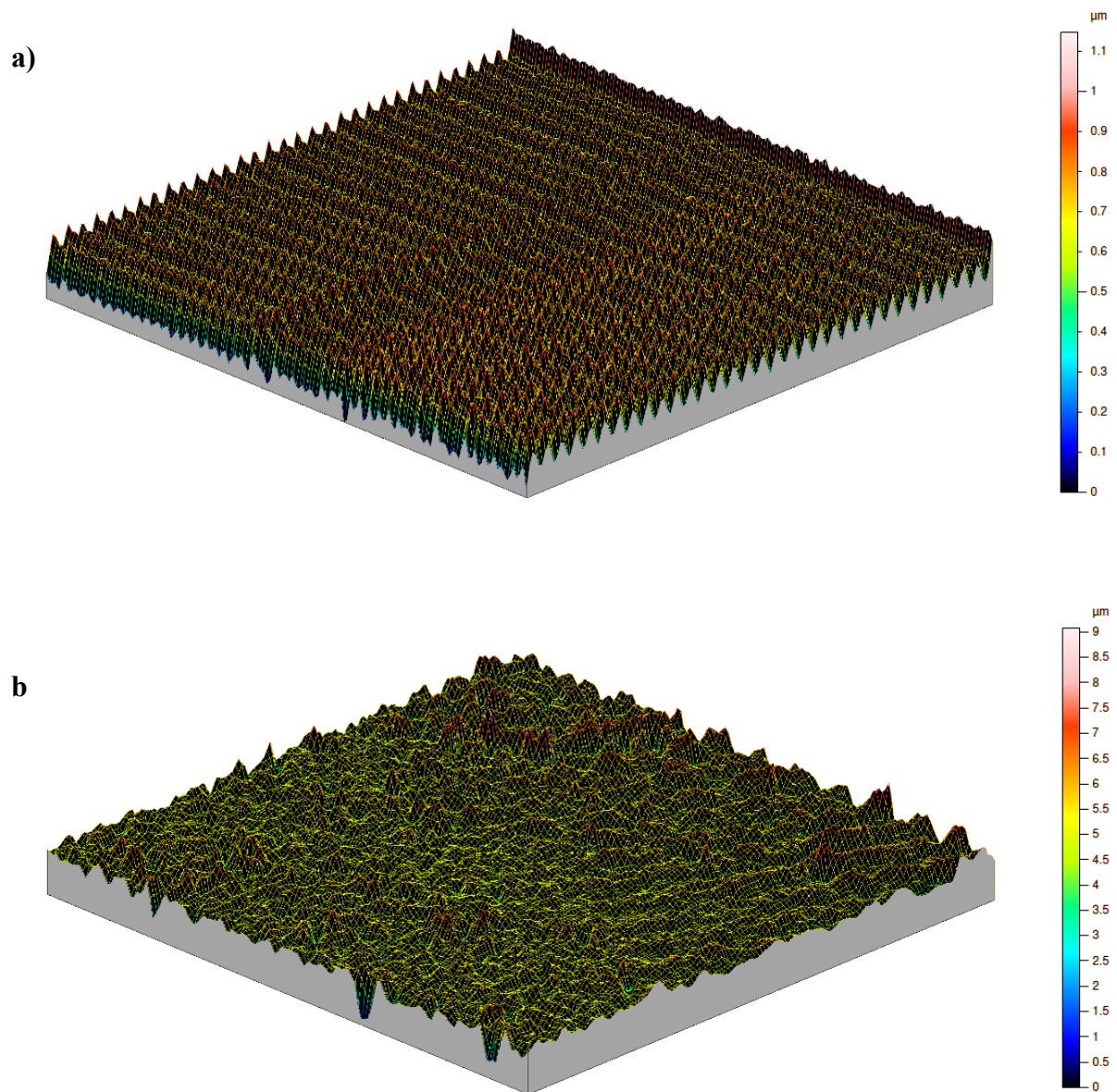


Figure 3.14. Surface roughness measurements of a) metal and b) polymer samples with ball radius 10 mm. The sampling length is 1.25×1.25 mm

After separation of roughness and waviness was performed by the appropriate filter, the quantitative results were obtained by the software. This method was used to measure the surface roughness of the generic metal and polymer samples, and the Charité® metal endplates. To obtain more reliable results, the surface roughness of each sample was measured six times.

3.3.3. General testing conditions for the current study according to the ISO and ASTM standards

3.3.3.1. Friction tests

It was mentioned in § 2.10 that in general, the experimental tests for TDAs are guided by the standards BS ISO 18192-1:2008 and ASTM F2423-05. The standards suggest appropriate values for load, angular motion and frequency, comparable to what TDAs may experience *in vivo*. Therefore, it was decided that the friction tests in this study follow the same standards. In each test, the major variables were *direction and magnitude of angular motion, frequency and compressive load*. Table 3.1 shows the suggested values by the above standards for different motions, compressive loads and total protein concentration of diluted calf serum (more details on the importance of protein concentration in Chapter 4), for testing lumbar TDA. Both standards suggest a frequency of 1 Hz and no larger than 2 Hz. In order to see whether change of frequency affects the friction results, tests were carried out at frequencies of 0.25, 0.5, 0.75, 1, 1.25, 1.5, 1.75 and 2 Hz. The general sinusoidally varying motions included axial rotation from 0° to +2°, flexion from 0° to +6°, extension from 0° to -3° and lateral bending from 0° to +2°. The compressive load varied according to each particular testing condition, but was selected within the range recommended by the above standards.

Table 3.1. The suggested values for different motions, compressive load and diluted calf serum protein concentration, for testing lumbar TDAs (*ASTM F2423-05*; *BS ISO 18192-1:2008*)

Standard	Axial Rotation	Flexion	Extension	Lateral Bend	Load (N)	Protein Concentration (g/L) \pm SD
<i>BS ISO 18192-1:2008</i>	$\pm 2^\circ$	$+ 6^\circ$	$- 3^\circ$	$\pm 2^\circ$	600 (min.) 2000 (max.)	30 ± 2
<i>ASTM F2423-05</i>	$\pm 3^\circ$	$+ 7.5^\circ$	$- 7.5^\circ$	$\pm 6^\circ$	1200	20

3.3.3.2. *Wear tests*

The wear tests were performed according to the recommendations by BS ISO 18192-1:2008 standard and SOP01.6. The sinusoidally varying motions included axial rotation from -2° to $+2^\circ$, flexion/extension from $+6^\circ$ to -3° , and lateral bending from -2° to $+2^\circ$. The load sinusoidally varied between 600 and 2000 N. The frequency was 1 Hz for angular motions and 2 Hz for the sinusoidally varying load. The wear test conditions are presented in greater detail in Chapter 7.

3.4. Summary

The generic models of metal-on-metal TDAs were designed based on dimensions of a metal-on-metal Maverick™ TDA, with ball radius of 10 mm and radial clearance of 0.015 mm. Different ball radii were then selected to enable comparison between different radii (10, 12, 14 and 16 mm). The generic models of metal and polymer TDAs were designed based on the dimensions of metal-on-polymer ProDisc-L®, with ball radius of 14 mm and radial clearance of 0.35 mm. Also, to enable comparison with metal-on-metal, a further sample was designed with ball radius 10 mm. The metal-on-metal wear tests were carried out using the metal-on-metal generic models with 10 mm ball radius. The metal-on-polymer wear tests were performed on the Charité® TDAs.

Friction and wear tests were performed using Bose SDWS-1 Spine Simulators and Bose ElectroForce® 3330 Series II Test Instrument. The friction tests were guided by ASTM F2423-05 and BS ISO 18192-1:2008, and the wear tests were guided by BS ISO 18192-1:2008 and SOP01.6. As part of the experiments, the surface roughness of the samples was measured, using a contact or non-contact method, depending on the size of the sample.

Chapter 4

*Effect of Lubricants
on the Friction in
Total Disc Arthroplasty*

4.1. Chapter overview

This chapter presents the study on the effect of two different lubricants on the friction of metal-on-metal total disc arthroplasty (TDA). An introduction to the purpose of the study is provided in § 4.2. Then the required materials and methods to approach the problem are described in § 4.3. Section 4.4 presents the results, followed by a discussion in § 4.5. The chapter is ended by a brief summary for the reader in § 4.6.

4.2. Introduction

A design of TDA is tested *in vitro* to simulate performance in the body. It is important to understand the tribological behaviour and performance of these designs and, therefore, reliable *in vitro* tests need to be carried out (Harsha and Joyce, 2011). As was mentioned in Chapter 2 (§ 2.10.3), hip and knee joints are lubricated by synovial fluid, but the intervertebral joint is not a synovial joint and is assumed to be lubricated by interstitial fluid. It was also mentioned that the lubricants used for tribological tests are divided into two groups: non-physiological fluids, such as Ringer's solution, and physiological fluids, which contain protein, such as calf serum. The lubricants in each group have different compositions, and may have appreciable effect on the results (Brockett et al., 2008; Harsha and Joyce, 2011; Scholes and Unsworth, 2000; Wang et al., 2004). Therefore, as tribological tests need to mimic the environment *in vivo* as closely as possible, it is important to select a lubricant with similar compositions to that in the body.

There are still doubts on the exact composition of the fluid that lubricates the bearing surfaces in TDAs, but it is likely to be somewhere between Ringer's solution and diluted calf serum (Fogh-Andersen, 1995; Sherwood, 2011; Streicher et al.1996). Therefore, the question is: does it make a difference which fluid is used as a lubricant in tribological tests of TDAs? My aim at this part of the study was to answer this question by investigating the effect of calf serum and Ringer's solution on friction in TDAs.

4.3. Materials and methods

4.3.1. Introduction

The samples used for this test were the generic metal-on-metal TDA models with ball radii 10 and 16 mm and radial clearance of 0.015 mm between the ball and socket, similar to the Maverick™ metal-on-metal TDA, as described in § 3.2.1.2 (Figure 4.1).

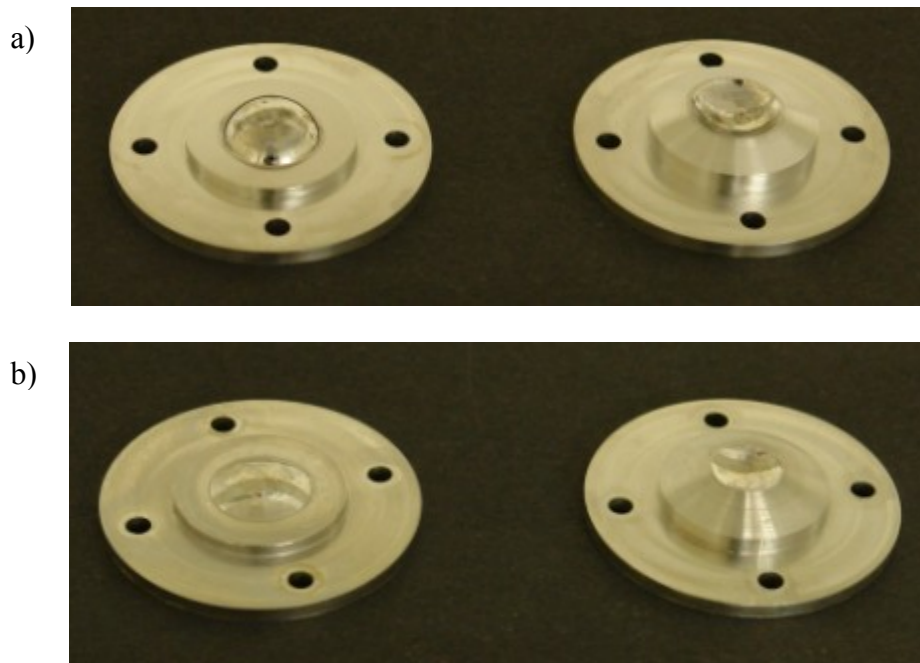


Figure 4.1. The generic metal-on-metal samples with a) 10 mm and b) 16 mm ball radii. The endplates are designed to enable easy fixation to the spine simulator

4.3.2. Fixtures

To be able to mount the specimens to the spine simulator, custom-designed fixtures were required. The fixtures were designed based on the dimensions and clearance of the working distance between the top and bottom plates of the Bose spine simulator (Figure 4.2). The diameters of the top and the bottom plates were 110 mm, with 100 mm clearance between them. To avoid creation of an unwanted external bending moment, the height of the fixtures was selected in such way that the centre of rotation (COR) for flexion/extension and lateral bending of the implants sits on the COR for flexion/extension and lateral bending of the simulator. The distance between top plate and COR of the simulator was 42.5 mm (Figure 4.2).

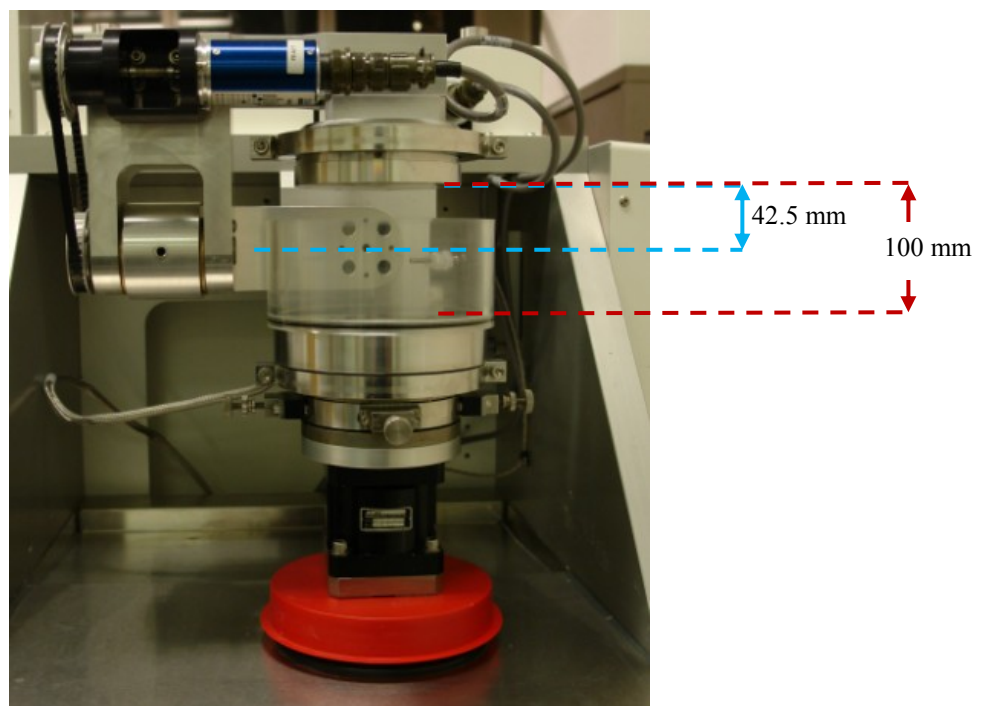


Figure 4.2. *The distance from the top plate to COR of the Bose spine simulator (42.5 mm) and to the bottom plate (100 mm)*

The COR of the implants is the centre of the sphere from which the ball is created. Since the ball radii were different, the COR of the 16 mm sample was different to that for the 10 mm sample. The fixtures were designed to fit the 16 mm sample. In order to be able to use the same fixture for both implants, the height of the upper fixture (i.e. the vertically stationary fixture) had to be adjusted to enable the sample with 10 mm ball radius to sit at the correct COR. To overcome the problem, a simple round plate was designed to be mounted onto the top plate. Two-dimensional models of the samples and fixtures were designed by SolidWorks2009 to identify the required thickness for the extra plate (Figure 4.3 and 4.4). It was measured that the thickness of the extra plate had to be 9 mm.

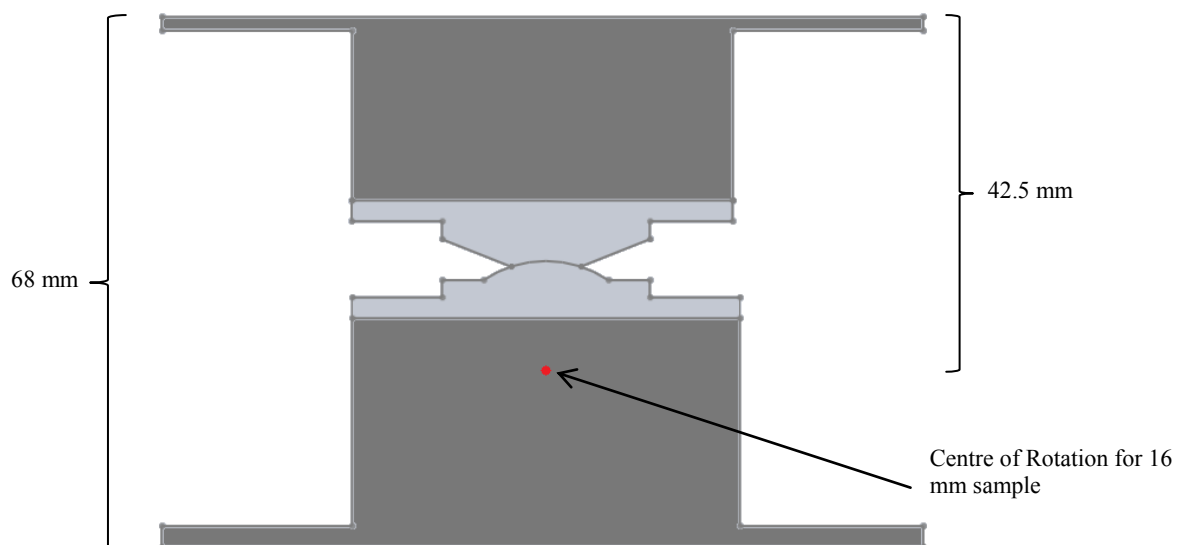


Figure 4.3. A 2D example of the sample with 16 mm ball radius, fitted to the fixtures. The red point indicates the COR of the sample, which is 42.5 mm to the top plate of the simulator.

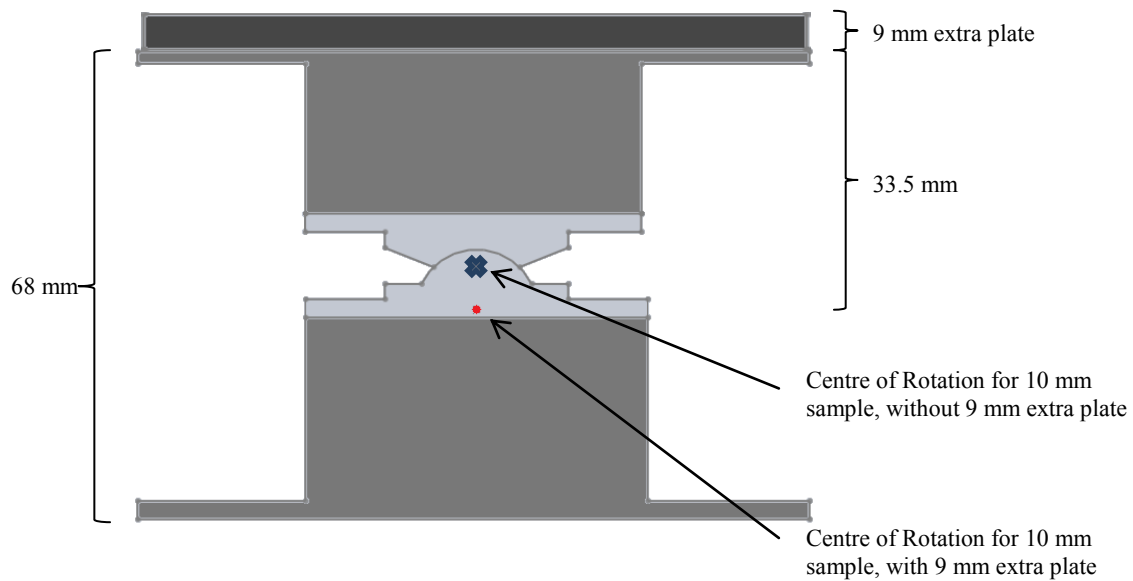


Figure 4.4. A 2D example of the sample with 10 mm ball radius, fitted to the same fixtures as those for the 16 mm sample. The red point indicates the COR of the sample, which has been adjusted to correct position by 9 mm extra plate, bringing the COR back to 42.5 mm. The cross indicates the COR of 10 mm sample, if the fixture were fitted to the simulator's top plate without the 9 mm extra plate.

The fixtures were manufactured by Westley Engineering Ltd. The material was stainless steel – Grade 316, as it corrodes in neither Ringer's solution nor diluted calf serum (which were the lubricants used in this study). Figure 4.5 shows the top fixture and the extra plate. The engineering drawings of the fixtures can be found in Appendix B.

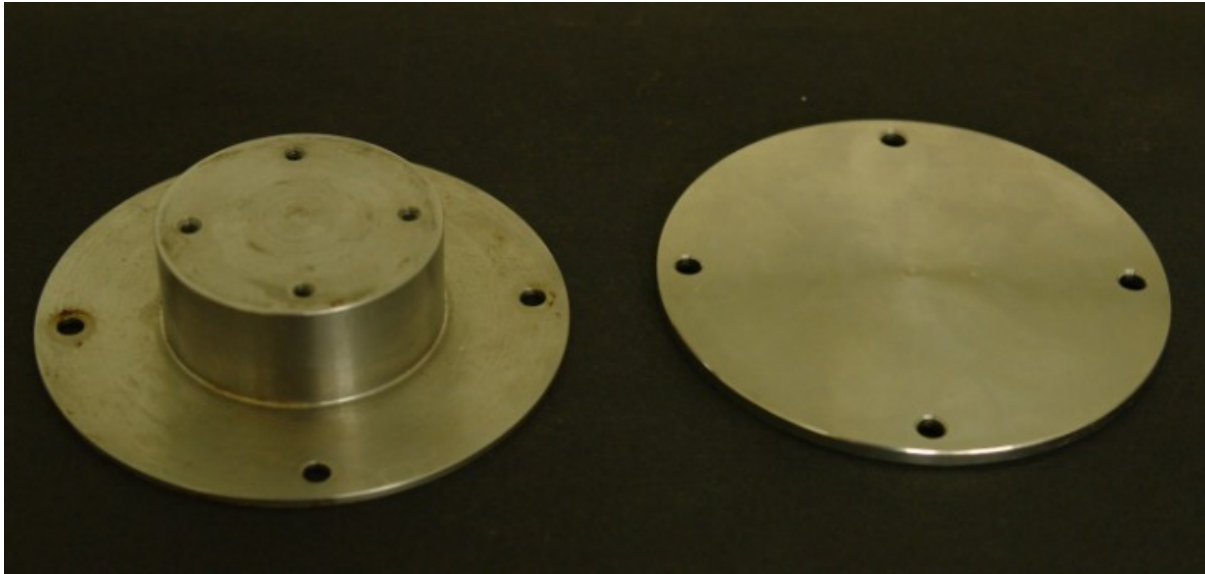


Figure 4.5. The top fixture (left) and the extra plate (right)

4.3.3. Lubricant preparation

The specimens were tested in two groups; the first group was tested in a solution of calf serum (SeraLab, West Sussex, UK) diluted with distilled water to a protein concentration of 30 ± 2 g/L, at a controlled temperature of 37°C (BS ISO 18192-1:2008). The serum was originally frozen, so it had to be defrosted before diluting with distilled water. To minimise biodegradation, instead of defrosting by hot water, the serum was left in a refrigerator at 5°C for 24 hours before testing. The second group was tested in Ringer's solution, also at a controlled temperature of 37°C. The solution was produced by dissolving a 1.2 g Ringer's solution tablet (Oxoid Ltd., Hampshire, UK) in 500 mL of distilled water.

4.3.4. Viscosity measurement of the lubricants

It is important to determine the viscosity of a lubricant because the value may affect the friction (Wang et al., 2008b). This was achieved by measuring the viscosity of both lubricants, using an AR-G2 cone-on-plate rheometer (TA Instruments, West Sussex, UK) under 0.5% constant strain (Figure 4.6). As temperature affects viscosity, measurements were made at 37° C, the same temperature as the testing condition.

To perform the viscosity measurement, about 6 to 8 drops of the lubricant were placed on the plate of the rheometer using a plastic pipette. Using the AR Instrument Control software (TA Instruments, West Sussex, UK), the cone was automatically brought down until it touched the surface of the lubricant. It was then rotated under 0.5% constant strain, at 1.166 and 1.122 s⁻¹ shear rates for diluted calf serum and Ringer's solution, respectively. The data was captured and processed by the same software. Finally, the processed data was transferred to Excel software (Microsoft Office, Redmond, WA, USA) and the average viscosity was calculated. The viscosity of the diluted calf serum and Ringer's solution were found to be 1.4 ± 0.4 and 0.72 ± 0.05 mPa.s, respectively.

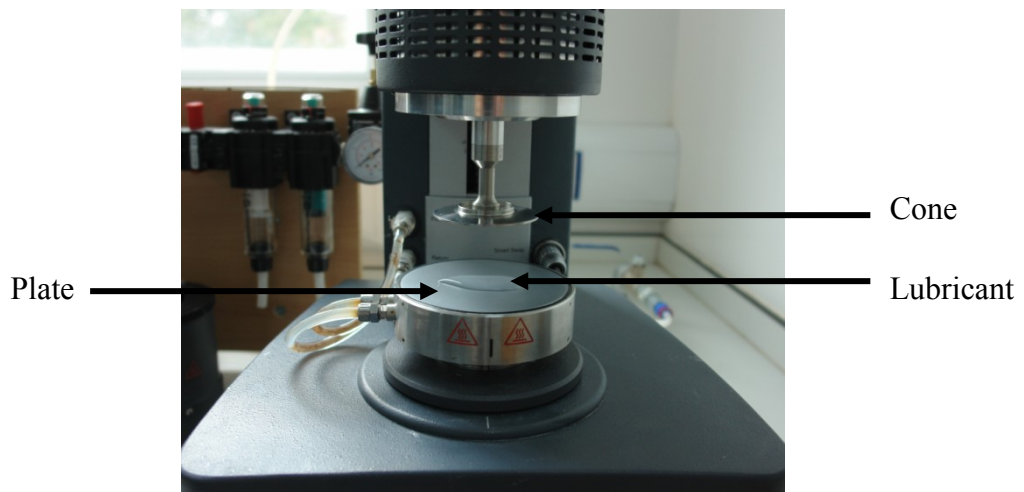


Figure 4.6. The AR-G2 cone-on-plate rheometer

4.3.5. Preparation of the metal samples

Before testing, the specimens were washed and cleaned as described in Chapter 3 (§ 3.3.1). The surface roughness of each sample was measured using the Taylor Hobson Form Talysurf-120L (as described in §3.3.2.2). The average surface roughness for the balls and sockets are shown in Table 4.1.

Table 4.1. The average surface roughness (S_a) of metal ball and socket samples with ball radii 10 and 16 mm, based on six measurements

Average roughness \pm Standard Deviation (μm)		
Specimen's ball radius	Ball	Socket
10	0.053 \pm 0.003	0.040 \pm 0.004
16	0.040 \pm 0.011	0.043 \pm 0.003

4.3.6 Frictional torque

Frictional torques were measured using the Bose SDWS-1 Spine Simulator, with multi-axial AMTI MC3-6-1000 load cell (§ 3.2.3.1). The specimens were mounted on custom-designed fixtures to allow the correct alignment within the simulator (§ 4.3.2). The fixtures were then placed inside the bath and mounted on the machine with the ball endplate connected to the bottom plate of the simulator and the socket to the top plate. The lubricant was then added to the bath and left until the temperature reached 37°C. Figure 4.7 shows the samples mounted to the simulator.

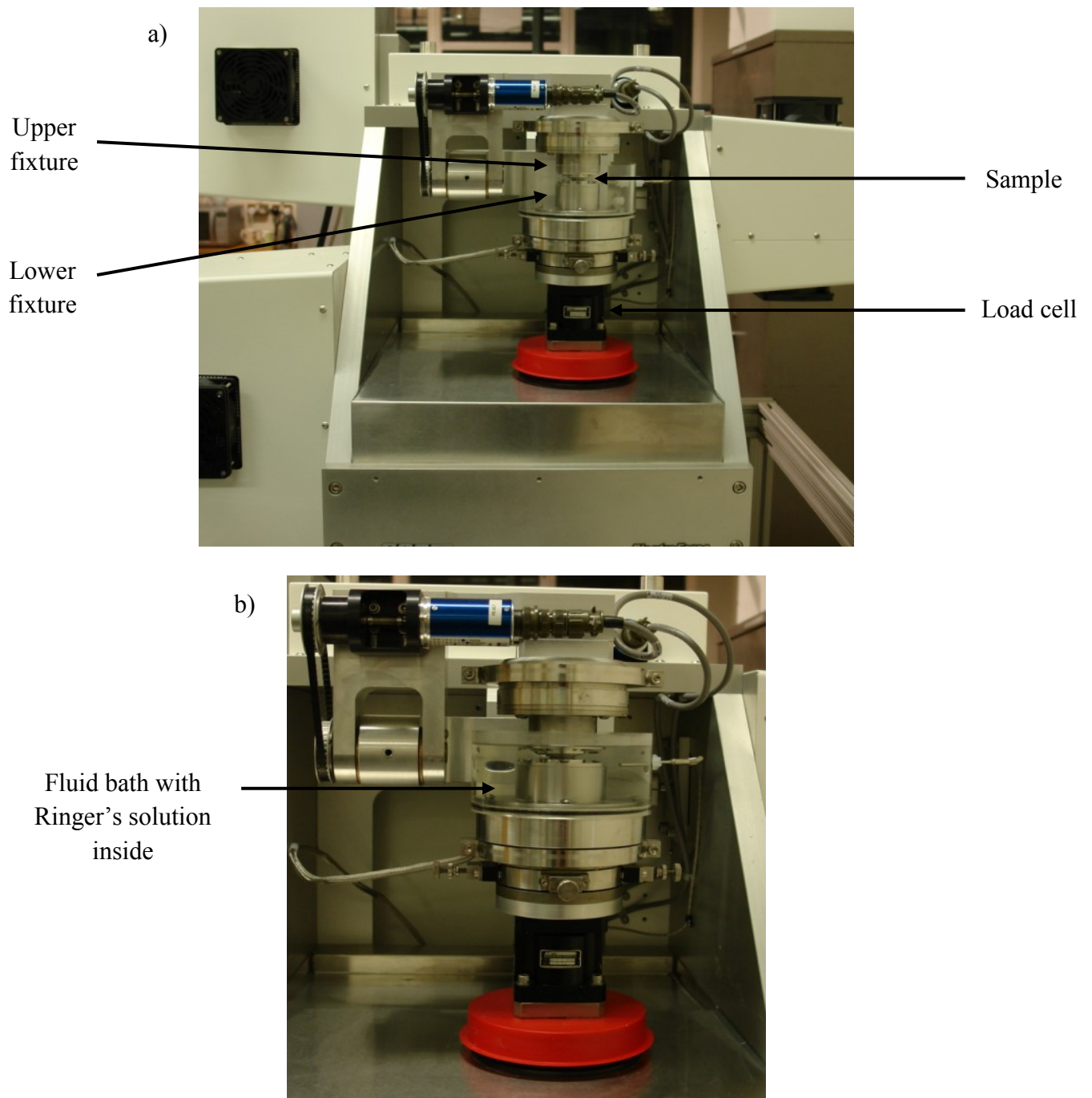


Figure 4.7. The Bose Spine Simulator with the 10 mm sample inside a) before and b) after adding lubricant

The testing was guided by standards BS ISO 18192-1:2008 and ASTM F2423-05. The direction and magnitude of motions, and range of frequencies were similar to that described in § 3.3.3.1 for friction tests. Each sample was subjected to an axial compressive load of 1200 N. The very first test was carried out in sinusoidally varying axial rotation from 0° to 2° for 100 cycles, in order to see whether the measured frictional torque was constant throughout the test. It was observed that the pattern for the frictional torque generated was constantly repeated after the first 30 cycles. Therefore, from then on, each test was carried out for 100 cycles and the frictional torque was measured. The procedure was then repeated under flexion to $+6^\circ$, extension to -3° and lateral bending to $+2^\circ$. Each sample was tested four times. The tests were not performed in consecutive manner, meaning that the decision of switching to a different lubricant at any point of testing on one particular sample at the time was random. This way the order of testing could not affect the results.

To determine the maximum torque generated in each test condition, a graph of frictional torque against angle of motion in 100 cycles was plotted for each test, using Excel software. An average frictional torque was calculated based on the values from the last 10 cycles. In order to compare the effect of different lubricants, graphs of mean frictional torque against frequency were plotted.

4.3.7. Statistical analysis

To investigate possible differences between the results from the two lubricants, error bars representing the 95% confidence intervals were added to the graphs of frictional torque against frequency. The 95% confidence intervals were calculated by multiplying the standard

error (equation 4) associated with each datum point on the graph, by 1.96 (James, 1993; Kreyszig, 2006). The standard error, S , is defined as

$$S = \frac{s}{\sqrt{n}} \quad 4$$

where s is the standard deviation and n is the number of measurements (James, 1993; Kreyszig, 2006).

These confidence intervals represent the regions in which there is a 95% probability of finding the true mean value (Kreyszig, 2006). Therefore, if there is an overlap between the two regions defined by the 95% confidence intervals, difference between them at the 5% level is not significant (James, 1993). No overlap would indicate a significant difference. This method has been used previously to determine whether materials used for implantation have different mechanical properties (Mahomed et al., 2009). (It should be noted that, strictly speaking, this method requires a large number of measurements for each data points. In this study, there were only four repeat measures, but the difference between the results for calf serum and Ringer's solution (see § 4.4) were so clear that no further statistical analysis was considered necessary).

4.3.8. Stribeck analysis

Stribeck analysis was performed to indicate the lubrication regime between the articulating surfaces. The analysis was performed using equations 1 to 3, as described in previous chapter (§ 2.10.4).

4.4. Results

4.4.1. Frictional torque analysis

The frictional torque was found to be significantly higher for a TDA with Ringer's solution as the lubricant, compared with those lubricated by diluted calf serum for both the 10 and 16 mm radii samples in axial rotation; Figure 4.8 presents the results for 16 mm samples in axial rotation, under a 1200 N load. At a frequency of 1 Hz (which is the frequency used for TDA wear testing, BS ISO 18192-1:2008) the frictional torque was 3.5 N.m for diluted calf serum and 4.5 N.m for Ringer's solution. Similar behaviour was observed for flexion, extension and lateral bending, for both ball radii. Figures 4.9, 4.10 and 4.11 show the results for 16 mm samples under 1200 N load during lateral bending, flexion and extension, respectively. It can be seen that the frictional torque in a TDA lubricated by Ringer's solution was always significantly higher than that in diluted calf serum, since in none of the graphs did the confidence interval error bars overlapped.

Results for the 10 mm radius TDA in flexion could not be obtained as the frictional torque, with Ringer's solution as the lubricant, was higher (> 15 N.m) than the limits for the spine simulator (see § 3.2.3.1). It can be seen that for the 16 mm radius sample (Figure 4.10), the friction in flexion with Ringer's solution as the lubricant, was around 14 N.m. The remaining 10 mm results can be found in Appendix C.

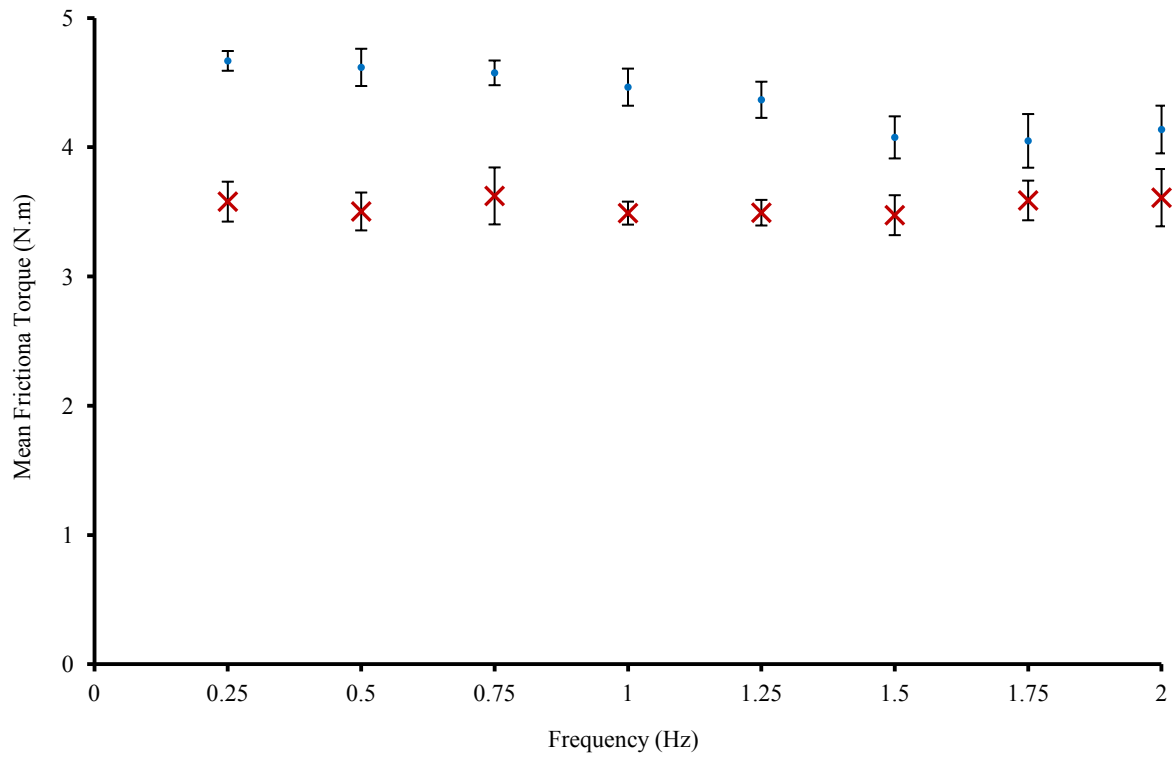


Figure 4.8. Mean frictional torque plotted against frequency, for the samples with 16 mm ball radius in diluted calf serum (x) and Ringer's solution (•) for axial rotation. Error bars represent 95% confidence intervals

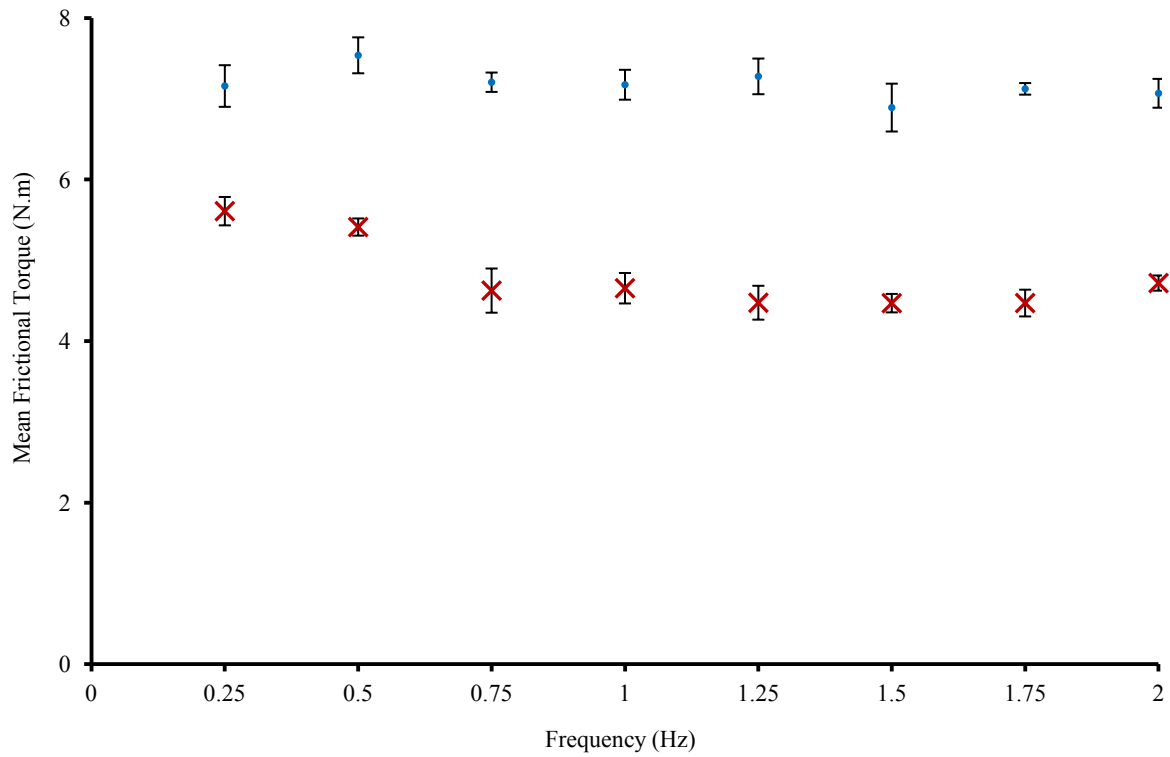


Figure 4.9 Mean frictional torque plotted against frequency, for the samples with 16 mm ball radius in diluted calf serum (×) and Ringer's solution (•) for lateral bending. Error bars represent 95% confidence intervals.

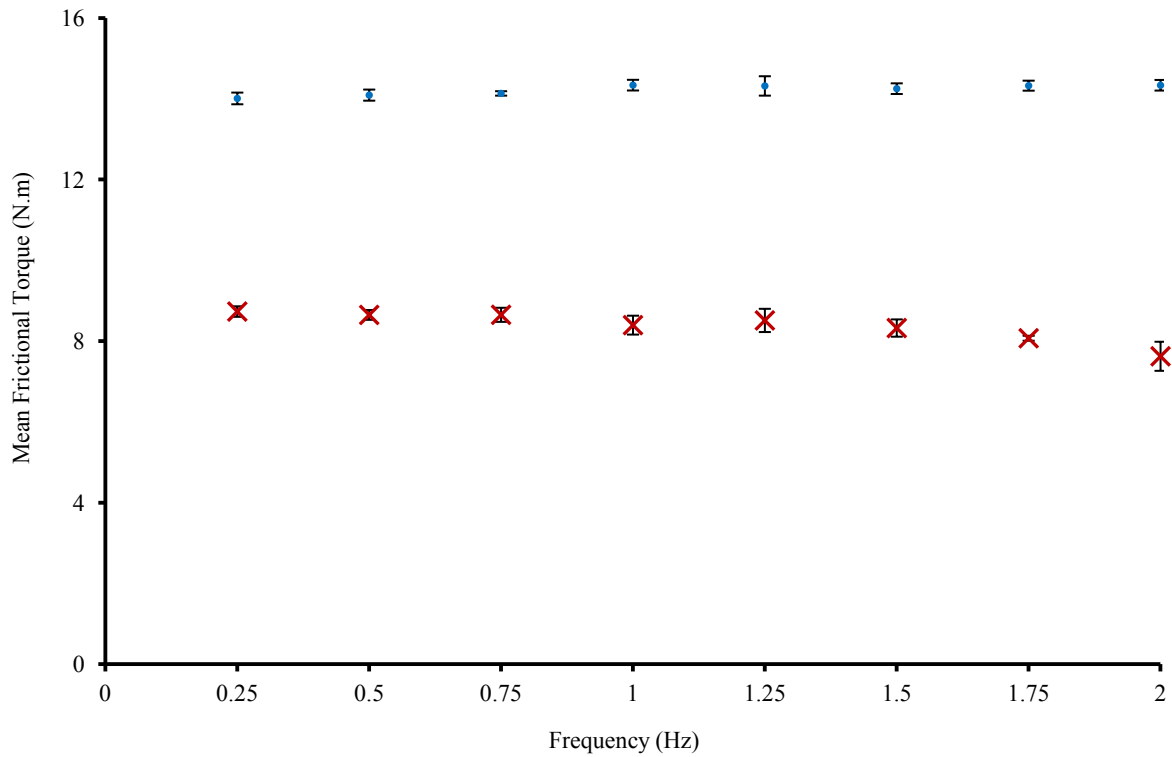


Figure 4.10. Mean frictional torque plotted against frequency, for the samples with 16 mm ball radius in diluted calf serum (x) and Ringer's solution (•) for flexion. Error bars represent 95% confidence intervals.

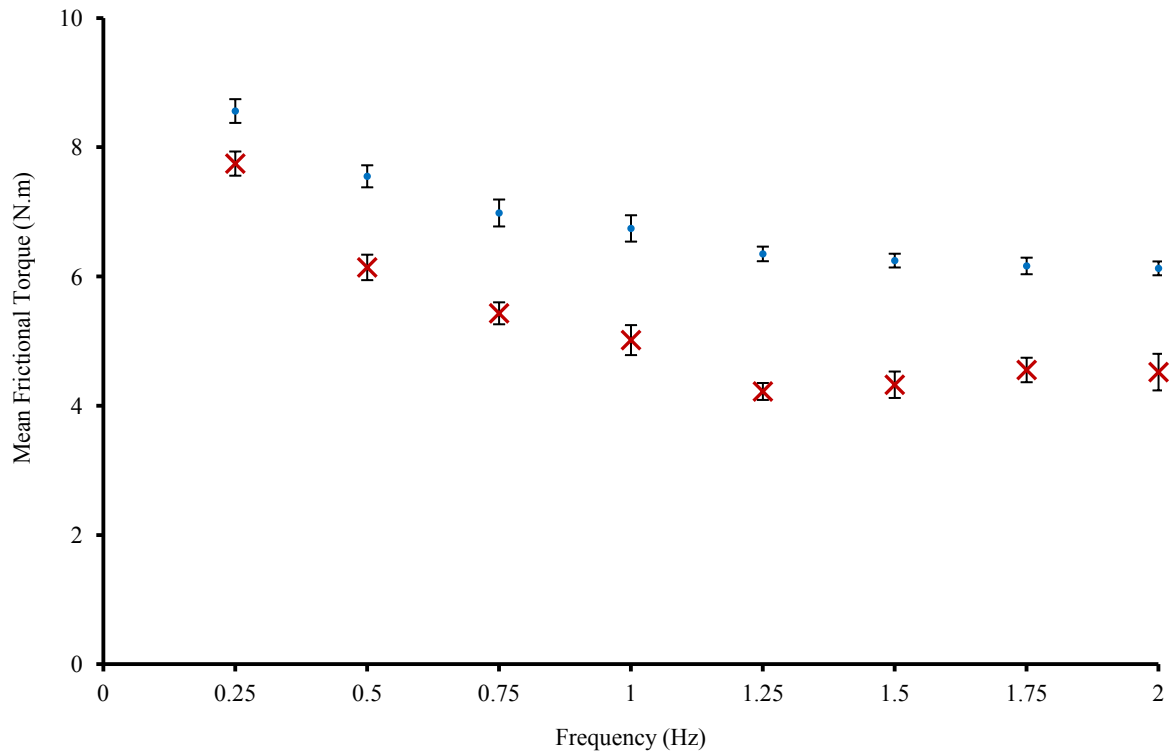


Figure 4.11. Mean frictional torque plotted against frequency, for the samples with 16 mm ball radius in diluted calf serum (x) and Ringer's solution (•) for extension. Error bars represent 95% confidence intervals.

4.4.2. Lubrication regime analysis

To investigate the lubrication regimes, Stribeck curves were plotted for each motion. Figure 4.12 presents the results for the sample with ball radius 16 mm, in axial rotation. It can be observed that in the case of Ringer's solution there was a decrease in friction factor and a gradual increase towards the end as Sommerfeld number increased. For the diluted calf serum, the graph was almost flat throughout.

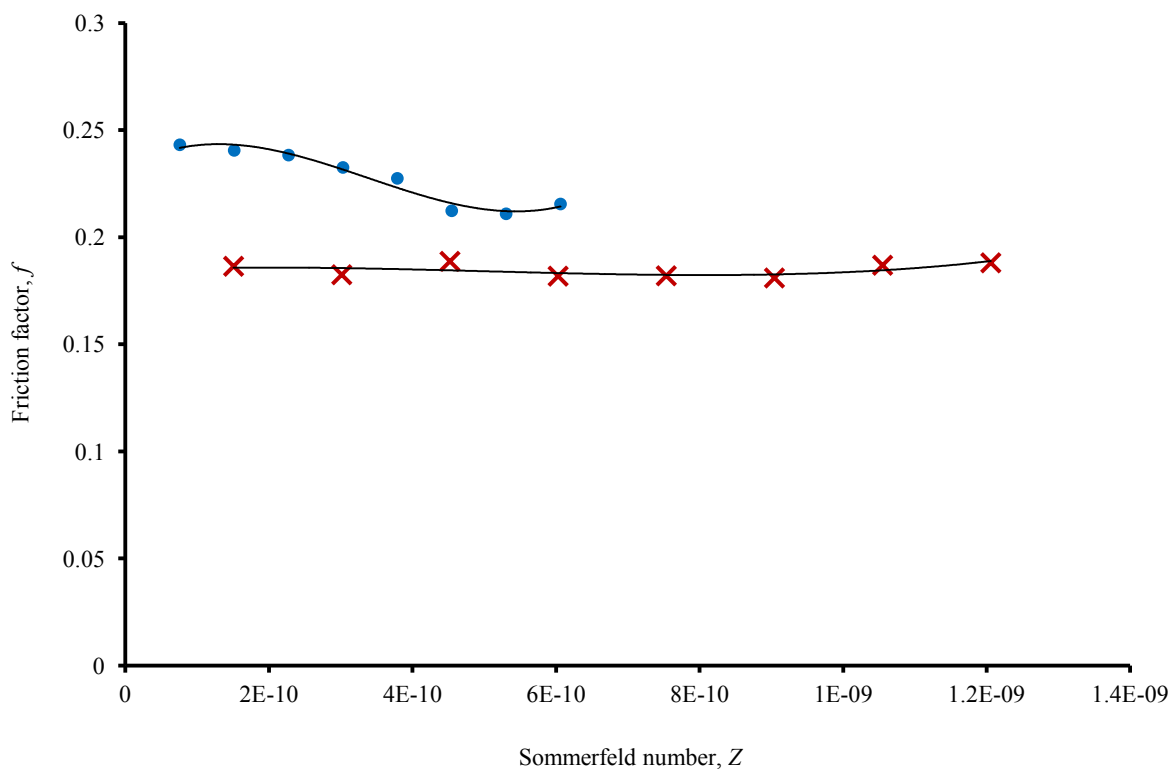


Figure 4.12. Stribeck curves for sample with a ball radius of 16 mm for diluted calf serum (×) and Ringer's solution (•), operated in axial rotation. A third order polynomial has been fitted to the points

For the same sample in lateral bend, friction factor for the test with Ringer's solution as lubricant had an initial increase with a gradual decrease as Sommerfeld number increased. For diluted calf serum, friction factor initially decreased and then flattened, with an increase at 2 Hz (Figure 4.13).

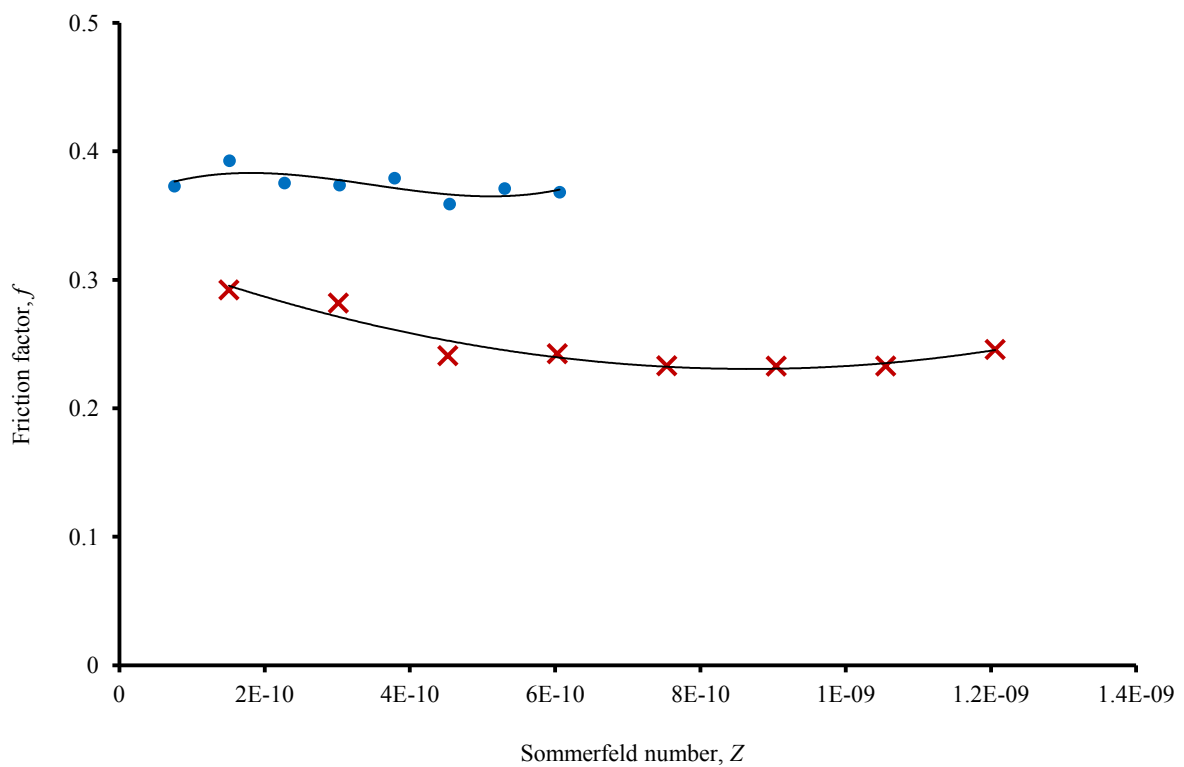


Figure 4.13. Stribeck curves for sample with a ball radius of 16 mm for diluted calf serum (×) and Ringer's solution (•), operated in lateral bend. A third order polynomial has been fitted to the points

In flexion, in the case for Ringer's solution, the friction factor had an increase at the beginning, similar to that in lateral bend, and then gradually flattened. For diluted calf serum, the friction factor initially decreased and then flattened out of a fairly constant value, with increasing Sommerfeld number (Figure 4.14).

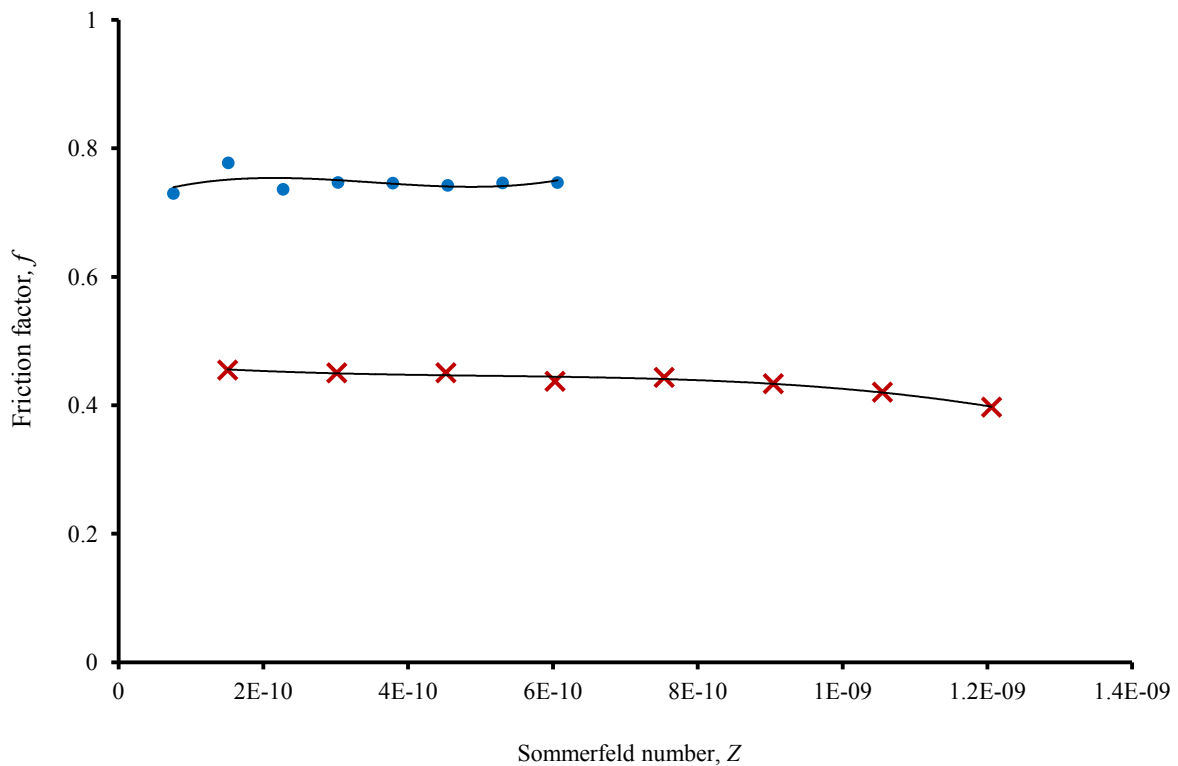


Figure 4.14. Stribeck curves for sample with a ball radius of 16 mm for diluted calf serum (\times) and Ringer's solution (\bullet), operated in flexion. A third order polynomial has been fitted to the points

The results for extension showed a decrease of friction factor with increasing Sommerfeld number in Ringer's solution, whilst for diluted calf serum friction factor decreased until the midway, where it gradually increased until flattened out at the end as Sommerfeld number increased.

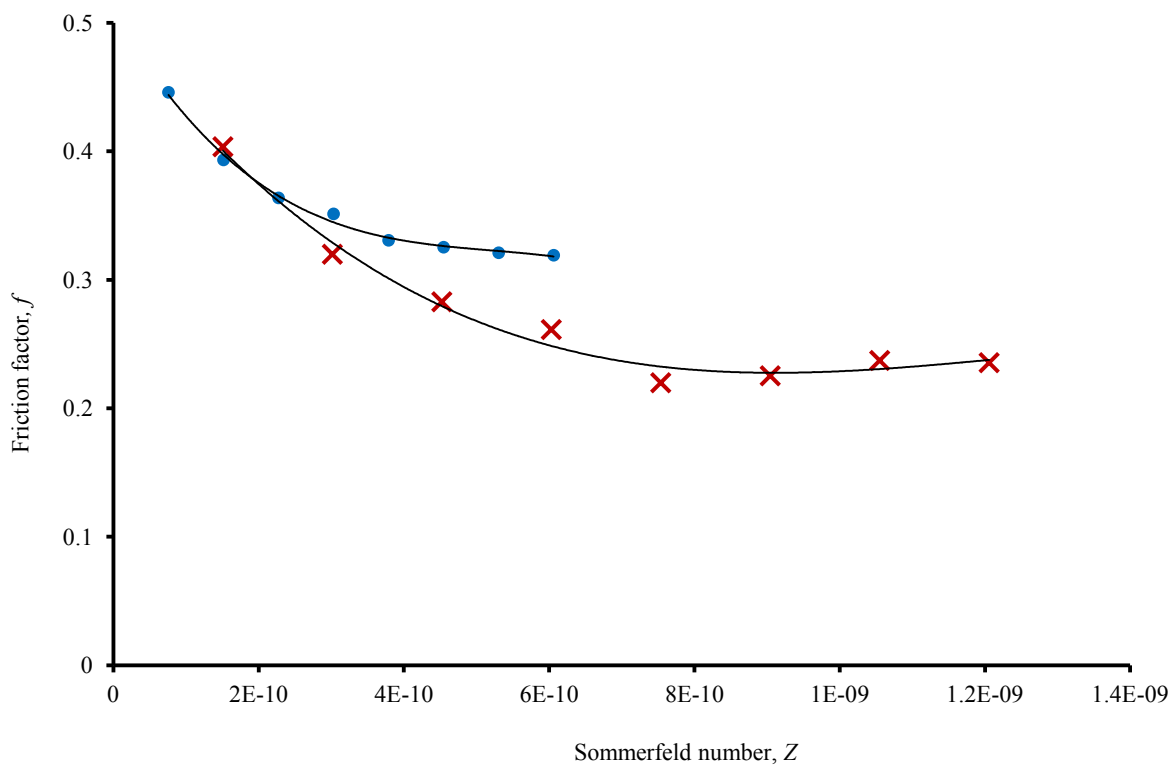


Figure 4.15. Stribeck curves for sample with a ball radius of 16 mm for diluted calf serum (x) and Ringer's solution (•), operated in extension. A third order polynomial has been fitted to the points

4.5. Discussion

TDA's with articulating bearing surfaces are currently tested, in the laboratory, using a lubricant of diluted calf serum. The exact nature of the lubricant found in TDA in the human spine is unknown, but is likely to be interstitial fluid (Shaheen and Shepherd, 2007; Yao and Gu, 2006). The composition of interstitial fluid is likely to be somewhere between that of Ringer's solution and diluted calf serum (Table 4.2). The protein content is expected to increase the viscosity (Roselli and Diller, 2011) and, therefore, the lubricity (Scholes and Unsworth, 2006a) of the fluid. The results of this study are consistent with this expectation by showing that frictional torques generated in diluted calf serum are significantly lower than those in Ringer's solution.

Table 4.2. Some of the major compositions of lubricants (Fogh-Andersen, 1995; Harsha and Joyce, 2011; Sherwood, 2011; Streicher et al.1996)

Constituent	Human Synovial fluid (g/L)	Human Interstitial fluid (g/L)	Diluted calf serum (g/L)	Ringer's solution (g/L)
Protein	17	20.6	30	-
Sodium	3.3	3.1 – 3.56	1.75-3.55	3.6
Potassium	0.16	0.12	0.07-0.11	0.21
Calcium	0.06	0.06	0.025-0.035	0.05
Chloride	3.8	4.44	1.5-2.5	5.7

The results presented here are consistent with those from studies of total hip arthroplasty (THA). In a study by Scholes and Unsworth (2006a) on metal-on-metal THAs, it was observed that the presence of proteins in the lubricant decreases the friction between the articulating surfaces. When the implant is lubricated by diluted calf serum, the proteins form a layer on the surface which reduces the contact and results in a mixture of metal-on-metal and protein-on-protein contact (Scholes and Unsworth, 2000; Unsworth, 1978). Such behaviour cannot be expected with Ringer's solution.

The results are also consistent with studies on the viscosity of Ringer's solution, diluted calf serum and interstitial fluid. Ringer's solution, diluted calf serum (Langer et al., 1987; Yao et al., 2003) and interstitial fluid (Roselli and Diller, 2011) are all Newtonian fluids. The viscosity of interstitial fluid lies between that of water and that of body plasma, and varies according to the total protein content and the relative fractions of large and small proteins (Roselli and Diller, 2011). The viscosity of water at body temperature is 0.70 mPa.s and the viscosity of body plasma ranges from 1.2 to 2 mPa.s at 37° (Das, 1978; Khurana, 2007). The measured viscosity of Ringer's solution at 37°, (see § 4.3.4) was 0.72 mPa.s which is comparable to that of water. The measured viscosity for diluted calf serum at 37°, at 1.4 mPa.s, was similar to that reported for plasma (Das, 1978; Khurana, 2007). Moreover, the viscosity of the plasma is very close to the average viscosity of interstitial fluid, which is 1.24 mPa.s (Shaheen and Shepherd, 2007; Zurovsky et al., 1995).

The Stribeck curves can give an indication of the lubrication regime (Scholes and Unsworth, 2000). As was previously mentioned in Chapter 2, § 2.10.4, when the friction factor is fairly constant with increasing Sommerfeld number, boundary lubrication occurs. A decrease in

friction factor with increasing Sommerfeld number is an indication of mixed lubrication. The results showed that both fluids lead to boundary or mixed lubrication. This shows that the bearing surfaces will be mostly in direct contact. However, in all cases the friction factor was higher in Ringer's solution than that in diluted calf serum. This was in agreement with previous results when friction was significantly higher in Ringer's solution.

Looking at the graphs of frictional torque against frequency, there appeared to be a dependence of frictional torque on the angle of motion. To understand it better, a graph of maximum frictional torque against maximum angular motion was plotted from the results obtained for both Ringer's solution and diluted calf serum (Figure 4.16). In the case of Ringer's solution, the coefficient of determination (R^2) suggests there may be a straight correlation between maximum frictional torque generated and maximum angular motion. It should be noted that the occurrence of maximum frictional torque was independent of frequency, meaning that once it could happen at frequency of 0.25 Hz (e.g. in extension for both lubricants), whilst another time it could happen at frequency of 0.75 Hz (e.g. in axial rotation for diluted calf serum). As other variables such as load and radius are constant, it may be considered that the difference between frictional torque values generated at maximum angular motions may be affected by possible change of lubrication regime as angular motion changes, and consequently by change in friction factor. On the other hand, in the case of diluted calf serum the R^2 value suggest that there may not be a strong evidence for a linear correlation. Therefore, even though there may be a relation between frictional torque generated and the angular motion, there is insufficient evidence to reach a clear conclusion.

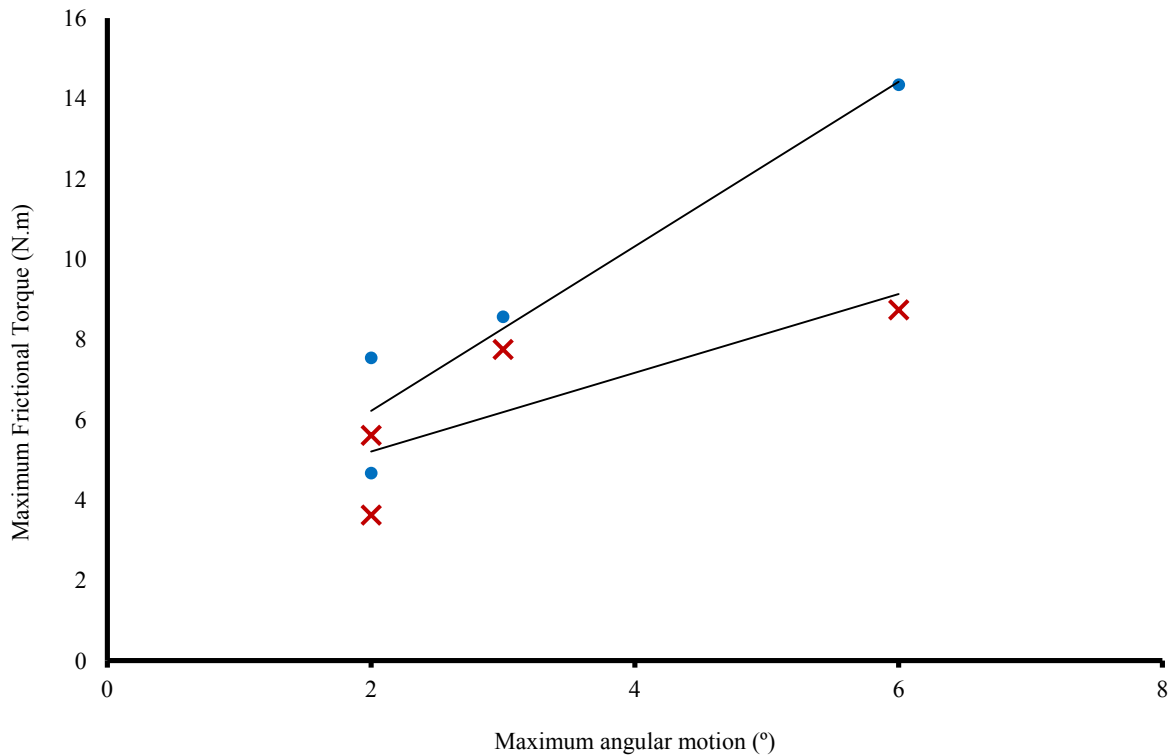


Figure 4.16. Maximum mean frictional torque plotted against maximum angular motion for sample with a ball radius of 16 mm for diluted calf serum (×) ($R^2 = 0.67$) and Ringer's solution (•) ($R^2 = 0.91$). Regression lines are fitted through the data points

The question that then arises is what lubricant should be used for laboratory testing of friction and wear on TDA. The results of this study show that Ringer's solution leads to significantly higher friction than a fluid containing protein. It is, therefore, likely to over-estimate the effects of friction and wear. However, it could be used for stringent tests to ensure that friction or wear problems were unlikely to occur *in vivo*. Diluted calf serum, as usually used for laboratory testing of TDAs, appears to have higher protein content than interstitial fluid and, therefore, might be expected to have a higher viscosity and lubricity, as discussed above. However, the average viscosity of interstitial fluid is closer to that in diluted calf serum, in

comparison to that in Ringer's solution. Therefore, it appears to be reasonable to use diluted calf serum to mimic the fluids surrounding a TDA. Also, the protein concentration of calf serum can be controlled by diluting with more distilled water; although, standards suggest 20 to 30 g/L protein concentration.

Currently, the exact nature of the fluid surrounding a TDA, and precise values for its physical properties are unknown. As a result, tribological studies of TDAs, in the laboratory, provide useful indications of the behaviour that may be obtained *in vivo*, but do not necessarily replicate the true behaviour. However, if the fluid surrounding a TDA is found to be interstitial fluid, then diluted calf serum appears to be a better lubricant than Ringer's solution. Therefore, in the remaining parts of the study, diluted calf serum was used as the lubricant; this has the further advantage of complying with international standards for TDA wear testing.

4.6. Summary

Total joint arthroplasty is tested *in vitro* to simulate performance in the body and therefore selection of an appropriate lubricant is essential. Currently, TDAs with articulating bearing surfaces is tested in diluted calf serum as the lubricant. It is believed that the lubricant found in TDAs is interstitial fluid that may have properties between that of Ringer's solution and diluted calf serum. To investigate the effect of lubricants, a set of friction tests were performed on metal-on-metal generic models of TDAs, using Ringer's solution and diluted

calf serum separately as lubricants. The results showed that the frictional torque generated between the bearing surfaces was significantly higher in Ringer's solution than that in diluted calf serum. The use of Ringer's solution as a lubricant provides a stringent test condition to detect possible problems. Diluted calf serum is more likely to provide an environment closer to that *in vivo*. Therefore, until the precise properties of the fluid lubricating a TDA is not known, diluted calf serum can be used for *in vitro* testing of TDAs, as has been done in the remaining studies in this work.

Chapter 5

Effect of Ball Radius on the Friction in Metal-on-Metal Total Disc Arthroplasty

5.1. Chapter overview

In this chapter, the study on the effect of ball radius on the friction in metal-on-metal total disc arthroplasty (TDA) is presented. A brief introduction, followed by materials and methods to perform the test and analyse the results are presented in § 5.2 and § 5.3, respectively. The results are shown in § 5.4, with a discussion on the results in § 5.5. A brief summary is provided in the final section (§ 5.6).

5.2. Introduction

It was mentioned in Chapter 2 that one of the methods to improve the performance of ball-and-socket TDAs may be changing the design. As one of the major design factors for such implants, changing the ball radius may be a step towards improving performance of TDAs. Studies on total hip arthroplasty (THA) report variation in performance with change in ball radius (Bishop et al., 2008; Smith et al., 2001a; Streicher et al., 1996). This may also be the case for TDAs; however, no studies under identical conditions have been performed to understand the effect of change in ball radius on the performance of such implants. Therefore, the aim of this part of the study was to investigate the effect of change in radius on friction in metal-on-metal TDAs. The work described in this chapter has already been published (Moghadas et al., 2012a).

5.3 Materials and methods

5.3.1. Introduction

For this study the metal samples with ball radii 10, 12, 14 and 16 mm were selected (see § 3.2.1.2). The same fixtures were used as detailed in § 4.3.2, except that for the 12 and 14 mm samples, two more extra plates with 5 and 2.5 mm thickness, respectively for each sample, were manufactured. This was to adjust the centre of rotation (COR) of the samples to the correct position for the spine simulator.

The same procedure as that in § 4.3.5 was followed for preparation of the samples for testing. After being left at room temperature for 48 hours, the surface roughness of each sample was measured using the Taylor Hobson Form Talysurf-120L. The measurements are presented in Table 5.1. Due to the limited number of samples available for the experiment, the samples with ball radii 10 and 16 mm from previous study was used; hence, the surface roughness was re-measured, in case of any differences caused by the previous experiment.

Table 5.1. The average surface roughness (S_a) of metal ball and socket samples with ball radii 10, 12, 14 and 16 mm, after six measurements

Average roughness \pm Standard Deviation (μm)		
Specimen's ball radius	Ball	Socket
10	0.054 ± 0.001	0.044 ± 0.011
12	0.050 ± 0.010	0.050 ± 0.004
14	0.052 ± 0.005	0.051 ± 0.002
16	0.045 ± 0.002	0.048 ± 0.002

5.3.2. Frictional torque

Frictional torque tests were performed using the Bose SDWS-1 Spine Simulator, with the multi-axial AMTI MC3-6-1000 load cell. The assembly of the samples in the simulator was similar to that in § 4.3.6. Similarly, the testing was guided by the standards BS ISO 18192-1:2008 and ASTM F2423-05. The specimens were tested in a solution of calf serum diluted with distilled water to a protein concentration of 30 ± 2 g/L, at a controlled temperature of 37°C.

As was mentioned in § 2.10.2, the BS ISO 18192-1:2008 recommendation on appropriate load values for wear testing of cervical TDAs is a minimum of 50 N (maximum 150 N), whilst for lumbar TDAs it ranges between 600 and 2000 N. On the other hand, the ASTM F2423-05 suggests a constant 1200 N load for wear testing of lumbar TDAs (constant 100 N for cervical TDA). Although the work here was focused on lumbar TDAs, a range of load values for both cervical and lumbar was investigated, for comparison with cervical TDAs in the future. Therefore, it was decided to perform the tests under all four recommended loads, to enable comparison between results under different loading conditions. Each specimen was tested under a constant axial compressive load of 50, 600, 1200 and 2000 N. The remaining testing conditions, such as angular motions and frequencies were identical to that described in § 3.3.3.1.

Using the procedure outlined in § 4.3.6 to determine the maximum torque generated in each test condition, a graph of frictional torque against angle was plotted for each test, using Excel software. An average peak frictional torque was calculated based on the values from the last 10 cycles. In order to observe the effects of frequency and load on frictional torque, graphs of

mean frictional torque against both frequency and load were plotted. For these graphs a linear regression analysis was performed, using Minitab software (Minitab Inc., State College, PA, USA).

5.3.3. Stribeck analysis

To indicate the lubrication regime under which the samples were acting, Stribeck analysis was used as described in § 2.10.4.

5.4. Results

5.4.1. Frictional torque analysis

The results showed that there was variation in frictional torque with frequency (Figure 5.1). The maximum mean frictional torque was about 9.5 N.m, which occurred for the specimen with a ball radius of 16 mm, in flexion at a frequency of 0.25 Hz, under a load of 2000 N. The results also showed that, for all four motions and for all four sample radii, frictional torque increased with load, as expected.

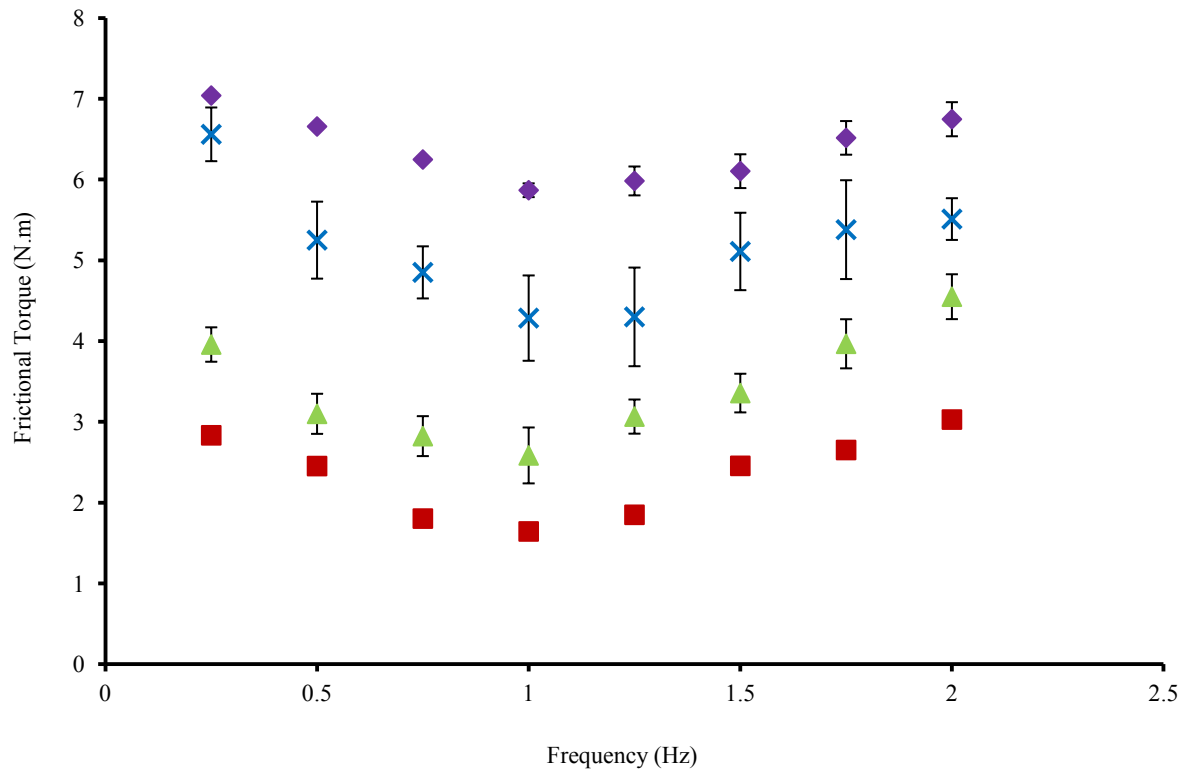


Figure 5.1. Mean frictional torque plotted against frequency for the sample with a ball radius of 10 mm, in flexion, under the loads of 50 (■), 600 (▲), 1200 (×) and 2000 N (◆). Error bars represent standard deviations; when error bars are not shown they are smaller than the symbols used to represent the data points

There was a positive linear correlation between mean frictional torque and load for all motions and all ball radii, in the range investigated, as expected. An example is shown in Figure 5.2, where there is a significant linear correlation between the mean frictional torque and load, in flexion, for all ball radii.

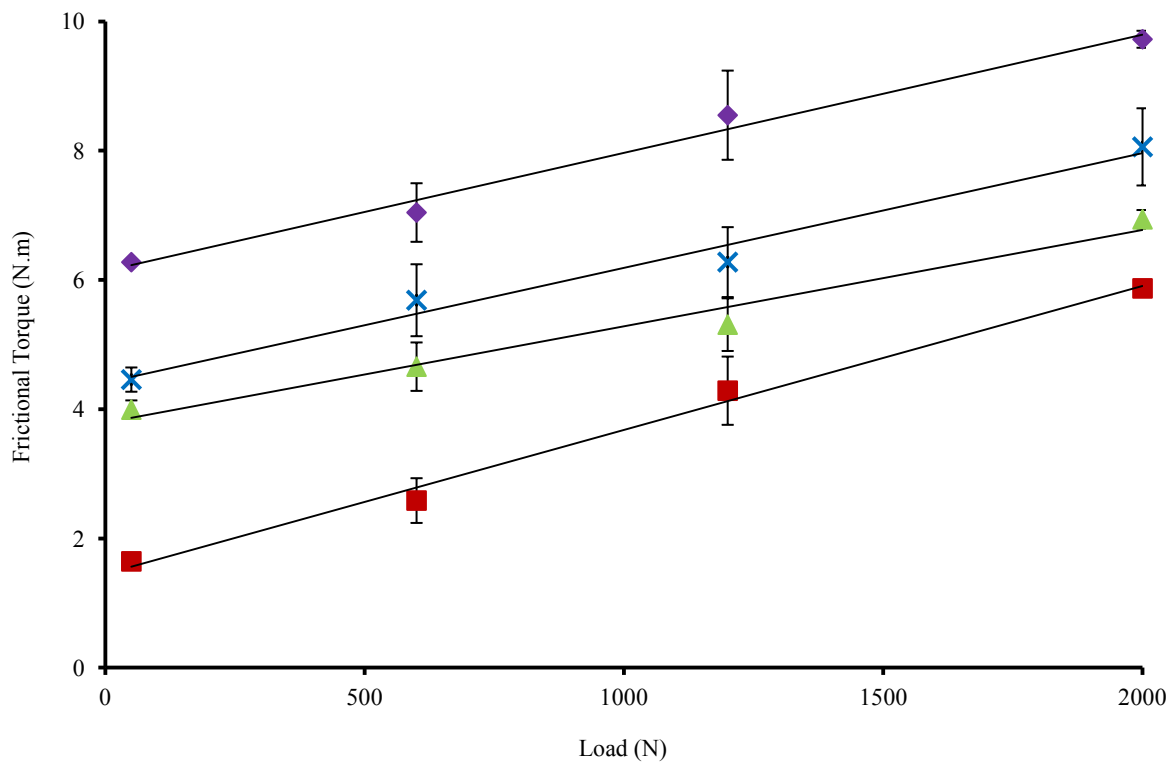


Figure 5.2. Mean frictional torque plotted against load for flexion at a frequency of 1 Hz, for implants with ball radii of 10 (■) ($R^2 = 0.99$, $p = 0.004$), 12 (▲) ($R^2 = 0.98$, $p = 0.012$), 14 (×) ($R^2 = 0.98$, $p = 0.009$) and 16 mm (◆) ($R^2 = 0.99$, $p = 0.006$). Error bars represent standard deviations; when error bars are not shown they are smaller than the symbols used to represent the data points. Regression lines are fitted through the data points

Figure 5.3 shows a significant linear correlation between frictional torque and radius, in flexion, at a frequency of 1 Hz, for the range of loads investigated. Similar results were observed for the other motions.

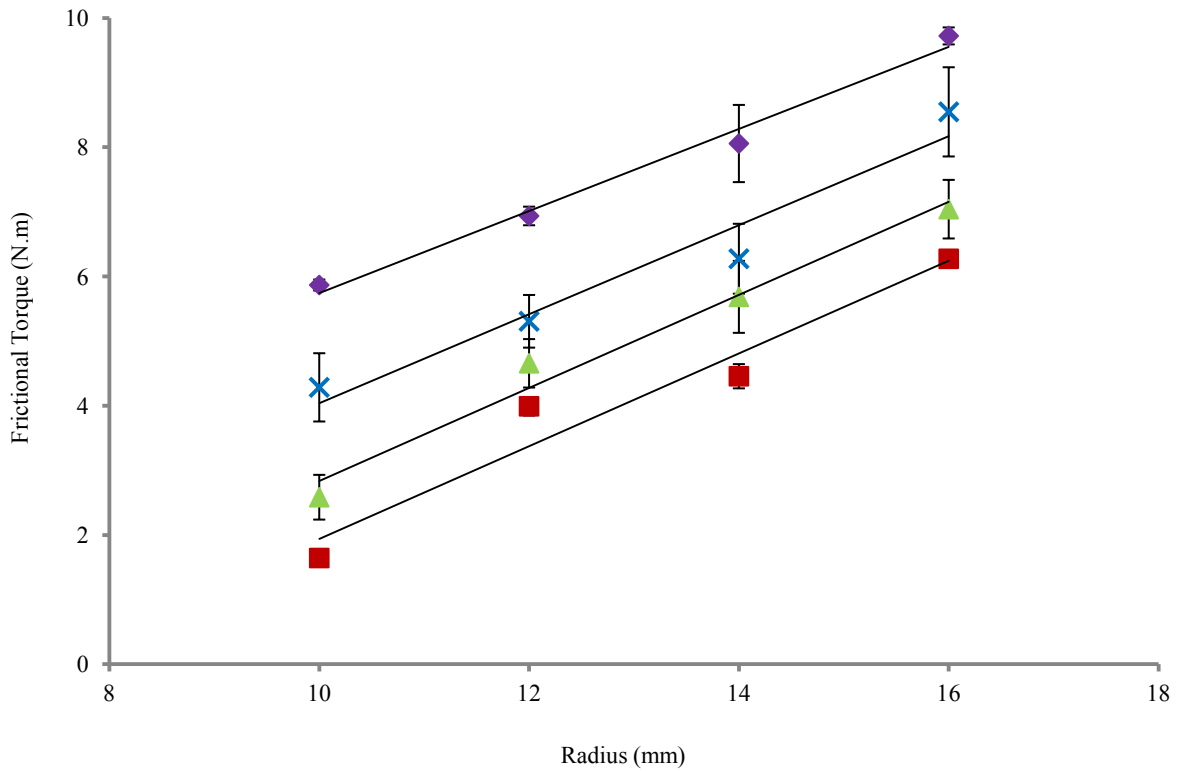


Figure 5.3. Mean frictional torque against radius for a frequency of 1 Hz in flexion motion, under the loads of 50 (■) ($R^2 = 0.95$, $p = 0.028$), 600 (▲) ($R^2 = 0.98$, $p = 0.011$), 1200 (×) ($R^2 = 0.95$, $p = 0.025$) and 2000 N (◆) ($R^2 = 0.99$, $p = 0.006$). Error bars represent standard deviations; when error bars are not shown they are smaller than the symbols used to represent the data points. Regression lines are fitted through the data points

5.4.2. Lubrication regime analysis

To investigate the lubrication regimes, Stribeck curves were plotted for each motion. The Stribeck curves for the sample with a ball radius of 10 mm, in flexion, (Figure 5.4) showed an initial decrease in friction factor and a gradual increase as Sommerfeld number increased. It was observed that the graphs go through a clear minimum. The results for 50 N load has been omitted from the graphs, as the values of friction factor were much higher than those for other loads and so could not be shown clearly on the same axes.

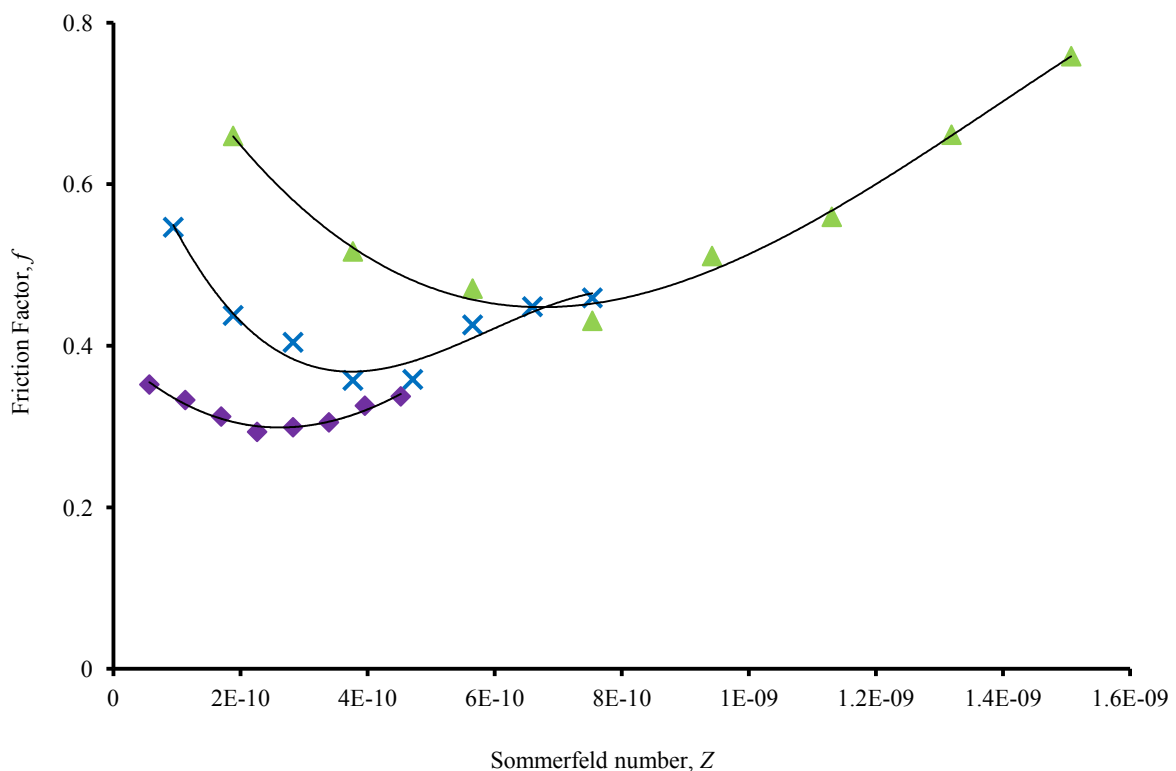


Figure 5.4. Stribeck curves for sample with a ball radius of 10 mm, under loads of 600 (\blacktriangle), 1200 (\times) and 2000 N (\blacklozenge), operated in flexion. A third order polynomial has been fitted to the points.

For the sample with 12 mm ball radius, in flexion, the friction factor showed a slight decrease and then a gradual increase with increasing Sommerfeld number. The pattern was similar to that in 10 mm sample, but flatter. Similarly, the graphs went through a clear minimum (Figure 5.5).

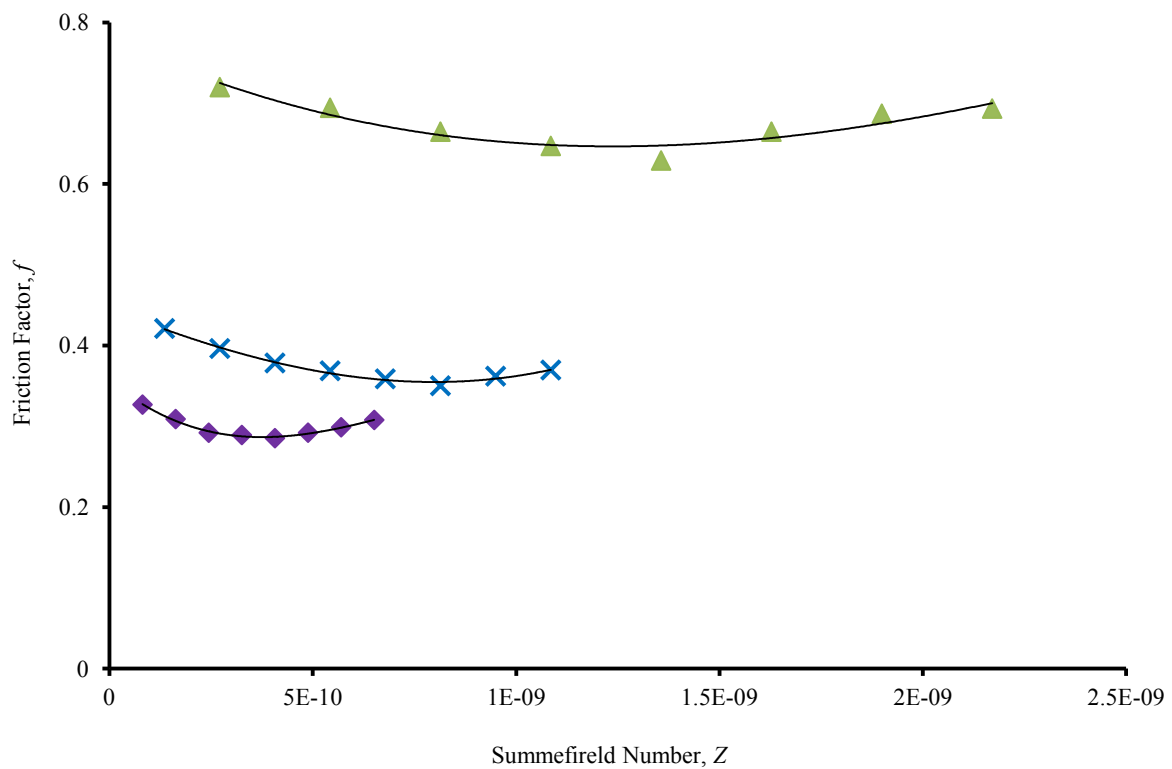


Figure 5.5. Stribeck curves for sample with a ball radius of 12 mm, under loads of 600 (\blacktriangle), 1200 (\times) and 2000 N (\blacklozenge), operated in flexion. A third order polynomial has been fitted to the points.

For the 14 mm ball, in flexion, curve at 600 and 1200 N followed the same pattern as those for 12 mm sample (Figure 5.6). At 2000 N, the friction factor initially decreased and then flattened out of a fairly constant value, with increasing Sommerfeld number. The graph had clear minimum for 600 and 1200 N but not for 2000 N loads.

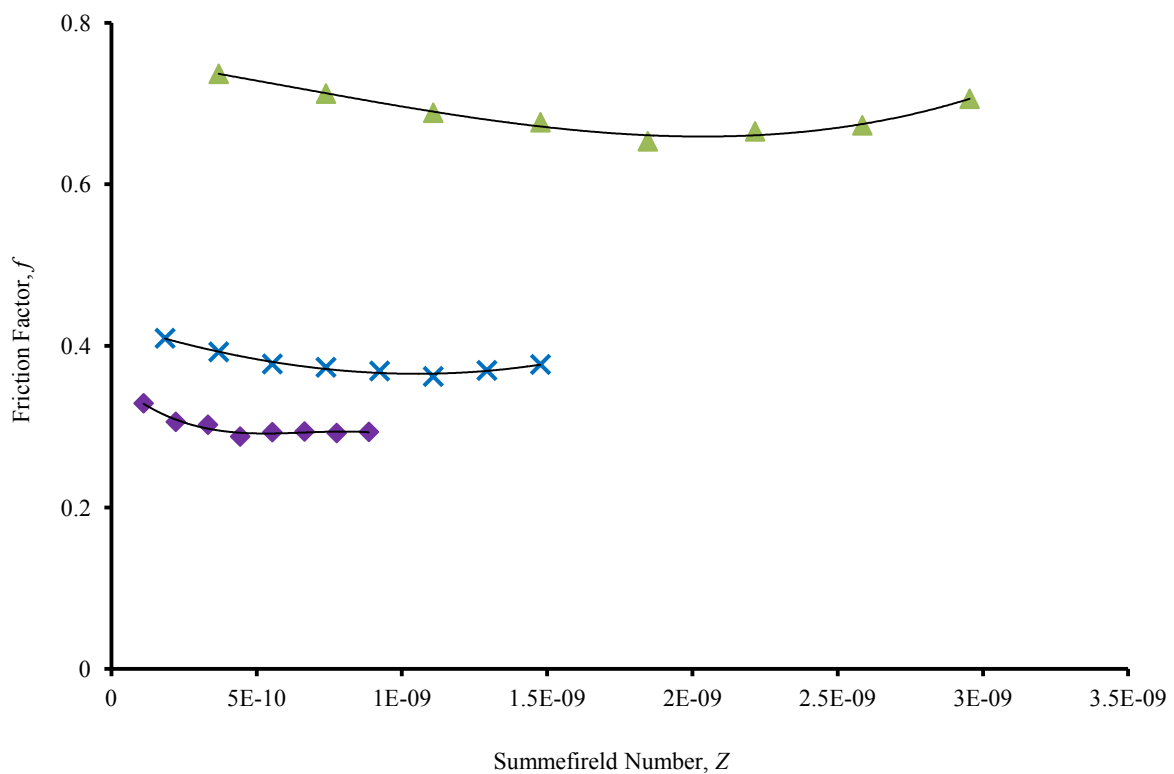


Figure 5.6. Stribeck curves for sample with a ball radius of 14 mm, under loads of 600 (\blacktriangle), 1200 (\times) and 2000 N (\blacklozenge), operated in flexion. A third order polynomial has been fitted to the points.

For the 16 mm ball, in flexion, (Figure 5.7), the friction factor at 600 N initially decreased and then slightly increased, with increasing Sommerfeld number. At 1200 and 2000 N, the friction factor initially decreased and then flattened out of a fairly constant value. The graph has clear minimum for 600 N but not for higher loads. For all ball radii, the results obtained from axial rotation, extension and lateral bend followed similar trend to those for flexion.

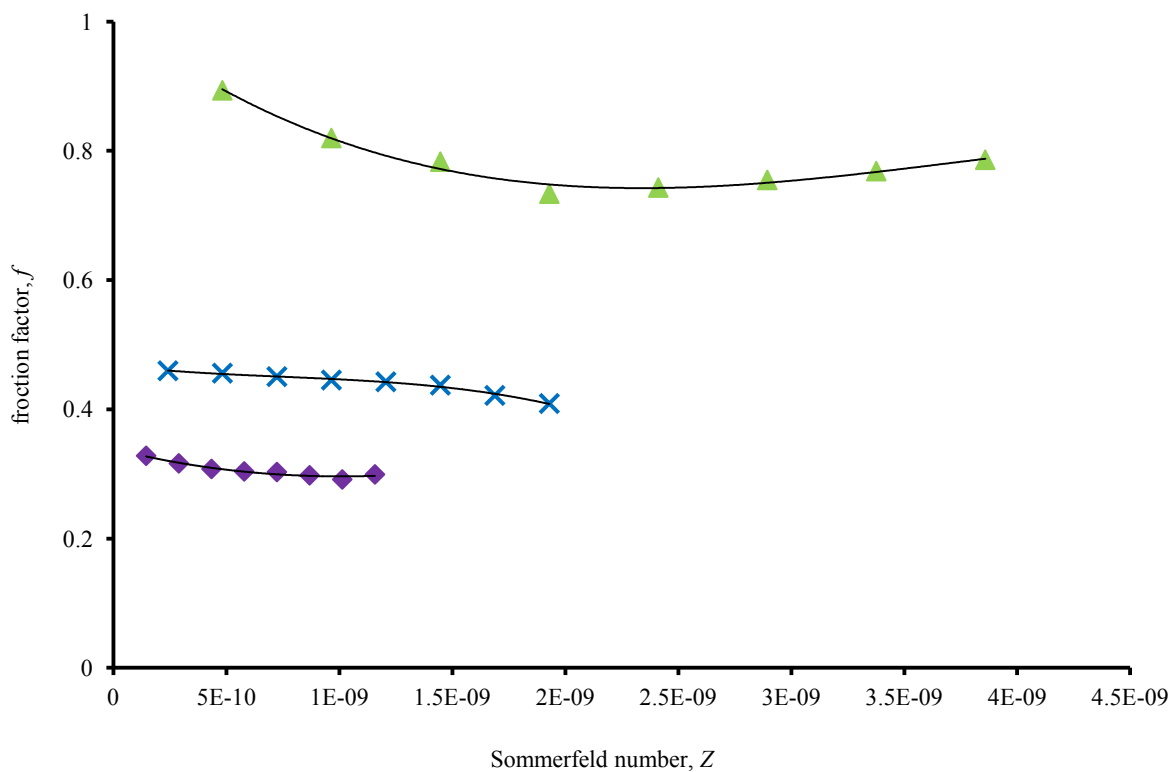


Figure 5.7. Stribeck curves for sample with a ball radius of 16 mm, under loads of 600 (\blacktriangle), 1200 (\times) and 2000 N (\blacklozenge), operated in flexion. A third order polynomial has been fitted to the points

5.5. Discussion

A linear correlation between frictional torque and load was found, as expected. This indicates that by increasing the axial load on TDAs, a higher frictional torque between the articulating surfaces is created. Ma et al. (1983) and Unsworth (1978) found a similar correlation between frictional torque and load in metal-on-metal and polymer-on-metal THAs. The frictional torque significantly decreased with ball radius; this result is also to be expected since the average frictional torque is given by $T = \frac{4}{\pi} \mu L r$, where μ is the coefficient of friction, L is the applied load and r is the ball radius (Gore et al., 1981). Streicher et al. (1996) reported similar results for metal-on-metal THAs; they observed that by reducing the diameter, the friction is reduced. Also, in a study by Wang et al. (2008b) on THAs, it was shown that an increase in ball diameter results in an increase in friction. Bishop et al. (2008) in another study on metal-on-metal hip joint bearings concluded that bearings with smaller diameter have lower frictional torques.

The friction factors in this study were found to be of the same order as those found in studies on metal-on-metal THAs under similar loads (Scholes et al., 2000a; Scholes et al., 2000b; Scholes and Unsworth, 2000). Frictional torque plotted against frequency showed varying trends that were analysed further by producing Stribeck curves which can give an indication of the lubrication regime (Scholes and Unsworth, 2000). The sample with ball radius of 10 mm showed mixed lubrication at low frequencies and the possibility of fluid film at higher frequency. However, within a motion cycle, it may be also possible that different lubrication regimes act at different times. The sample with ball radius of 16 mm appeared to demonstrate

boundary lubrication as the friction factor was fairly constant with increasing Sommerfeld number. Although a theoretical study (Shaheen and Shepherd, 2007) of ball-and-socket TDAs with radii of 14, 21 and 28 mm, suggested that metal-on-metal disc implants are more likely to show boundary lubrication, the current experimental study showed that it is also possible to achieve mixed or fluid film lubrication. Such lubrication regimes were also found in a study (Smith et al., 2001a) of metal-on-metal THAs, where hip implants with 14 and 18 mm femoral head radii showed mixed and fluid film lubrication, respectively.

The ultimate test of a TDA is after implantation into the human body, but pre-clinical wear testing can be used to determine the potential performance of devices. This is investigated in Chapter 7 of this work.

5.6. Summary

This study has investigated the friction in metal-on-metal TDAs. Frictional torque has been found to increase with load and also with the radius of the bearing surface. The analysis of the Stribeck curves indicated that most metal-on-metal TDAs operate in the boundary/mixed lubrication regime. However, TDAs with a ball radius of 10 mm offer the possibility of fluid film lubrication under high loads and frequencies.

Chapter 6

Polymer-on-Metal or Metal-on-Polymer

Total Disc Arthroplasty?

Effect of Material Combination

on the Friction

6.1. Chapter overview

In this chapter, the two possibilities with polymer and metal combinations for ball-and-socket total disc arthroplasty (TDA) is studied; a metal socket/polymer ball and a polymer socket/metal ball combination. The chapter starts with a brief introduction in § 6.2 on metal-on-polymer TDAs and the reason behind the selection of the new material combination. In § 6.3, the material and method used for this study is described. Results of the study are presented in § 6.4, followed by a discussion in § 6.5. The chapter is closed by a brief summary in § 6.6.

6.2. Introduction

Previously, it was mentioned that the articulation between ball and socket bearing surfaces leads to friction and that the friction needs to be minimised to possibly reduce the generation of wear debris and improve performance of the TDAs (see § 2.10.4). As was previously mentioned in Chapter 2 (§ 2.9.3), in total hip arthroplasty (THA) the idea of “low friction arthroplasty” was initiated by Charnley; he designed a hip replacement with a metal femoral head articulating against polymer acetabular cup (Hall et al., 1994; Joyce, 2009). TDAs have been designed with the material combination the other way round, with a polymer ball articulating against a metal socket. The material combination of THAs has never been applied for ball-and-socket TDAs; hence, one may ask whether a similar approach to the Charnley THA can benefit TDAs by means of generating less friction between the bearing surfaces. The aim of this part of the work was to compare the friction between TDAs with a polymer ball/metal socket and metal ball/polymer socket. The work described in this chapter has already been accepted for publication (Moghadas et al., 2012b).

6.3. Materials and methods

6.3.1. Introduction

In this study the metal and polymer samples were used, where one design had a metal socket/polymer ball and the other a polymer socket/metal ball (see § 3.2.1.3). In both groups, two ball radii of 10 and 14 mm were used, with each sample having a radial clearance of 0.35

mm between the ball and socket (Figure 6.1). Similar fixtures to those in metal-on-metal friction test were used. In order to align the centre of rotation (COR, see § 4.3.2) of the samples correctly to the COR of the simulator, extra plates with thickness of 9 and 2.5 mm were employed for the samples with ball radii 10 and 14 mm, respectively (see § 4.3.2 and § 5.3.1).

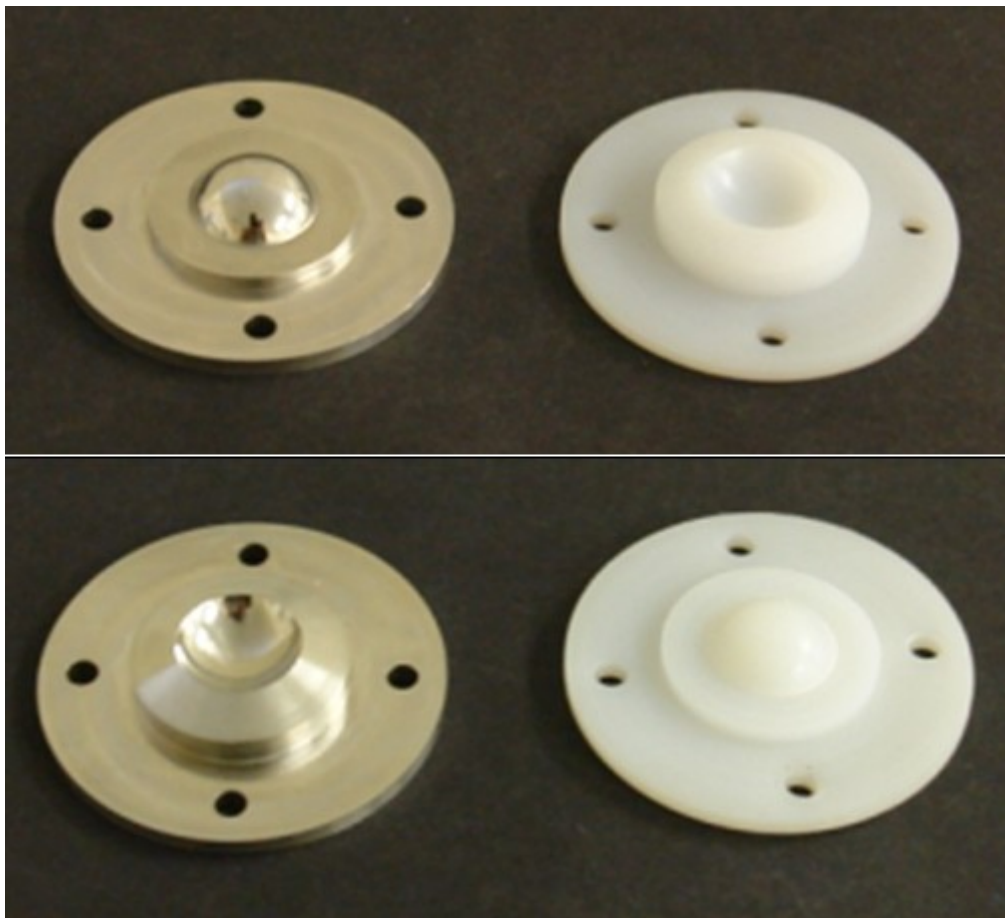


Figure 6.1. The generic model with polymer socket (top right) on metal ball (top left), and metal socket (bottom left) on polymer ball (bottom right) with 10 mm ball radius

The preparation method for both metal and polymer samples followed the same procedure as that described in Chapter 4 (§ 4.3.5). The surface roughness of the samples was measured using the Taylor Hobson Form Talysurf-120L, after they were left at room temperature for 48 hours. The average surface roughness for the balls and sockets are shown in Table 6.1 and were comparable to suggested values for metal and polymer THAs (Jin et al., 1997; Mattei et al., 2011), as well as the in-house measurements of the Maverick™ and the Charite® TDAs, where the average values of surface roughness for metal and polymer bearing surfaces were 0.05 ± 0.001 and 0.80 ± 0.052 μm , respectively. The polymer samples were soaked in distilled water and kept at 37° C for two weeks before the start of each test to allow for any fluid uptake to stabilise.

Table 6.1. The average surface roughness (S_a) of polymer and metal samples, after six measurements

Ball radius (mm)	material	specimen	Average roughness, S_a (μm) \pm Standard Deviation
10	UHMWPE	ball	1.04 ± 0.010
10	CoCr	socket	0.05 ± 0.003
14	UHMWPE	ball	1.05 ± 0.010
14	CoCr	socket	0.05 ± 0.001
10	CoCr	ball	0.05 ± 0.001
10	UHMWPE	socket	0.94 ± 0.075
14	CoCr	ball	0.05 ± 0.002
14	UHMWPE	socket	0.96 ± 0.006

6.3.2 Frictional torque

The samples were mounted to the spine simulator as described in Chapter 4 (§ 4.3.2). Standards BS ISO 18192-1:2008 and ASTM F2423-05 were used to guide through the experiments. The lubricant for this part of the study was diluted calf serum with a protein concentration of 30 ± 2 g/L, at a controlled temperature of 37°C.

The testing conditions were identical to that described in Chapter 4, § 4.3.6. Each sample was tested four times in total; tests were not necessarily performed consecutively, to ensure reproducibility of the results. This means that the decision of switching to a different TDA sample at any point of testing was random; hence, the order of testing could not affect the results. As in previous studies in this thesis, a graph of frictional torque against angle was plotted for each test, using Excel software, to determine the maximum torque generated in each test condition. An average frictional torque was calculated based on the values from the last 10 cycles.

In order to compare the effect of different material combinations and ball radii in similar frequencies, graphs of mean frictional torque against frequency were plotted.

6.3.3. Statistical analysis

To investigate significant differences between the material combinations, error bars to represent the 95% confidence intervals were added to the graphs of frictional torque against frequency. The method of calculating the confidence intervals are presented in Chapter 4, § 4.3.7.

6.3.4. Stribeck analysis

The Stribeck analysis was performed, as described in Chapter 4 (§ 4.3.8), to compare between lubrication regimes under which the samples were acting.

6.4. Results

6.4.1. Frictional torque analysis

The frictional torque was found to be significantly higher for a TDA with a metal socket/polymer ball compared with a TDA with a polymer socket/metal ball for both the 10 and 14 mm samples in axial rotation, since in none of the graphs did the confidence interval error bars overlap (Figure 6.2). At a frequency of 1 Hz, the frictional torque for the samples with 10 mm ball radius was 1.49 N.m for the metal socket/polymer ball combination and 0.66 N.m for the polymer socket/metal ball. The 14 mm radii had frictional torque values of 2.31 N.m (metal socket/polymer ball) and 1.28 N.m (polymer socket/metal ball).

Similar results were also found for lateral bending (graph is shown in Appendix D). In extension (0° to -3°), in most cases the results were significantly different. However, in rare occasions, the results overlapped (Figure 6.3). No overlap between the results was observed when extension motion was reduced to 0° to -2° (see Appendix D).

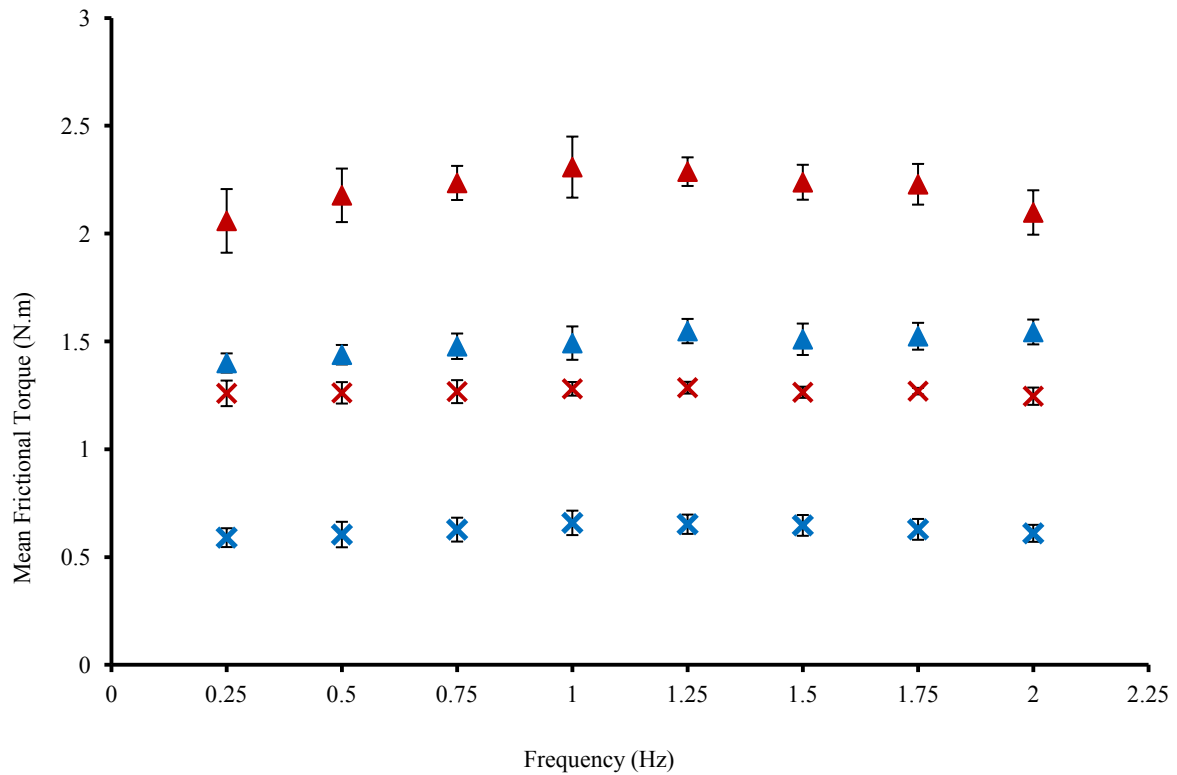


Figure 6.2. Mean frictional torque plotted against frequency, in axial rotation, for the samples with 10 mm ball radius in polymer socket/metal ball (×) and metal socket/polymer ball (▲) combination, and samples with 14 mm ball radius in polymer socket/metal ball (×) and metal socket/polymer ball (▲) combination. Error bars represent 95% confidence intervals; where error bars are not shown, they are smaller than the data points.

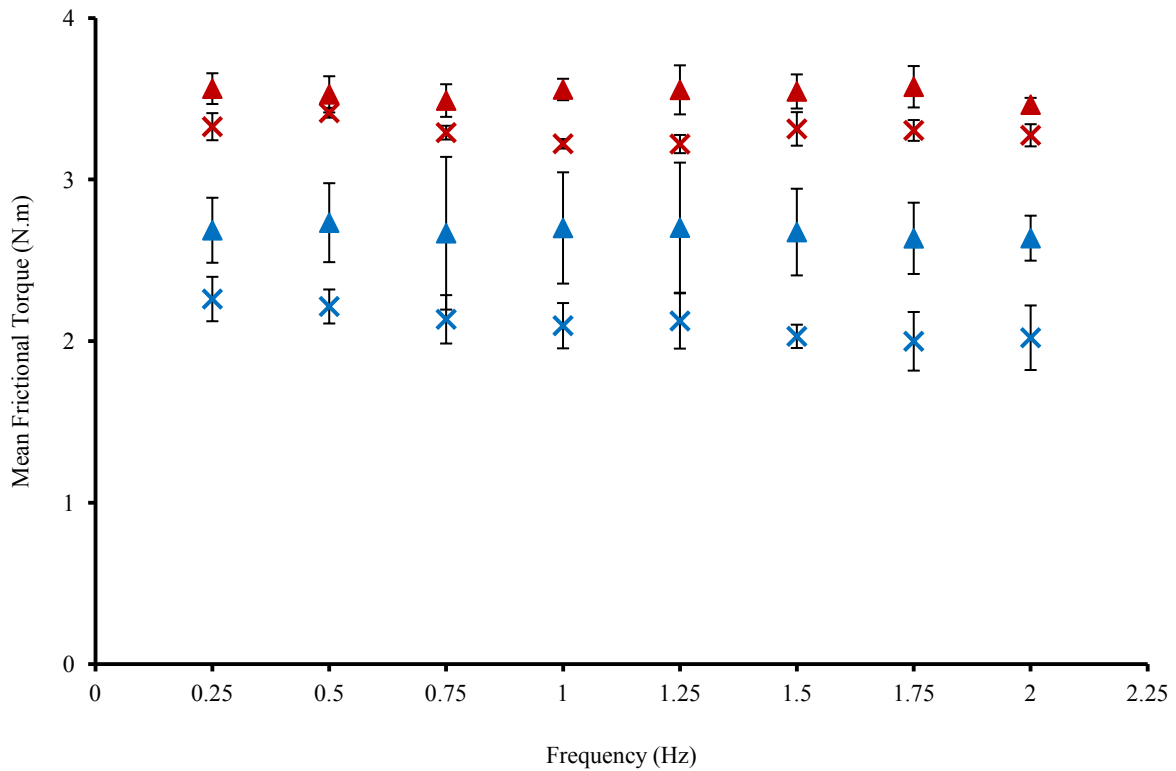


Figure 6.3. Mean frictional torque plotted against frequency, in extension between 0° to -3° , for the samples with 10 mm ball radius in polymer socket/metal ball (×) and metal socket/polymer ball (▲) combination, and samples with 14 mm ball radius in polymer socket/metal ball (×) and metal socket/polymer ball (▲) combination. Error bars represent 95% confidence intervals; where error bars are not shown, they are smaller than the data points.

The frictional torque in flexion (0° to 6°) was not found to be significantly different between the two different material combinations (Figure 6.4). However, when the flexion motion was reduced to 0° to 2° , the friction for the metal socket/polymer ball was found to be significantly higher than for the polymer socket/metal ball (Figure 6.5). At 1 Hz, the metal socket/polymer ball frictional torque was 2.34 N.m, while the polymer socket/metal ball was 1.39 N.m, for the 10 mm radii; values for the 14 mm radii were 3.21 N.m and 1.78 N.m for the metal socket/polymer ball and polymer socket/metal ball, respectively.

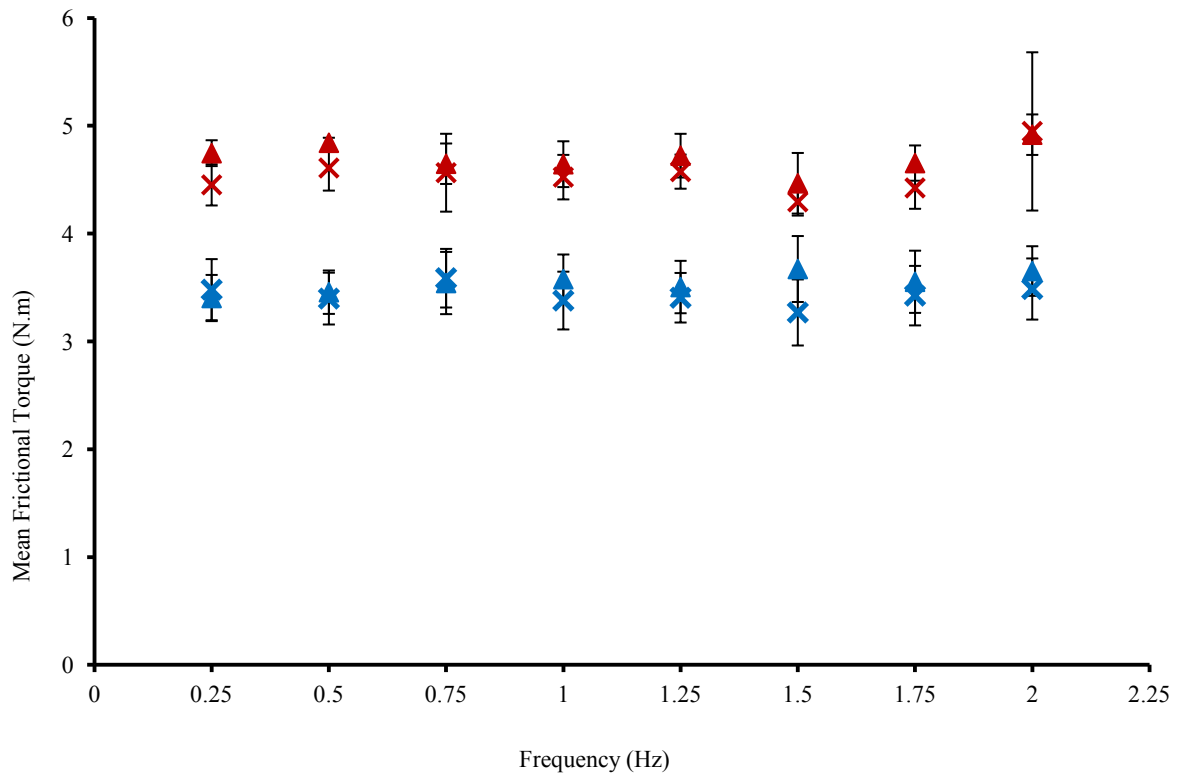


Figure 6.4. Mean frictional torque plotted against frequency, in flexion between 0° to 6° , for the samples with 10 mm ball radius in polymer socket/metal ball (\times) and metal socket/polymer ball (\blacktriangle) combination, and samples with 14 mm ball radius in polymer socket/metal ball (\times) and metal socket/polymer ball (\blacktriangle) combination. Error bars represent 95% confidence intervals; where error bars are not shown, they are smaller than the data points.

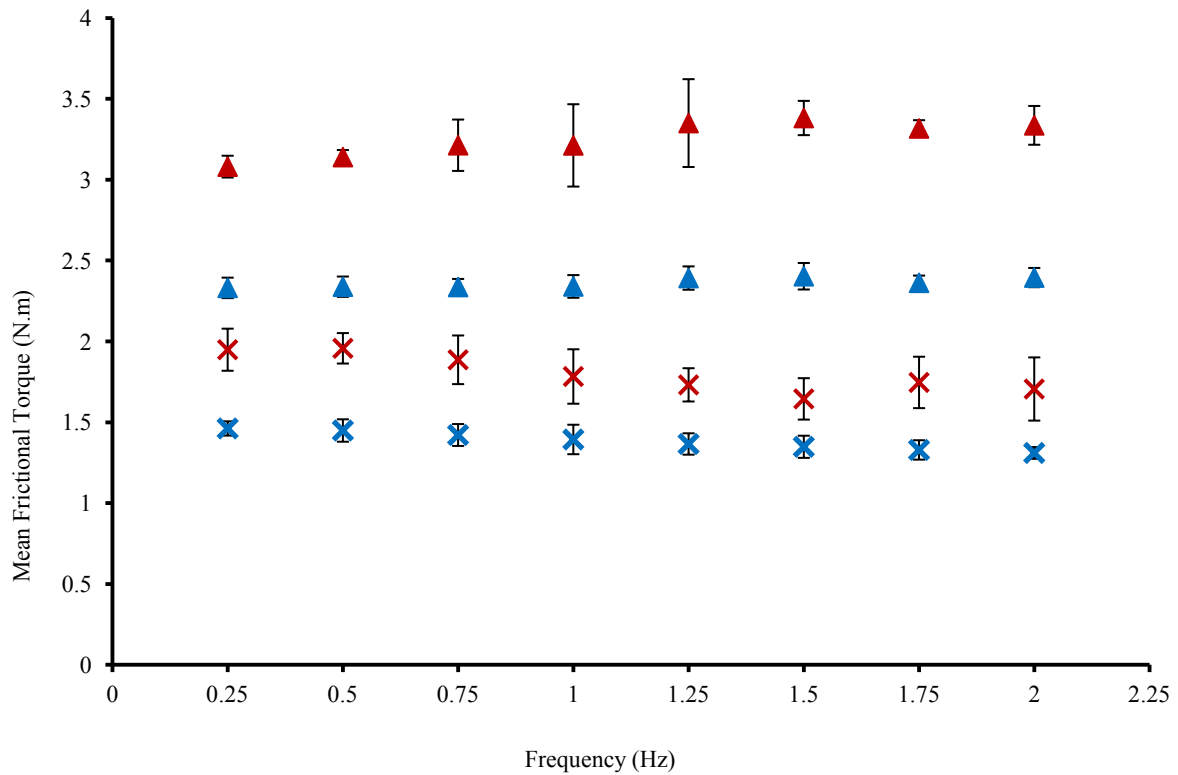


Figure 6.5. Mean frictional torque plotted against frequency, in flexion between 0° to 2° , for the samples with 10 mm ball radius in polymer socket/metal ball (\times) and metal socket/polymer ball (\blacktriangle) combination, and samples with 14 mm ball radius in polymer socket/metal ball (\times) and metal socket/polymer ball (\blacktriangle) combination. Error bars represent 95% confidence intervals; where error bars are not shown, they are smaller than the data points.

6.4.2. Lubrication regime analysis

The Stribeck curves were plotted in order to indicate the lubrication regimes in the samples, under 1200 N compressive axial load. Figure 6.6 presents the results for both material combination of the samples with ball radii 10 and 14 mm, in axial rotation. It can be observed that the friction factor almost flattened with increasing Sommerfeld number for both sample sizes in the case of the polymer socket/metal ball. For the 10 mm sample with the metal socket/polymer ball combination, friction factor gradually increased with increasing Sommerfeld number and then flattened towards the end. With the same material combination for the 14 mm sample, there was a gradual increase and then a gradual decrease from midpoint. This graph passed through a clear maximum.

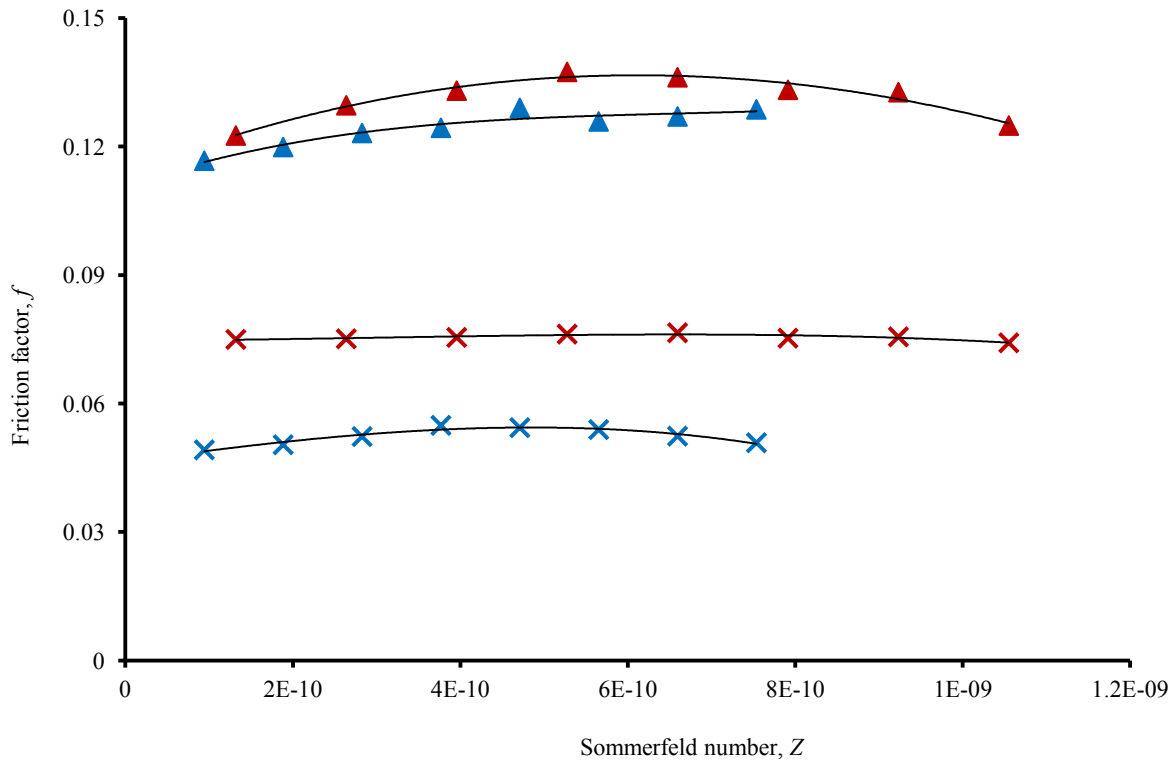


Figure 6.6. Stribeck curves for the samples with 10 mm ball radius in polymer socket/metal ball (×) and metal socket/polymer ball (▲) combination, and samples with 14 mm ball radius in polymer socket/metal ball (×) and metal socket/polymer ball (▲) combination, in axial rotation. A third order polynomial has been fitted to the points.

In Flexion (between 0° to 6°, Figure 6.7), graphs of 14 mm sample for both combinations, and graph of 10 mm sample for polymer socket/metal ball combination showed an initial increase in friction factor, then a gradual decrease and finally a gradual increase as Sommerfeld number increased. The 10 mm sample with metal socket/polymer ball combination showed a gradual increase of friction factor with increasing Sommerfeld number up to the frequency of 1 Hz, and then a sinusoidally-like decrease and increase of friction factor with Sommerfeld number.

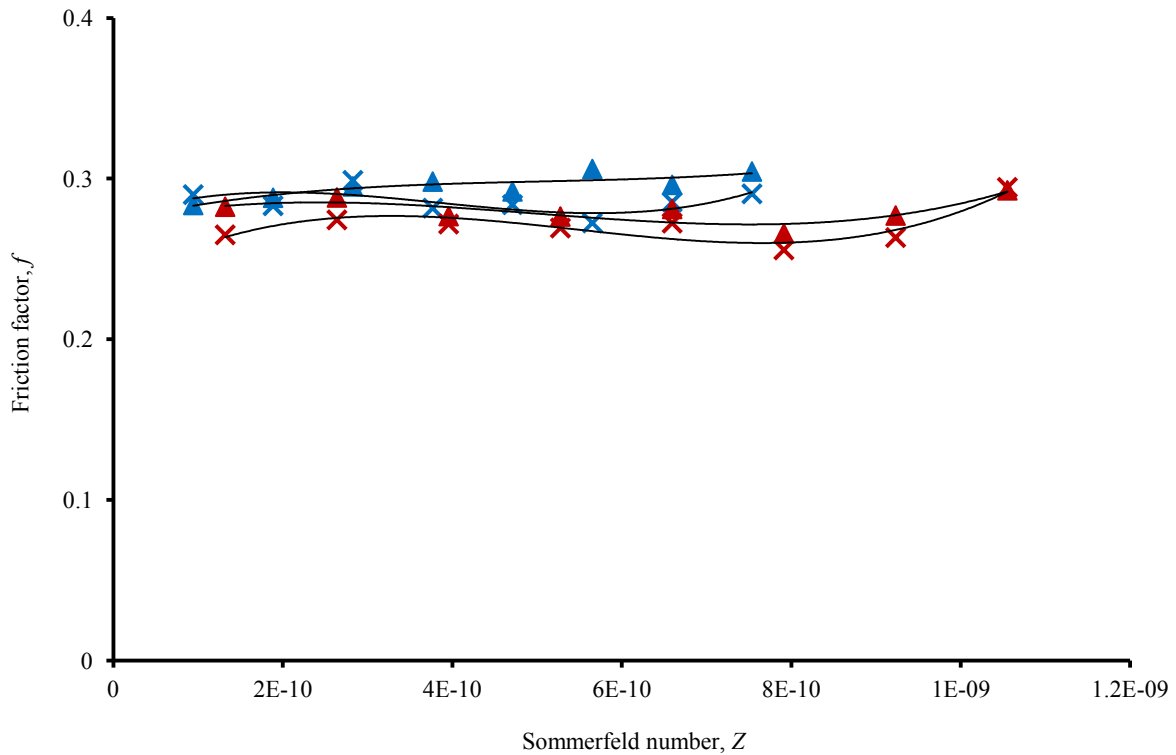


Figure 6.7. Stribeck curves for the samples with 10 mm ball radius in polymer socket/metal ball (×) and metal socket/polymer ball (▲) combination, and samples with 14 mm ball radius in polymer socket/metal ball (×) and metal socket/polymer ball (▲) combination, in flexion between 0° to 6°. A third order polynomial has been fitted to the points.

In lateral bending (see Appendix D), graphs for polymer socket/metal ball for both radii showed a gradual decrease in friction factor with increasing Sommerfeld number. For metal socket/polymer ball combinations, an initial decrease and then an increase towards the end was observed. In extension, between 0° to -3° (also in Appendix D), graphs for 10 mm samples showed a gradual decrease in friction factor as Sommerfeld number increased. For 14 mm samples, the graphs were almost flat.

6.5. Discussion

Current designs of ball-and-socket TDAs have a metal socket articulating against a polymer ball. This is the opposite way round to THAs that have a polymer socket articulating against a metal ball. This study compared the friction between TDAs with metal socket/polymer ball and polymer socket/metal ball articulations. The frictional torques for metal socket/polymer ball devices were found to be significantly higher than frictional torques for polymer socket/metal ball devices in axial rotation, lateral bending and most of the time in extension. A significant difference was also found in flexion and extension, when the range of motion was limited to 0 to 2° and 0 to -2°, respectively. These findings have implications in the design of TDA, where friction should be minimised to reduce the generation of wear debris and implant loosening (Punt et al., 2009). Future designs of TDAs may benefit from having a metal ball articulating against a polymer socket. However, this study has only investigated one aspect of the design, namely friction, and further development and testing would be required to investigate the concept fully, such as wear testing.

The reasons for the difference seen between TDAs with a metal socket/polymer ball and a polymer socket/metal ball articulation at low angular motions (i.e. up to 3°) may be due to deformation of the polymer under load. For the design with a metal socket/ polymer ball, as the load is applied the polymer ball will deform to take up the shape of the metal socket (which has a radius of 10.35 mm or 14.35 mm in this study). For the design with a polymer socket/ metal ball, as the load is applied the polymer socket will deform and take up the shape of the metal ball (which has a radius of 10 mm or 14 mm in this study). By analogy to the previous study in Chapter 5, a smaller radius can be expected to create less friction. Since the

new ball radius of the former at the contact becomes larger than its initial radius, and therefore larger than that in polymer socket/metal ball, it may be concluded that the friction in the metal socket/polymer ball combination becomes higher. Another possibility could be that for the metal socket/polymer ball in low angular motions, the deformation at the point of contact makes it difficult for the metal socket to move in small degrees, since the deformed ball may not roll or slide as well as a non-deformed ball; hence, higher friction is created. However, when the ball moves in higher degrees (up to 6°), the effect of deformation does not disturb the socket movement. This will not be the case for samples with polymer socket/metal ball as the deforming part is the socket. Although conventionally friction is assumed to be independent of area, it has been shown for THAs (with a polymer socket and a metal head) that friction coefficient decreases with increasing contact stress (Wang et al., 2001). Therefore, for the metal socket/polymer ball device in this study, the contact stress will be low (as the contact area is larger) and the friction will be higher.

Regardless of the material combination, the implants with 10 mm ball radius showed lower frictional torque than the implant with 14 mm ball radius. This is in agreement with the results presented in Chapter 5. It is also in agreement with studies on polymer-on-metal THAs (Scholes et al., 2003). For example, Charnley designed a “low friction” THA by reducing femoral head (ball) diameter (Hall et al., 1994).

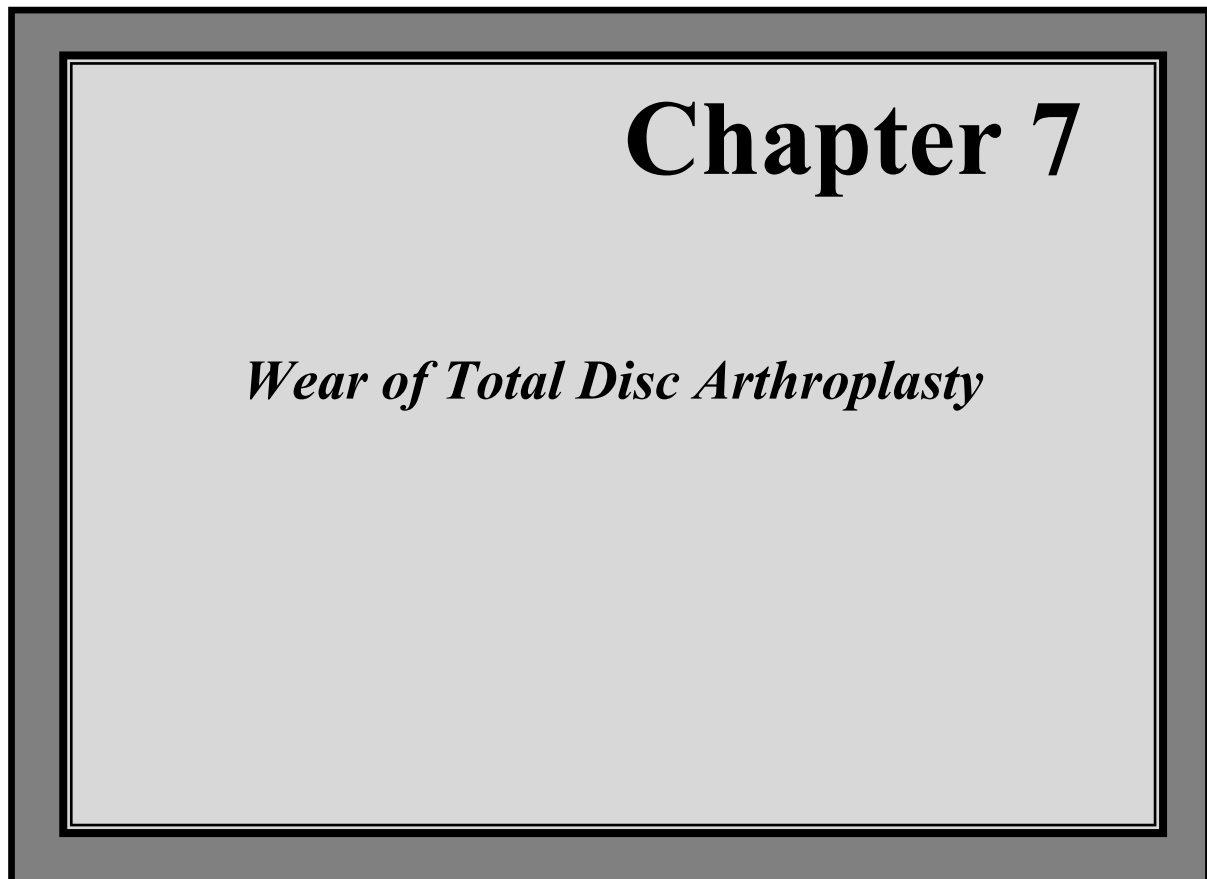
The lubrication regimes for each sample were investigated by plotting the Stribeck curves. The results showed that both radii indicate boundary or mixed lubrication. However, in all cases, except in flexion, the friction factor for the 10 mm sample with polymer socket/ metal ball was the lowest, meaning that less friction was created between the articulating surfaces.

This was in agreement with the results obtained earlier, where in all cases frictional torque was the lowest for the 10 mm sample with polymer socket/ metal ball.

It can be concluded that TDAs with a combination of a polymer socket/metal ball has lower friction than conventional TDAs that have a metal socket/polymer ball. Also, in comparison, the implant with smaller ball radius creates less friction. These findings have implications in the design of TDAs since future designs may benefit from this material combination.

6.6. Summary

Friction between articulating surfaces of ball-and-socket TDAs needs to be minimised to reduce the creation of wear debris and loosening. One of the common material combinations in TDA is the articulation of a metal socket on polymer ball. However, the combination of a polymer socket/ metal ball (which is used in THAs) has not been investigated for TDAs. Therefore, the objective of this part of the study was to compare the friction between a polymer socket/ metal ball and metal socket/ polymer ball TDA. The frictional torque was generally found to be significantly higher for samples with a metal socket/polymer ball compared with samples with a polymer socket/metal ball for both 10 and 14 mm radii. It can be concluded that TDAs with a combination of a polymer socket/metal ball has lower friction than the conventional TDAs with metal socket/polymer ball.



7.1. Chapter overview

The friction studies have been described in previous chapters. In this chapter the wear of metal-on-metal samples and metal-on-polymer Charité® total disc arthroplasty (TDA) are described. The chapter starts with a brief introduction in § 7.2, then the materials and methods for both tests are described in § 7.3. The results of the wear tests are presented in § 7.4 and discussed in § 7.5. A summary of the chapter is provided in § 7.6.

7.2. Introduction

The study of wear has been widely carried out on total hip arthroplasty (THA) and total knee arthroplasty (TKA), to better understand the behaviour of the implants *in vivo*. Wear studies on TDA must be similarly performed in order to reduce wear-related problems. As mentioned in previous chapters, the most common material combinations for TDAs are articulations of metal-on-metal and metal-on-polymer. It was also mentioned that the metal-on-metal articulation offers a very low wear rate in comparison to metal-on-polymer TDAs. The metal-on-polymer articulation experiences much higher wear as a result of a hard-on-soft contact between the bearing surfaces. Such combination creates larger wear particles, in comparison to metal-on-metal wear debris (Anissian et al., 1999; Huang et al., 2002; Tipper et al., 1999). However, in both cases the wear particles create problems, such as toxicity, inflammatory tissue response, bone loss and, therefore, implant loosening.

With wear being one of the leading factors for failure, it is important to understand the behaviour of such implants *in vitro* and compare the two combinations under equal conditions. Since such comparison have never been done under the same conditions before, the first aim of this part of the study was to investigate the wear rate of metal-on-metal samples and the Charité® TDAs, and compare the results under equivalent conditions. A secondary aim was to compare wear of Charité® TDAs under similar conditions but using two different spine simulators: the Bose SDWS-1 Spine Simulators at the University of Birmingham and a six-station Prosim Spine Wear Simulator (Simulation Solutions Ltd., Stockport, UK) at the University of Leeds. This comparison was made to ensure that Bose spine simulator gave comparable results to the established Prosim spine simulator.

7.3. Materials and methods

7.3.1. Materials

7.3.1.1. Implant and fixtures for the Charité® wear test

For this part of the study, four samples of Charité® TDA with the smallest size (Size 1) and thinnest (7.5 mm) UHMWPE core, and parallel (0 degree) Size 1 endplates were used (Charité® Artificial Disc, 2006) (Figure 7.1).



Figure 7.1. The Charité® TDA

As the geometry and shape of the implants were different from those in previous studies, new fixtures were designed to enable complete fixation of the Charité® to the simulator. The basic structure of the fixtures was similar to the previous designs in Chapters 4 to 6, and the heights of the fixtures were modified to enable correct positioning of the centre of rotation (COR). The difficult part was how to fix the endplates into the fixture, so that it rigidly sits exactly at the centre. In some studies on TDAs (Serhan et al., 2006; Vicars et al., 2010), the fixtures include a semi-hollow cylinder with the hollow part being slightly larger than the

endplates. The hole is filled with bone cement and the endplate is placed into the hole. Although the endplate in this case is rigid, there are several disadvantages with such fixtures. Bone cement cures fast; therefore, it is important to position the implant quickly and correctly to the centre of the fixture. This may be difficult to achieve without a marker or an external object which can guide the endplate to the centre. Even if that was achieved, the endplates need to be perfectly horizontal, hence, a further problem is created as a plate or lid needs to be placed on top of the endplate to insure it will settle in the bone cement horizontally. Another disadvantage is that once the test is complete, it may be impossible to take the endplates out of the fixtures and therefore, neither the endplates nor the fixture can be used for further analysis or studies.

To overcome the problems associated with the current fixtures, I decided to design fixtures that do not require bone cement fixation. Therefore, instead of having a semi-hollow cylinder much larger than the endplate, the fixtures were designed based on the actual shape of the endplates to enable perfect fit to the fixture with clearance of ± 0.1 mm. To assure the endplate is fixed into place and does not come out or move, hollow lids were designed to screw on top of the endplates after insertion. To avoid overlapping with the socket of the endplates, the lid thickness was very small (1 mm). An extra hole was designed through the centre of the fixture to enable the endplate to be easily removed by tapping it with a metal rod.

The fixtures and lids were manufactured by Westley Engineering Ltd., using stainless steel – Grade 316. Figure 7.2 shows an example of the endplate, fixture and the lid and Figure 7.3 presents the assembly method. The engineering drawings can be found in Appendix E.

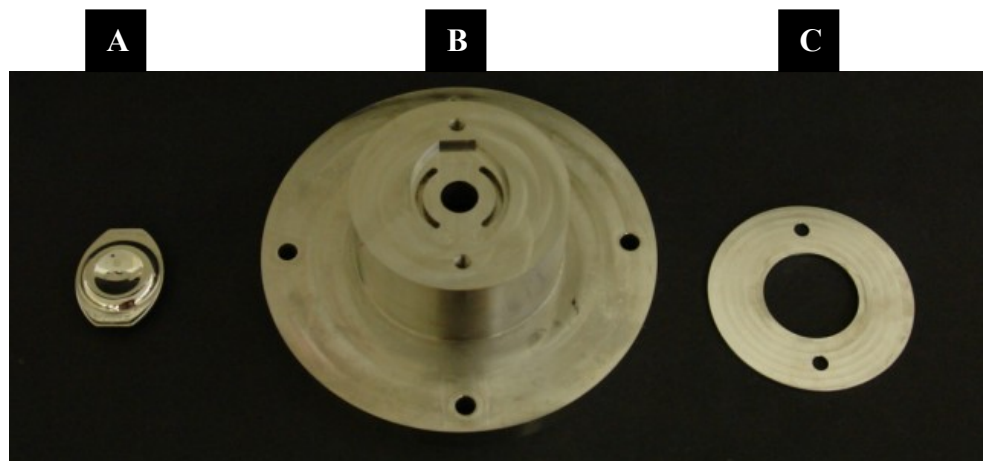


Figure 7.2. The endplate (A), fixture (B) and lid (C)

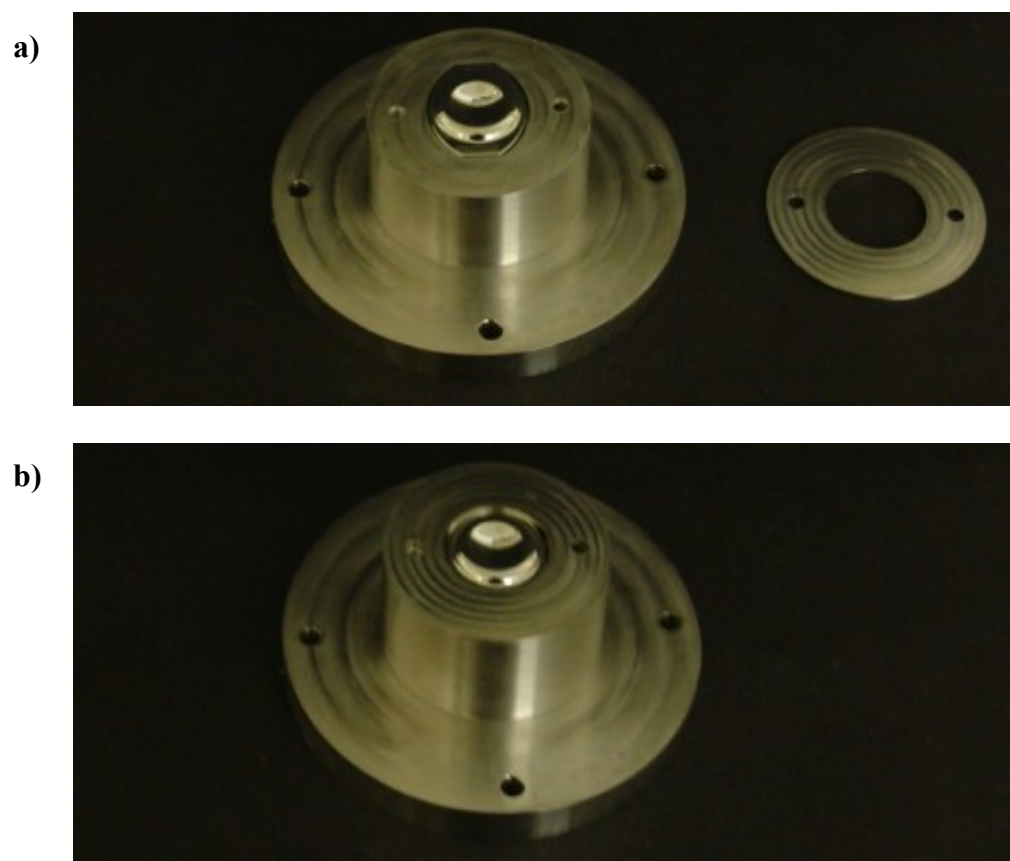


Figure 7.3. The assembly method of the Charité® endplate to the fixture. a) The metal endplate is placed into the fixture, and b) the lid is placed on top to secure the endplate in place

7.3.1.2. Implant and fixtures for the metal-on-metal wear test

The samples used for the metal-on-metal wear test were the generic TDA models (described in Chapter 3, § 3.2.1.2) with a ball radius 10 mm and a radial clearance of 0.015 mm between the ball and socket. Three specimens were used to enable comparison of wear between similar implants.

Two fixtures were manufactured by Westley Engineering Ltd., similar to those for friction test (see § 4.3.2). As the new fixtures were purely made for the purpose of this test, their overall length was increased to 9 mm, instead of using the “extra plates” method that was used for the friction tests in Chapter 4 to 6.

7.3.1.3. Testing equipment

For the Charité® wear tests three machines were used: two spine simulators with a uni-axial Bose 1010CCH-1K-B load cell (Chapter 3, §3.2.3.1), and one Bose ElectroForce® 3330 Series II Test Instrument (Chapter 3, §3.2.3.2), that was used as the load soak control station (more details in § 7.3.2.7). For the wear tests of the metal-on-metal samples, only the two spine simulators with a uni-axial Bose 1010CCH-1K-B load cell were used.

7.3.2. Methods

7.3.2.1. Preparing samples for measurement

The wear tests were performed according to the International Standard BS ISO 18192-1:2008 on wear of TDAs and Standard Operating Protocol for Spine Wear Simulator Studies (SOP01.6) by the Institute of Medical and Biological Engineering, University of Leeds. The initial cleaning procedure for the generic metal samples was identical to that described in

Chapter 3, § 3.3.1 (the cleaning procedure after the initial phase of the tests is described in § 7.3.2.7, as it is slightly different). After samples were cleaned for the first time and left at room temperature for 48 hours, the gravimetric, volumetric and surface roughness measurements were performed (more details in § 7.3.2.2, § 7.3.2.3 and § 7.3.2.4).

It should be noted that neither the Charité® cores, nor the endplates were washed as they had been gamma irradiated and packed in double sealed plastic packages. However, air spray (RS Components Ltd., Northants, UK) was used to remove any possible pores or dust after opening the packs. Before testing, the UHMWPE Charité® cores were kept in plastic containers filled with distilled water, so they could soak. The whole containers were kept in a water bath at 37° C for two weeks, to allow for any fluid uptake to stabilise.

It should be also mentioned that the Charité® TDA contains a metal rim that passes through the groove around the UHMWPE core. This rim was removed right after the implant was taken out of the packages. The rim is designed to detect the location of the UHMWPE core when implanted to the body, since the X-rays cannot detect polymers. As the wear tests of the Charité® TDAs in this study needed to be similar to that in the University of Leeds, the rims were removed.

7.3.2.2. Gravimetric measurement

According to BS ISO 18192-1:2008, gravimetric measurements should be performed to monitor mass loss of the implant during wear testing. The measurements of both metal samples and UHMWPE Charité® cores were carried out using an Ohaus GA200D balance (Ohaus Scales and Balances, Norfolk, UK), with ± 0.2 mg precision. To do the measurement,

each sample was placed on the tray of the balance and the mass was measured and displayed digitally. Each sample was taken off and put back on the tray for further measurement six times and the average mass was calculated. In the case of Charité® test, as the components of interest were the UHMWPE cores, there was no need to measure the mass of the endplates.

7.3.2.3. Volumetric measurement

Another method to monitor wear of the implant is volumetric measurement, which is also recommended by the BS ISO 18192-1:2008. The volume of the UHMWPE Charité® cores were measured with a SkyScan-1172 High-resolution desk-top MicroCT system (SkyScan, Kontich, Belgium), which performs micro-computed tomography (microCT) scans of an object by taking a series of radiographs which are then reconstructed to form 2D and 3D greyscale images. The equipment was available in the School of Dentistry at the University of Birmingham.

The scanning process was carried out by a specialist technician (Dr. Michelle Holder). To perform the measurement, each sample was placed on the base of the scanner. To hold the specimen in place, a cube of packaging foam was grooved and fixed to the base of the scanner with double-sided tape. The specimen was then placed into the groove (Figure 7.4). At the time of scanning the door of the scanner was completely closed.

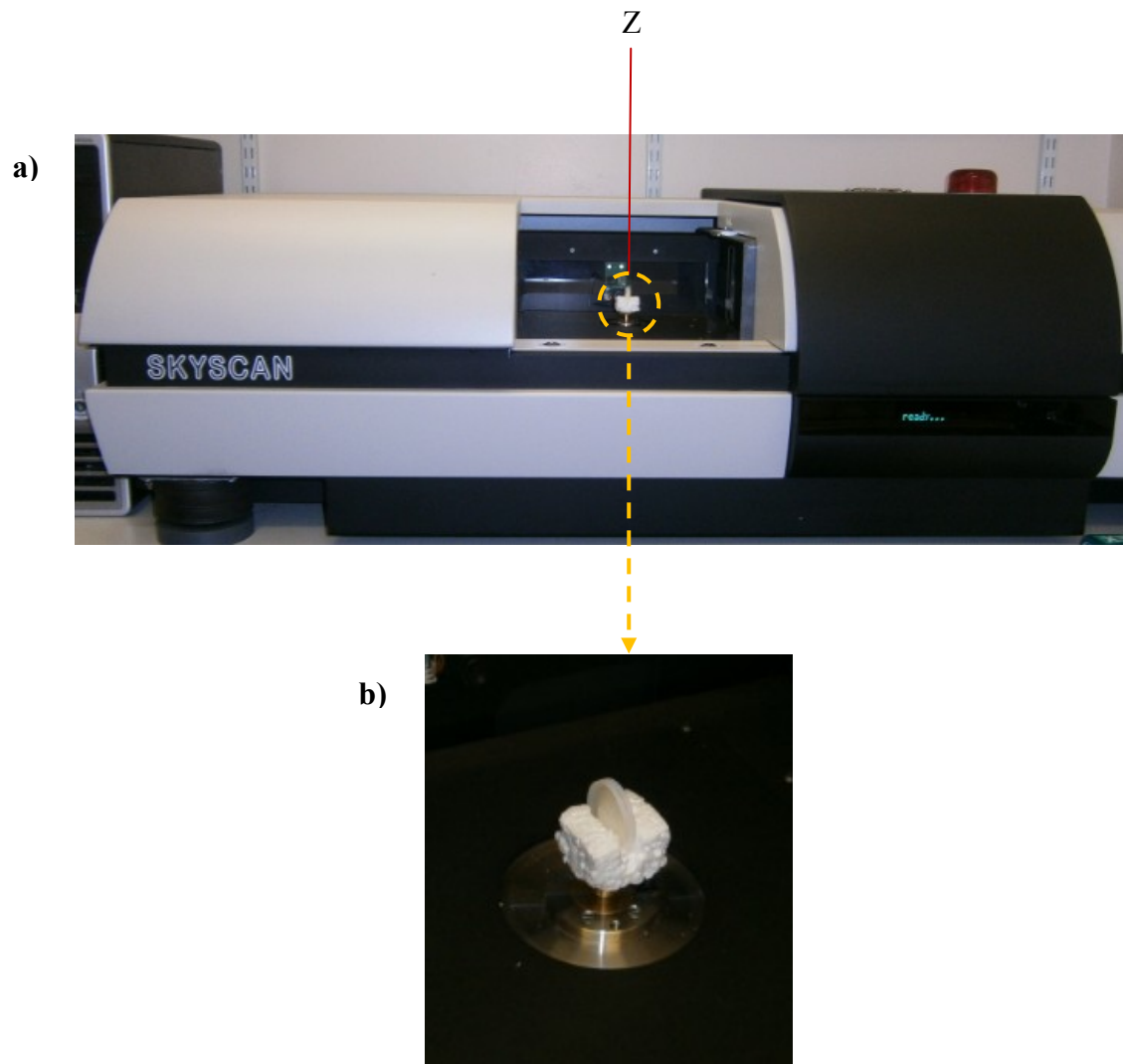


Figure 7.4. a) The SkyScan-1172 High-resolution desk-top MicroCT system and b) the Charite® core inside a grooved packaging foam

The scanning process was controlled by the SkyScan-1172 MicroCT software (SkyScan, Kontich, Belgium). A series of images was taken by the camera inside the scanner. According to the size and material of the specimen, the SkyScan-1172 MicroCT manual suggested the medium camera resolution of 1000×575 plane image matrix. The sample was set to rotate 360° around the Z-axis, as shown in Figure 7.4. The machine was set to take 10 images at every degree of rotation (specialist technician's preference). The voltage of the X-ray discharge was set to 70 kV and the current to 114 mA. These values were all selected by the specialist technician.

After the scanning was completed, the images were reconstructed to form a greyscale 2D image, using the SkyScan-1172 MicroCT software. Images were smoothed by the CTAn software (SkyScan, Kontich, Belgium), where the shadows and lines created by noise were removed from the image, to give a more accurate representation of the core. After smoothing was performed, the images were converted to a 3D greyscale image of the core and the quantitative measurement of the volume was produced. The height of the core was also measured by the software. This procedure was repeated for all four UHMWPE cores.

As the generic metal-on-metal TDA samples were too large for the scanner, volumetric measurement was not possible.

7.3.2.4. Surface roughness measurements of the metal samples

After gravimetric measurements were performed, the 3D surface roughness measurements of the metal samples were carried out using the Taylor Hobson Form Talysurf-120L stylus profiler, as described in Chapter 3 (§ 3.3.2.3).

7.3.2.5. Lubricant preparation

Both metal samples and Charité® TDAs were tested in a solution of calf serum diluted with distilled water to a protein concentration of 15 g/L, at a controlled temperature of 37°C (BS ISO 18192-1:2008). Whilst BS ISO 18192-1:2008 suggests a 30 g/L protein concentration, the SOP01.6 suggests a 15 g/L protein concentration. As one of the aims of the Charité® wear test was to compare between the results obtained from similar tests performed at the University of Leeds, the protein concentration was selected according to the SOP01.6 recommendation. For easy comparison between results obtained from Charité® wear test and the metal-on-metal wear test, the protein concentration for the latter was also taken to be 15 g/L.

The wear test is a long-term process and can be continued for 10 million cycles. It is recommended by BS ISO 18192-1:2008 to replace the fluid completely at least every 0.5 million cycles. To minimise bacterial contamination, it is also suggested to add sodium azide to the diluted lubricant. According to the SOP01.6, 0.3 g of sodium azide powder (Sigma-Aldrich, MO, USA) was added to one litre of diluted calf serum.

7.3.2.6. Viscosity measurement of the lubricant

As the protein concentration of the lubricant for wear testing was different from that for friction tests, the viscosity was measured again in case of any differences. The procedure for the measurement was the same as that described in Chapter 4, § 4.3.4. The viscosity of the 15 g/L protein concentration was 1.2 ± 0.3 mPa.s, in comparison to 1.4 ± 0.4 mPa.s for the same lubricant with 30 g/L protein concentration.

7.3.2.7. *Performing the tests*

After initial gravimetric, volumetric and surface roughness measurements, the samples were fixed to the simulators, using the custom-designed fixtures described in § 7.3.1. The metal samples were mounted to the fixtures by screws, with the sockets fixed to the top and the balls to the bottom plates of the simulators, similar to that for the friction tests. For the Charité®, the metal endplates were first assembled and fitted to the fixture, as described in § 7.3.1.1. Using the split clamps, the top fixtures were mounted to the top plates and the bottom fixtures to the bottom plates of the simulators. The bottom plate on the simulator was then moved down by about 5 mm, to provide enough space for the UHMWPE cores to be placed on the bottom endplates manually. Once the cores were correctly positioned on the bottom plates, the bottom fixtures were moved up until the face of the cores touched the face of the top plates.

According to the BS ISO 18192-1:2008 standard, when performing wear tests on a TDA that includes a polymer component, at least one TDA should be kept in load soak control environment. The load soak control sample only undergoes sinusoidally varying compressive load, with no angular motions. This is to determine any fluid intake of the polymer component. Therefore, one of the Charité® TDAs was kept under the load soak control condition, in the Bose ElectroForce® 3330 Series II Test Instrument. The method of assembly was similar to that for spine simulators; however, since the top plate was the moving part (as described in Chapter 3), the upper fixture was moved up first to enable easy positioning of the core and then moved back down so that the two surfaces meet. After assembly was complete, lubricant was added to the fluid bath and left to reach 37° C. The remaining lubricant was kept in a refrigerator at 5°C, for no longer than seven days. Tables 7.1 and 7.2

show the parameters for lumbar TDA wear test by BS ISO 18192-1:2008 that were used in this study. The two samples inside the spine simulators underwent sinusoidally varying axial rotation, flexion/extension and lateral bending and load, according to the parameters given in Tables 7.1 and 7.2, whilst the load soak control sample only underwent sinusoidally varying compressive load.

Table 7.1. Required angular displacements for lumbar TDA wear test, by the BS ISO 18192-1: 2008

	Flexion/extension	Axial rotation	Lateral bend
Min.	-3°	2°	2°
Max.	6°	-2°	-2°
Frequency (Hz)	1	1	1

Table 7.2. Load parameters for lumbar TDA wear test, by the BS ISO 18192-1:2008

	Load (N)
Min.	600
Max.	2000
Frequency (Hz)	2

Each sample was subjected to a wear test for 5 million cycles. Although the standard suggests 10 million cycles, it has been shown that the wear rate of THAs reaches steady-state after the first few million cycles (Nechtow et al., 2006; Vicars et al., 2010). Similar behaviour was predicted for the wear tests in this study. Therefore, the tests were performed up to 5 million cycles.

To overcome evaporation of the lubricant, the fluid bath was topped up with the diluted calf serum every day. The testing was stopped and the lubricant was completely replaced after every 0.25 million cycles. The procedure was as described below.

- After the whole lubricant was drained out of the fluid bath, the bath was washed with household detergent.
- A solution of Virkon disinfectant powder diluted with tap water (10 mg of powder with 1 litre water) was added to the fluid bath and left for 2 hours, to destroy bacterial contamination.
- The fluid bath was washed once with tap water and twice with distilled water.
- Fresh lubricant was added to the bath and the tests carried out for a further 0.25 million cycles.
- The procedure was repeated every 0.25 million cycles.

The testing was stopped and the specimens were taken out for measurement at 0.5, 1, 2, 3, 4 and 5 million cycles. For the metal-on-metal samples, both components were measured. For the Charité® TDAs, only the UHMWPE cores were taken out and measured. The fluid baths were cleaned as described above. The specimens that were taken out were cleaned as follows:

- washed with household detergents
- soaked in Vircon solution (Vircon powder diluted with tap water, as described before) for 20 minutes
- washed once with tap water and twice with distilled water
- ultrasonically cleaned in a propan-2-ol bath (see § 3.3.1)
- washed again with acetone to remove any traces of grease or dirt
- dried and wiped over with low lint clean-room wipes and kept in plastic boxes in room temperature for 48 hours

After 48 hours, the gravimetric measurements for both metal samples and Charité® cores, volumetric measurements for Charité® cores and surface roughness measurements of metal samples were performed as described in § 7.3.2.2, § 7.3.2.3 and § 7.3.2.4, respectively. This procedure was repeated for all three generic metal-on-metal samples and four Charité® cores at 0.5, 1, 2, 3, 4 and 5 million cycles.

7.3.2.8. Statistical analysis

Based on the gravimetric measurement results, the mass loss was calculated and graphs of mass loss against number of cycles were plotted using Excel software. For these graphs a linear regression analysis was performed, using Minitab software. The mean gravimetric wear rate was calculated from the gradient of the regression line. Also, linear regression analysis was performed, using Minitab software. A similar procedure was applied to measure volumetric wear rate. For the metal samples, as it was not possible to measure volume loss, it was calculated from:

$$V = \frac{m}{\rho} \quad 5$$

where V is the volume, m is the mass and of the sample and ρ is the density of cobalt chrome which is 8.29 mg/mm^3 (Paré et al., 2007). Then from the results, graphs of volumetric wear rates against number of cycles were plotted and the mean wear rate was calculated as described above. The volumes of the Charité® cores were measured by the CTAn software (see § 7.3.2.3). However, in order to compare with the gravimetric measurements, the gravimetric wear results were used to calculate a volumetric wear value using equation 5, with the density of UHMWPE assumed to be 0.94 mg/mm^3 (Vicars et al., 2009).

To investigate whether the two volumetric measurement techniques were in agreement, the Bland-Altman test (Bland and Altman, 1986) was used. Bland and Altman (1986) showed that if a graph of sample one against sample two is plotted (in this case measurement method one against measurement method two) and a high correlation is observed at the line of equality (Figure 7.5.a), they may not necessarily be in agreement. Therefore, in order to find out whether two samples (in this case two measurement methods) are in agreement, a Bland-Altman test needs to be performed. To achieve, scatter-plot of the differences between the means of the values from the two measurement methods (y-axis) was plotted against the means (x-axis) (Figure 7.5.b). Lines of mean difference (\bar{d}) and limits were also plotted. The limits were defined from the following:

$$\bar{d} \pm .96\sigma \quad 6$$

where σ is the standard deviation of the differences (Bland and Altman, 1986). If the two volume measurement methods were in agreement, 95% of differences lie between the limits. Figure 7.5.a shows as example of the correlation between the results from two sets of measurements and Figure 7.5.b gives as example of a Bland-Altman graph, where results are in agreement.

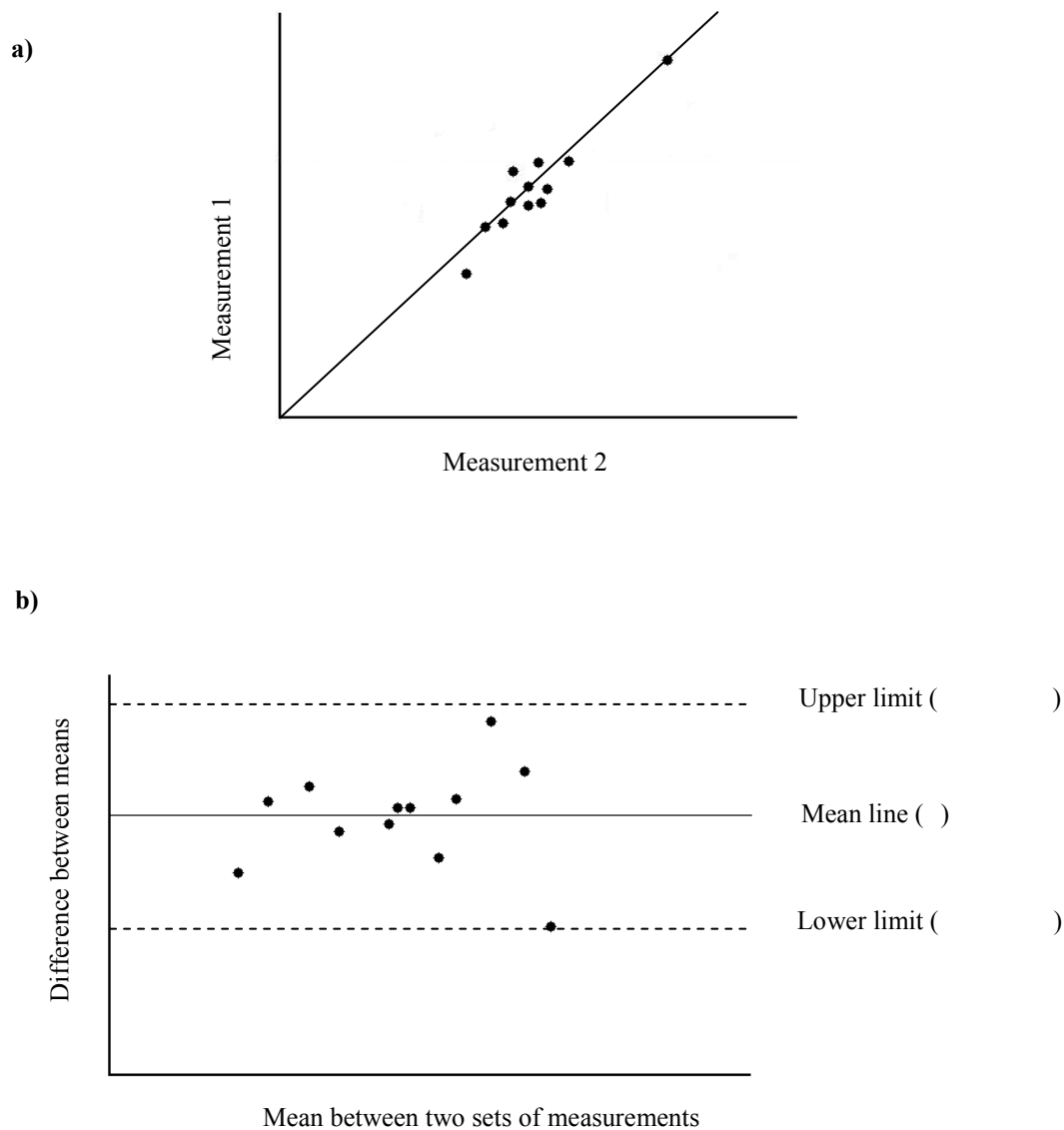


Figure 7.5. An example of a) two measurements with correlation at line of equality and b) Bland-Altman graph with results in agreement (author's own graphs, adapted from Bland and Altman, 1986)

7.4. Results

7.4.1. Wear study of the Charité® cores

The Charité® wear test produced a mean gravimetric wear rate of 12.0 ± 1.4 mg per million cycles, giving an overall mass loss of 60.3 ± 4.6 mg. This, of course, was observed for the three UHMWPE cores that were tested in the spine simulators. A linear mass loss was observed, as can be seen in Figure 7.6. In the gravimetric measurements of the load soak control sample, the mass of the sample appeared to increase from 1277.3 to 1277.8 mg (i.e. an increase of 0.1 mg every 1 million cycles). However, as the mass measured was less than the precision of the balance (0.2 mg), there was no reliable evidence for fluid uptake.

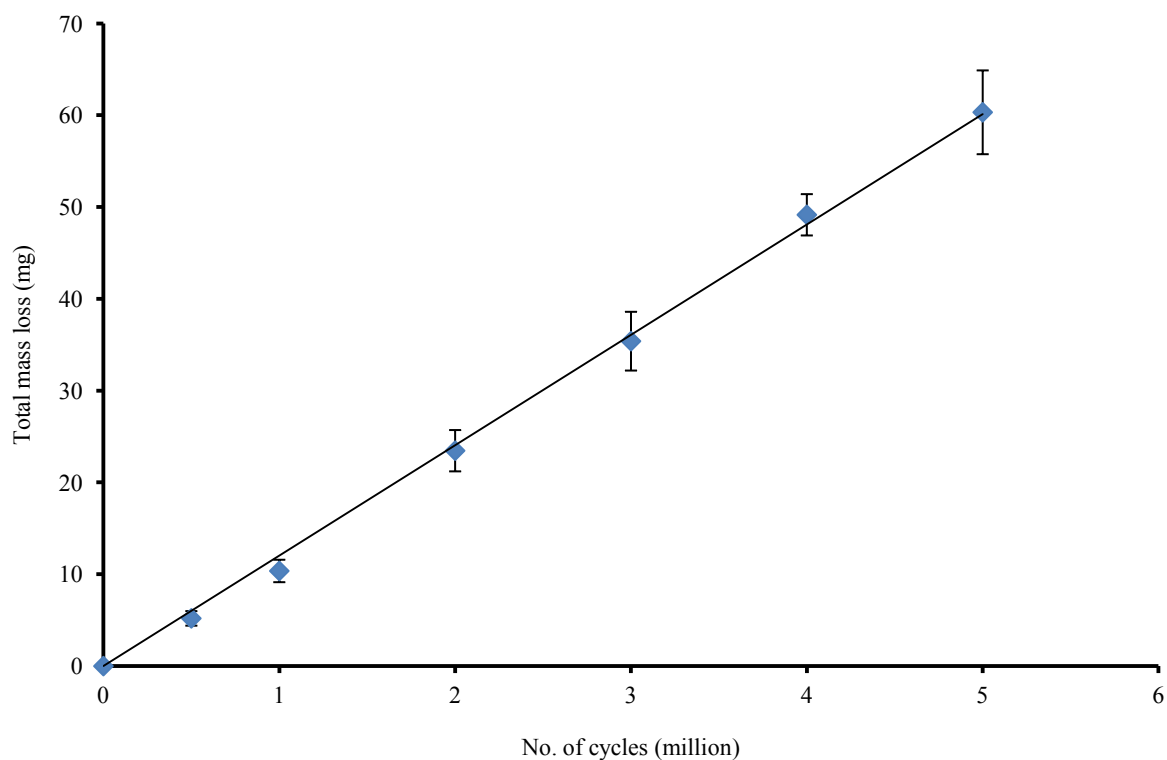


Figure 7.6. The mean mass loss of the Charité® cores. A regression line is fitted through the data points ($R^2 = 0.99$, $p = 0.00$). Error bars represent standard deviations

The experimental mean volumetric wear rate was $12.8 \pm 1.2 \text{ mm}^3$ per million cycles, with an overall volume loss of $64.6 \pm 6.0 \text{ mm}^3$. Results are presented in Figure 7.7. The Bland-Altman plot showed that the two volumetric measurement techniques were in agreement. Figure 7.8 shows that all differences lay between the limits.

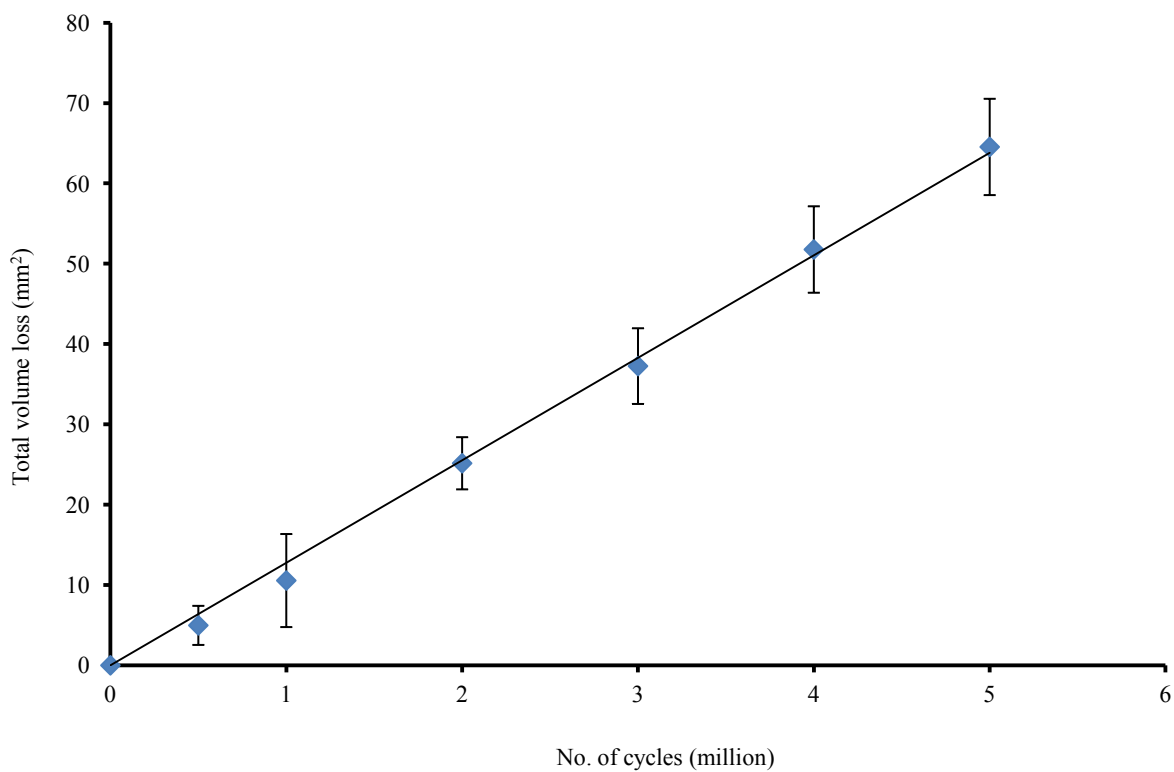


Figure 7.7. The mean volume loss of the Charité® cores. A regression line is fitted through the data points ($R^2 = 0.99$, $p = 0.00$). Error bars represent standard deviations

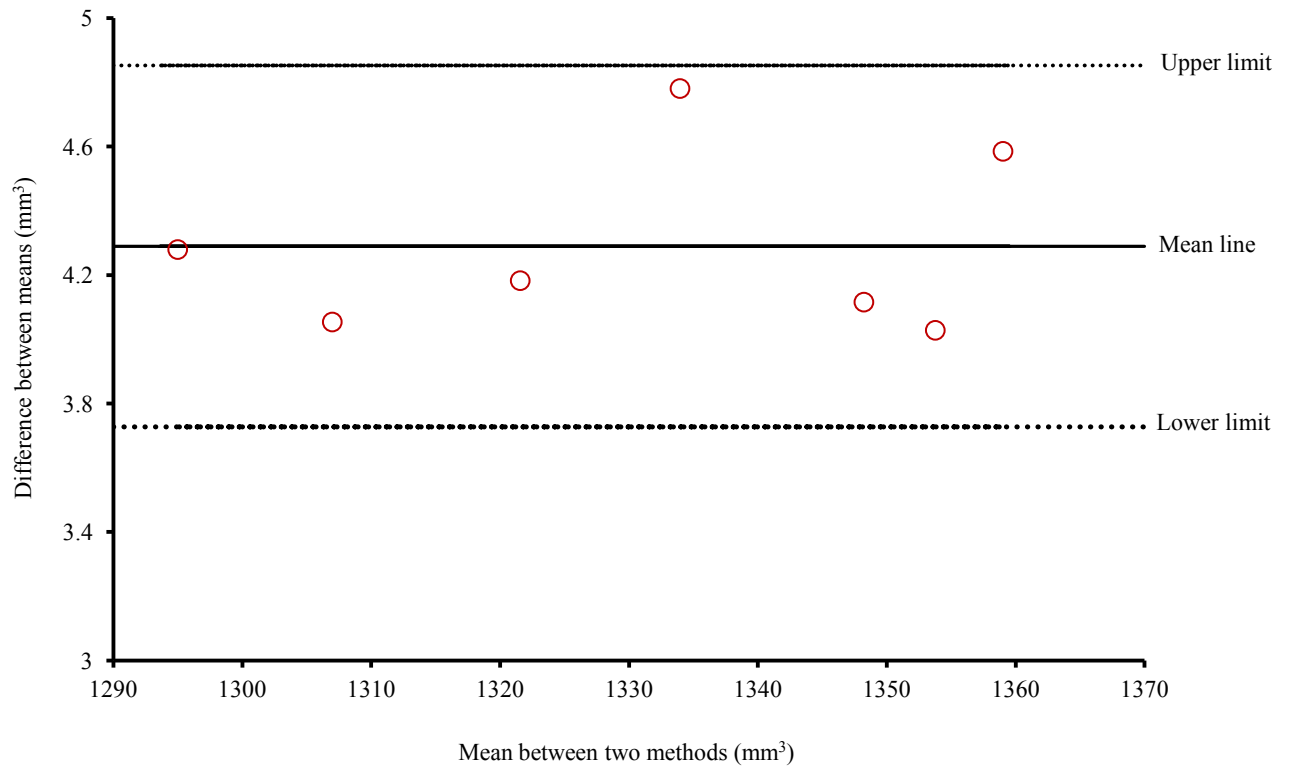


Figure 7.8. *The Bland-Altman graph, with the difference between the means of the values from the two measurement methods against the means*

The 3D microCT images showed a decrease in height for all three samples, where the height changed from 7.5 ± 0.0 (brand new) to 7.1 ± 0.1 mm (after 5 million cycles). No difference in height was observed for the load soak control sample. Figure 7.9 gives an example of the UHMWPE core a) before the test and b) after 5 million cycles.

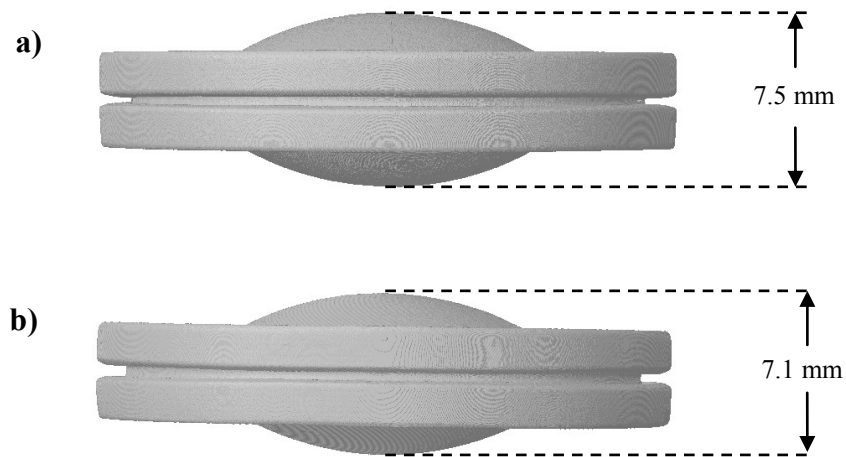


Figure 7.9. The 3D microCT images of the UHMWPE Charité® core a) brand new and b) after 5 million cycles of wear test

7.4.2. Wear study of the metal-on-metal samples

The wear of the metal-on-metal samples exhibited an initial run-in period for the first million cycles, followed by a steady-state wear rate. As two mechanisms happened, two separate regression lines were fit through each phase of data. The gravimetric wear rate in the run-in period was 8.5 ± 0.7 mg per million cycles, followed by a steady-state wear rate of 3.2 ± 0.3 mg per million cycles. The overall mass loss was 21.0 ± 1.0 mg. Figure 7.10 shows the mean mass loss for all three samples.

In order to understand whether the fit obtained by splitting the graph into two linear sections was statistically significant, an F-test (Bevington, 1969) was performed by Excel. In this approach:

$$F = \frac{Q_1 + 2Q_2}{(N - 1) / 2Q_2} \quad 7$$

where Q_1 is the sum of the squared deviations for a single line and Q_2 is that for two lines; N is the number of data points. The F-values obtained from the results are compared with $F_{2, N-4}$ tabulated at the 5% level (the table can be found in Bevington, 1969). If the calculated F exceeds the tabulated value, the two lines are considered significantly better fit than one. In the case of this study, the number of data points were 7, therefore for the two lines to be significantly better fit, the F-value needed to be larger than 9.55 (according to the table in Bevington, 1969). The results obtained from Excel showed that the two lines gave a significantly better fit ($F > 9.55$, $p < 0.05$).

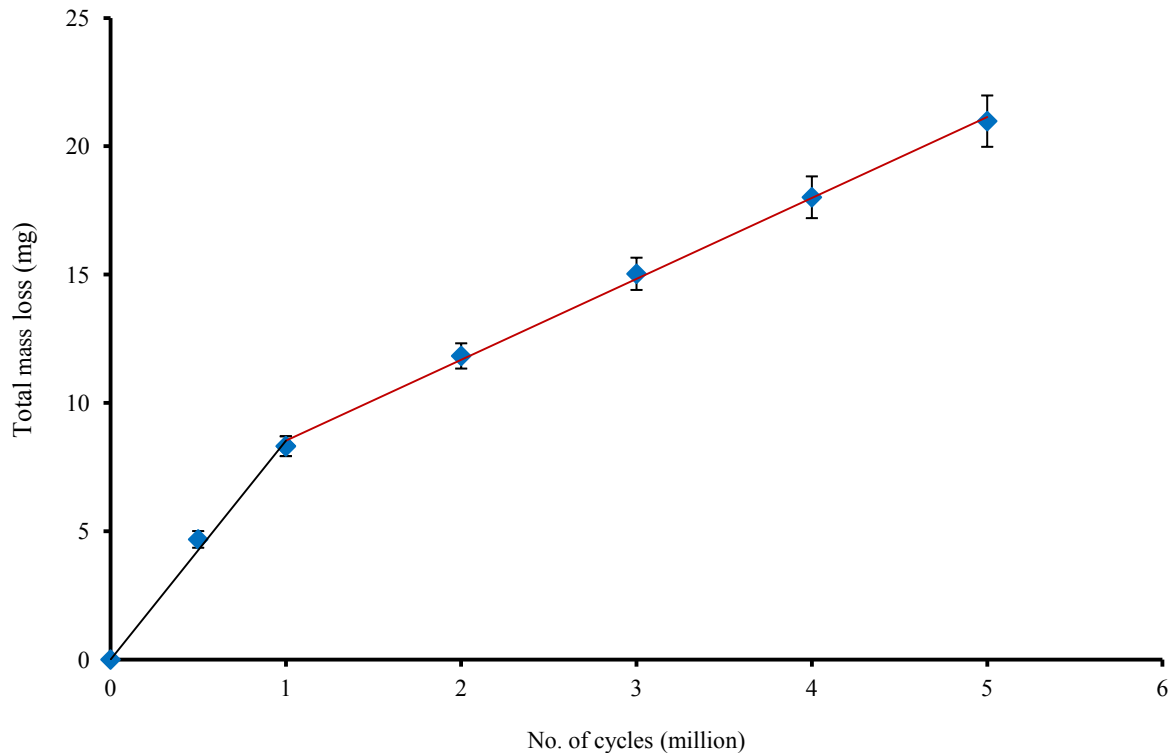


Figure 7.10. The mean mass loss of the metal-on-metal samples. A regression line is fitted through the data points (for 0 to 1 million cycles, $R^2 = 0.99$, $p = 0.046$; for 1 to 5 million cycles, $R^2 = 0.99$, $p = 0.00$). Error bars represent standard deviations

The volumetric wear was calculated as described in § 7.3.2.8. Similar to gravimetric wear, there were two phases; hence, a similar approach was applied to find the wear rate. For the initial run-in phase in the first million cycles, the wear rate was $1.0 \pm 0.1 \text{ mm}^3$ per million cycles, followed by a steady-state wear rate of $0.4 \pm 0.03 \text{ mm}^3$ per million cycles thereafter. The overall volume loss was $2.5 \pm 0.1 \text{ mm}^3$. Figure 7.11 presents the mean volume loss for all three samples. The F-test showed that the two lines gave a significantly better fit ($F > 9.55$, $p < 0.05$).

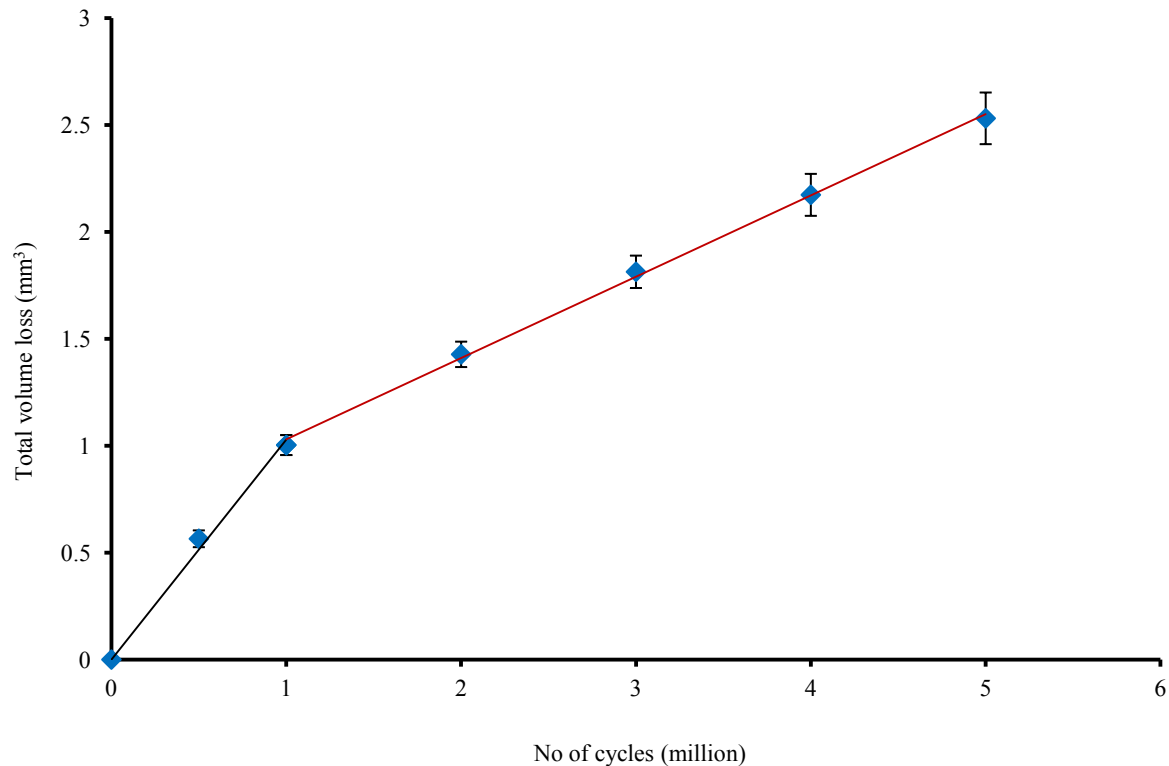


Figure 7.11. The mean volume loss of the metal-on-metal samples. A regression line is fitted through the data points (for 0 to 1 million cycles, $R^2 = 0.99$, $p = 0.046$; for 1 to 5 million cycles, $R^2 = 0.99$, $p = 0.00$). Error bars represent standard deviations

7.4.3. Surface study of the metal-on-metal samples

When the metal-on-metal samples were taken out of the simulator for measurements after the first 0.5 million cycles, multi-directional wear patterns on the articulating surfaces could be observed by the naked eye. The surface roughness measurements showed an average increase of $0.005 \pm 0.001 \mu\text{m}$ for balls and $0.006 \pm 0.001 \mu\text{m}$ for sockets during that period. The multi-directional wear patterns were observed during the 5 million cycles of testing. After the tests were complete, the average surface roughness for balls increased from $0.044 \pm 0.002 \mu\text{m}$ to $0.059 \pm 0.002 \mu\text{m}$, and for sockets from $0.047 \pm 0.006 \mu\text{m}$ to $0.063 \pm 0.007 \mu\text{m}$. Table 7.3

presents the average surface roughness values of the brand new balls and sockets, which can be compared to that after 5 million cycles in Table 7.4.

Table 7.3. The average surface roughness (S_a) of brand new metal ball and socket samples, after six measurements

Average roughness \pm Standard Deviation (μm)		
Specimen number	Ball	Socket
1	0.045 ± 0.005	0.053 ± 0.004
2	0.046 ± 0.012	0.041 ± 0.010
3	0.042 ± 0.009	0.047 ± 0.010
Average	0.044 ± 0.002	0.047 ± 0.006

Table 7.4. The average surface roughness (S_a) of metal ball and socket samples after 5 million cycles, after six measurements

Average roughness \pm Standard Deviation (μm)		
Specimen number	Ball	Socket
1	0.06 ± 0.001	0.069 ± 0.004
2	0.059 ± 0.002	0.056 ± 0.007
3	0.057 ± 0.003	0.065 ± 0.009
Average	0.059 ± 0.002	0.063 ± 0.007

It appeared that the average surface roughness also increased in two stages; an initial run-in period, followed by a steady-state phase. The change in the average surface roughness of all samples (balls and sockets) is presented in Figure 7.12 (the F-test showed that two lines gave a significantly better fit ($F > 9.55$, $p < 0.05$)).

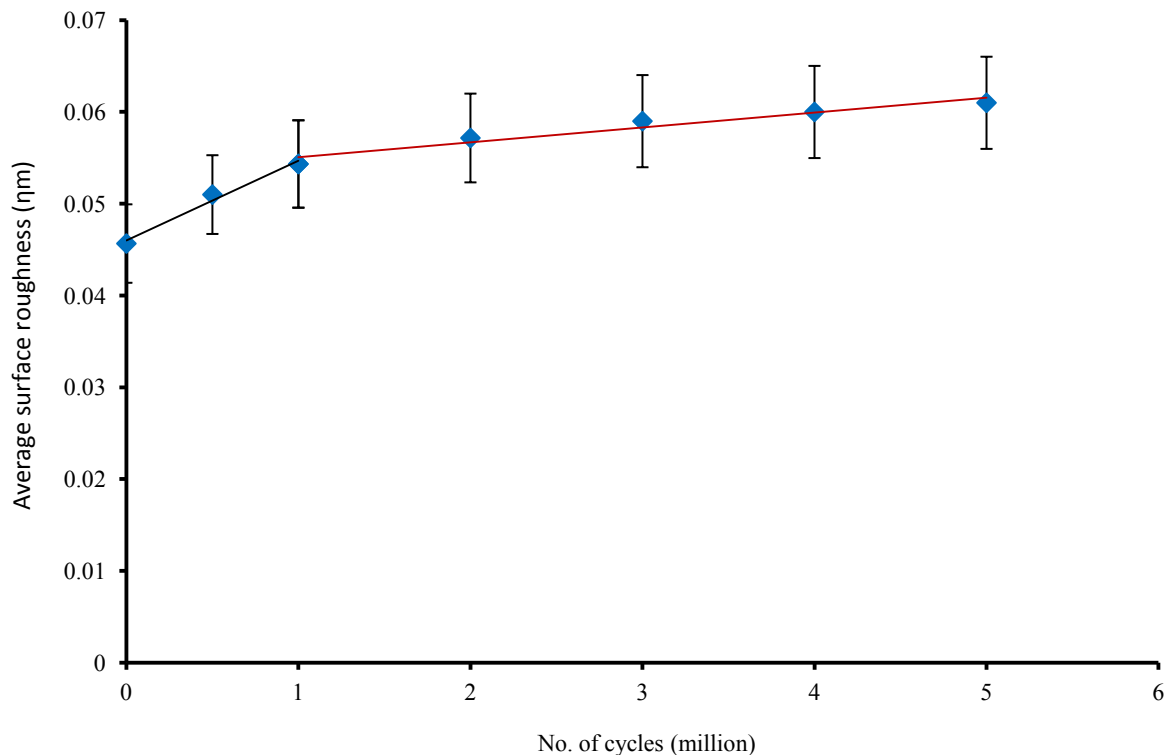


Figure 7.12. The average surface roughness of metal-on-metal samples (for 0 to 1 million cycles, $R^2 = 0.98$, $p = 0.039$; for 1 to 5 million cycles, $R^2 = 0.94$, $p = 0.012$). Error bars represent standard deviations

Although the surface roughness increased after 1 million cycles and scratches were still observed, the surfaces seemed to be smoothed by self-polishing of the articulating surfaces. Figure 7.13 shows the difference in the surface texture of a ball sample a) when brand new, b) after 1 million cycles and c) after 5 million cycles.

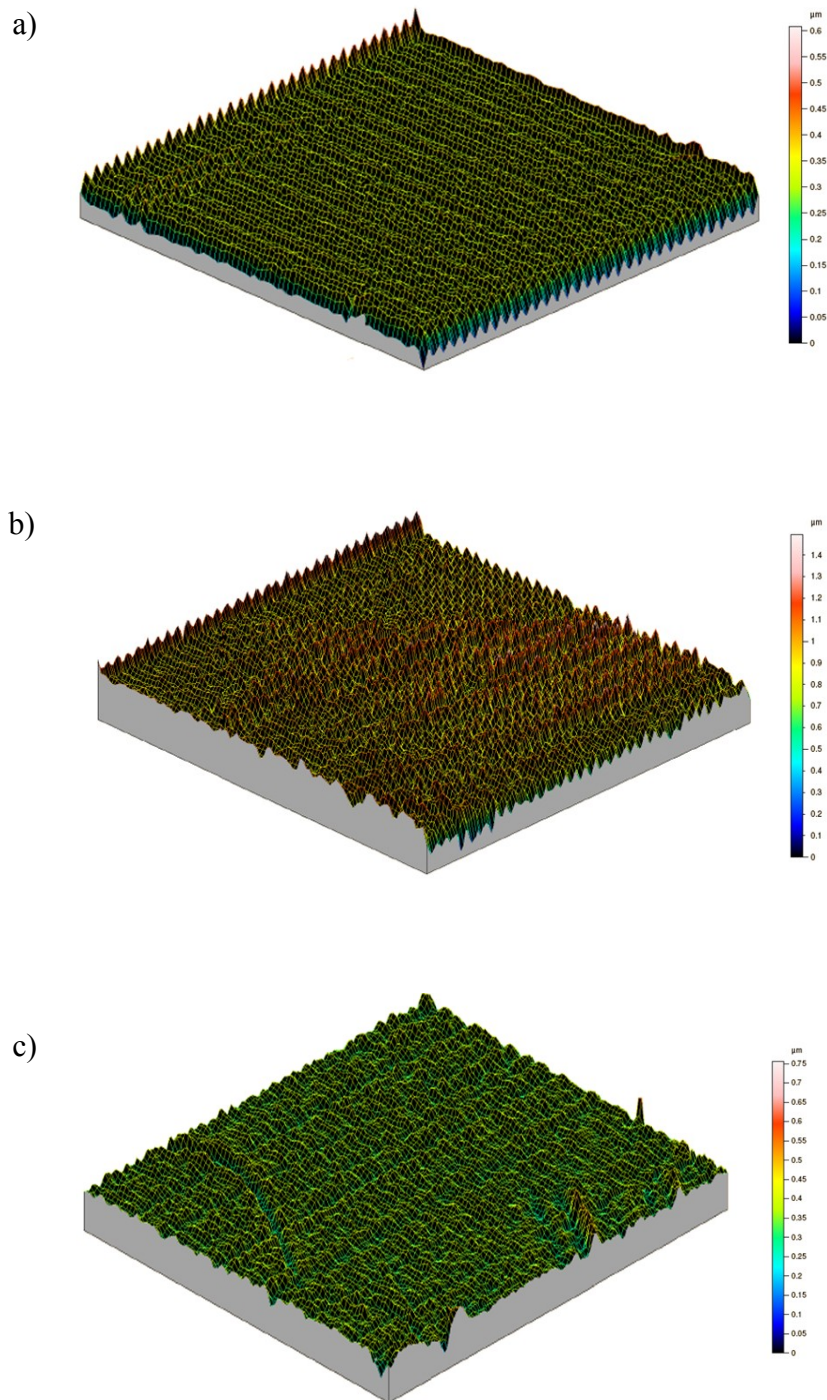


Figure 7.13. The 3D Taylor Hobson Form Talysurf-120L surface roughness measurement images of a ball sample a) when brand new, b) after 1 million cycles and c) after 5 million cycles

7.4.4. Comparison between wear of the Charité® TDAs and the metal-on-metal samples

For easy comparison between the volumetric wear rate of both metal-on-metal samples and Charité® cores, the results are presented together in Figure 7.14. As expected from previous results in § 7.4.1 and § 7.4.2, it can be seen that the mean volume loss for Charité® cores was at least 23 times more than that in metal-on-metal samples.

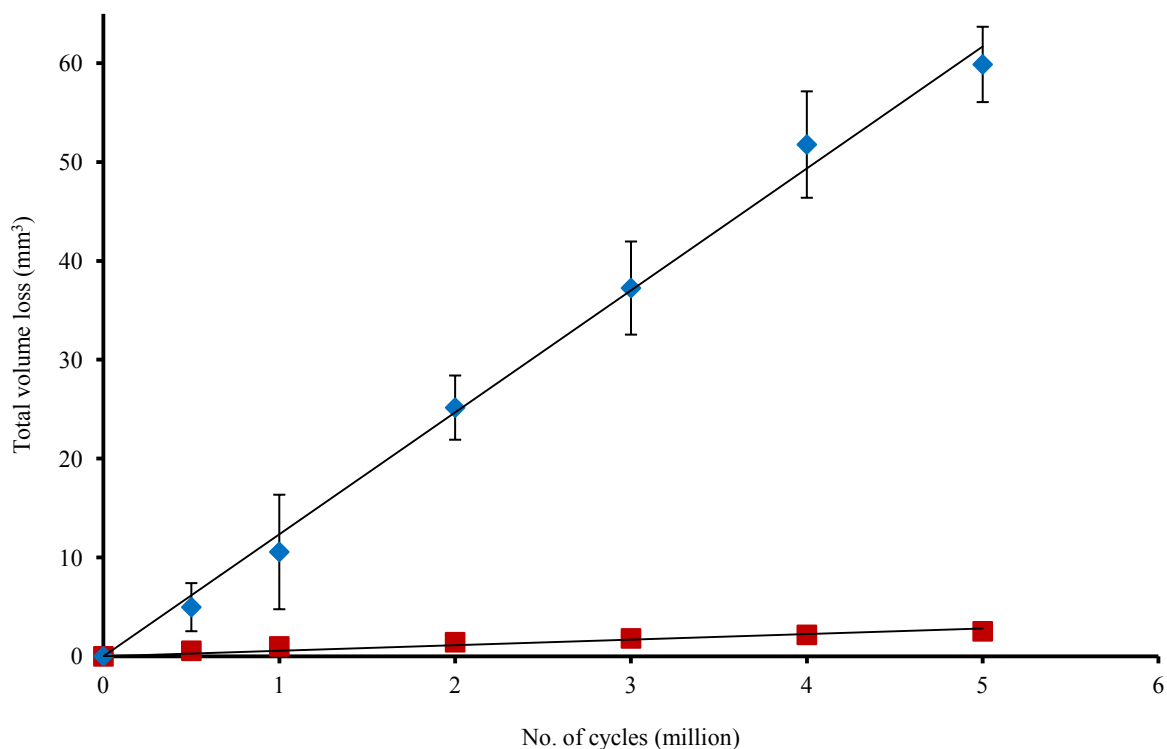


Figure 7.14. The mean volume loss of the Charité® cores (◆) and metal-on-metal samples (■). A regression line is fitted through the data points. Error bars represent standard deviations; when error bars are not shown they are smaller than the symbols used to represent the data points

7.5. Discussion

7.5.1. The Charité® TDA

The wear rate of the Charité® found in this study was consistent with those in similar studies on Charité® TDAs (Paré et al., 2007; Prokopovich et al., 2011; Vicars et al., 2009) and unlike metal-on-metal samples, a linear trend was exhibited. The mean wear rate was found to be $12.8 \pm 1.2 \text{ mm}^3$ per million cycles. This is in contrast with a study on similar TDAs by Serhan et al. (2006), where there was a 0.8 mm^3 per million cycles initial running-in wear rate followed by a steady-state 0.2 mm^3 per million cycles thereafter. It should be noted that the latter study was performed using a hip simulator and in accordance to ASTM Standards for TDA wear test; therefore, different angular motions and loading conditions were applied. Prokopovich et al. (2011) reported a mean wear rate of $12.9 \pm 2.5 \text{ mm}^3$ per million cycles for the Charité® TDAs, which is comparable to the results obtained in this study. Also, in a similar study by Vicars et al. (2009) on the same TDAs, a mean wear rate of $12.5 \pm 1.3 \text{ mm}^3$ per million cycles was observed.

The total mass loss of the polymer parts was $60.3 \pm 4.6 \text{ mg}$, which was in agreement with a similar study by Vicars et al. (2010) on ProDisc-L®, using a 6-station Prosim spine simulator; a mean mass loss of $63.3 \pm 10.4 \text{ mg}$ was reported. In the same study, a mean wear rate of $11.6 \pm 1.2 \text{ mg}$ per million cycles was reported, that was also comparable to the $12.03 \pm 1.4 \text{ mg}$ per million cycles mean wear rate of the present study. In the parallel study on wear of the Charité® TDAs carried out at the University of Leeds, also using a 6-station Prosim spine simulator, a mean wear rate of $11.5 \pm 1.6 \text{ mg}$ per million cycles was measured (personal communication from Mr. Phillip Hyde, PhD research student, University of Leeds),

which was also in agreement with the values obtained in this work. Therefore, it may be concluded that both simulators are capable of producing comparable results under similar conditions.

Studies on the surface topography of the Charité® UHMWPE core and other metal-on-polymer TDAs commonly report abrasive and adhesive wear, and burnishing (Anderson et al., 2006; Kurtz et al., 2007; Prokopovich et al., 2011). When a metal surface is in contact with a polymer surface, the microscopic irregularities or the locally stiffer asperities of each surface scratch the opposing surface, which results in creation of wear debris and scratches. This is known as abrasive wear, which is very common in metal-on-metal and metal-on-polymer implants with articulating surfaces (Anderson et al., 2006; Hutchings, 1992; Wimmer and Fischer, 2007). Adhesive wear occurs when material from one surface is transferred to another due to adhesion between the articulating surfaces (Jin and Wei, 2009; Stolarski, 1990). It may well be possible that both UHMWPE core and metal endplates experienced abrasive and adhesive wear, since light scratches were barely observed by the naked eye on all articulating surfaces. Burnishing is associated with an adhesive wear mechanism when the polymer surface wear occurs by adhesion to the metal articulating surface, resulting in a polished glossy appearance (Anderson et al., 2006; Kurtz et al., 2009). The glossy appearance of the surfaces was visible to the naked eye, therefore, it may be said that burnishing also occurred.

The height of the load soak control UHMWPE core did not change, whilst the height of the other cores decreased by 0.4 ± 0.1 mm. Therefore, it may be concluded that the decrease in height was a result of wear and material loss only and there was negligible plastic deformation.

7.5.2. Wear of the metal-on-metal samples

In metal-on-metal samples, the trend of the results obtained for volumetric wear was in agreement with a typical trend for metal-on-metal THAs (Dowson et al., 2004; Vassiliou et al., 2006). During the first million cycles of articulation, higher but steadily decrease in wear rate was observed in a running-in period. Thereafter, a lower but steady-state wear was evident.

The metal-on-metal wear rate obtained in this study was partly in agreement with a similar study by Paré et al. (2007) on the metal-on-metal A-Mav™ lumbar TDA (Medtronic, Memphis, TN, USA). They reported an initial wear rate of about 0.6 ± 0.1 mm³ per million cycles in the first 0.5 million cycles. Both the initial wear rate and the run-in period were in contrast to the present study. However, the steady-state wear rate was 0.4 ± 0.1 mm³ per million cycles, which was comparable to the 0.4 ± 0.03 mm³ per million cycles obtained in the present work. Similar studies on THAs suggest different wear rates ranging from 0.2 to 6.3 mm³ per million cycles, some of which are in agreement with that obtained in this study (Affatato et al., 2008; Goldsmith et al., 2000; Scholes et al., 2001; Scholes and Unsworth, 2006b; Vassilou et al., 2006). In a study by Goldsmith et al. (2000) on metal-on-metal hip implants, an initial wear rate of 0.5 mm³ per million cycles during the first million cycles was reported followed by a steady-state wear rate of 0.4 mm³ per million cycles thereafter. The

wear rate in the run-in phase was almost twice that of the present study, but the steady-state wear rates were comparable. It can be said that the metal-on-metal wear rate in this study was comparable to other studies on metal-on-metal THAs.

The trend of change in surface roughness followed that of gravimetric wear measurements. The surface roughness also had a more rapid, linear change in the first million cycles, followed by a slower, linear change thereafter. The increase of surface roughness is a result of direct or partly-direct contact between the two surfaces. Therefore, it may be concluded that boundary or mixed lubrication regime occurred, which follows similar conclusions obtained in friction studies in Chapter 5.

When the two metal surfaces are in contact, abrasive wear may occur, as described in § 7.5.1. The multi-directional wear pattern of the metal samples may also result in surface fatigue which occurs as a result of cyclic crack growth due to debris detachment (Wimmer et al., 2001; Wimmer and Fischer, 2007). Explanted metal-on-metal Maverick™ TDAs have confirmed the multi-directional nature of the wear scars (Paré et al., 2007).

At the initial stages of the wear testing, the irregularities on the surfaces increased with continuous contact, resulting in an increase in surface roughness. However, it appeared that after the first million cycles the two metal surfaces underwent a self-polishing mechanism (McKellop et al., 1996; Rieker et al., 2001), which usually results in a decrease in wear (Paré et al., 2007).

7.5.3. A comparison between wear of the Charité® TDAs and metal -on-metal samples

The difference between the wear rate of the metal samples and the Charité® TDAs showed that the wear rate for metal-on-polymer implants can be over 23 times larger than that for metal-on-metal TDAs. This is in agreement with other studies on TDAs and THAs, where the wear rate of metal-on-polymer implants were between two to ten times larger than that for metal-on-metal (Paré et al., 2007; Scholes et al., 2001). The reason for such large differences may be in the material combination. In hard-on-soft contact, more particles are removed from the surface by the harder material, whilst in hard-on-hard articulation a self-polishing mechanism occurs which results in creating less wear debris with possibly smaller size than softer materials.

7.6. Summary

This part of the study investigated the wear rate of the generic metal-on-metal samples and the metal-on-polymer Charité® TDAs. Under similar conditions, the metal-on-metal samples showed wear rate 23 times smaller than that for metal-on-polymer Charité® TDAs. The results were in agreement with some of the studies with similar conditions, and varied with those performed under different conditions.

Chapter 8

General Conclusions

This thesis aimed at investigating the tribology of ball-and-socket total disc arthroplasty (TDA) under laboratory conditions; this attempts to simulate the environment a TDA experiences in the body. It was mentioned in previous chapters that TDAs are likely to be lubricated by interstitial fluid. In experimental studies both Ringer's solution and calf serum are used as lubricants for *in vitro* tests; diluted calf serum is recommended by BS ISO 18192-1:2008 (ASTM F2423-05 recommends bovine serum). Therefore, towards investigating the objectives of this work, the first question was: does it make a difference if Ringer's solution or diluted calf serum is used in tribological tests of TDA? The study in Chapter 4 showed that it does make an appreciable difference which fluid is used. If there were no differences, Ringer's solution could be used for future tests, as it is easier to make, does not become contaminated by bacteria and is cheaper. But since the two liquids performed appreciably differently, the next question was: which fluid should be selected as the lubricant? Interstitial fluid contains protein, as so does diluted calf serum. Based on the comparison of different fluids in Table 4.2, it was found that the properties of interstitial fluid are likely to be closer to that found in diluted calf serum rather than Ringer's solution. Until the full properties of interstitial fluid lubricating TDAs are understood, laboratory tests on TDAs should use diluted calf serum.

As one of the objectives of this work, the effect of change in ball radius on performance of ball-and-socket TDAs was investigated in Chapter 5. Friction tests were performed on metal-on-metal samples with 10, 12, 14 and 16 mm ball radii, under 50, 600, 1200 and 2000 N compressive loads. The results showed that, as expected, the lower the ball radius, the lower the frictional torque. Similar reports were observed on several studies on metal-on-metal and polymer-on-metal total hip arthroplasty (THA), as was discussed in Chapter 5. The study

presented in Chapter 6 showed that in both metal-on-polymer (metal socket/ polymer ball) and polymer-on-metal (polymer socket/ metal ball) combinations, the smaller radius showed lower friction, even in the case of flexion from 0 to 6°, where there was no significant difference between frictional torque created by the two material combinations. Hence, it may be concluded that regardless of the material combination, the smaller radius creates less friction and hence may perform better.

Stribeck analysis in this work showed that for similar ball radii, friction factors in metal-on-metal samples were larger than that for metal and polymer samples. This means that metal-on-metal samples experience higher friction. It could be thought that the higher metal-on-metal friction could lead to more wear. However, wear studies in Chapter 7 showed that the wear rate of metal-on-polymer TDAs was 23 times higher than that in metal-on-metal. This is mainly a result of different material combination. Metal-on-metal is an articulation of two identical hard materials, whereas for metal-on-polymer one is harder than the other, which may result in creating larger polymer wear particles by metal (Anissian et al., 1999; Huang et al., 2002; Tipper et al., 1999). Studies on metal-on-metal THA show that the size of the metal wear particles can range between 10 to 120 nm (Billi et al., 2011; Brown et al., 2006; Yan et al., 2009). In a study by Punt et al. (2012) on metal and polymer TDAs and THAs, it was observed that the size of the polymer wear particles can be as large as 944 μm for TDAs and 311 μm for THAs. This consequently results in a higher wear rate of metal-on-polymer TDAs in comparison to metal-on-metal, even though Yan et al., (2009) in a study on THAs state that the number of metal wear particles generated could be more than polymer wear particles by about a factor of 2.

It was mentioned in a number of occasions that wear particles can lead to bone loss and implant loosening. Studies on TDAs and THAs show that the wear particle of both materials can cause inflammatory reaction of the adjacent tissue to the presence of foreign-body particles (Catelas and Wimmer, 2011; Punt et al., 2012; Zeh et al., 2007). In addition to that, in case of metal particles, early adverse local tissue reaction and toxicity is a major concern; this compromises the lower wear rate of metal-on-metal TDAs in comparison to metal-on-polymer and makes the latter more favourable (Catelas and Wimmer, 2011; Langton et al., 2010; Zeh et al., 2007). The question here was: now that metal-on-polymer combination is preferred, can performance of TDAs improve by reversing the material of ball and socket (i.e. polymer socket/ metal ball instead of metal socket/ polymer ball)? The difference between polymer-on-metal and metal-on-polymer material combination was investigated in Chapter 6. The material combination was identical and surface roughnesses of identical materials were similar; therefore, one could expect that the friction does not change significantly between both types of TDAs. However, the results showed that in small angular motions (up to 3°), friction may be significantly lower in polymer-on-metal TDAs (possible reasons for such difference are discussed in Chapter 6, § 6.5). This part of the study only investigated the friction between the two types. Future work could include performing wear tests on polymer-on-metal and metal-on-polymer TDAs under identical conditions to see whether still polymer-on-metal performs better. In Chapter 7, the wear study of the metal-on-polymer Charité® TDAs showed a linear wear rate during 5 million cycles and the overall thickness of the polymer socket decreased. This may well be the case for polymer-on-metal TDAs. However, the wear rate could vary as a result of reversing the ball and socket material. It should be reminded that in the wear test, all three angular motions (i.e. axial rotation, flexion/extension and lateral bending) were combined. Friction tests showed a difference in

behaviour only when the angular motion was small. Therefore, we cannot say whether or not this would significantly affect the wear rate until long-term wear tests are performed. This could be a further step ahead towards improving future designs of TDAs, especially since metal and polymer TDAs are more favourable than metal-on-metals.

Tribological experiments in this study were an attempt towards better understanding the behaviour and performance of TDAs with different design combinations. The overall conclusions of this work are:

- within the range of 10 to 16 mm ball radii, performance of ball and socket TDAs with smaller ball radii is better than those with larger ball radii
- if a metal-on-metal combination is not to be used because of concerns associated with metal wear debris, polymer-on-metal may be an alternative material combination for future designs of TDAs, as opposed to the traditional metal-on-polymer
- when performing laboratory tests, diluted calf serum can be used as an alternative to Ringer's solution, until the composition of the fluid lubricating TDAs is fully understood

In future studies, it may be interesting to perform wear tests on TDAs with identical material combination and different ball radii to understand whether the wear rate of TDAs with smaller ball radii is also lower than that with larger radii. It was mentioned in Chapter 2 that one of the design factors that can affect tribological performance is radial clearance. Several studies on THAs show that decreasing radial clearance between the articulating surfaces reduces friction (Brockett et al., 2008; Liu et al., 2005; Smith et al., 2001b). The main reason can be explained by the possible decrease of lubricant film thickness when radial clearance

increases, which consequently results in higher friction between the articulating surfaces. This may also be the case for TDAs. Therefore, as part of any future work, similar studies presented in this thesis could be repeated for TDAs with different radial clearance, to investigate the effects of change in radial clearance on friction and wear.

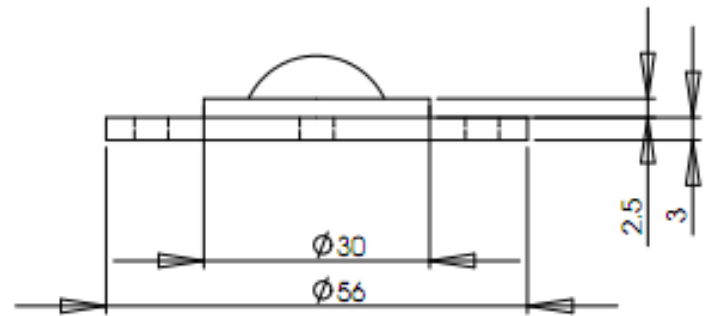
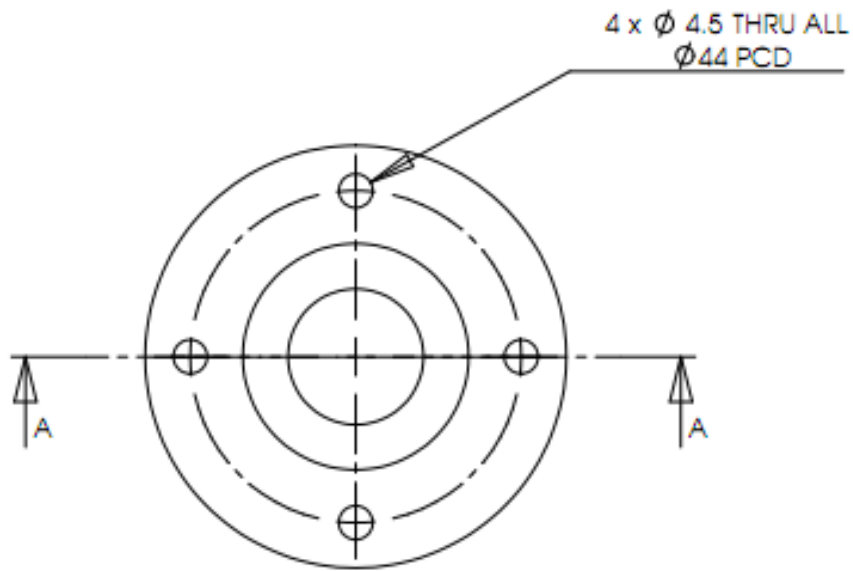
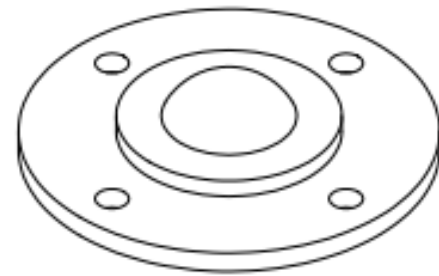
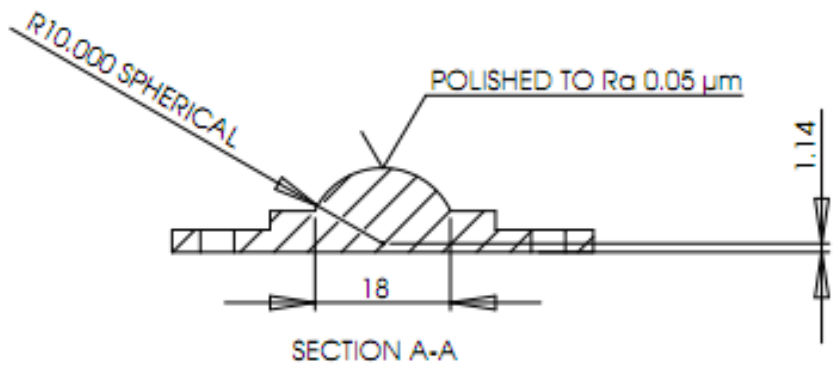
Appendix A

The engineering drawings of the metal and
polymer TDA samples

(see § 3.2.2)

Note: LB (Lower Block) refers to the samples mounted to the bottom plates

UB (Upper Block) refers to the samples mounted to the top plates



PROPRIETARY AND CONFIDENTIAL

THE INFORMATION CONTAINED IN THIS DRAWING IS THE SOLE PROPERTY OF THE UNIVERSITY OF BIRMINGHAM. ANY REPRODUCTION IN PART OR AS A WHOLE WITHOUT THE WRITTEN PERMISSION OF THE UNIVERSITY OF BIRMINGHAM IS PROHIBITED.

Tolerance unless otherwise stated:
 whole numbers ± 0.25
 one decimal place ± 0.10
 two decimal places ± 0.05

MATERIAL

Cobalt Chrome to ASTM F799-96
 (Co-27 Cr-5.5 Mo-0.06C)

DIMENSIONS ARE IN MM

DRAWN BY:

PARSHA MOGHADAS
 08 JULY 2009

SIZE
A

DWG. NO.
LB-implant-10

REV
2

SCALE: 1:1

SHEET 1 OF 1

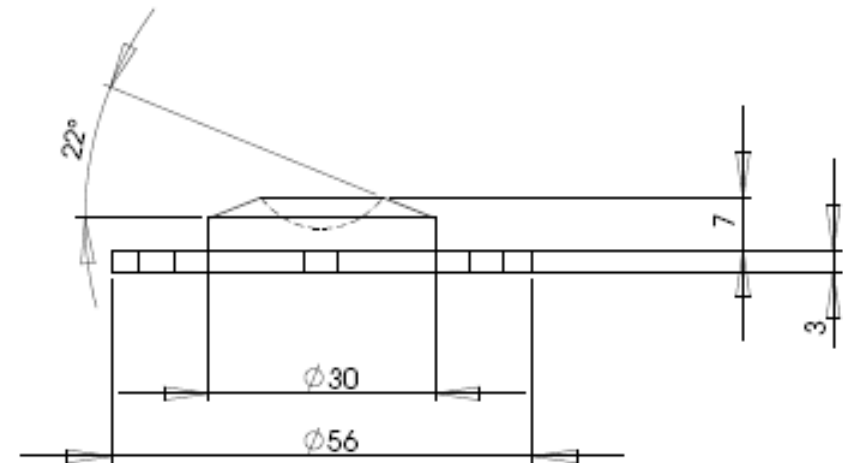
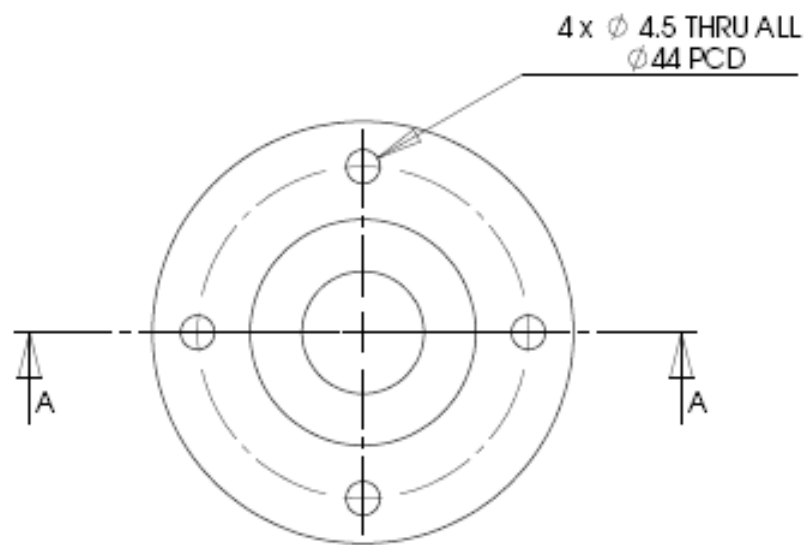
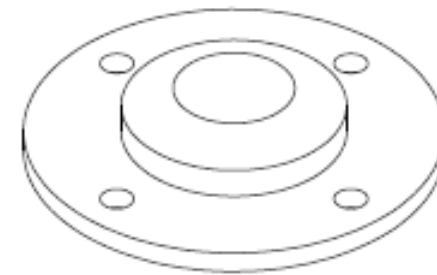
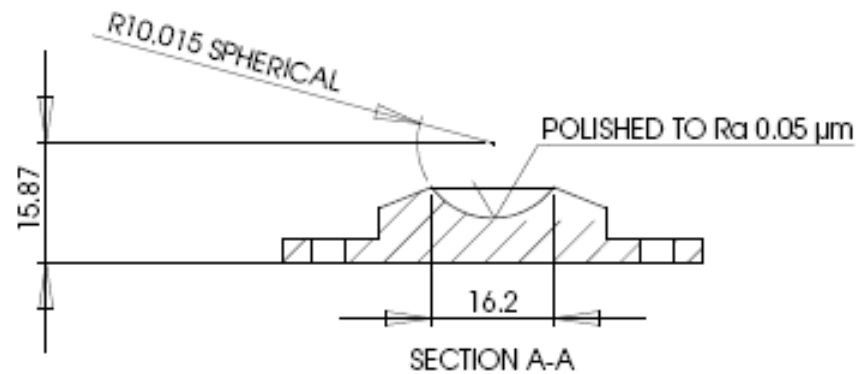
5

4

3

2

1



PROPRIETARY AND CONFIDENTIAL

THE INFORMATION CONTAINED IN THIS DRAWING IS THE SOLE PROPERTY OF THE UNIVERSITY OF BIRMINGHAM. ANY REPRODUCTION IN PART OR AS A WHOLE WITHOUT THE WRITTEN PERMISSION OF THE UNIVERSITY OF BIRMINGHAM IS PROHIBITED.

Tolerance unless otherwise stated:
whole numbers ± 0.25
one decimal place ± 0.10
two decimal places ± 0.05

MATERIAL
Cobalt Chrome to ASTM F799-96
(Co-27 Cr-5.5 Mo-0.05C)

DIMENSIONS ARE IN MM

DRAWN BY:

PARSHIA MOGHADAS
08 JULY 2009

SIZE

A

DWG. NO.

UB-implant-10

REV

2

SCALE: 1:1

SHEET 1 OF 1

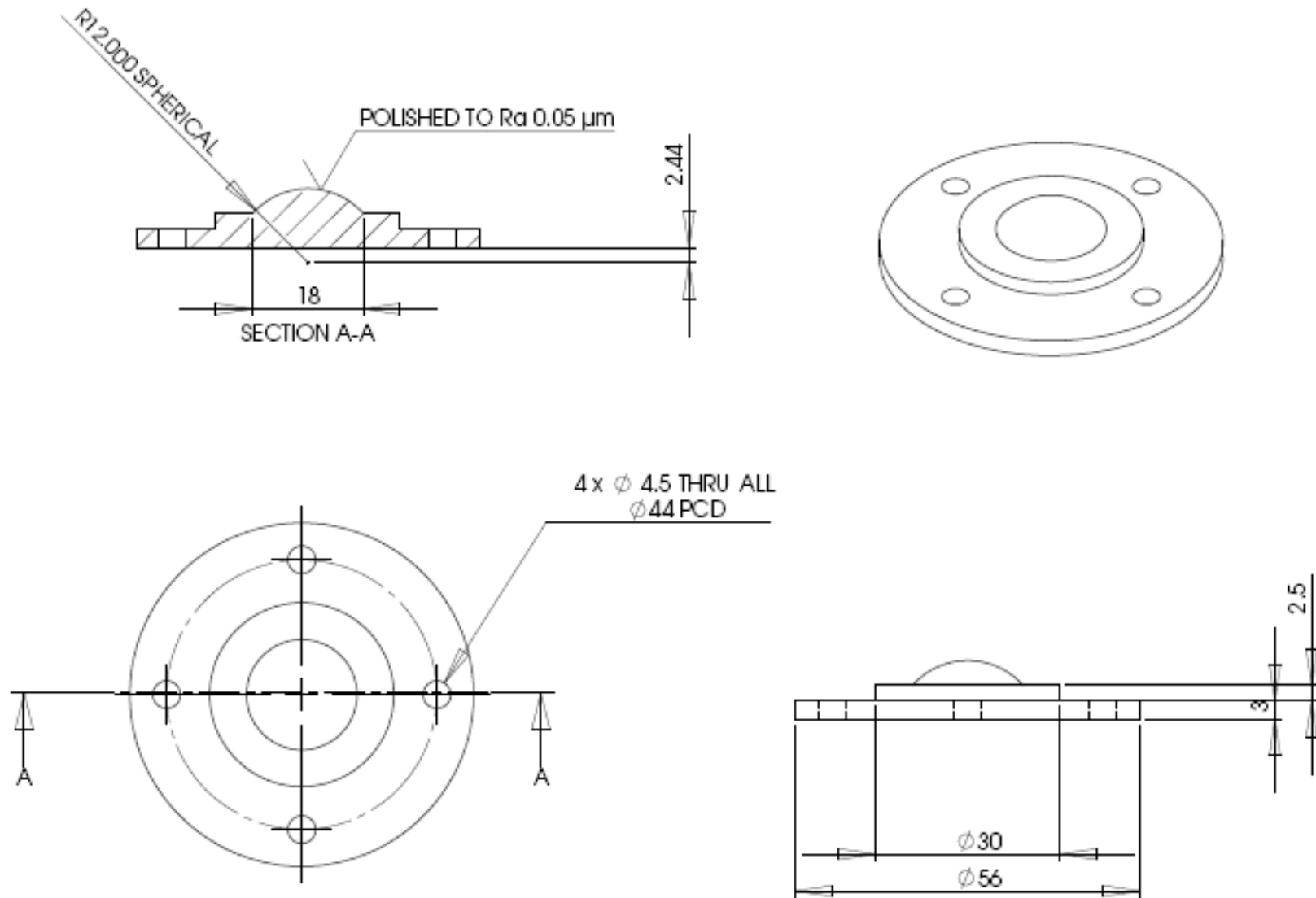
5

4

3

2

1



PROPRIETARY AND CONFIDENTIAL

THE INFORMATION CONTAINED IN THIS DRAWING IS THE SOLE PROPERTY OF THE UNIVERSITY OF BIRMINGHAM. ANY REPRODUCTION IN PART OR AS A WHOLE WITHOUT THE WRITTEN PERMISSION OF THE UNIVERSITY OF BIRMINGHAM IS PROHIBITED.

Tolerance unless otherwise stated:
 whole numbers ± 0.25
 one decimal place ± 0.10
 two decimal places ± 0.05

MATERIAL
 Cobalt Chrome to ASTM F799-96
 (Co-27 Cr-5.5 Mo-0.06C)

DIMENSIONS ARE IN MM

DRAWN BY:

PARSHIA MOGHADAS
 08 JULY 2009

SIZE
A

DWG. NO.
LB-implant-12

REV
2

SCALE: 1:1

SHEET 1 OF 1

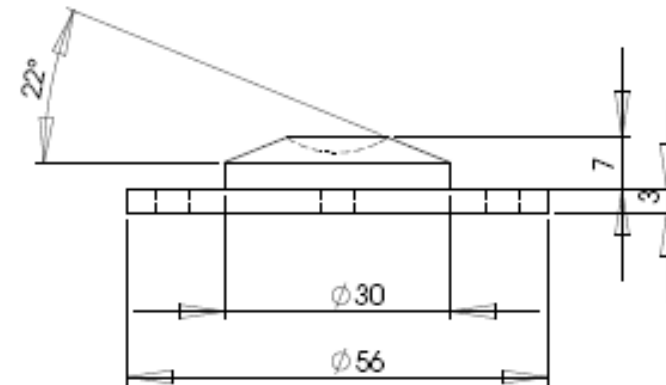
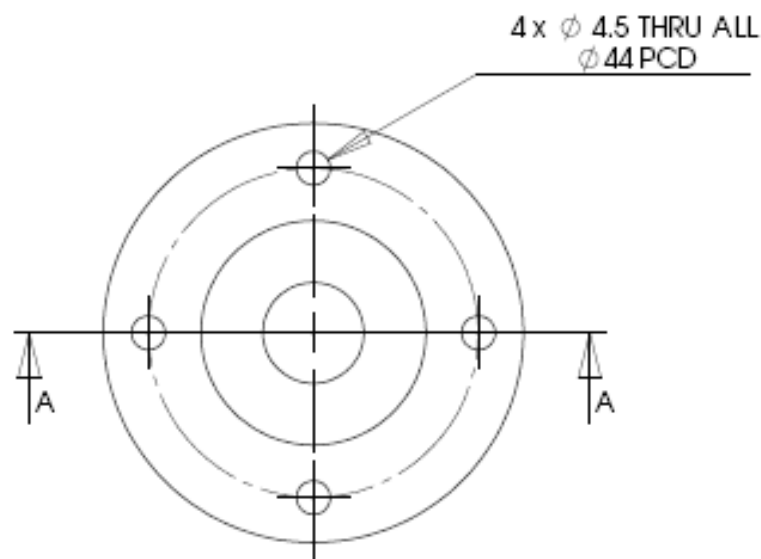
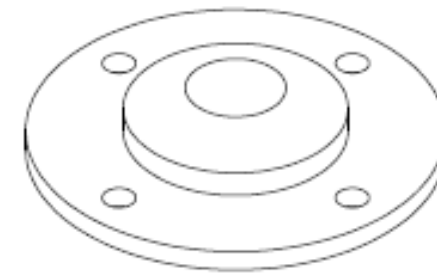
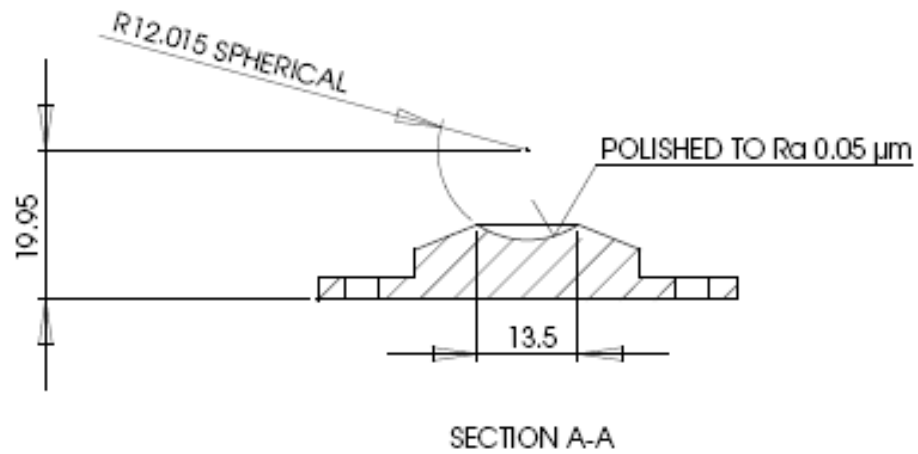
5

4

3

2

1



PROPRIETARY AND CONFIDENTIAL

THE INFORMATION CONTAINED IN THIS DRAWING IS THE SOLE PROPERTY OF THE UNIVERSITY OF BIRMINGHAM. ANY REPRODUCTION IN PART OR AS A WHOLE WITHOUT THE WRITTEN PERMISSION OF THE UNIVERSITY OF BIRMINGHAM IS PROHIBITED.

Tolerance unless otherwise stated:
 whole numbers ± 0.25
 one decimal place ± 0.10
 two decimal places ± 0.05

MATERIAL

Cobalt Chrome to ASTM F792-96
 (Co-27 Cr-5.5 Mo-0.05C)

DIMENSIONS ARE IN MM

DRAWN BY:

PARSHIA MOGHADAS
 08 JULY 2009

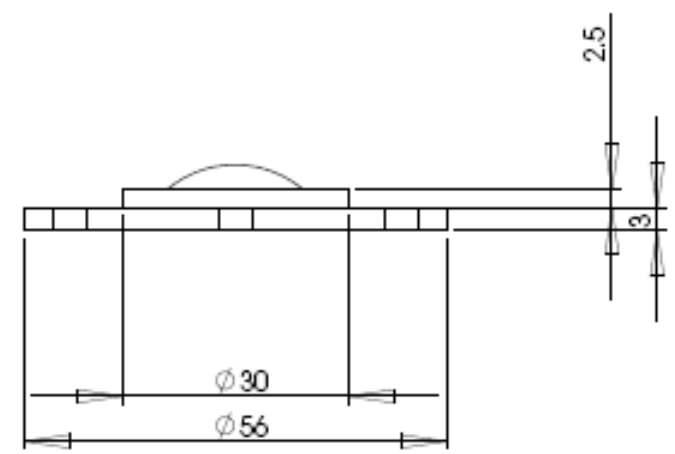
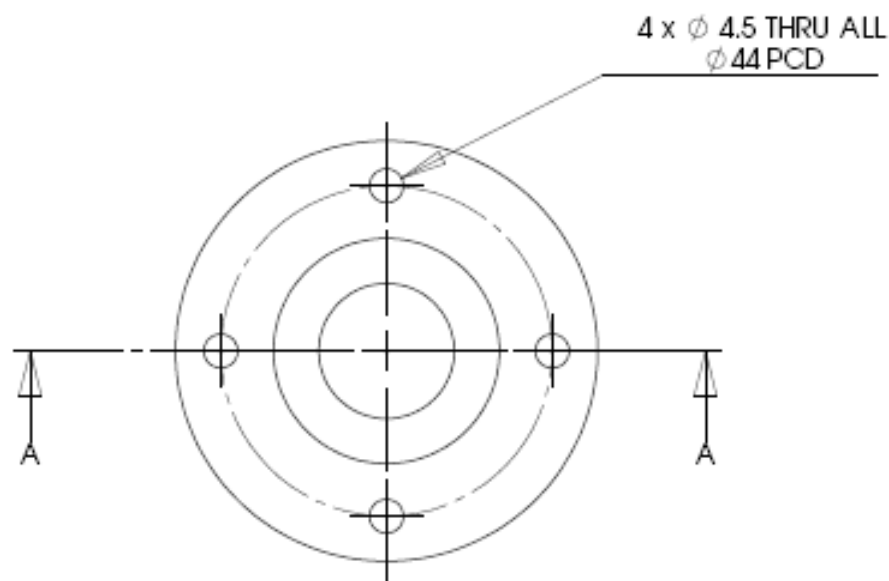
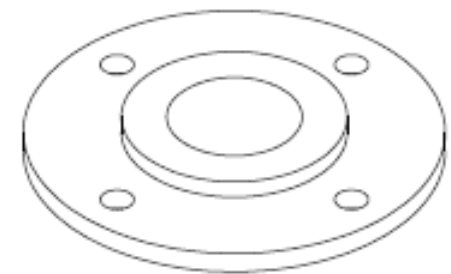
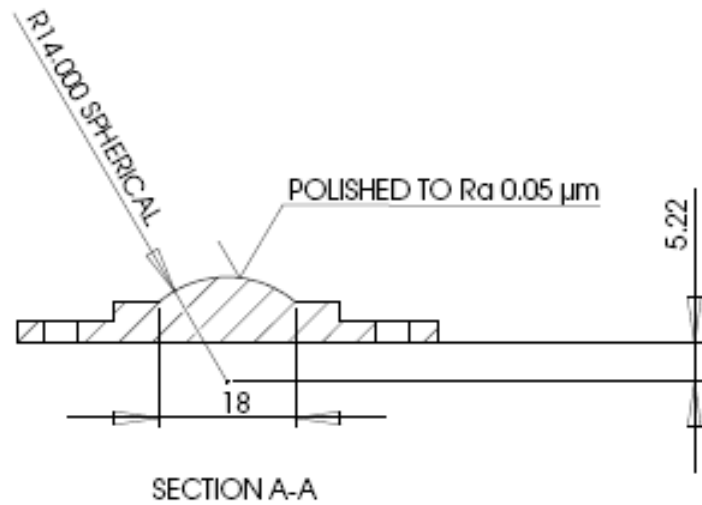
SIZE
A

DWG. NO.
UB-implant-12

REV
2

SCALE: 1:1

SHEET 1 OF 1



PROPRIETARY AND CONFIDENTIAL

THE INFORMATION CONTAINED IN THIS DRAWING IS THE SOLE PROPERTY OF THE UNIVERSITY OF BIRMINGHAM. ANY REPRODUCTION IN PART OR AS A WHOLE WITHOUT THE WRITTEN PERMISSION OF THE UNIVERSITY OF BIRMINGHAM IS PROHIBITED.

Tolerance unless otherwise stated:
 whole numbers ± 0.25
 one decimal place ± 0.10
 two decimal places ± 0.05

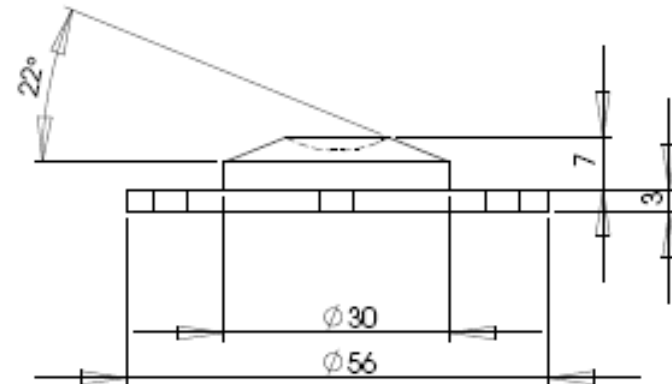
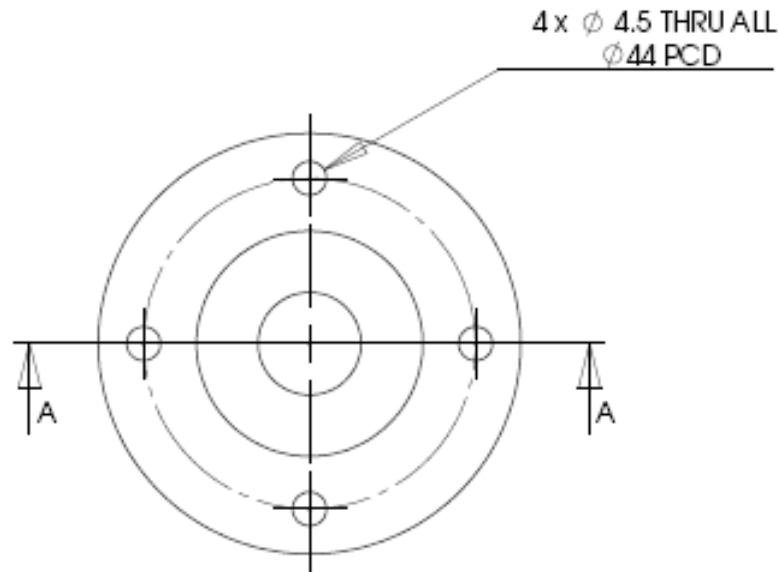
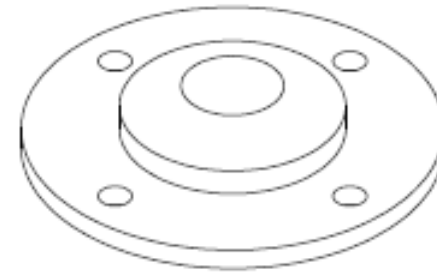
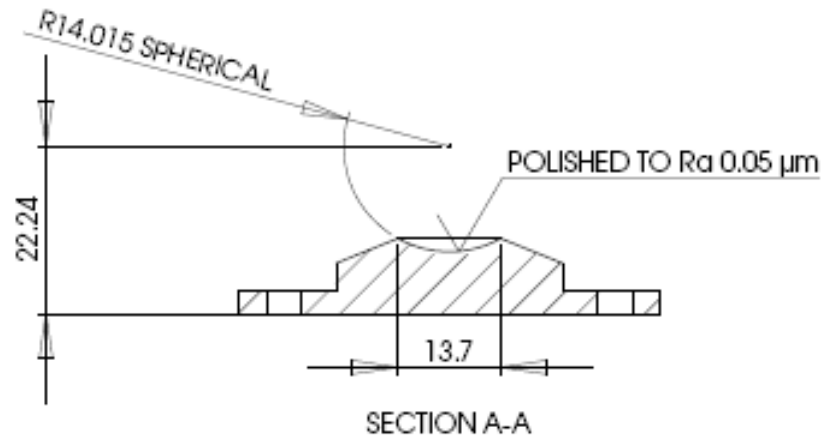
MATERIAL
 Cobalt Chrome to ASTM F799-96
 (Co-27 Cr-5.5 Mo-0.05C)

DIMENSIONS ARE IN MM

DRAWN BY:
 PARSHIA MOGHADAS
 08 JULY 2009

SIZE A	DWG. NO. LB-implant-14	REV 2
------------------	----------------------------------	-----------------

SCALE: 1:1 SHEET 1 OF 1



PROPRIETARY AND CONFIDENTIAL

THE INFORMATION CONTAINED IN THIS DRAWING IS THE SOLE PROPERTY OF THE UNIVERSITY OF BIRMINGHAM. ANY REPRODUCTION IN PART OR AS A WHOLE WITHOUT THE WRITTEN PERMISSION OF THE UNIVERSITY OF BIRMINGHAM IS PROHIBITED.

Tolerance unless otherwise stated:
whole numbers ± 0.25
one decimal place ± 0.10
two decimal places ± 0.05

MATERIAL
Cobalt Chrome to ASTM F799-96
(Co-27 Cr-5.5 Mo-0.05C)

DIMENSIONS ARE IN MM

DRAWN BY:

PARSHIA MOGHADAS
08 JULY 2009

SIZE DWG. NO.

A UB-implant-14

REV

2

SCALE: 1:1

SHEET 1 OF 1

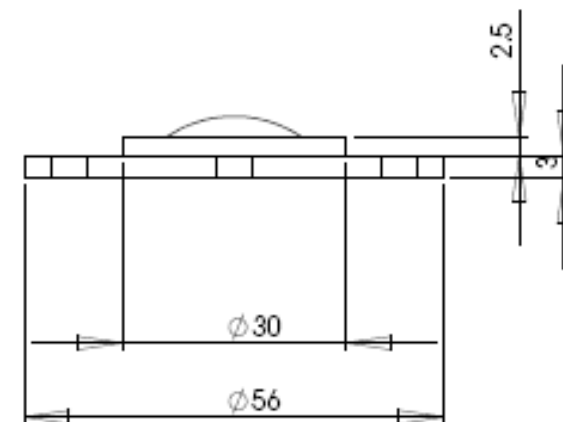
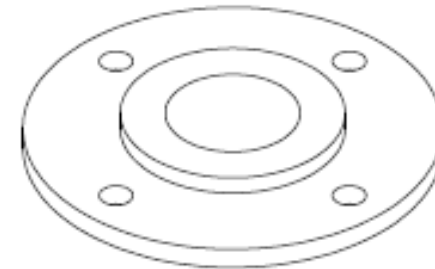
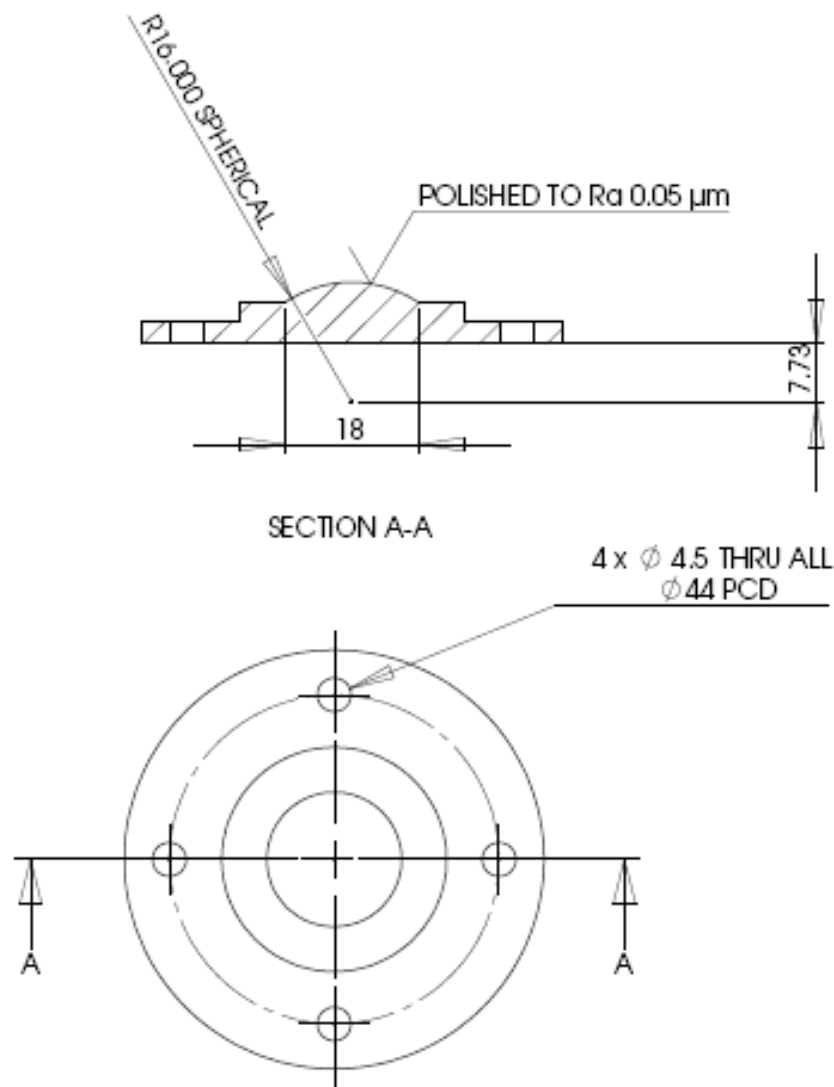
5

4

3

2

1



PROPRIETARY AND CONFIDENTIAL

THE INFORMATION CONTAINED IN THIS DRAWING IS THE SOLE PROPERTY OF THE UNIVERSITY OF BIRMINGHAM. ANY REPRODUCTION IN PART OR AS A WHOLE WITHOUT THE WRITTEN PERMISSION OF THE UNIVERSITY OF BIRMINGHAM IS PROHIBITED.

Tolerance unless otherwise stated:
 whole numbers ± 0.25
 one decimal place ± 0.10
 two decimal places ± 0.05

MATERIAL
 Cobalt Chrome to ASTM F799-96
 (Co-27 Cr-5.5 Mo-0.06C)

DIMENSIONS ARE IN MM

DRAWN BY:

PARSHIA MOGHADAS
 08 JULY 2009

SIZE
A

DWG. NO.
LB-implant-16

REV
2

SCALE: 1:1

SHEET 1 OF 1

5

4

4

3

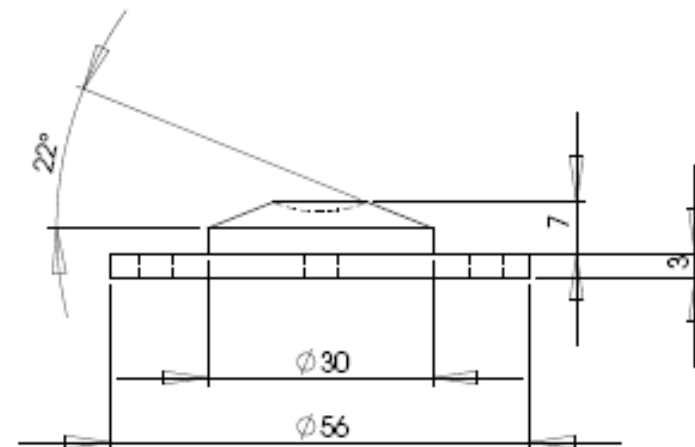
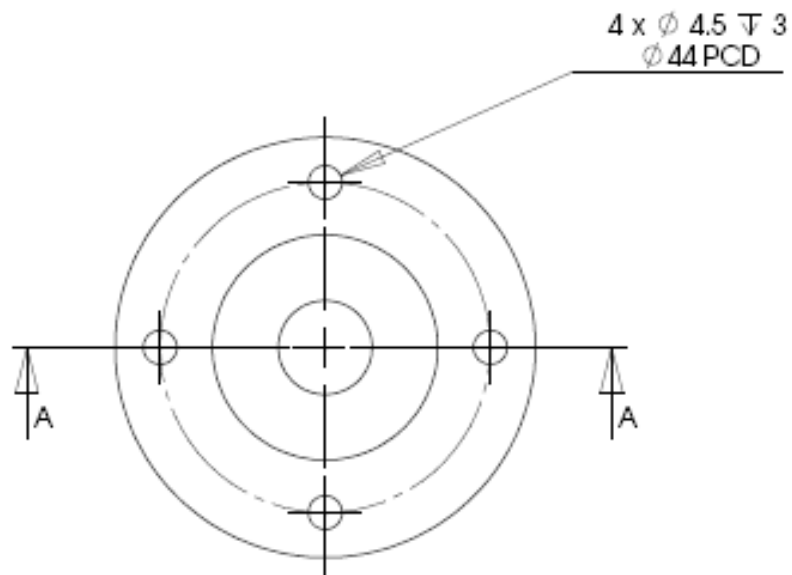
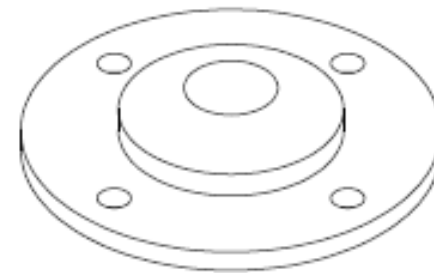
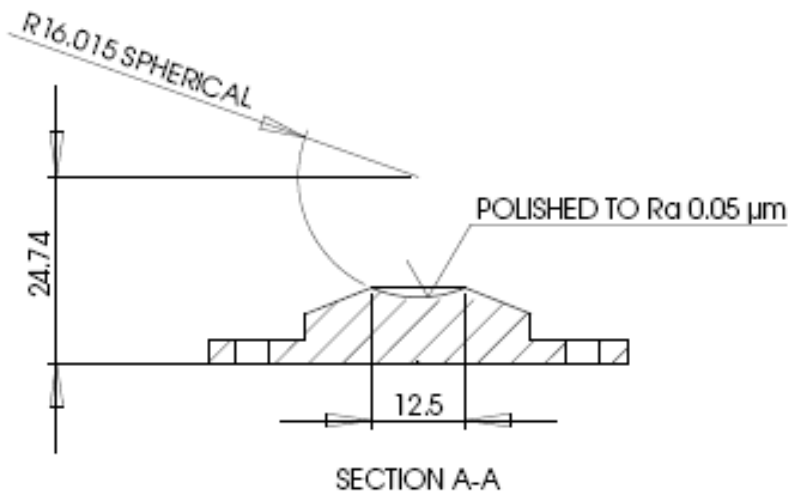
3

2

2

1

1



PROPRIETARY AND CONFIDENTIAL

THE INFORMATION CONTAINED IN THIS DRAWING IS THE SOLE PROPERTY OF THE UNIVERSITY OF BIRMINGHAM. ANY REPRODUCTION IN PART OR AS A WHOLE WITHOUT THE WRITTEN PERMISSION OF THE UNIVERSITY OF BIRMINGHAM IS PROHIBITED.

Tolerance unless otherwise stated:

whole numbers ± 0.25
 one decimal place ± 0.10
 two decimal places ± 0.05

MATERIAL

Cobalt Chrome to ASTM F799-96
 (Co-27 Cr-5.5 Mo-0.06C)

DIMENSIONS ARE IN MM

DRAWN BY:

PARSHA MOGHADAS
 08 JULY 2009

SIZE

A

DWG. NO.

UB-implant-16

REV

2

SCALE: 1:1

SHEET 1 OF 1

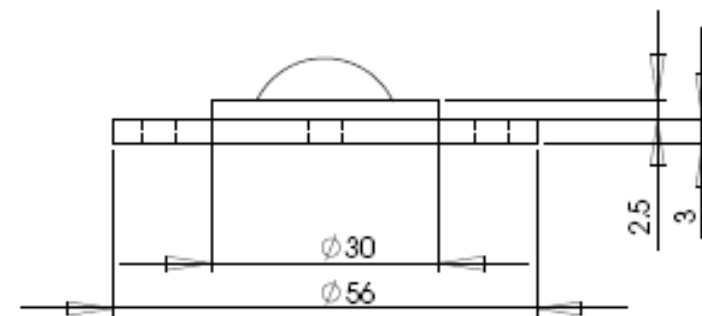
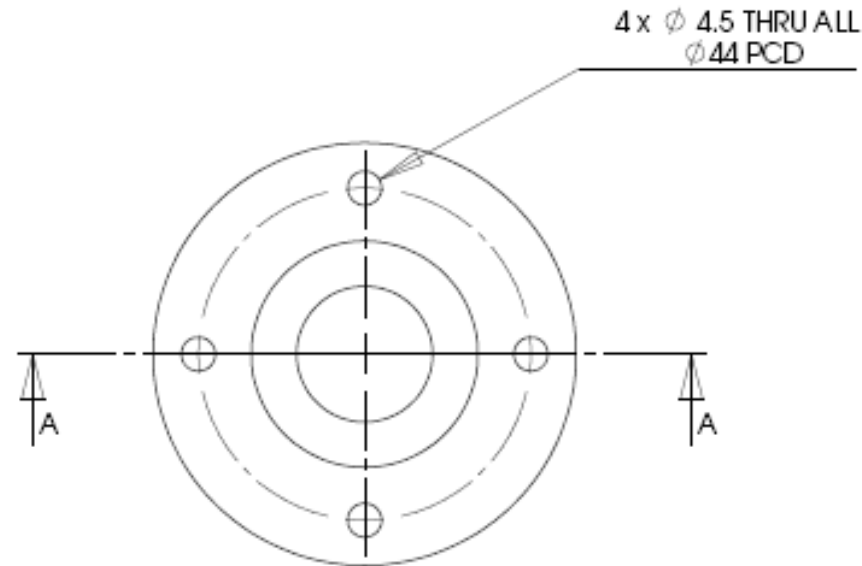
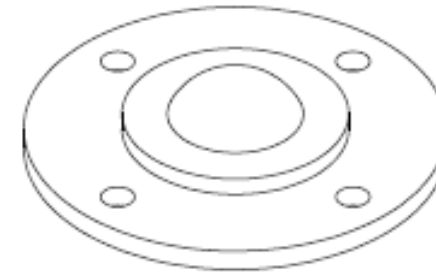
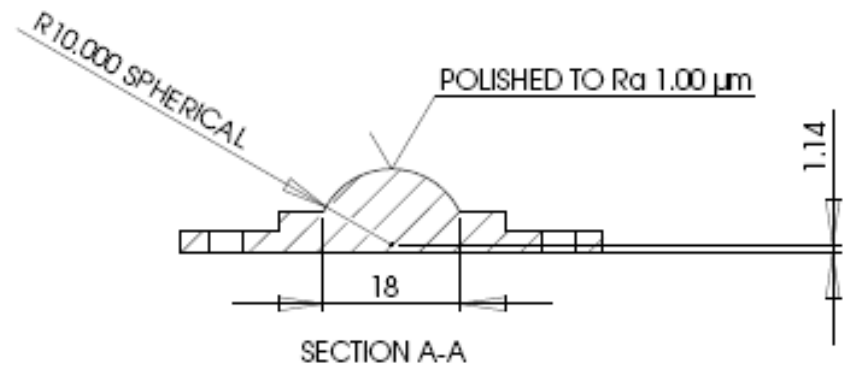
5

4

3

2

1



PROPRIETARY AND CONFIDENTIAL

THE INFORMATION CONTAINED IN THIS DRAWING IS THE SOLE PROPERTY OF THE UNIVERSITY OF BIRMINGHAM. ANY REPRODUCTION IN PART OR AS A WHOLE WITHOUT THE WRITTEN PERMISSION OF THE UNIVERSITY OF BIRMINGHAM IS PROHIBITED.

Tolerance unless otherwise stated:
whole numbers ± 0.25
one decimal place ± 0.10
two decimal places ± 0.05

MATERIAL
UHMWPE

DIMENSIONS ARE IN MM

DRAWN BY:

PARSHIA MOGHADAS
09 DECEMBER 2010

SIZE
A

DWG. NO.
LB-implant-10-MOP

REV
2

SCALE: 1:1

SHEET 1 OF 1

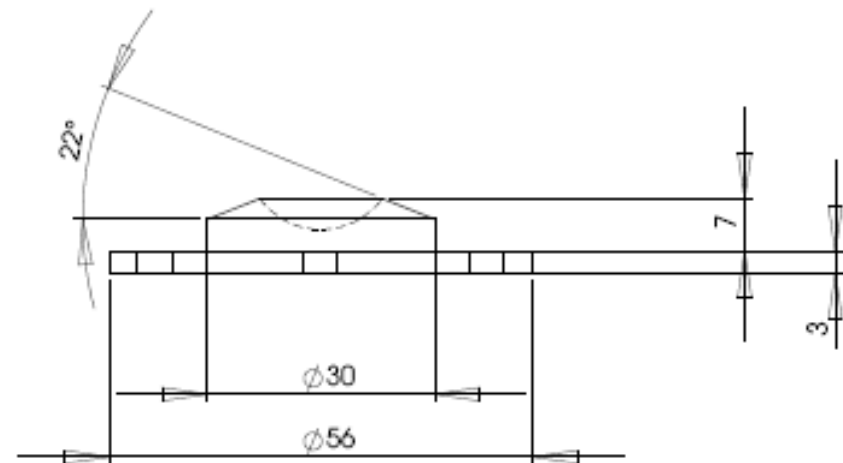
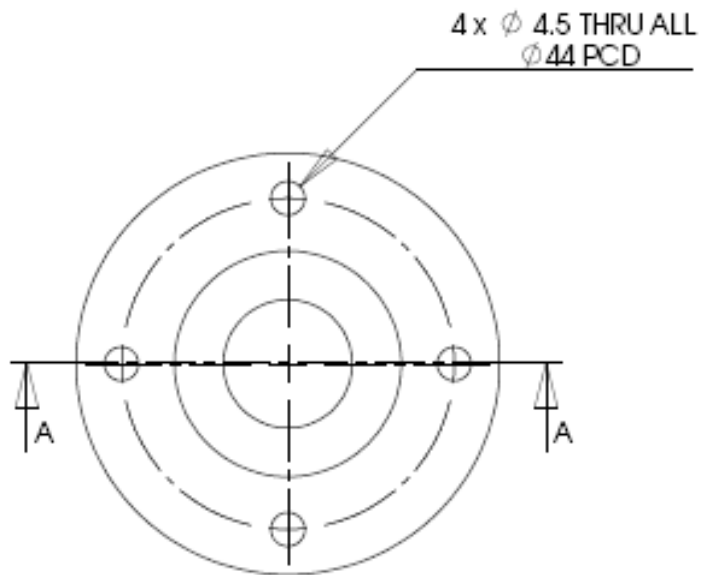
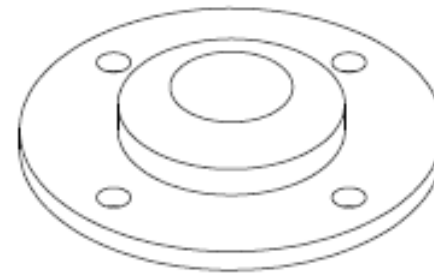
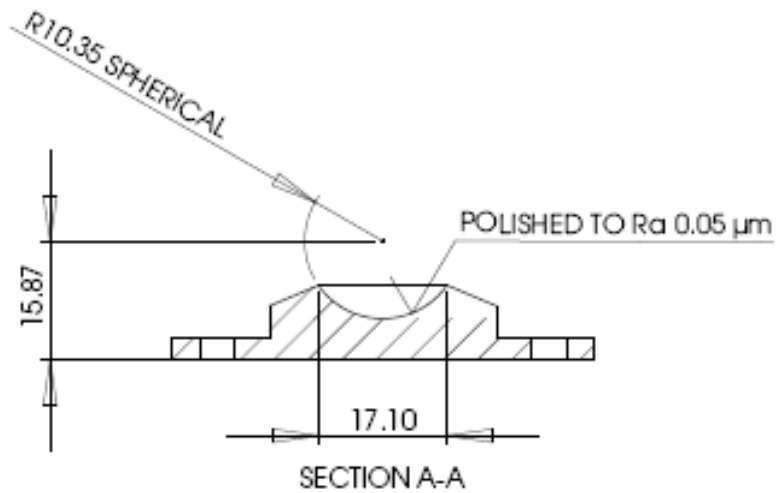
5

4

3

2

1



PROPRIETARY AND CONFIDENTIAL

THE INFORMATION CONTAINED IN THIS DRAWING IS THE SOLE PROPERTY OF THE UNIVERSITY OF BIRMINGHAM. ANY REPRODUCTION IN PART OR AS A WHOLE WITHOUT THE WRITTEN PERMISSION OF THE UNIVERSITY OF BIRMINGHAM IS PROHIBITED.

Tolerance unless otherwise stated:
whole numbers ± 0.25
one decimal place ± 0.10
two decimal places ± 0.05

MATERIAL
Cobalt Chrome to ASTM F799-96
(Co-27 Cr-5.5 Mo-0.06C)

DIMENSIONS ARE IN MM

DRAWN BY:

PARSHIA MOGHADAS
09 DECEMBER 2010

SIZE
A

DWG. NO.
UB-implant-10-MOP

REV
2

SCALE: 1:1

SHEET 1 OF 1

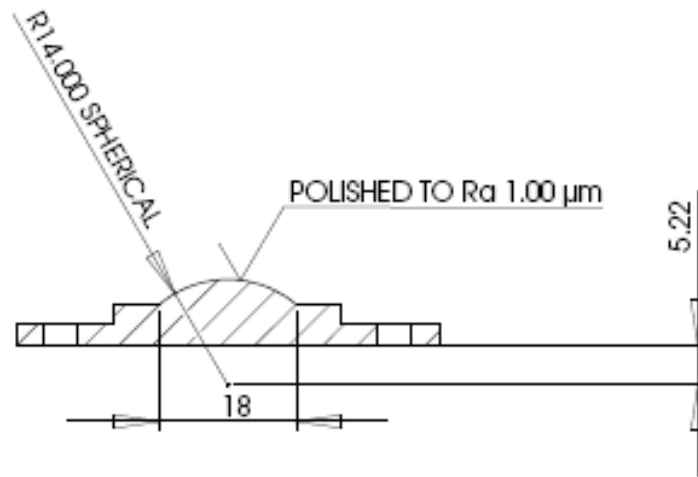
5

4

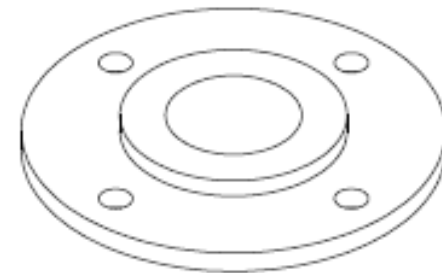
3

2

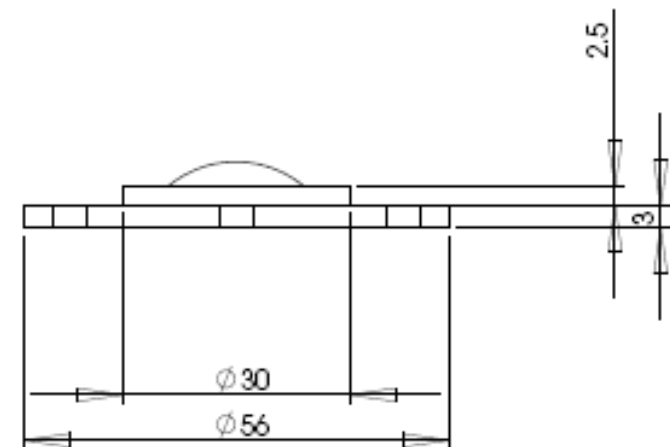
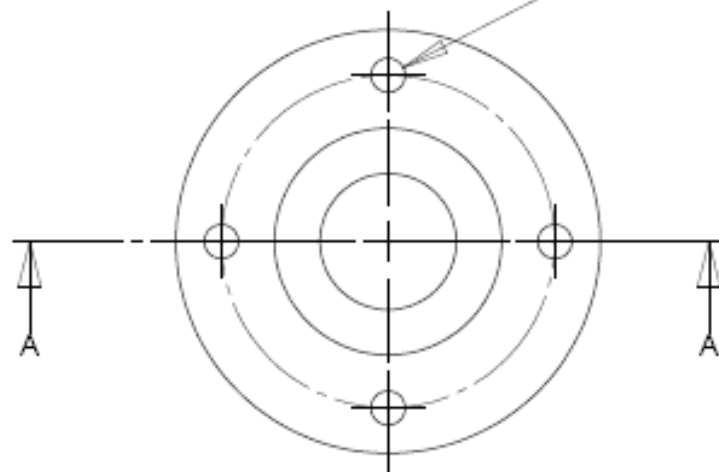
1



SECTION A-A



4 x ϕ 4.5 THRU ALL
 ϕ 44 PCD



PROPRIETARY AND CONFIDENTIAL

THE INFORMATION CONTAINED IN THIS DRAWING IS THE SOLE PROPERTY OF THE UNIVERSITY OF BIRMINGHAM. ANY REPRODUCTION IN PART OR AS A WHOLE WITHOUT THE WRITTEN PERMISSION OF THE UNIVERSITY OF BIRMINGHAM IS PROHIBITED.

Tolerance unless otherwise stated:
whole numbers ± 0.25
one decimal place ± 0.10
two decimal places ± 0.05
MATERIAL
UHMWPE

DIMENSIONS ARE IN MM

DRAWN BY:

PARSHIA MOGHADAS
09 DECEMBER 2010

SIZE
A

DWG. NO.
LB-implant-14-MOP

REV
2

SCALE: 1:1

SHEET 1 OF 1

5

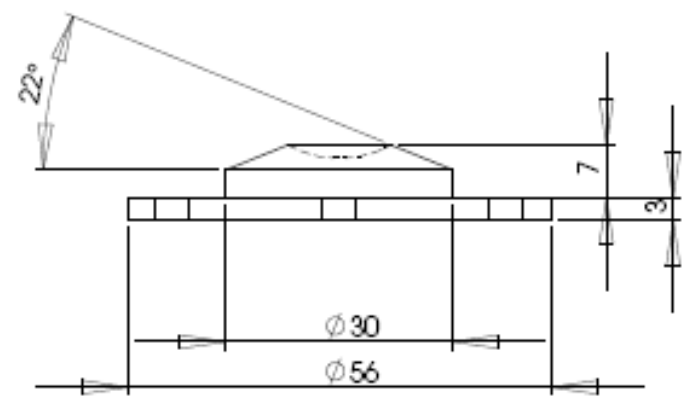
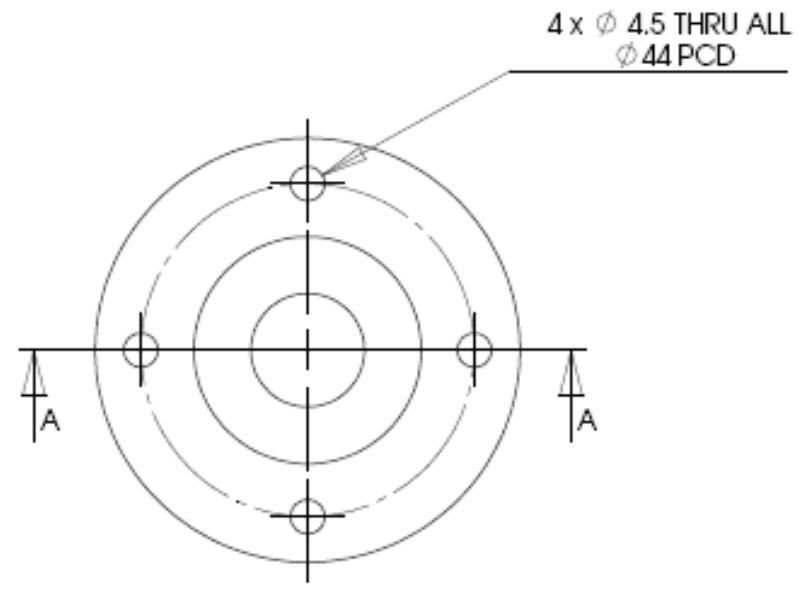
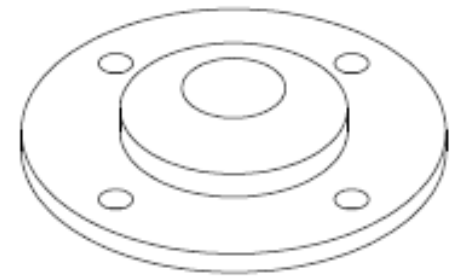
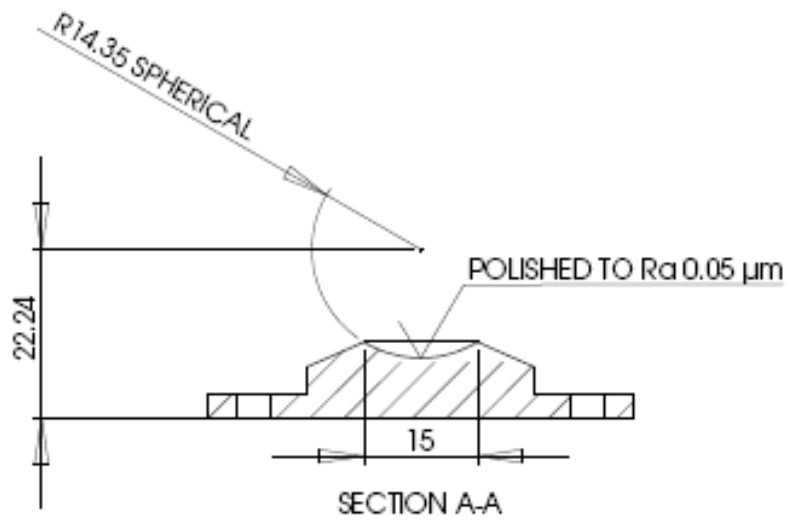
4

3

2

1

1



PROPRIETARY AND CONFIDENTIAL

THE INFORMATION CONTAINED IN THIS DRAWING IS THE SOLE PROPERTY OF THE UNIVERSITY OF BIRMINGHAM. ANY REPRODUCTION IN PART OR AS A WHOLE WITHOUT THE WRITTEN PERMISSION OF THE UNIVERSITY OF BIRMINGHAM IS PROHIBITED.

Tolerance unless otherwise stated:
 whole numbers ± 0.25
 one decimal place ± 0.10
 two decimal places ± 0.05

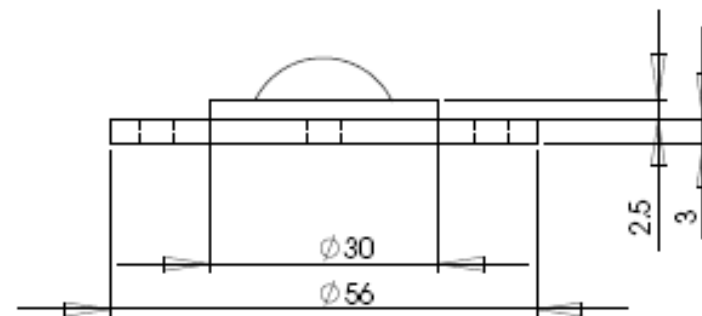
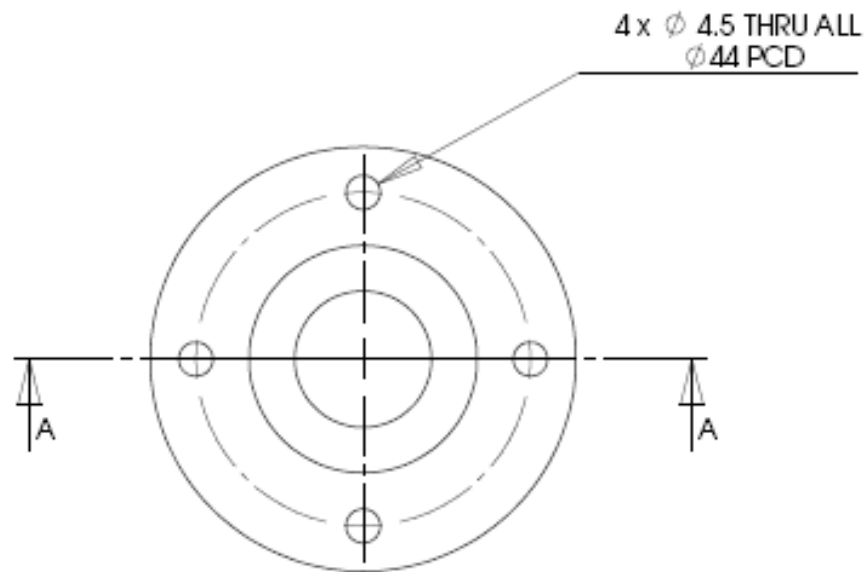
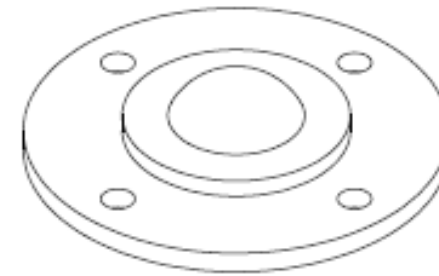
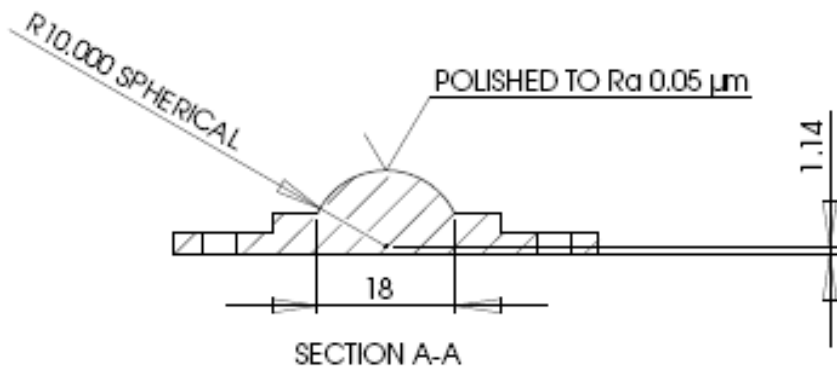
MATERIAL
 Cobalt Chrome to ASTM F799-96
 (Co-27 Cr-5.5 Mo-0.06C)

DIMENSIONS ARE IN MM

DRAWN BY:
 PARSHA MOGHADAS
 09 DECEMBER 2010

SIZE A	DWG. NO. UB-implant-14-MOP	REV 2
	SCALE: 1:1	SHEET 1 OF 1

5 4 3 2 1



PROPRIETARY AND CONFIDENTIAL

THE INFORMATION CONTAINED IN THIS DRAWING IS THE SOLE PROPERTY OF THE UNIVERSITY OF BIRMINGHAM. ANY REPRODUCTION IN PART OR AS A WHOLE WITHOUT THE WRITTEN PERMISSION OF THE UNIVERSITY OF BIRMINGHAM IS PROHIBITED.

Tolerance unless otherwise stated:
whole numbers ± 0.25
one decimal place ± 0.10
two decimal places ± 0.05

MATERIAL
Cobalt Chrome to ASTM F799-96
(Co-27 Cr-5.5 Mo-0.05C)

DIMENSIONS ARE IN MM

DRAWN BY:

PARSHA MOGHADAS
09 December 2010

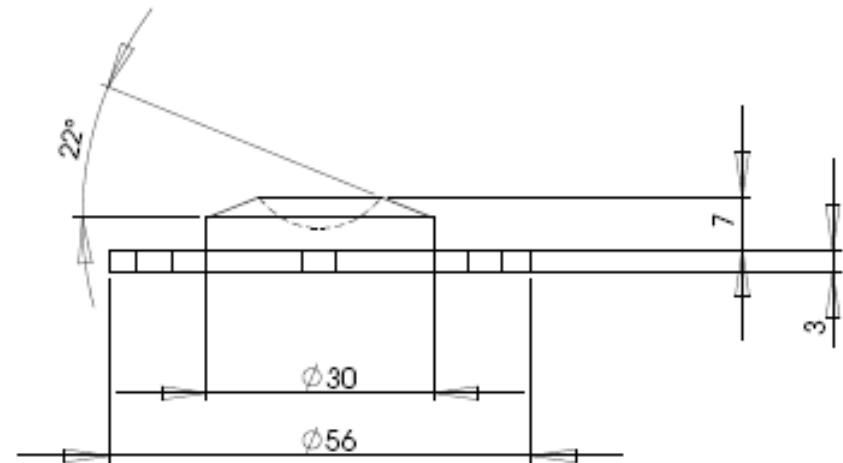
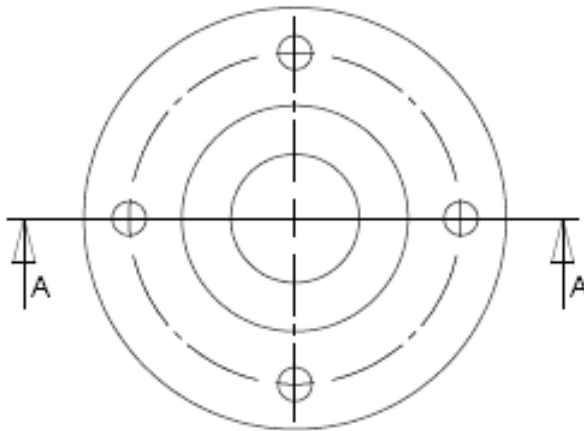
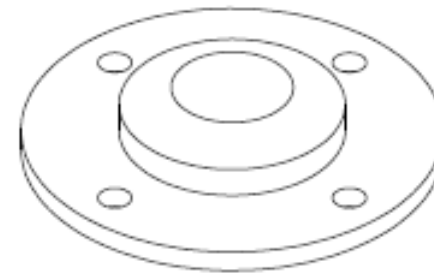
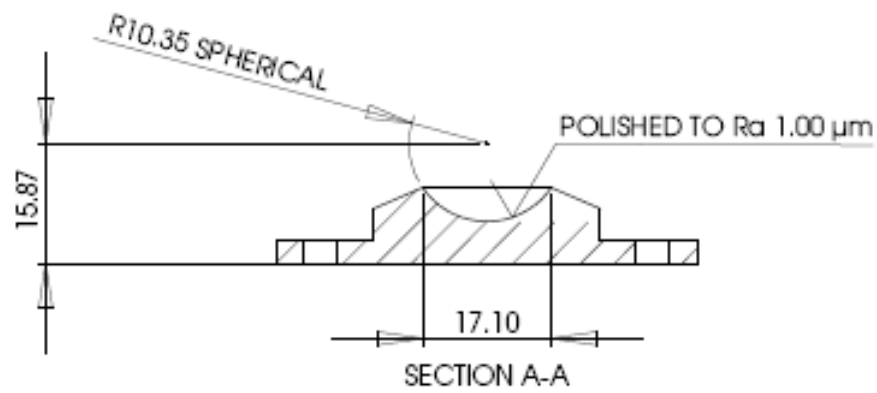
SIZE
A

DWG. NO.
LB-implant-10-POM

REV
2

SCALE: 1:1

SHEET 1 OF 1



PROPRIETARY AND CONFIDENTIAL

THE INFORMATION CONTAINED IN THIS DRAWING IS THE SOLE PROPERTY OF THE UNIVERSITY OF BIRMINGHAM. ANY REPRODUCTION IN PART OR AS A WHOLE WITHOUT THE WRITTEN PERMISSION OF THE UNIVERSITY OF BIRMINGHAM IS PROHIBITED.

Tolerance unless otherwise stated:
whole numbers ± 0.25
one decimal place ± 0.10
two decimal places ± 0.05

MATERIAL
UHMWPE

DIMENSIONS ARE IN MM

DRAWN BY:

PARSHIA MOGHADAS
09 DECEMBER 2010

SIZE
A

DWG. NO.
UB-implant-10-POM

REV
2

SCALE: 1:1

SHEET 1 OF 1

5

4

4

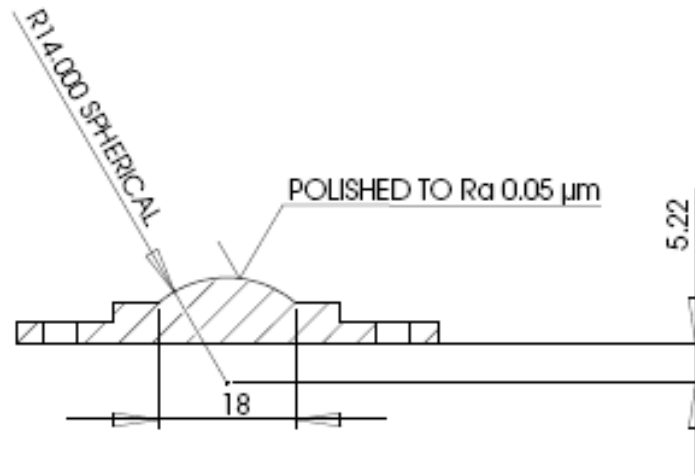
3

3

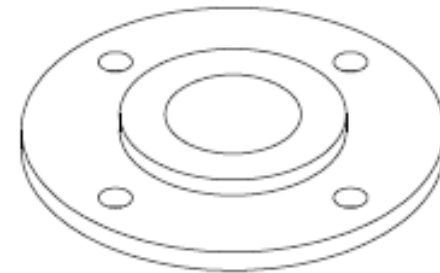
2

1

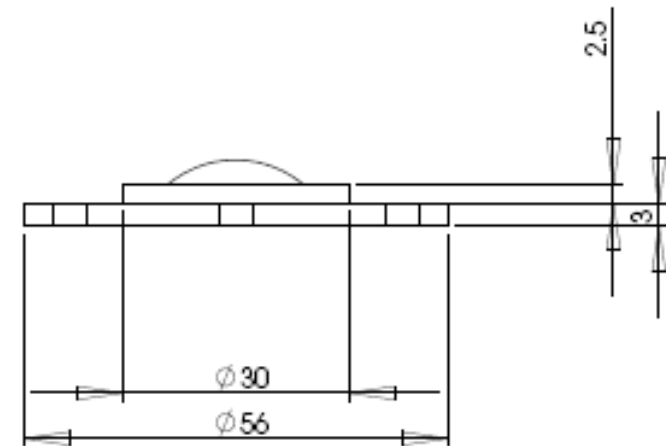
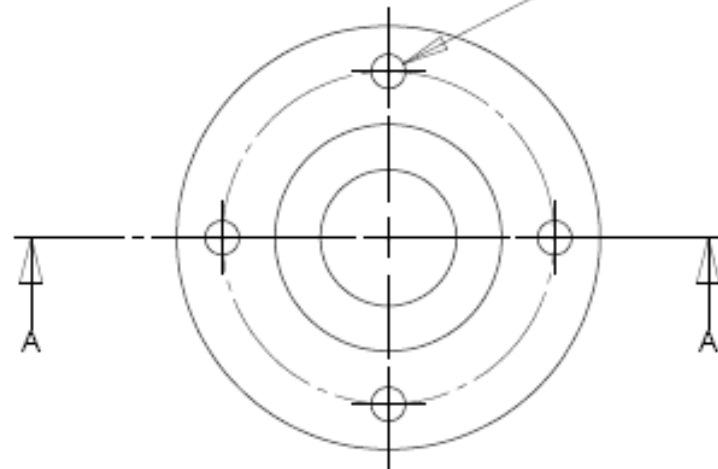
1



SECTION A-A



4 x ϕ 4.5 THRU ALL
 ϕ 44 PCD



PROPRIETARY AND CONFIDENTIAL

THE INFORMATION CONTAINED IN THIS DRAWING IS THE SOLE PROPERTY OF THE UNIVERSITY OF BIRMINGHAM. ANY REPRODUCTION IN PART OR AS A WHOLE WITHOUT THE WRITTEN PERMISSION OF THE UNIVERSITY OF BIRMINGHAM IS PROHIBITED.

Tolerance unless otherwise stated:
whole numbers ± 0.25
one decimal place ± 0.10
two decimal places ± 0.05

MATERIAL
Cobalt Chrome to ASTM F799-96
(Co-27 Cr-5.5 Mo-0.05C)

DIMENSIONS ARE IN MM

DRAWN BY:

PARSHA MOGHADAS
09 DECEMBER 2010

SIZE
A

DWG. NO.
LB-implant-14-POM

REV
2

SCALE: 1:1

SHEET 1 OF 1

5

f

4

1

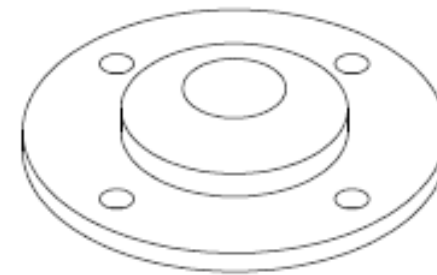
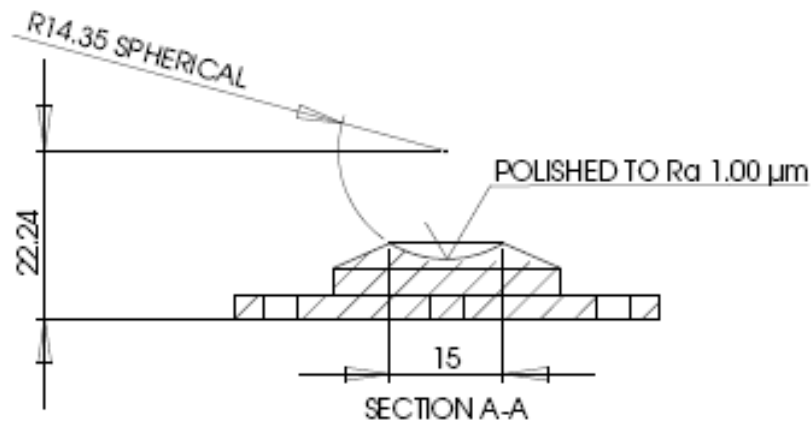
3

2

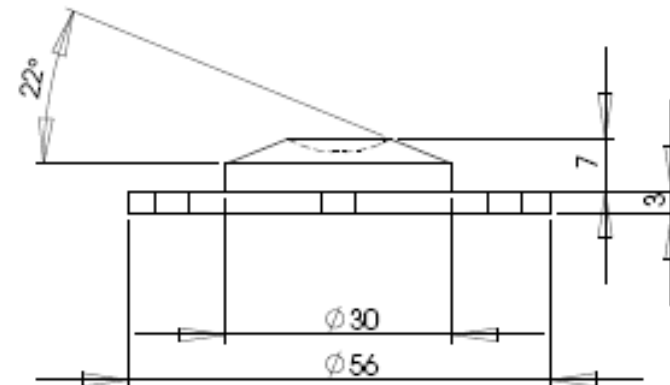
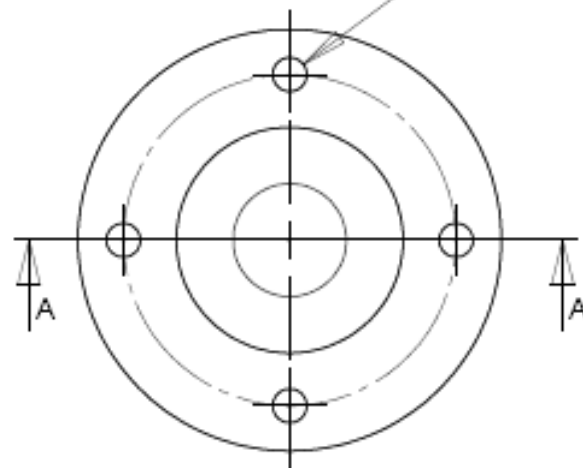
2

1

1



4 x ϕ 4.5 THRU ALL
 ϕ 44 PCD



PROPRIETARY AND CONFIDENTIAL

THE INFORMATION CONTAINED IN THIS DRAWING IS THE SOLE PROPERTY OF THE UNIVERSITY OF BIRMINGHAM. ANY REPRODUCTION IN PART OR AS A WHOLE WITHOUT THE WRITTEN PERMISSION OF THE UNIVERSITY OF BIRMINGHAM IS PROHIBITED.

Tolerance unless otherwise stated:
 whole numbers ± 0.25
 one decimal place ± 0.10
 two decimal places ± 0.05

MATERIAL
 UHMWPE

DIMENSIONS ARE IN MM

DRAWN BY:

PARSHA MOGHADA'S
 09 DECEMBER 2010

SIZE
A

DWG. NO.
UB-implant-14-POM

REV
2

SCALE: 1:1

SHEET 1 OF 1

Appendix B

The engineering drawings of the fixtures

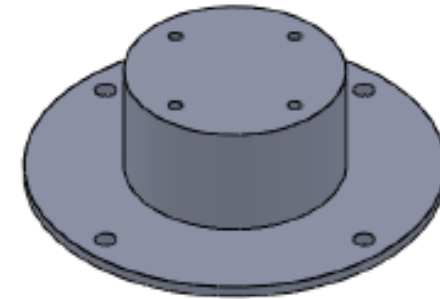
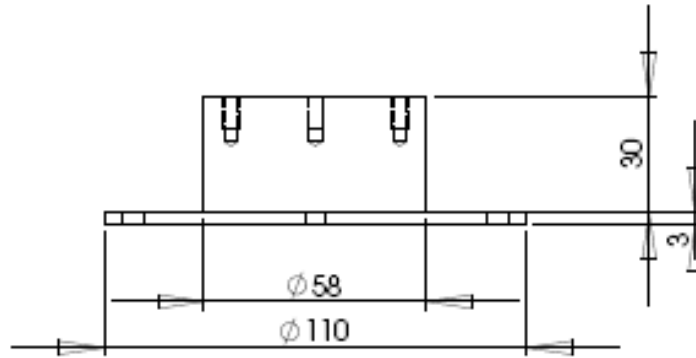
and the extra plate

(see § 4.3.2)

Note: LB (Lower Block) refers to the fixture mounted to the bottom plates

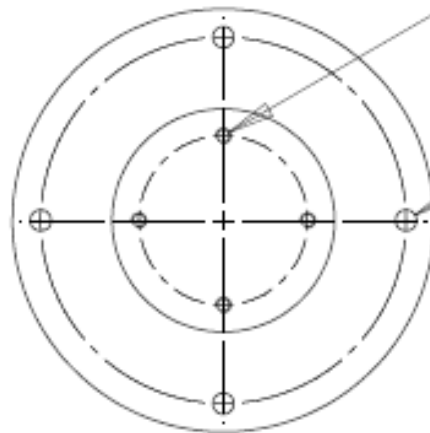
UB (Upper Block) refers to the fixture mounted to the top plates

EP is the abbreviation for extra plate



4 x ϕ 3.3 ∇ 11.5
 M4x0.7 - 6H ∇ 8
 ϕ 44 PCD

4 x ϕ 5.5 THRU ALL
 ϕ 95.25 PCD



PROPRIETARY AND CONFIDENTIAL

THE INFORMATION CONTAINED IN THIS DRAWING IS THE SOLE PROPERTY OF THE UNIVERSITY OF BIRMINGHAM. ANY REPRODUCTION IN PART OR AS A WHOLE WITHOUT THE WRITTEN PERMISSION OF THE UNIVERSITY OF BIRMINGHAM IS PROHIBITED.

Tolerance unless otherwise stated:
 whole numbers ± 0.25
 one decimal place ± 0.10
 two decimal places ± 0.05

MATERIAL
 MEDICAL GRADE STAINLESS STEEL

DIMENSIONS ARE IN MM

DRAWN BY:

PARSHA MOGHADAS
 19 October 2009

SIZE DWG. NO.

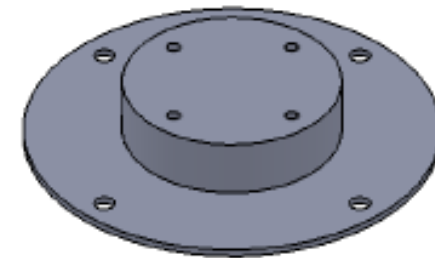
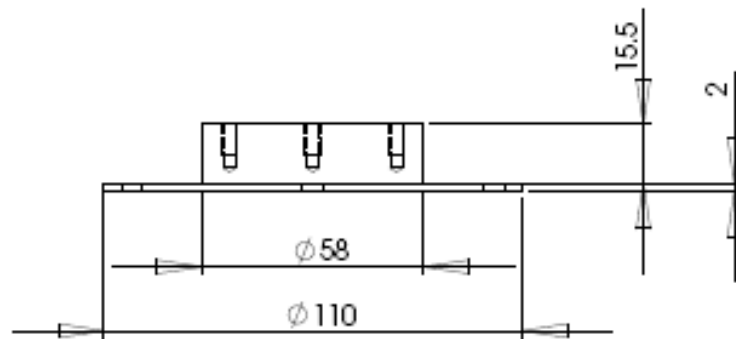
A **LB-jig-Flat**

REV

1

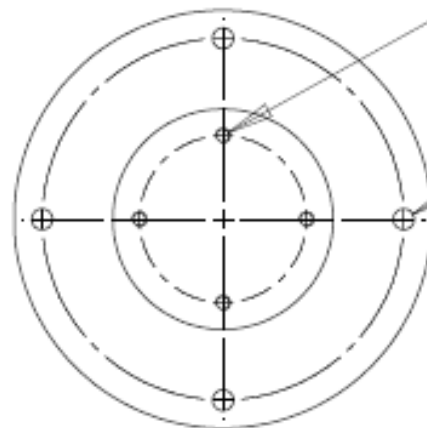
SCALE: 1:2

SHEET 1 OF 1



4 x ϕ 3.3 ∇ 11.5
 M4x0.7 - 6H ∇ 8
 ϕ 44 PCD

4 x ϕ 5.5 THRU ALL
 ϕ 95.25 PCD



PROPRIETARY AND CONFIDENTIAL

THE INFORMATION CONTAINED IN THIS DRAWING IS THE SOLE PROPERTY OF THE UNIVERSITY OF BIRMINGHAM. ANY REPRODUCTION IN PART OR AS A WHOLE WITHOUT THE WRITTEN PERMISSION OF THE UNIVERSITY OF BIRMINGHAM IS PROHIBITED.

Tolerance unless otherwise stated:
 whole numbers ± 0.25
 one decimal place ± 0.10
 two decimal places ± 0.05

MATERIAL
 MEDICAL GRADE STAINLESS STEEL

DIMENSIONS ARE IN MM

DRAWN BY:

PARSHA MOGHADAS
 19 October 2009

SIZE
A

DWG. NO.
UB-jig-Flat

REV
1

SCALE: 1:2

SHEET 1 OF 1

5

↑

4

↓

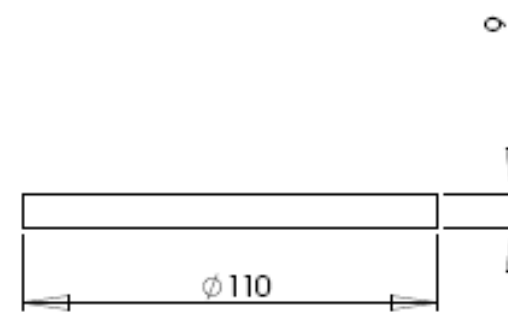
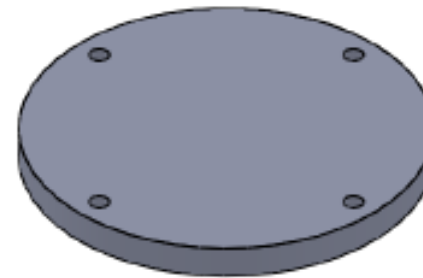
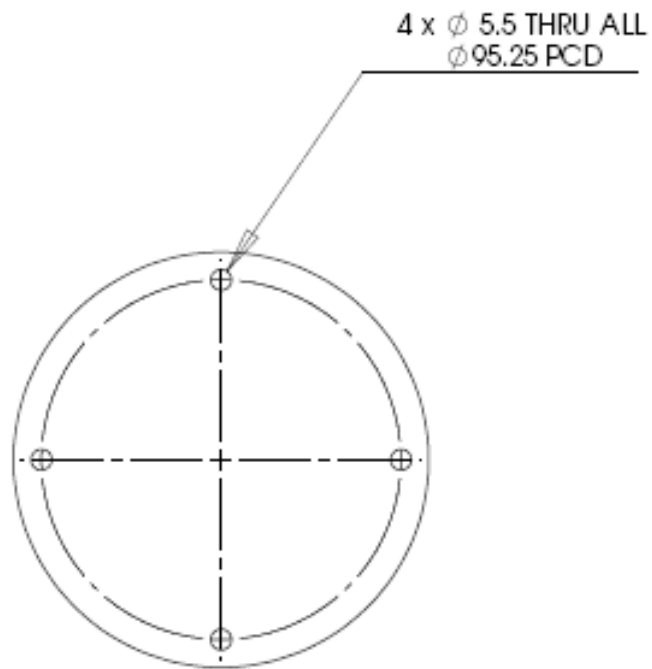
3

↓

2

↓

1



PROPRIETARY AND CONFIDENTIAL

THE INFORMATION CONTAINED IN THIS DRAWING IS THE SOLE PROPERTY OF THE UNIVERSITY OF BIRMINGHAM. ANY REPRODUCTION IN PART OR AS A WHOLE WITHOUT THE WRITTEN PERMISSION OF THE UNIVERSITY OF BIRMINGHAM IS PROHIBITED.

Tolerance unless otherwise stated:
 whole numbers ± 0.25
 one decimal place ± 0.10
 two decimal places ± 0.05

MATERIAL
 MEDICAL GRADE STAINLESS STEEL

DIMENSIONS ARE IN MM

DRAWN BY:

PARSHA MOGHADAS
 19 October 2009

SIZE
A

DWG. NO.
EP-9

REV
1

SCALE: 1:2

SHEET 1 OF 1

5

4

3

2

1

Appendix C

Graphs of mean frictional torque against frequency, for diluted calf serum and Ringer's solution

(part of the results from the study in Chapter 4)

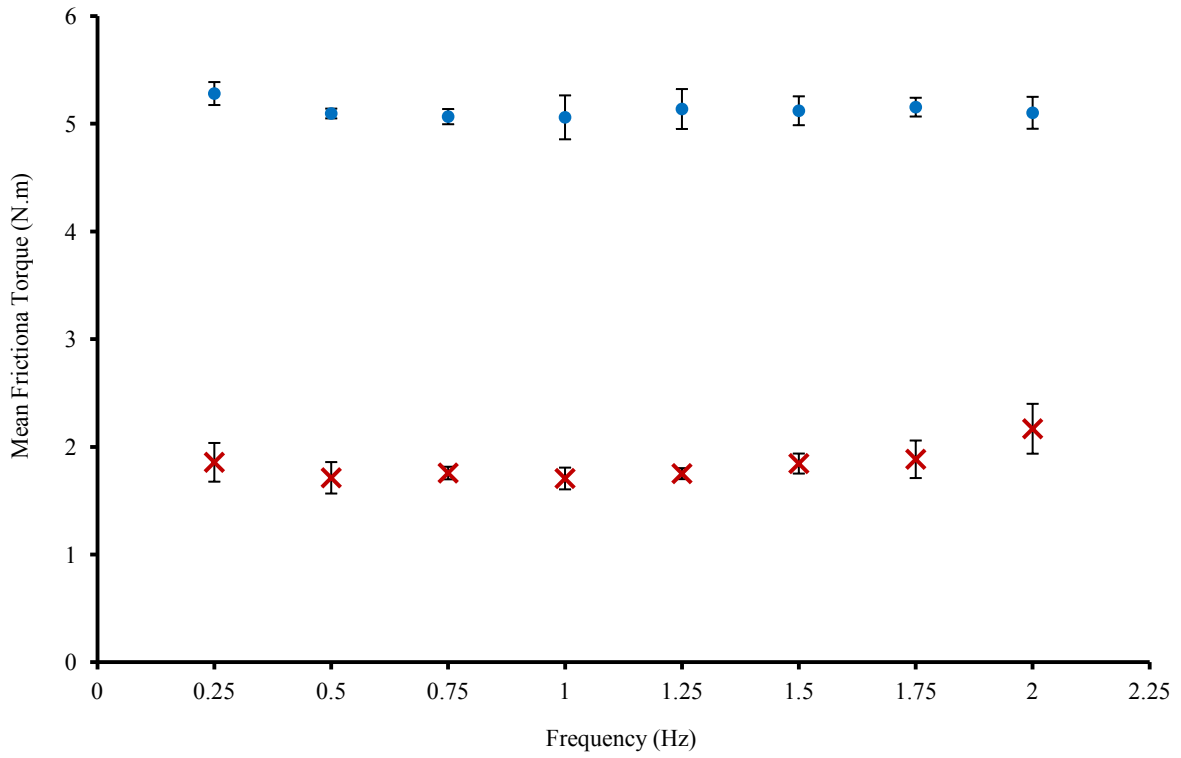


Figure C.1. Mean frictional torque plotted against frequency, for the samples with 10 mm ball radius in diluted calf serum (×) and Ringer's solution (•) for axial rotation. Error bars represent 95% confidence intervals

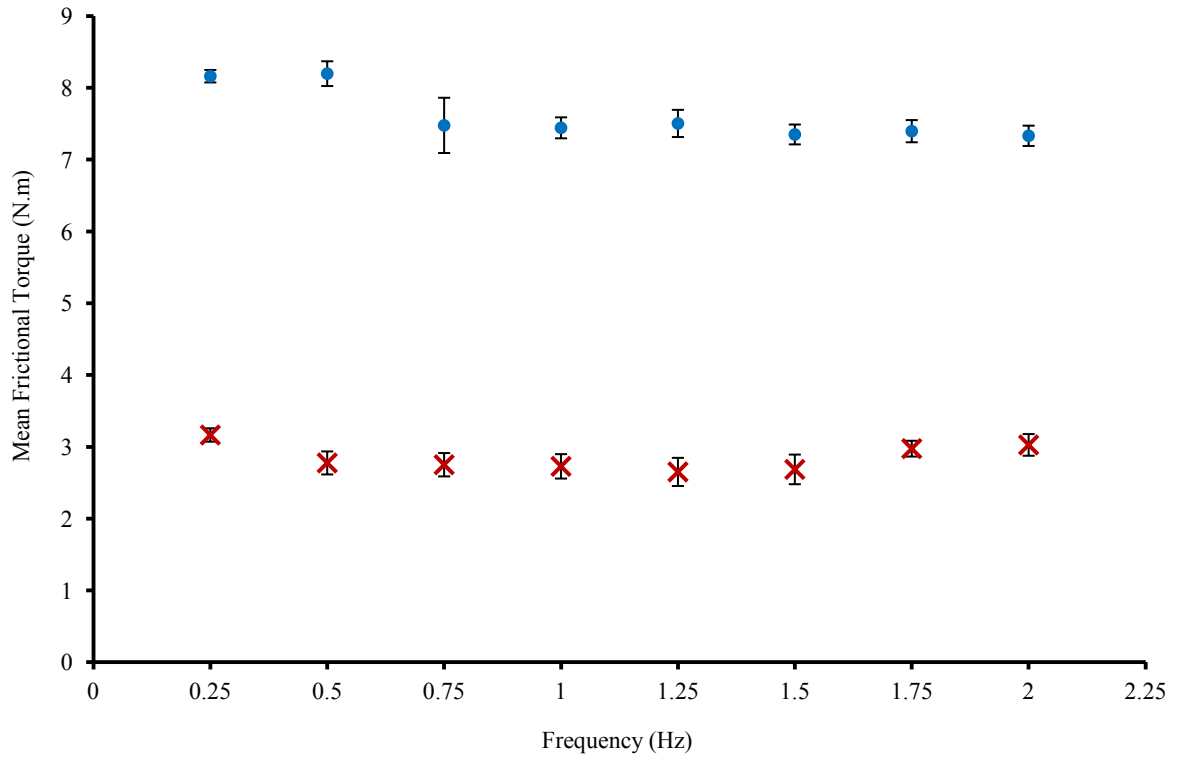


Figure C.2. Mean frictional torque plotted against frequency, for the samples with 10 mm ball radius in diluted calf serum (×) and Ringer's solution (•) for lateral bending. Error bars represent 95% confidence intervals

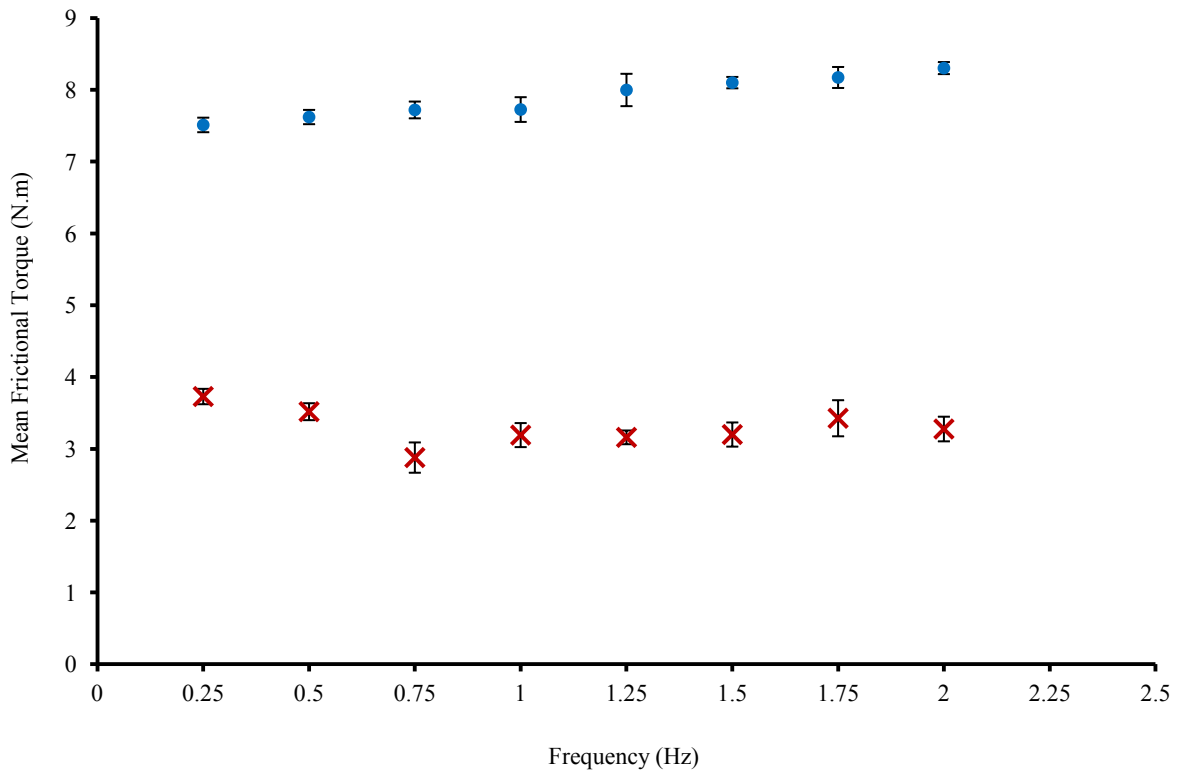


Figure C.3. Mean frictional torque plotted against frequency, for the samples with 10 mm ball radius in diluted calf serum (×) and Ringer's solution (•) for extension. Error bars represent 95% confidence intervals

Appendix D

Graphs of mean frictional torque against frequency and Stribeck curves, for polymer-on-metal and metal-on-polymer TDA samples
(part of the results from the study in Chapter 6)

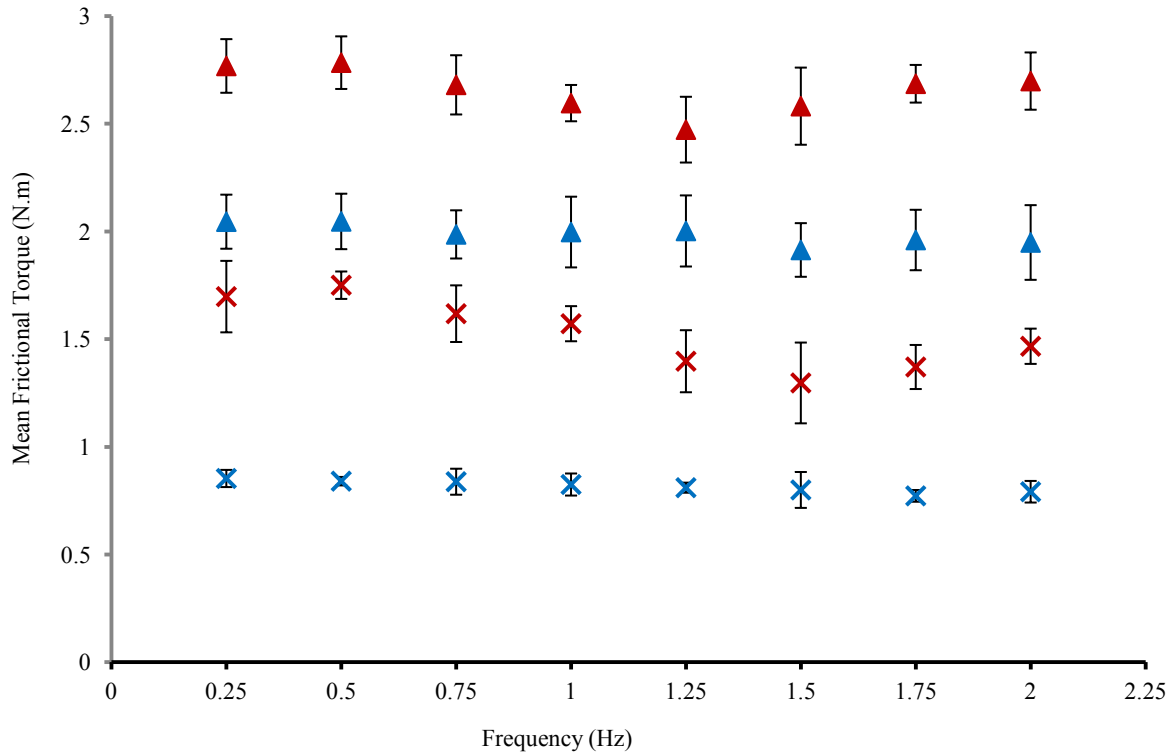


Figure D.1. Mean frictional torque plotted against frequency, in lateral bending between 0° to 2° , for the samples with 10 mm ball radius in polymer socket/metal ball (x) and metal socket/polymer ball (▲) combination, and samples with 14 mm ball radius in polymer socket/metal ball (x) and metal socket/polymer ball (▲) combination. Error bars represent 95% confidence intervals; where error bars are not shown, they are smaller than the data points. Same comment.

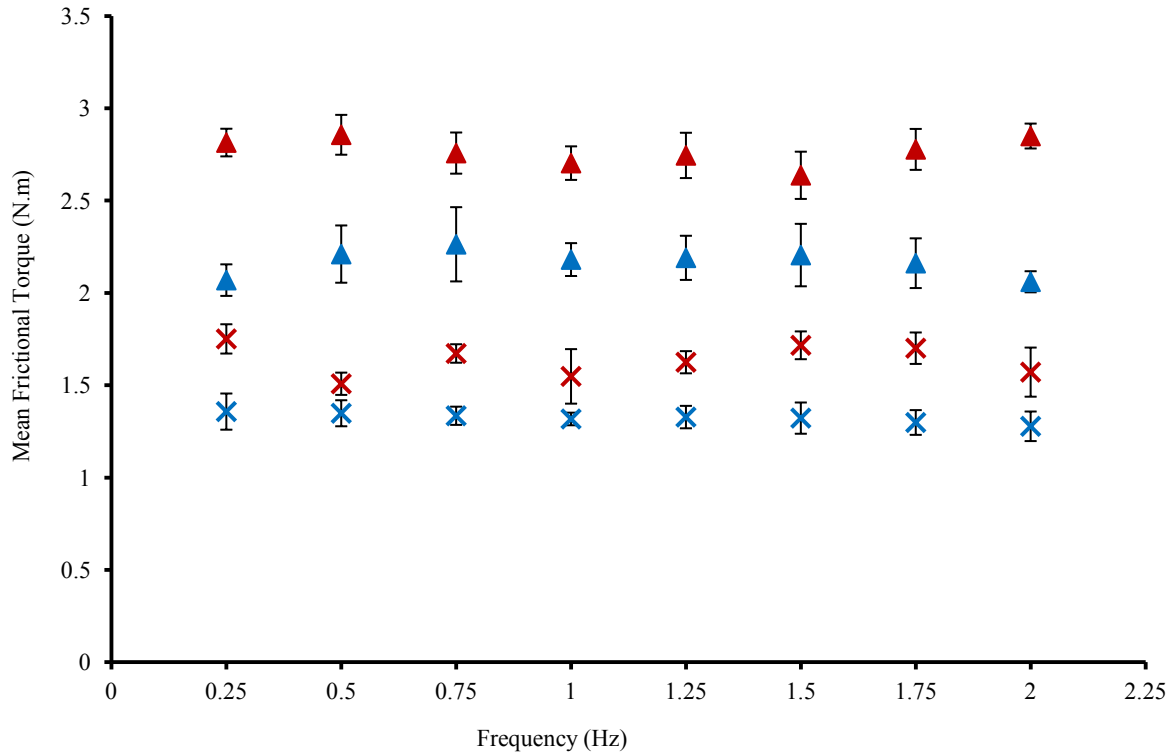


Figure D.2. Mean frictional torque plotted against frequency, in extension between 0° to -2° , for the samples with 10 mm ball radius in polymer socket/metal ball (\times) and metal socket/polymer ball (\blacktriangle) combination, and samples with 14 mm ball radius in polymer socket/metal ball (\times) and metal socket/polymer ball (\blacktriangle) combination. Error bars represent 95% confidence intervals; where error bars are not shown, they are smaller than the data points. Same comment.

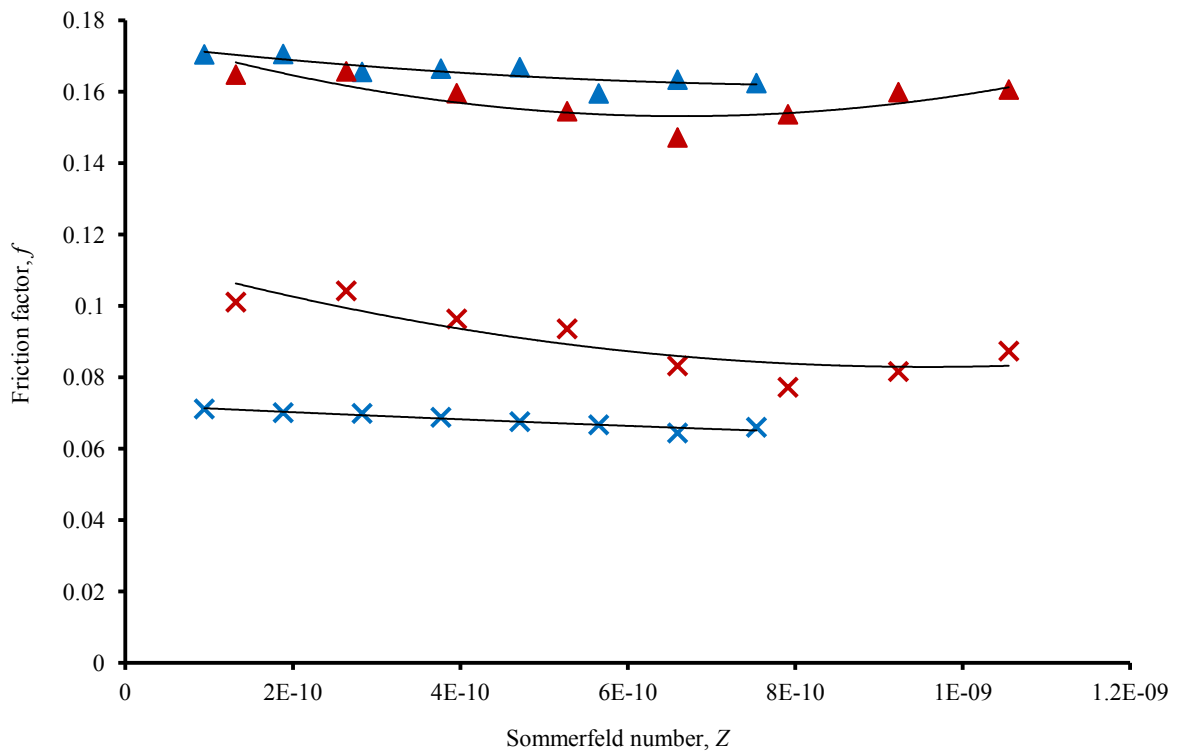


Figure D.3. Stribeck curves for the samples with 10 mm ball radius in polymer socket/metal ball (×) and metal socket/polymer ball (▲) combination, and samples with 14 mm ball radius in polymer socket/metal ball (×) and metal socket/polymer ball (▲) combination, in lateral bending between 0° to 2°. A third order polynomial has been fitted to the points.

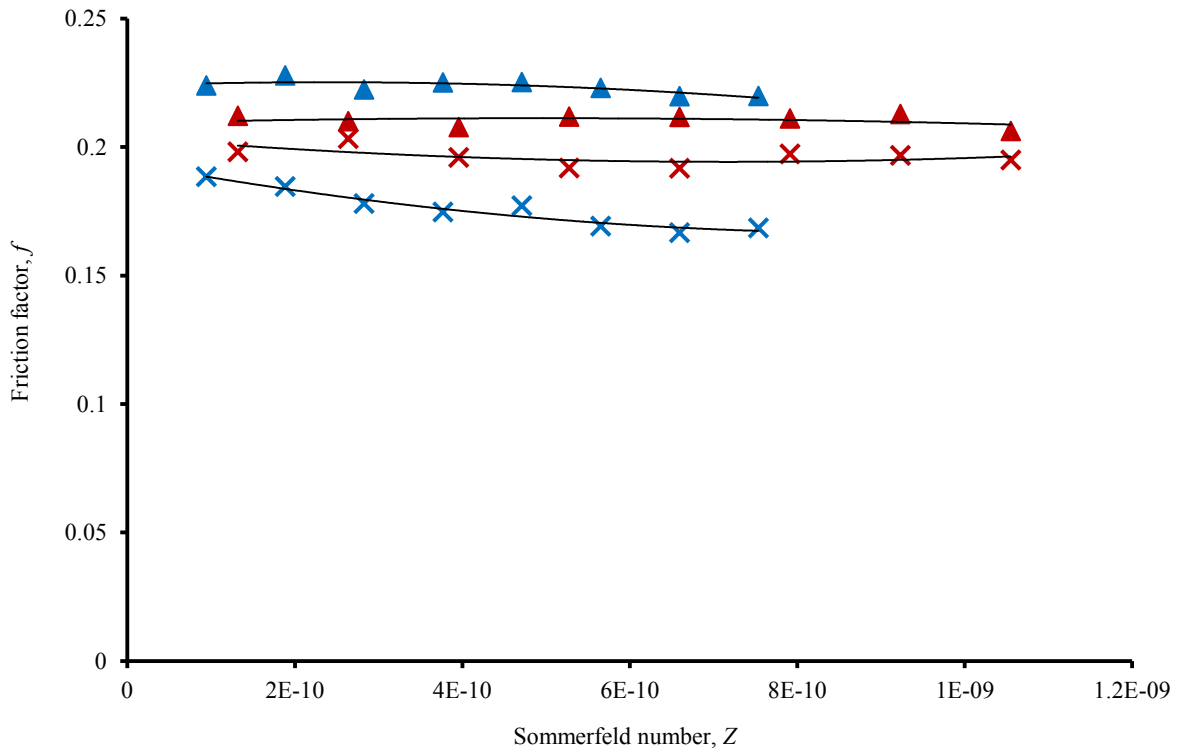
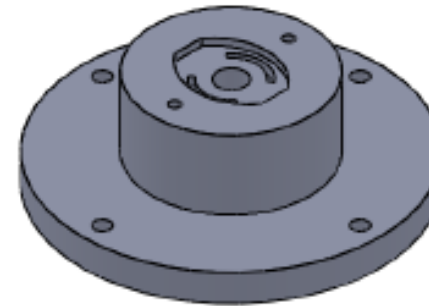
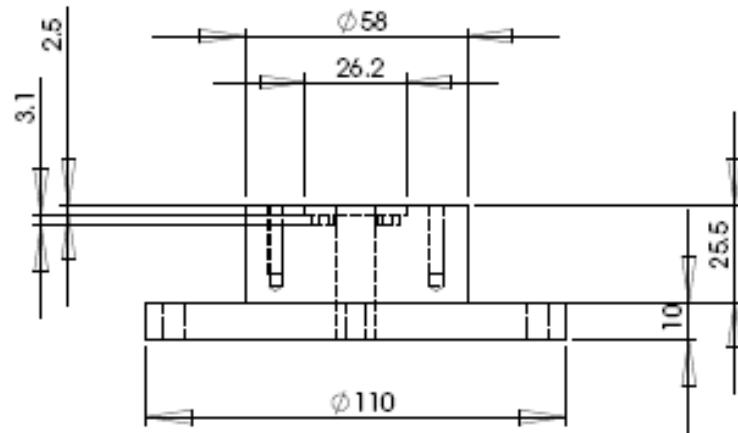


Figure D.4. *Stribeck curves for the samples with 10 mm ball radius in polymer socket/metal ball (×) and metal socket/polymer ball (▲) combination, and samples with 14 mm ball radius in polymer socket/metal ball (×) and metal socket/polymer ball (▲) combination, in extension between 0° to -3°. A third order polynomial has been fitted to the points.*

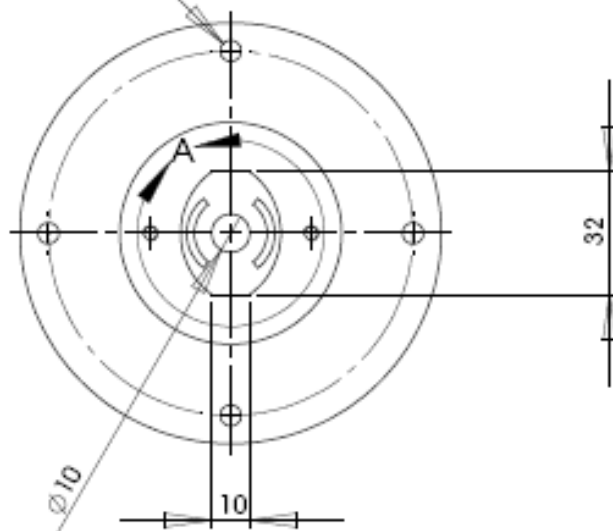
Appendix E

The engineering drawings of the fixtures for the
Charité® wear test

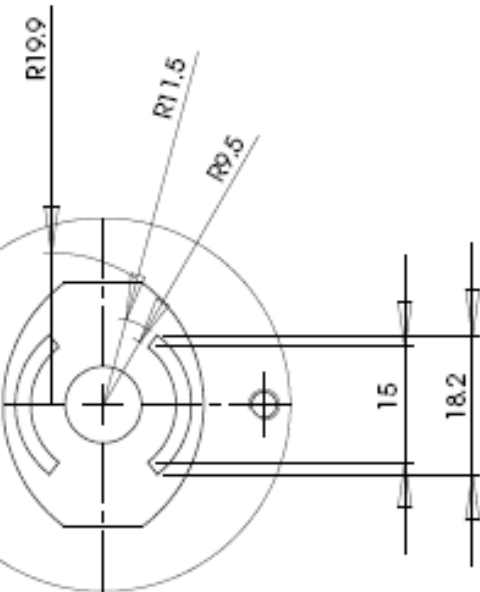
(see § 7.3.1)



4x ϕ 5.5 THRU ALL
 ϕ 95.25 PCD



2x ϕ 3.3 ∇ 21.5
 M4x0.7 - 6H ∇ 18



DETAIL A

PROPRIETARY AND CONFIDENTIAL

THE INFORMATION CONTAINED IN THIS DRAWING IS THE SOLE PROPERTY OF THE UNIVERSITY OF BIRMINGHAM. ANY REPRODUCTION IN PART OR AS A WHOLE WITHOUT THE WRITTEN PERMISSION OF THE UNIVERSITY OF BIRMINGHAM IS PROHIBITED.

Tolerance unless otherwise stated:
 whole numbers ± 0.25
 one decimal place ± 0.10
 two decimal places ± 0.05

MATERIAL
 MEDICAL GRADE STAINLESS STEEL

DIMENSIONS ARE IN MM

DRAWN BY:
 PARSHA MOGHADAS
 04 May 2010

SIZE DWG. NO.
A Lower Jig

REV
 2

SCALE: 1:2

SHEET 1 OF 1

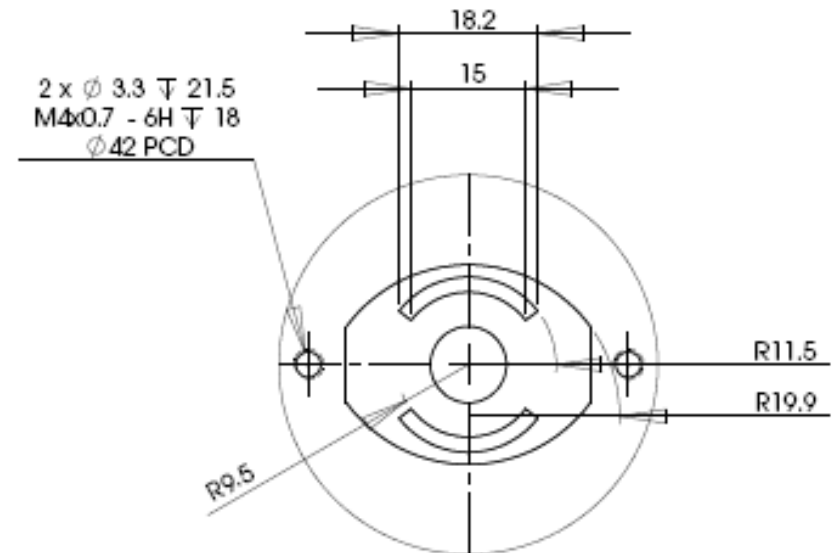
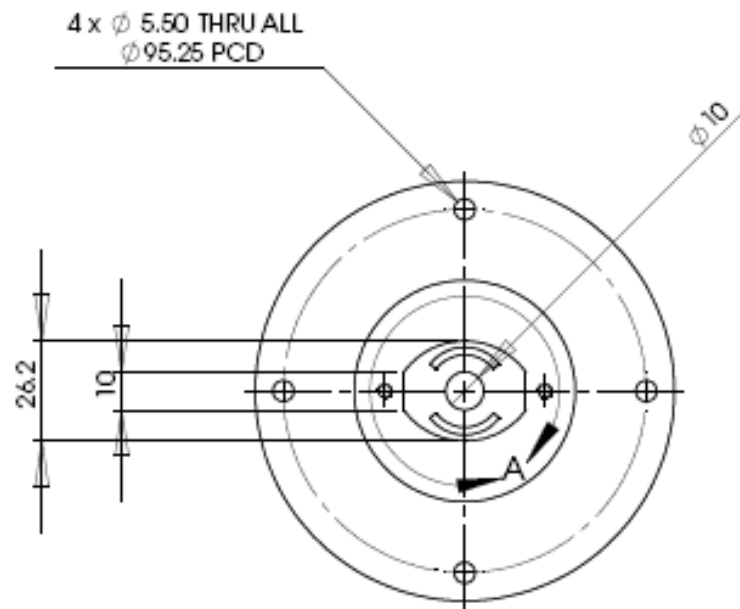
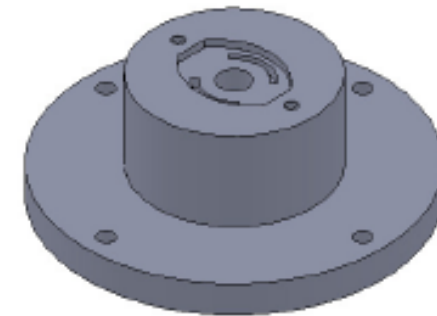
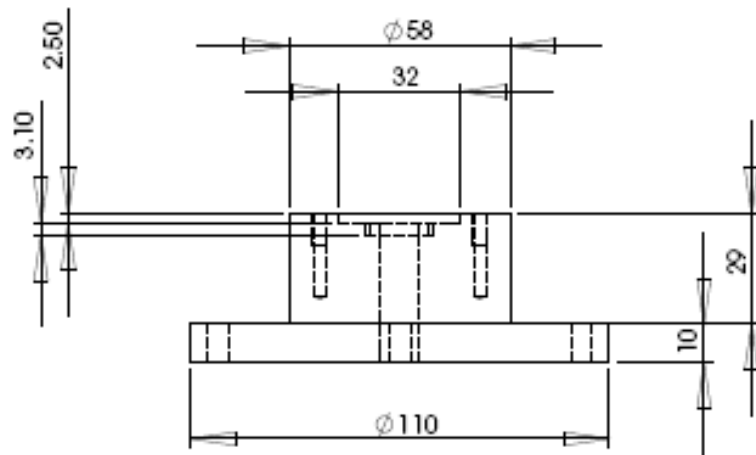
5

4

3

2

1



DETAIL A

PROPRIETARY AND CONFIDENTIAL

THE INFORMATION CONTAINED IN THIS DRAWING IS THE SOLE PROPERTY OF THE UNIVERSITY OF BIRMINGHAM. ANY REPRODUCTION IN PART OR AS A WHOLE WITHOUT THE WRITTEN PERMISSION OF THE UNIVERSITY OF BIRMINGHAM IS PROHIBITED.

Tolerance unless otherwise stated:
 whole numbers ± 0.25
 one decimal place ± 0.10
 two decimal places ± 0.05

MATERIAL
 MEDICAL GRADE STAINLESS STEEL

DIMENSIONS ARE IN MM

DRAWN BY:
 PARSHA MOGHADAS
 04 May 2010

SIZE
A

DWG. NO.
Upper Jig

REV
2

SCALE: 1:2

SHEET 1 OF 1

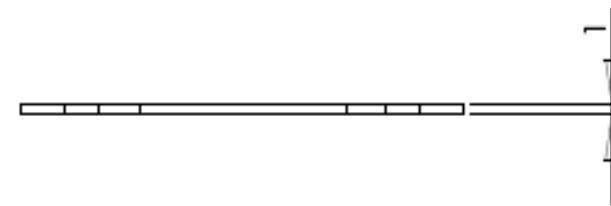
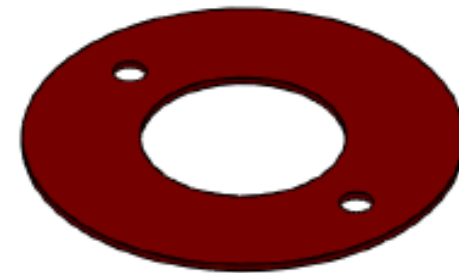
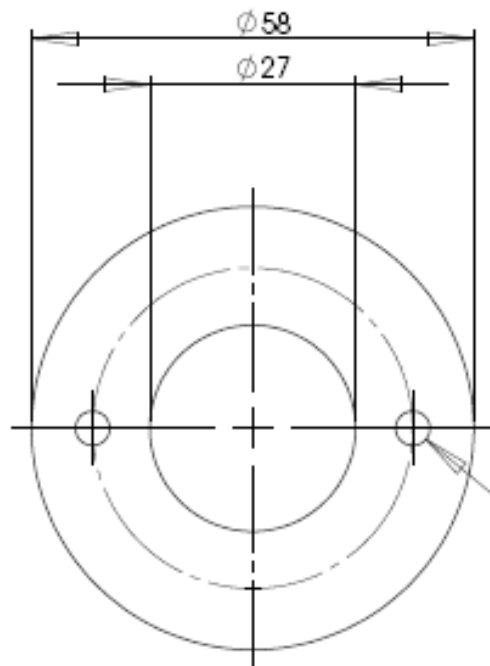
5

4

3

2

1



2 x $\phi 4.5$ THRU ALL
 $\phi 42$ PCD

PROPRIETARY AND CONFIDENTIAL

THE INFORMATION CONTAINED IN THIS DRAWING IS THE SOLE PROPERTY OF THE UNIVERSITY OF BIRMINGHAM. ANY REPRODUCTION IN PART OR AS A WHOLE WITHOUT THE WRITTEN PERMISSION OF THE UNIVERSITY OF BIRMINGHAM IS PROHIBITED.

Tolerance unless otherwise stated:
 whole numbers ± 0.25
 one decimal place ± 0.10
 two decimal places ± 0.05

MATERIAL
 MEDICAL GRADE STAINLESS STEEL

DIMENSIONS ARE IN MM

DRAWN BY:

PARSHA MOGHADAS
 06 May 2010

SIZE
A

DWG. NO.
Plate

REV
2

SCALE: 1:1

SHEET 1 OF 1

5

4

3

2

1

1

REFERENCES

Abramovitz, J. N., Neff, S. R. (1991) Lumbar disc surgery: results of the Prospective Lumbar Discectomy Study of the Joint Section on Disorders of the Spine and Peripheral Nerves of the American Association of Neurological Surgeons and the Congress of Neurological Surgeons. *Neurosurgery* **29**, 301-307; discussion 307-308

Adams, M. A., Freeman, B. J., Morrison, H. P., Nelson, I. W., Dolan, P. (2000) Mechanical initiation of intervertebral disc degeneration. *Spine* **25**, 1625-1636

Adams, M. A., Hutton, W. C. (1988) Mechanics of the intervertebral disc. In: *The Biology of the Intervertebral Disc*, edited by Ghosh, P. Volume II, Boca Raton, FL, CRC Press, pp 176-180

Adams, M. A., Hutton, W. C., Stott, J. R. (1980) The resistance to flexion of the lumbar intervertebral joint. *Spine* **5**, 245-253

Affatato, S., Spinelli, M., Zavalloni, M., Leardini, W., Viceconti, M. (2008) Predictive role of the Lambda ratio in the evaluation of metal-on-metal total hip replacement. *Proceedings of the Institution of Mechanical Engineers Part H-Journal of Engineering in Medicine* **222**, 617-628

Ahn, S. H. (2002) Comparison of clinical outcomes and natural morphologic changes between sequestered and large central extruded disc herniations. *Yonsei Medical Journal* **43**, 283-290

Anderson, P. A., Kurtz, S. M., Toth, J. M. (2006) Explant analysis of total disc replacement. *Seminars in Spine Surgery* **18**, 109-116

Anderson, P. A., Rouleau, J. P., Toth, J. M., Riew, K. D. (2004) A Comparison of simulator-tested and retrieved cervical disc prostheses. Invited submission from the Joint Section Meeting on Disorders of the Spine and Peripheral Nerves, March 2004. *Journal of Neurosurgery, Spine* **1**, 202–210

Anissian, H. L., Stark, A., Gustafson, A., Good, V., Clarke, I. C. (1999) Metal-on-metal bearing in hip prosthesis generates 100-fold less wear debris than metal-on-polyethylene. *Acta Orthopaedica Scandinavica* **70**, 578-82

ASTM F 1537 – 08: *Standard Specification for Wrought Cobalt-28Chromium-6Molybdenum Alloys for Surgical Implants (UNS R31537, UNS R31538, and UNS R31539)*. Pennsylvania, American Society for Testing and Materials

ASTM F 2423 – 05: *Standard Guide for Functional, Kinematic, and Wear Assessment of Total Disc Prostheses*. Pennsylvania, American Society for Testing and Materials

ASTM F 2848 – 10: *Standard Specification for Medical-Grade Ultra-High Molecular Weight Polyethylene Yarns*. Pennsylvania, American Society for Testing and Materials

Basho, R., Bhalla, A., Wang, J. C. (2011) Neck pain from a spine surgeon's perspective. *Physical Medicine and Rehabilitation Clinics of North America* **22**, 551-555

Berry, J. L., Moran, J. M., Berg, W. S., Steffee, A. D. (1987) A morphometric study of the human lumbar and selected thoracic vertebrae. *Spine* **12**, 362-367

Bertagnoli, R., Zigler, J., Karg, A., Voigt, S. (2005) Complications and strategies for revision surgery in total disc replacement. *The Orthopaedic Clinics of North America* **36**, 389-395

Bevington, P. R. (1969) *Data Reduction and Error Analysis in the Physical Sciences*. New York, McGraw Hill

Billi, F., Benya, P., Kavanaugh, A., Adams, J., McKellop, H., Ebrahimzadeh, E. (2011) The John Charnley Award: an accurate and extremely sensitive method to separate, display, and characterize wear debris, Part 2: metal and ceramic particles. *Clinical Orthopaedics and Related Research* **470**, 339-350

Bishop, N. E., Waldow, F., Morlock, M. M. (2008) Friction moments of large metal-on-metal hip joint bearings and other modern designs. *Medical Engineering and Physics* **30**, 1057-1064

Bland, J. M., Altman, D. G. (1986) Statistical methods for assessing agreement between two methods of clinical measurement. *The Lancet* **327**, 307-310

Bogduk, N. (2005) *Clinical Anatomy of the Lumbar Spine and Sacrum*. 4th edition, Edinburgh, Elsevier Churchill Livingstone

Broberg, K. B., von Essen, H. O. (1980) Modelling of intervertebral discs. *Spine* **5**, 155-167

Brockett, C. L., Harper, P., Williams, S., Isaac, G. H., Dwyer-Joyce, R. S., Jin, Z., Fisher, J. (2008) The influence of clearance on friction, lubrication and squeaking in large diameter metal-on-metal hip replacements. *Journal of Materials Science: Materials in Medicine* **19**, 1575–1579

Brown, C., Fisher, J., Ingham, E. (2006) Biological effects of clinically relevant wear particles from metal-on-metal hip prostheses. *Proceedings of the Institution of Mechanical Engineers Part H-Journal of Engineering in Medicine* **220**, 355-369

BS ISO 14242-2:2000: *Implants for Surgery- Wear of Total Hip Joint Prostheses. Methods of Measurement*. London, British Standard Institution

BS ISO 18192-1:2008: *Implants for Surgery- Wear of Total Intervertebral Spinal Disc Prostheses. Part 1: Loading and Displacement Parameters for Wear Testing and Corresponding Environmental Conditions for Test*. London, British Standard Institution

BS ISO 3274:1996: *Geometric Product Specifications (GPS)- Surface Texture: Profile Method. Nominal Characteristics of Contact (stylus) Instruments*. London, British Standard Institution

BS ISO 4287:1997: *Geometric Product Specifications (GPS)- Surface Texture: Profile Method. Terms, Definitions and Surface Texture Parameters.* London, British Standard Institution

BS ISO 4288:1996: *Geometric Product Specification (GPS)- Surface Texture: Profile Method: Rules and Procedures for the Assessment of Surface Texture.* London, British Standard Institution

Bush, K., Cowan, N., Katz, D. E., Gishen, P. (1992) The natural history of sciatica associated with disc pathology. *Spine* **17**, 1205-1212

Cairns, D., Mooney, V., Crane, P. (1984) Spinal pain rehabilitation: inpatient and outpatient treatment results and development of predictions for outcome. *Spine* **9**, 91-95

Catelas, I., Wimmer, M. A. (2011) New insights into wear and biological effects of metal-on-metal bearings. *The Journal of Bone and Joint Surgery, American Volume* **93**, 76-83

Charité® Artificial Disc (2006) *The User Manual.* DePuy Spine, Inc., Raynham, MA, USA

Clarke, I. C., Good, V., Williams, P., Schroeder, D., Anissian, L., Stark, A., Oonishi, H., Schuldies, J., Gustafson, G. (2000) Ultra-low wear rates for rigid-on-rigid bearings in total hip replacements. *Proceedings of the Institution of Mechanical Engineers Part H-Journal of Engineering in Medicine* **214**, 331-347

Crockett, R., Roba, M., Naka, M., Gasser, B., Delfosse, D., Frauchiger, V., Spencer, N. D. (2009) Friction, lubrication, and polymer transfer between UHMWPE and CoCrMo hip-implant materials: A fluorescence microscopy study. *Journal of Biomedical Materials Research Part A* **89A**, 1011-1018

Cunningham, B. W., Hu, N., Beatson, H. J., Serhan, H., Seftor, J. C., McAfee, P. C. (2009) Revision strategies for single- and two-level total disc arthroplasty procedures: a biomechanical perspective. *The Spine Journal* **9**, 735-743

Dang, L. (2007) *Minimally Invasive Spinal Surgery : Feasibility of Replacement of the Nucleus Pulposus and Fusion*. PhD, The University of Birmingham

Das, D. (1978) *Biochemistry*. Kolkata, Academic Publishers

David, T. (2005) Revision of a Charité artificial disc 9.5 years in vivo to a new Charité artificial disc: case report and explant analysis. *European Spine Journal* **14**, 507–511

Deyo, R. A., Mirza, S. K., Martin, B. I. (2006) Back pain prevalence and visit rates: estimates from U.S. national surveys, 2002. *Spine* **31**, 2724-2727

Dowson, D., Hardaker, C., Flett, M., Isaac, G. H. (2004) A hip joint simulator study of the performance of metal-on-metal joints: Part I: the role of materials. *Journal of Arthroplasty* **19**, 118-123

Dowson, D., Jin, Z. M. (2006) Metal-on-metal hip joint tribology. *Proceedings of the Institution of Mechanical Engineers Part H-Journal of Engineering in Medicine* **220**, 107-118

Erkan, S., Rivera, Y., Wu, C., Mehbod, A. A., Transfeldt, E. E. (2009) Biomechanical comparison of a two-level Maverick disc replacement with a hybrid one-level disc replacement and one-level anterior lumbar interbody fusion. *Spine Journal* **9**, 830-835

Evans, P., Starly, B., Sun, W. (2005) Computer aided tissue engineering design for a spinal intervertebral disc. *Proceedings of the IEEE 31st Annual Northeast Bioengineering Conference*, Stevens Institute of Technology, Hoboken, New Jersey

Farfan, H. F., Huberdeu, R. M., Dubow, H. I. (1972) Lumbar intervertebral disc degeneration: the influence of geometrical features on the pattern of disc degeneration- a post mortem study. *The Journal of Bone and Joint Surgery, American Volume* **54**, 492-510

Fogh-Andersen, N., Altura, B. M., Altura, B. T., Siggaard-Andersen, O. (1995) Composition of interstitial fluid. *Clinical Chemistry* **41**, 1522-1525

Frymoyer, J. W., Cats-Baril, W. L. (1991) An overview of the incidences and costs of low back pain. *The Orthopaedics Clinics of North America* **22**, 263-271

Fujiwara, A., Tamai, K., Yamato, M., An, H. S., Yoshida, H., Saotome, K., Kurihashi, A. (1999) The relationship between facet joint osteoarthritis and disc degeneration of the lumbar spine: an MRI study. *European Spine Journal* **8**, 396-401

Gale, L. R., Chen, Y., Hills, B. A., Crawford, R. (2007) Boundary lubrication of joints - Characterization of surface-active phospholipids found on retrieved implants. *Acta Orthopaedica* **78**, 309-314

Gilad, I., Nissan, M. (1986) A study of vertebra and disc geometric relations of the human cervical and lumbar spine. *Spine* **11**, 154-157

Gillet P. (2003) The fate of the adjacent motion segments after lumbar fusion. *Journal of Spinal Disorders and Techniques* **16**, 338-345

Goldsmith, A. A., Dowson, D., Isaac, G. H., Lancaster, J. G. (2000) A comparative joint simulator study of the wear of metal-on-metal and alternative material combinations in hip replacements. *Proceedings of the Institution of Mechanical Engineers Part H- Journal of Engineering in Medicine* **214**, 39-47

Gore, T. A., Higginson, G. R., Kornberg, R. E. (1981) Some evidence of squeeze-film lubrication in hip prostheses. *Engineering in Medicine* **10**, 89-95

Gower, W. E., Pedrini, V. (1969) Age-related variations in proteinpolysaccharides from human nucleus pulposus, annulus fibrosus, and costal cartilage. *The Journal of Bone and Joint Surgery* **51**, 1154-1162

Grupp, T. M., Meisel, H. J., Cotton, J. A., Schwiesau, J., Fritz, B., Blömer, W., Jansson, V. (2010) Alternative bearing materials for intervertebral disc arthroplasty. *Biomaterials* **31**, 523-531

Guerin, H. A. L., Elliott, D. M. (2006) Structure and properties of soft tissues in the spine. In: *Spine Technology Handbook*, edited by Kurtz, S. M., Edidin, A. A., Amsterdam, Elsevier Academic Press, pp 35-56

Gwynne, J. H., Oyen, M. L., Cameron, R. E. (2010) Preparation of polymeric samples containing a graduated modulus region and development of nanoindentation linescan techniques. *Polymer Testing* **29**, 494-502

Hall, R. M., Unsworth, A., Wroblewski, B. M., Burgessa, I. C. (1994) Frictional characterisation of explanted Charnley hip prosthesis. *Wear* **175**, 159-166

Hallab, N., Link, H. D., McAfee, P. C. (2003) Biomaterial optimization in total disc arthroplasty. *Spine* **28**, S139-S152

Hammond, W. H., Brena, S. F., Unikel, I. P. (1978) Compensation for work-related injuries and rehabilitation of patients with chronic pain. *Southern Medical Journal* **71**, 664-666

Hardy, R. W. (1982) *Lumbar Disc Disease*. New York, Raven Press

Harris, R. I., MacNab, I. (1954) Structural changes in the lumbar intervertebral discs: their relationship to low back pain and sciatica. *Journal of Bone and Joint Surgery, British Volume* **36**, 304-322

Harsha, A. P., Joyce, T. J. (2011) Challenges associated with using bovine serum in wear testing orthopaedic biopolymers. *Proceedings of the Institution of Mechanical Engineers, Part H- Journal of Engineering in Medicine* **225**, 948-58

Hickey, D. S., Hukins, D. W. L. (1980) Relationship between the structure of the annulus fibrosus and the function and failure of the intervertebral disc. *Spine* **5**, 106-116

Huang, C. H., Ho, F. Y., Ma, H. M., Yang, C. T., Liao, J. J., Kao, H. C., Young, T. H., Cheng, C. K. (2002) Particle size and morphology of UHMWPE wear debris in failed total knee arthroplasties- a comparison between mobile bearing and fixed bearing knees. *Journal of Orthopaedic Research* **20**, 1038-1041

Hughes, S. P. F., Freemont, A. J., Hukins, D. W. L., McGregor, A. H., Roberts, S. (2012) The pathogenesis of intervertebral disc degeneration and new and emerging therapies in managing back pain. *Journal of Bone and Joint Surgery, British Volume* (submitted)

Hukins, D. W. L. (1987) properties of spinal materials. In: *The Lumbar Spine and Back Pain*, edited by Jayson, M. I. V., 3rd edition, Edinburgh, Churchill Livingstone, pp 138-160

Hukins, D. W. L. (1988) Disc structure and function. In: *The Biology of the Intervertebral Disc*, edited by Ghosh, P. Volume I, Boca Raton, FL, CRC Press, pp 1-37

Hukins, D. W. L. (1992) A simple model for the function of proteoglycans and collagen in the response to compression of the intervertebral disc. *Proceedings of the Royal Society Part B- Biological Sciences* **249**, 281-285

Hukins, D. W. L., Aspden, R. M. (1985) Composition and properties of connective tissues. *Trends in Biochemical Sciences* **10**, 260-264

Hukins, D. W. L., Kirby, M. C., Sikoryn, T. A., Aspden, R. M., Cox, A. J. (1990) Comparison of structure, mechanical properties and functions of lumbar spinal ligaments. *Spine* **15**, 787-795

Hutchings, I. M. (1992) *Tribology- Friction and Wear of Engineering Materials*. London, Arnold

Iatridis, J. C., Weidenbaum, M., Setton, L. A., Mow, V. C. (1996) Is the nucleus pulposus a solid or a fluid? Mechanical behaviors of the nucleus pulposus of the human intervertebral disc. *Spine* **21**, 1174-1184

Jacobs, M. A., Schmidt, M. B., Farrar, R. (1998) The effect of clearance and diameter on the debris generation in a metal-on-metal hip. *The Journal of Arthroplasty* **13**, 224

James, G. (1993) *Advanced Modern Engineering Mathematics*. Wokingham, Addison-Wesley Publishing Company, pp 778-88

Jin, C., Wei, W. (2009) Wear. In: *Biomedical Materials*, edited by Narayan, R., New York, Springer, pp 183-196

Jin, Z. M., Dowson, D., Fisher, J. (1997) Analysis of fluid film lubrication in artificial hip joint replacements with surfaces of high elastic modulus. *Proceedings of the Institution of Mechanical Engineers Part H-Journal of Engineering in Medicine* **211**, 247-256

Jones, E., Scholes, S. C., Burgess, I. C., Ash, H. E., Unsworth, A. (2009) Compliant layer bearings in artificial joints. Part 2: simulator and fatigue testing to assess the durability of the interface between an elastomeric layer and a rigid substrate. *Proceedings of the Institution of Mechanical Engineers Part H-Journal of Engineering in Medicine* **223**, 1-12

Joseph, J. (1986) *Aids to Human Osteology*. 7th edition, London, Baillière Tindall

Joyce, T. (2009) Biopolymer tribology. In: *Polymer Tribology*, edited by Sinha, S. K., Briscoe, B. J., London, Imperial College Press, pp 227-266

Khurana, L. (2007) *Textbook of Human Physiology for Dental Students*. New Delhi, Elsevier, p 212

Klein, J. A., Hickey, D. S. Hukins, D. W. L. (1983) Radial bulging of the annulus fibrosus during compression of the intervertebral disc. *Journal of Biomechanics* **16**, 211-217

Klein, J. A., Hukins, D. W. L. (1982) Collagen fibre orientation in the annulus fibrosus of intervertebral disc during bending and torsion measured by X-ray diffraction. *Biochimica et Biophysica Acta* **719**, 98-101

Koes, B. W., van Tulder, M. W., Ostelo, R., Kim Burton, A., Waddell, G. (2001) Clinical guidelines for the management of low back pain in primary care: an international comparison. *Spine* **26**, 2504-2513; discussion 2513-2514

Kreyszig, E. (2006) *Advanced Engineering Mathematics*. 9th edition, Hoboken, NJ, John Wiley & Sons Inc., pp 1049-1057

Kurtz, S. M. (2006) Total disc arthroplasty. In: *Spine Technology Handbook*, edited by Kurtz, S. M., Edidin, A. A., Amsterdam, Elsevier Academic Press, pp. 313-351

Kurtz, S. M., Edidin, A. A. (2006) The basic tools and terminology of spine treatment. In: *Spine Technology Handbook*, edited by Kurtz, S. M., Edidin, A. A., Amsterdam, Elsevier Academic Press, pp. 1-7

Kurtz, S. M., Pelozo, J., Siskey, R., Villarraga, M. L. (2005) Analysis of a retrieved polyethylene total disc replacement component. *Spine Journal* **5**, 344–350

Kurtz, S. M., Steinbeck, M., Ianuzzi, A., van Ooij, A., Punt, I. M., Isaza, J., Ross, E.R.S. (2009) Retrieval analysis of motion preserving spinal devices and periprosthetic tissues. *International Journal of Spine Surgery* **3**, 161-177

Kurtz, S. M., van Ooij, A., Ross, R., de Waal Malefijt, J., Pelozo, J., Ciccarelli, L., Villarraga, M. L. (2007) Polyethylene wear and rim fracture in total disc arthroplasty. *Spine Journal* **7**, 12-21

Langer, H. E., Altmann, S., Lührs, W., Zeidler, H. (1987) The lubrication of the natural joint: viscosity of hyaluronic acid and friction in the human hip. In: *Biomechanics: Basic and Applied Research*, edited by Bergmann G., Kölbl, R., Rohlmann, A., Dordrecht, Martinus Nijhoff Publishers, pp 273-278

Langton, D. J., Jameson, S. S., Joyce, T. J., Hallab, N. J., Natu, S., Nargol, A. V. (2010) Early failure of metal-on-metal bearings in hip resurfacing and large-diameter total hip replacement: a consequence of excess wear. *The Journal of Bone and Joint Surgery, British Volume* **92**, 38-46

Liu, F., Jin, Z. M., Hirt, F., Rieker, C., Roberts, P., Grigoris, P. (2005) Effect of wear of bearing surfaces on elastohydrodynamic lubrication of metal-on-metal hip implants. *Proceedings of the Institution of Mechanical Engineers Part H-Journal of Engineering in Medicine* **219**, 319-328

Lyons, G., Eisenstein, S. M., Sweet, M. B. (1981) Biochemical changes in intervertebral disc degeneration. *Biochimica et Biophysica Acta* **673**, 443-53

Ma, S. M., Kabo, J. M., Amstutz, H. C. (1983) Frictional torque in surface and conventional hip replacement. *Journal of Bone and Joint Surgery, American Volume* **65**, 366-370

Mahomed, A., Chidi, N. M., Hukins, D. W. L., Kukureka, S. N., Shepherd, D. E. T. (2009). Frequency dependence of viscoelastic properties of medical grade silicones. *Journal of Biomedical Materials Research Part B: Applied Biomaterials* **89**, 210-216

Mahomed, A., Moghadas, P. M., Shepherd, D. E. T., Hukins, D. W. L., Roome, A., Johnson, S. (2012) Effect of axial load on the flexural properties of an elastomeric total disc replacement. *Spine* (in press)

Marchand, F., Ahmed, A. M. (1990) Investigation of the laminate structure of lumbar disc annulus fibrosus. *Spine* **15**, 402-410

Marcolongo, M. S., Cannella, M., Massey, C. J. (2006) Nucleus replacement of the intervertebral disc. In: *Spine Technology Handbook*, edited by Kurtz, S. M., Edidin, A. A., Amsterdam, Elsevier Academic Press, pp 282-298

Maroudas, A., Urban, J. P. G. (1980) Swelling pressure of cartilaginous tissues. In: *Studies in Joint Disease*, edited by Maroudas, A., Holborrow, E. J. Volume I, London, Pitman Medical, Tunbridge Wells. pp. 87-116

Mattei, L., Di Puccio, F., Piccigallo, B., Ciulli, E. (2011) Lubrication and wear modelling of artificial hip joints: A review. *Tribology International* **44**, 532-549

McAfee, P. C., Cunningham, B., Holsapple, G., Adams, K., Blumenthal, S., Guyer, R. D., Dmitriev, A., Maxwell, J. H., Regan, J. J., Isaza, J. (2005) A prospective, randomized, multicenter food and drug administration investigational device exemption study of lumbar total disc replacement with the Charité Artificial Disc versus lumbar fusion. Part II: evaluation of radiographic outcomes and correlation of surgical technique accuracy with clinical outcomes. *Spine* **30**, 1576-1583, discussion E388-E390

McGregor, A. H., Hukins, D. W. L. (2009) Lower limb involvement in spinal function and low back pain. *Journal of Back and Musculoskeletal Rehabilitation* **22**, 219-222

McKellop, H., Park, S. H., Chiesa, R., Doorn, P., Lu, B., Normand, P., Grigoris, P., Amstutz, H. (1996) In vivo wear of three types of metal on metal hip prostheses during two decades of use. *Clinical Orthopaedics and Related Research* **329**, S128-S140

McNally, D. S., Arridge, R. G. C. (1995) An analytical model of intervertebral disc mechanics. *Journal of Biomechanics* **28**, 53-68

Meakin, J. R., Hukins, D. W. L. (2000) Effect of removing the nucleus pulposus on the deformation of the annulus fibrosus during compression of the intervertebral disc. *Journal of Biomechanics* **33**, 575-580

Middleditch, A., Oliver, J. (2005) *Functional Anatomy of the Spine*. 2nd edition, Edinburgh, Elsevier Butterworth Heinemann

Modic, M. T., Ross, J. S. (2007) Lumbar degenerative disk disease. *Radiology* **245**, 43-61

Moghadas, P., Mahomed, A., Hukins, D. W. L., Shepherd, D. E. T. (2012a) Friction in metal-on-metal total disc arthroplasty: effect of ball radius. *Journal of Biomechanics* **45**, 504-509

Moghadas, P. M., Shepherd, D. E. T., Hukins, D. W. L., Mahomed, A. (2012b) Polymer-on-metal or metal-on-polymer total disc arthroplasty: does it make a difference? *Spine* (in press)

Nachemson, A. L. (1976) The lumbar spine: an orthopaedic challenge. *Spine* **1**, 59-71

National Institute for Health and Clinical Excellence (2009) Low back pain: Early management of persistent non-specific low back pain. *Clinical Guideline 88*, The National Collaborating Centre for Primary Care, UK

Nechtow, W., Hinter, M., Bushelow, M., Kaddick, C. (2006) IVD replacement mechanical performance depends strongly on input parameters. *Transactions of the 52nd Annual Meeting of the Orthopaedic Research Society*, Chicago, IL

Orozco, L., Soler, R., Morera, C., Alberca, M., Sánchez, A., García-Sancho, J. (2011) Intervertebral disc repair by autologous mesenchymal bone marrow cells: a pilot study. *Transplantation* **92**, 822-828

Panjabi, M. M., Duranceau, J., Goel, V., Oxland, T., Takata, K. (1991) Cervical human vertebrae: quantitative three-dimensional anatomy of the middle and lower regions. *Spine* **16**, 861-869

Panjabi, M. M., White, A. A., Keller, D., Southwick, W. O., Friedlaender, G. (1978) Stability of the cervical spine under tension. *Journal of Biomechanics* **11**, 189-197

Paré, P. E., Chan, F. W., Powell, M. L. (2007) Wear characterisation of the A-MAV™ anterior motion replacement using a spine wear simulator. *Wear* **263**, 1055–1059

Porchet, F., Metcalf, N. H. (2004) Clinical outcomes with the Prestige II Cervical Disc: preliminary results from a prospective randomized clinical trial. *Neurosurgical Focus* **17**, E6

Prokopovich, P., Perni, S., Fisher, J., Hall, R. M. (2011) Spatial variation of wear on Charité lumbar discs. *Acta Biomaterialia* **7**, 3914-3926

Punt, I. M., Austen, S., Cleutjens, J. P. M., Kurtz, S. M., ten Broeke, R. H. M., van Rhijn, L. W., Willems, P., van Ooij, A. (2012) Are periprosthetic tissue reactions observed after revision of total disc replacement comparable to the reactions observed after total hip or knee revision surgery? *Spine* **37**, 150-159

Punt, I. M., Cleutjens, J. P., de Bruin, T., Willems, P. C., Kurtz, S. M., van Rhijn, L. W., Schurink, G. W., van Ooij, A. (2009) Periprosthetic tissue reactions observed at revision of total intervertebral disc arthroplasty. *Biomaterials* **30**, 2079-2084

Punt, I. M., Visser, V. M., Van Rhijn, L. W., Kurtz, S. M., Antonis, J., Schurink, G. W. H., Van Ooij, A. (2008). Complications and reoperations of the SB Charité lumbar disc prosthesis: experience in 75 patients. *European Spine Journal* **17**, 36-43

Rawlinson, J. J., Punga, K. P., Gunsallus, K. L., Bartel, D. L., Wright, T. M. (2007) Wear simulation of the ProDisc-L disc replacement using adaptive finite element analysis. *Journal of Neurosurgery: Spine* **7**, 165-173

Rieker, C., Konrad, R., Schoun, R. (2001) In vitro comparison of the two hard-hard articulations for total hip replacements. *Proceedings of the Institution of Mechanical Engineers Part H-Journal of Engineering in Medicine* **215**, 153-160

Roselli, R. J., Diller, K. R. (2011) *Biotransport: principles and applications*. New York, Springer, p139

Scholes, S. C., Green, S. M., Unsworth, A. (2001) The wear of metal-on-metal total hip prostheses measured in a hip simulator. *Proceedings of the Institution of Mechanical Engineers Part H-Journal of Engineering in Medicine* **215**, 523-530

Scholes, S. C., Smith, S. L., Ash, H. E., Unsworth, A. (2003) The lubrication and friction of conventional UHMWPE, novel compliant layer, and hard bearing surfaces for use in total hip prostheses. In: *Friction, Lubrication, and Wear of Artificial Joints*, edited by Hutchings, I. M., London, Professional Engineering Publishing, pp 59-74

Scholes, S. C., Unsworth, A. (2000) Comparison of friction and lubrication of different hip prostheses. *Proceedings of the Institution of Mechanical Engineers Part H-Journal of Engineering in Medicine* **214**, 49-57

Scholes, S. C., Unsworth, A. (2006a) The effects of proteins on the friction and lubrication of artificial joints. *Proceedings of the Institution of Mechanical Engineers Part H-Journal of Engineering in Medicine* **220**, 687-693

Scholes, S. C., Unsworth, A. (2006b) The tribology of metal-on-metal total hip replacements. *Proceedings of the Institution of Mechanical Engineers Part H-Journal of Engineering in Medicine* **220**, 183-194

Scholes, S. C., Unsworth, A. (2010) The wear performance of PEEK-OPTIMA based self-mating couples. *Wear* **268**, 380-387

Scholes, S. C., Unsworth, A., Goldsmith, A. A. J. (2000a) A frictional study of total hip joint replacements. *Physics in Medicine and Biology* **45**, 3721–3735

Scholes, S. C., Unsworth, A., Hall, R. M., Scott, R. (2000b) The effects of material combination and lubricant on the friction of total hip prostheses. *Wear* **241**, 209-213

Scott, R. A., Schroeder, D. W. (1997) The effect of radial mismatch on the wear of metal on metal hip prosthesis: a hip simulator study. *43rd Annual Meeting of the Orthopaedic Research Society*, San Francisco, CA, USA, p.764

Serhan, H. A., Dooris, A. P., Parsons, M. L., Ares, P. J., Gabriel, S. M. (2006) In vitro wear assessment of the Charité artificial disc according to ASTM recommendations. *Spine* **31**, 1900-1910

Shaheen, A., Shepherd, D. E. T. (2007) Lubrication regimes in lumbar total disc arthroplasty. *Proceedings of the Institution of Mechanical Engineers Part H-Journal of Engineering in Medicine* **221**, 621-627

Sherwood, L. (2011) *Fundamentals of Human Physiology*. California, Brooks/Cole Cengage Learning, pp 417-420

Shim, C. S., Lee, S., Maeng, D. H., Lee, S. H. (2005) Vertical split fracture of the vertebral body following total disc replacement using ProDisc: report of two cases. *Journal of Spinal Disorders and Techniques* **18**, 465–469

Smith, S. L., Dowson, D., Goldsmith, A. A. J. (2001a) The lubrication of metal-on-metal total hip joints: a slide down the Stribeck curve. *Proceedings of the Institution of Mechanical Engineers Part J- Journal of Engineering Tribology* **215**, 483-493

Smith, S. L., Dowson, D., Goldsmith, A. A. J. (2001b) The effect of diametral clearance, motion and loading cycles upon lubrication of metal-on-metal total hip replacements. *Proceedings of the Institution of Mechanical Engineers, Part C- Journal of Mechanical Engineering Science* **215**, 1-5

SOP01.6: *Standard Operating Protocol for Spine Wear Simulator Studies*. Leeds, Institute of Medical and Biological Engineering, University of Leeds

Steffee, A. D. (1992) The Steffee artificial disc. In *Clinical Efficacy and Outcome in the Diagnosis and Treatment of Low Back Pain*, edited by Weinstein, J. N., New York, Raven Press

Stolarski, T. A. (1990) *Tribology in Machine Design*. Oxford, Butterworth-Heinemann, pp 14-19

Streicher, R. M., Semlitsch, M., Schön, R., Weber, H., Rieker, C. (1996) Metal-on-metal articulation for artificial hip joints: laboratory study and clinical results. *Proceedings of the Institution of Mechanical Engineers Part H-Journal of Engineering in Medicine* **210**, 223-232

Taylor Hobson (1990) *The Taylor Hobson Form Talysurf-120L User Manual*, Taylor Hobson, Leicester, UK

Tipper, J. L., Firkins, P. J., Ingham, E., Fisher, J., Stone, H., Farrar, R. (1999) Quantitative analysis of the wear and wear debris from low and high carbon content cobalt chrome alloys used in metal on metal total hip replacements. *Journal of Materials Science: Materials in Medicine* **10**, 353-362

Unsworth, A. (1978) The effects of lubrication in hip joint prostheses. *Physics in Medicine and Biology* **23**, 253-268

Urban, J. P. G., Maroudas, A. (1981) Swelling of the intervertebral disc in vitro. *Connective Tissue Research* **9**, 1-10

Vassilou, K., Elfick, A. P. D., Scholes, S. C., Unsworth, A. (2006) The effect of 'running-in' on the tribology and surface morphology of metal-on-metal Birmingham hip resurfacing device in simulator studies. *Proceedings of the Institution of Mechanical Engineers Part H-Journal of Engineering in Medicine* **220**, 269-277

Vernon-Roberts, B., Pirie C. J. (1977) Degenerative changes in the intervertebral discs of the lumbar spine and their sequelae. *Rheumatology and Rehabilitation* **16**, 13-21

Vicars, R., Fisher, J., Hall, R. M. (2009) The accuracy and precision of a micro computer tomography volumetric measurement technique for the analysis of in-vitro tested total disc replacements. *Proceedings of the Institution of Mechanical Engineers Part H-Journal of Engineering in Medicine* **223**, 383-388

Vicars, R., Hyde, P. J., Brown, T. D., Tipper, J. L., Ingham, E., Fisher J., Hall, R. M. (2010) The effect of anterior-posterior shear load on the wear of ProDisc-L TDR. *European Spine Journal* **19**, 1356-1362

Virgin, W. J. (1951) Experimental investigations into the physical properties of the intervertebral disc. *The Journal of Bone and Joint Surgery. British Volume* **33**, 607-611

Wang, A., Essner, A., Klein, R. (2001) Effect of contact stress on friction and wear of ultra-high molecular weight polyethylene in total hip replacement. *Proceedings of the Institution of Mechanical Engineers Part H-Journal of Engineering in Medicine* **215**, 133-139

Wang, A., Essner, A., Schmidig, G. (2004) The effects of lubricant composition on in vitro wear testing of polymeric acetabular components. *Journal of Biomedical Materials Research Part B- Applied Biomaterials* **68B**, 45–52

Wang, F. C., Brockett, C., Williams, S., Udofia, I., Fisher, J., Jin, Z. M. (2008a) Lubrication and friction prediction in metal-on-metal hip implants. *Physics in Medicine and Biology* **53**, 1277-1293

Wang, Q. M., Cheng, H. B., Mao, Z. X., Qi, X. S., Zhang, M., Chen, Y. (2011) Clinical and radiographic results after treatment of cervical degenerative disc disease with the Bryan discprosthesis: A prospective study with 2-year follow-up. *Acta Orthopaedica Belgica* **77**, 809-815

Wang, W. Z., Jin, Z. M., Dowson, D., Hu, Y. Z. (2008b) A study of the effect of model geometry and lubricant rheology upon the elastohydrodynamic lubrication performance of metal-on-metal hip joints. *Proceedings of the Institution of Mechanical Engineers Part J- Journal of Engineering Tribology* **222**, 493-501

White, A. A., Panjabi, M. M. (1978) The basic kinematics of the human spine, *Spine* **3**, 12-20

White, A. A., Panjabi, M. M. (1990) *Clinical Biomechanics of the Spine*. Philadelphia, J. P. Lippincott

White, A. P., Grossman, E. L., Hilibrand, A. S. (2010) Clinical presentation of disc degeneration. In: *The lumbar Intervertebral disc*, edited by Phillips, F. M., Laurysen, C., New York, Thieme Medical

Wicke, L. (1998) *Atlas of Radiologic Anatomy*. 6th English edition, Baltimore, Williams & Wilkins

Williams, F. M. K., Sambrook, P. N. (2011) Neck and back pain and intervertebral disc degeneration: role of occupational factors. *Best Practice and Research Clinical Rheumatology* **25**, 69-79

Wimmer, M. A., Fischer, A. (2007) Tribology In: *The Adult Hip*, edited by Callaghan, J. J., Rosenberg, A. G., Rubash, H. E. Volume I, Philadelphia, Lippincott Williams & Wilkins, pp 215-303

Wimmer, M. A., Loos, J., Nassutt, R., Heitkemper, M., Fischer, A. (2001) The acting wear mechanisms on metal-on-metal hip joint bearings: in vitro results. *Wear* **250**, 129-139

Yan, Y., Neville, A., Dowson, D., Williams, S., Fisher, J. (2009) Effect of metallic nanoparticles on the biotribocorrosion behaviour of metal-on-metal hip prostheses. *Wear* **267**, 683-688

Yao, H., Gu, W. Y. (2006) Physical signals and solute transport in human intervertebral disc during compressive stress relaxation: 3D finite element analysis. *Biorheology* **43**, 323-335

Yao, J. Q., Laurent, M. P., Johnson, T. S., Blanchard, C. R., Crowninshield, R. D. (2003) The influences of lubricant and material on polymer/CoCr sliding friction. *Wear* **255**, 780-784

Yoganandan, N., Kumaresan, S., Pintar, F. A. (2001) Biomechanics of the cervical spine- Part 2: Cervical spine soft tissue responses and biomechanical modelling. *Clinical Biomechanics* **16**, 1-27

Zeh, A., Planert, M., Siegert, G., Lattke, P., Held, A., Hein, W. (2007) Release of cobalt and chromium ions into the serum following implantation of the metal-on-metal Maverick-type artificial lumbar disc (Medtronic Sofamor Danek). *Spine* **32**, 348-352

Zurovsky, Y., Mitchell, G., Hattingh, J. (1995) Composition and viscosity of interstitial fluid of rabbits. *Experimental Physiology* **80**, 203-207